Imperial College
London

Insulin growth-factor 1Ea gene transfer therapy after myocardial infarction

A thesis submitted for the degree of Doctor of Philosophy and the Diploma of Imperial College
by

Enrique Gallego-Colon

National Heart & Lung Institute
Hammersmith Campus
Imperial College London

August 2015

Abstract

Cardiovascular diseases (CVD) are the major cause of death globally with myocardial infarction (MI) being one of the main causes of mortality. The limited regenerative capacity of adult human tissues is particularly pertinent to the heart, which cannot repair itself fully after injury; instead, the damaged myocardium is replaced by fibrotic scar tissue and the heart progressively decrement in function. To date, efforts to develop interventions for alleviation of this inevitable destructive progression have proven largely ineffective. Although over the past decades, treatment for myocardial ischemia has made significant progress, myocardial infarction remains an unsolved therapeutic target.

In attempting to address this problem, insulin growth factor splicing variant 4 (IGF-1Ea) has been extensively tested for its therapeutic properties in the resolution of tissue injury. In the heart, constitutive overexpression of IGF-1Ea (αMHC.IGF-1Ea) restored heart functionality post-infarct, reducing scar formation and increased anti-apoptotic signalling.

This thesis provides deeper understanding on the role of IGF-1Ea in early modulation of the inflammatory process after myocardial infarction in αMHC.IGF-1Ea transgenic mice. In fact, the enhanced repair in αMHC.IGF-1Ea after myocardial infarction is due to IGF-1Ea modulating several aspects of the cellular repair process after MI, including immune cell recruitment, cytokine expression, and reduction of the extracellular matrix turnover. However, the heart-specific transgene is constitutively expressed from birth and does not simulate delivery to humans in the clinic. With a better understanding of IGF-1Ea in cardiac repair, this thesis also focused on the design of both cell- and gene-based approaches to deliver the IGF-1Ea therapeutic payload into the heart by (i) adoptive immunotherapy approach using bone-marrow derived-macrophages mediated cell delivery of IGF-1Ea and (ii) IGF-1Ea gene transfer to the heart using a cardiotropic adeno-associated viral vector (AAV9) after ischemia/reperfusion. Of the two approaches, only the gene-based approach was able to deliver IGF-1Ea into the heart achieving therapeutically relevant levels. AAV9-mediated IGF1Ea gene transfer proved to be a potential therapeutic clinical approach to prevent the adverse ventricular remodeling after myocardial infarct. The knowledge acquired in this thesis will be relevant to inform and design future therapeutic approaches for the treatment of patients suffering from myocardial infarction.

Acknowledgements

I would like to thank my supervisor Nadia Rosenthal for her vast knowledge, imagination and creativity, as it has been for me the thrust I needed to push forward this thesis. I would like to thank her as well for the opportunity of taking me in with an amazing fellowship as CardioNet. I am in debt to my secondary supervisor Sian Harding for her advice during the writing of this thesis.

There are no words that could explain my experience as a CardioNet-Marie Curie Fellow, as I believe that being a CardioNet fellow it has been one of the greatest career opportunities I ever had. Within the CardioNet network, I also had the opportunity to learn new techniques all over Europe which opened my mind to the scientific world, as well as having the chance to met the best scientist in the Cardiovascular field. I also had the chance to built strong friendships with all the PhD students within the network, like Adriana, Megan R, Megan M, Ghislaine, Francesco P, Francesco M, Alberto, Dimitris, Mayyasa, Stuti, Adrian, Andrea, Vikas. I will always remember our meeting, dinners and parties.

My special thank you goes to Enrique Lara for providing me with the opportunity to conduct part of my PhD work at the CNIC, Madrid, Spain. I shall always cherish the moments with the people in his lab, a friendship that we extended further outside the lab. Here at ICTEM, I only have words of gratitude to all past and present members of Nadia's group particularly Susanne, Teresa and Jo. I am deeply indebted to Jo, who has always been honest with me as well as though when needed. One of the things that I learnt from Jo was to ask me every time while doing experiments, why are you doing this experiment? What question do you want to answer? Second, I cherish a lot our long conversations about life, science and other stuff looking through the window of our floor and pretending we were somewhere sunny. The last but not least, my special gratitude to "The Pineapple team", Tom , Ellie, Marty, Carolina, Poppins, Ari, Anselmito, Alice, Katy, Magda, Imeldita. I thank you all for sharing some of the great times of my PhD both inside and outside the lab, I hope our friendship will last forever.

I would like to thank to all the people I collaborated with here at Imperial College, such as Eduardo Oliver for his scientific advice and encouragement. My friend, Oscar Pello, for reading this thesis from an external point of view. Finally, Robert D. Sampson for his help with the isolation cells from the heart – through this collaboration we ended up being close friends.

Statement of originality

All the work described in this thesis was performed by the author except were specifically indicated below or in the text. The ITR 3D structure and sequence in Methodology, Figure 2.8 was kindly provided by Fran Cruz at the Spanish Centre for Cardiovascular Research (CNIC). The Neonatal Rat Cardiomyocytes as well as the transfection, in Figure 5.1, were provided and performed by Dr. Wenhua. Sectioning and staining of Figures 3.3, 4.1, 5.2, 5.11, 5.12 were performed by Padmini Sarathchandra. Sectioning and staining of Figure 5.9 were performed at CNIC's sectioning core facility. Antibody titrations, heart digestions in Chapter 3 were performed with the assistance of Robert D. Sampson. Adeno-associated viruses were produced at University of Pennsylvania, Penn vector core.

Copyright declaration

'The copyright of this thesis rests with the author and is made available under a Creative Commons Attribution Non-Commercial No Derivatives licence. Researchers are free to copy, distribute or transmit the thesis on the condition that they attribute it, that they do not use it for commercial purposes and that they do not alter, transform or build upon it. For any reuse or redistribution, researchers must make clear to others the licence terms of this work'

Imagination is more important than knowledge.

A. Einstein

Abbreviations

AAV9	Adeno-associated virus serotype 9
AAV9.GFP	Adeno-associated virus serotype 9 green fluorescence protein
AAV9.IGF-1Ea	Adeno-associated virus serotype 9 insulin-like growth factor isoform Ea
ACE	Angiotensin-converting-enzyme
ACTA	Actin-alpha 1 skeletal muscle
Ads	Adenoviruses
ANP	Atrial natriuretic peptide
ARB	Angiotensin-II receptor blockers
BMCs	Marrow-derived cells
BMdM	Bone marrow derived macrophages
BNP	Brain natriuretic peptide
BRDU	Bromodeoxyuridine
BSA	Bovine serum albumin
BW	Body weight
CABG	Coronary artery bypass graft surgery
CAPRICORN	Carvedilol post-infarct survival control in LV dysfunction
CCR2	C-C chemokine receptor type 2
CDK-1	Cyclin-dependent kinase 1
cDNA	Complementary DNA
CF	Cardiac fibroblast
CFSE	Carboxyfluorescein succinimidyl ester
CHD	Cardiovascular heart diseases
CMV	Cytomegalovirus promoter
CnAβ1	Calcineurin splicing variant
Col Iα1	Collagen type I
Col Iα3	Collagen type III
CSC	Cardiac stem cells
cTNT	Cardiac troponin promoter
CTX	Cardiotoxin
CUPID	Calcium upregulation by percutaneous administration of gene therapy in cardiac disease
CVD	Cardiovascular diseases
CX3CR1	CX3C chemokine receptor 1 (CX3CR1) also known as the fractalkine receptor or G-protein coupled receptor 13 (GPR13)

DKO-MΦs	Luciferase-labelled macrophages
DNA	Deoxyribonucleic acid
DTT	Dithiothreitol
EC	Endothelial cells
ECL	Enhance chemiluminescence
ECM	Extracellular matrix
ELISA	Enzyme-linked immunosorbent assay
EPDC	Epicardium-derived cells
FACS	Flow cytometry cell sorting
FBS	Fetal bovine serum
FDA	Food and drug administration
FOXO	Forkhead box O sub class family
FS	Fractional shortening
GC	Genome copies
GFP	Green fluorescence protein
GOI	Genes of interest
GSK-3α	Glycogen synthase-serine kinase 3α
HEK293 cells	Human embryonic kidney 293 cells
HRE	Hypoxia regulatory element
HSV	Herpes simplex virus
I.V	Intravenous administration
I/R	Ischemia/reperfusion injury
ICD	Implantable cardioverter-defibrillator
IFN-γ	Interferon gamma
IGF-1Ea	Insulin Growth Factor 1 Ea peptide
IGF-1Eb	Insulin Growth Factor 1 Eb peptide
IGF-1R	IGF-receptor
IGF-2	Insulin-like Growth Factor-2 or mechano growth factor (MGF)
IGFBP	IGF-1 binding proteins
IL	Interleukin
iPS cells	Induced pluripotent stem cells
IRES	Internal ribosomal entry site
ITR	Inverted terminal repeats
IVIS	*In vivo* imaging sytem
LB	Luria broth
Lox	Lysyl oxidase

LV	Left ventricule
LVAD	Left ventricular assist devices
LVEDd	Left ventricular end-diastolic diameter
LVEDV	Left ventricular end-diastolic volume
LVEF	Left ventricular ejection fraction
LVESV	Ventricular end-systolic volume
M-CSF	Macrophage colony-stimulating factor
M1	Inflammatory IFNγ/LPS stimulated macrophages
M2	Reparative IL-4 stimulated macrophages
MAGIC	Myoblast autologous grafting in ischemic cardiomyopathy
MAP-kinase	Mitogen activated protein kinase signalling or extracellular-signal-regulated kinases (ERKs)
MBCK	MB isozyme fraction of creatine kinase MB
MCP-1	Monocyte chemoattractant protein-1
MI	Myocardial infarction
miRNA	microRNA
MMP	Matrix metalloproteinase
MRC	Medical research council
mRNA	messenger ribonucleic acid
mTOR	Mammalian target of rapamycin
Mθ	Day 7-non-polarised bone marrow derived macrophages
Nab	Neutralizing antibodies
NO	Nitric Oxide
Nppb	N-terminal probrain natriuretic peptide
NT-proBNP	Pro-brain natriuretic peptide
pAAV9.IGF1Ea	Plasmid containing IGF-1Ea, IRES, luciferase gene, and ampicillin resistance gene.
PBS	Phosphate buffered saline
PCI	Percutaneous coronary intervention
PI(3)/AKT	Phosphatidylinositol-4,5-bisphosphate 3-kinase/ AKT signaling pathway
pIRES2.eGFP	Plasmid containing IGF-1Ea, IRES, enhanced GFP gene
PMN	Polymorphonuclear leukocyte
qRT-PCR	Real-time polymerase chain reaction
RALDH2	Retinaldehyde dehydrogenase 2
RIPA	Radioimmunoprecipitation

ROS	Reactive oxygen species
RT	Room temperature
RV	Right ventricle
SAVE	Survival and ventricular enlargement
SDS	Sodium dodecyl sulphate
SEM	Stantard error of the mean
SERCA2	Sarco/endoplasmic reticulum Ca2+-ATPase, or SR Ca2+-ATPase
siRNA	Small interfering RNA
TA	Tibialis anterior
TGFβ	Tranforming growth factor beta 1
TIMPs	Inhibitors of metalloproteinases
UCP-1	Uncoupling protein1
VF	Ventricular fibrillation
VT	Ventricular tachycardia
VSMC	Vascular mesenchymal stem cells
WMSI	Wall motion score index
WT	Wild type
αMHC.IGF-1Ea	Alpha-myosin heavy chain promoter of IGF-1Ea

TABLE OF CONTENTS

Abstract 2
Acknowledgments 3
Statement of originality 4
Copyright declaration 5
Abbreviations 7
Table of Contents 11
List of Figures 16
List of Tables 19

Chapter 1 – Introduction 20
1.1 The Heart 20
1.2 Regeneration of the mammalian heart 22
1.3 Cardiovascular heart diseases 23
1.3.1 Clinical features of myocardial infarction 24
1.3.2 Immune system response after myocardial infarction 25
1.3.2.1 Activation of the inflammatory process 25
1.3.2.2 Neutrophil- and macrophage-mediated inflammatory responses 26
1.3.2.3 Wound healing and heart remodeling 29
1.3.3 Current treatments after myocardial infarction-derived heart failure 30
1.3.3.1 Interventional cardiology after myocardial infarction 30
1.3.3.2 Pharmacological treatment after myocardial infarction 31
1.3.3.3 Other post-MI treatments: implantable medical devices 32
1.4 Therapeutic approaches for myocardial infarction injury 33
1.4.1 Cell-based therapeutic approaches 33
1.4.1.1 Immunological therapies 35
1.4.2 Gene-based therapeutic approaches 37
1.4.2.1 Viral vectors for cardiac transfer 38
1.4.2.2 Adeno-associated virus biology 39
1.4.2.2.1 AAV neutralizing antibodies 40
1.4.2.2.2 Production of recombinant AAVs 41

1.5 The insulin-like growth factor family 43
1.5.1 Insulin-like growth factor 1 structure and post-translational modification. 43
1.5.2 Insulin-like growth factor 1 receptor and signalling pathways 45
1.5.2.1 MAP-kinase signalling 46
1.5.2.2 PI(3)/AKT-signalling 46
1.5.2.3 Calcineurin signalling 47
1.5.3 IGF-1 isoforms in skeletal muscle regeneration 47
1.5.4 IGF-1 in cardiac repair 48
1.5.5 IGF-1 therapeutic applications 50
1.5.5.1 Viral delivery of IGF-1 51
1.6 Hypothesis and aims 52

Chapter 2 – Methodology 53
2.1 Mouse model 53
2.1.1 αMHC.IGF-1Ea mice 53
2.1.2 αMHC.IGF-1Ea genotyping 53
2.2 RNA extraction and quantification 54
2.2.1 RNA isolation from cells and from tissue 54
2.2.2 RNA quantification 55
2.2.3 cDNA synthesis 55
2.2.4 Quantitative Real-Time polymerase chain reaction (qRT-PCR) 55
2.2.4.1 qPCR data analysis: comparative $\Delta\Delta C_t$ method 56
2.2.4.2 Taqman® probe-based gene expression analysis 57
2.3 Protein biochemistry 57
2.3.1 Protein extraction and quantification 58
2.3.2 Immunoblotting 58
2.4 Immune single cell isolation from heart 59
2.4.1 Flow cytometry and cell sorting 60
2.5 Generation and differentiation of bone marrow-derived macrophages 63
2.5.1 Mouse bone marrow cell isolation 63
2.5.2 Cryopreservation of mouse bone marrow cells 63
2.5.3 Differentiation and culture of bone marrow-derived macrophages 63
2.5.4 M1/M2 polarization of bone marrow-derived macrophages 64
2.5.5 Monocyte isolation from blood and spleen 64
2.5.6 Bone marrow-derived macrophage flow cytometry characterisation 64
2.5.7 Bone marrow-derived macrophage CFSE staining 65

2.6 Bone marrow-derived macrophages transfection 65
2.7 *In vivo* model of cardiac injury 66
2.7.1 Left descending coronary artery ligation as model myocardial infarction 66
2.7.2 Ischemia reperfusion injury as a model of myocardial infarction 66
2.7.3 Skeletal muscle CTX injury as model for muscle regeneration 67
2.8 Echocardiography 67
2.8.1 Transthoracic echocardiography with Vevo 770 67
2.8.2 Transthoracic echocardiography with Vevo 2100. 67
2.9 Histology of paraffin-embedded tissue 69
2.9.1 Masson's Trichrome Staining 69
2.9.1.1 Determination of scar length and total fibrosis 69
2.9.2 Picrosirius red staining 70
2.9.3 Heart immunohistochemistry 70
2.9.4 Heart immunofluorescence 71
2.10 Amplification and purification of IGF-1Ea vector from E.coli 71
2.11 IGF-1Ea cloning strategy: from pIRES2.eGFP to pAAV9.IGF-1Ea 72
2.11.1 Amplification and purification of IGF-1Ea PCR product 73
2.11.2 IGF-1Ea PCR product digestion and ligation into the pAC-cTNT 74
2.11.3 One Shot® Stbl3 Transformation. 75
2.11.4 Amplification of positive clones, bacterial amplification and plasmid isolation 75
2.11.5 Confirmation of correct IGF-1Ea cloning: PCR and restriction enzyme digestion 75
2.11.6 pIRES.eGFP and pAAV9.IGF-1Ea sequencing 76
2.11.7 Sequencing GC-rich regions of the ITRs 77
2.11.8 pAAV9.IGF-1Ea vector quality control, construction, production, and purification 79
2.12 *In vivo* injections of both GFP- and CFSE-macrophages after CTX injury 80
2.13 AAV9.IGF-1Ea *in vivo* gene transfer 81
2.13.1 IVIS - Bioluminescence analysis of *in vivo* gene transfer 80
2.13.2 Detection of serum IGF-1 protein 80
2.14 Statistics 81

Chapter 3 – Study of IGF-1Ea-mediated inflammatory response and extracellular matrix remodeling after myocardial infarction in αMHC.IGF-1Ea 82
3.1 Introduction 82
3.2 IGF-1Ea improves cardiac function after myocardial infarction 83
3.3 Altered tissue remodeling in αMHC.IGF-1Ea after injury 87
3.4 Distinct chemokine and cytokine production in αMHC-IGF-1Ea hearts after myocardial infarct 90
3.5 IGF-1Ea modulates myeloid cell recruitment after myocardial infarction 91
3.6 Discussion 95
3.6.1 Limitation of the project 97
3.6.2 Outcomes 98

Chapter 4 – Delivery of therapeutic growth factors to the injured heart by bone marrow-derived macrophages 99
4.1 Introduction 99
4.2 Rationale behind the skeletal muscle injury model 99
4.3 IGF-1Ea levels in macrophages and monocytes 100
4.4 Bone marrow-derived macrophage characterisation for transplantation 101
4.5 Bone marrow-derived macrophage immunotherapy 102
4.5.1 Effect of IGF-1Ea on transfected BMdMs *in vitro* 106
4.6 Homing of transplanted bone marrow-derived macrophages following TA injury and the effect of 'priming' macrophages with cytokines 106
4.6.1 Homing of IGF-1Ea.GFP M1- and M2-like macrophages 108
4.6.2 Homing of CFSE-positive bone marrow-derived macrophages 110
4.7 Discussion 111
4.7.1 Limitation of the approach 114
4.7.2 Outcomes 114

Chapter 5 - Adeno-associated virus type 9 (AAV9) IGF-1Ea gene transfer into the damaged heart after ischemia/reperfusion injury 115
5.1 Introduction 115
5.2 pAAV9.IGF-1Ea expression on neonatal cardiomyocytes and AAV9.IGF-1Ea infection of HL-1 cells 115
5.3 Characteristics of intravenous AAV9.IGF-1Ea gene transfer 116
5.4 Echocardiography assessment of AAV9.IGF-1Ea gene delivery after ischemia/reperfusion 120

5.4.1 AAV9.IGF-1Ea gene transfer improves global left ventricular function after ischemia/reperfusion 121
5.4.2 Left ventricular regional wall motion is enhanced by 28 days after AAV9.IGF-1Ea gene transfer 122
5.5 IGF-1Ea gene transfer reduces infarct size and cardiac fibrosis 124
5.6 BrdU+ quantification nuclei after IGF-1Ea gene transfer 125
5.7 AAV9.IGF-1Ea treatment promotes cardiac Akt-mediated signalling 128
5.8 Discussion 129
5.8.1 Limitation of the project 131
5.8.2 Outcomes 132

Chapter 6 – Concluding remarks and future directions 133
6.1 Concluding remarks 133
6.2 Future directions 135
6.3 Future work 135

Publications and Presentations 140
Publications 140
Presentations 140
Awards 142
Outreach activities 143

Appendix 144
References 146

List of figures

Figure 1.1. Internal view of the 4-chambered healthy heart 21
Figure 1.2. Biphasic monocyte/macrophage inflammatory response and remodeling process after myocardial infarction in the mice. 27
Figure 1.3. Potential lineage relationships of monocytes and macrophages after myocardial infarction 28
Figure 1.4. Basic structure of a wild-type adeno-associated viral genome 39
Figure 1.5. Structure of the rodent IGF-1 gene 44
Figure 1.6. Different IGF-1 pre-propeptides cleavage 45
Figure 1.7. IGF-1/IGF-1R signalling pathway 46
Figure 1.8. Enhanced cardiac repair in αMHC-IGF1Ea transgenic mice after myocardial infarction 49
Figure 2.1. IGF-1Ea genotyping PCR product 54
Figure 2.2. Bovine Serum Albumin (BSA) representative standard curve 58
Figure 2.3. Identification of positive stained cells using the fluorescence minus one (FMO) strategy for Ly6G, CD11c and CD11b 61
Figure 2.4. Identification of positive stained cells using the fluorescence minus one (FMO) strategy for F4/80, Ly6C and CD206 62
Figure 2.5. Echocardiographic representation of parasternal short and long axis orientation and schematics of LV walls 68
Figure 2.6. Schematic illustration of pIRES2.eGFP backbone and IGF-1Ea PCR product. 72
Figure 2.7. Schematic illustration of pAAV9.IGF-1Ea vector backbone and IGF-1Ea restriction enzyme digestion 76
Figure 2.8. Predicted structure of the inverted terminal repeats (ITR) in the pAAV.IGF-1Ea 77
Figure 2.9. ITR PCR product agarose gel 79
Figure 3.1. IGF-1Ea relative mRNA levels in the heart after myocardial infarct in WT and αMHC.IGF-1Ea mice compared throughout a 28-day timecourse 84
Figure 3.2. Expression of IGF-1Ea improves cardiac function and reduces dilation as early as 7 days after myocardial infarction 85
Figure 3.3. IGF-1Ea enhanced repair after myocardial infarction 87
Figure 3.4. Changes in gene expression of extracellular matrix suggesting a distinct remodeling in αMHC.IGF-1Ea mice after myocardial infarction 88
Figure 3.5. Infarct region mRNA levels of matrix genes of the newly synthesised extracellular matrix of αMHC.IGF-1Ea mice 89

Figure 3.6. Cytokine dynamics in the infarcted hearts of αMHC.IGF-1Ea 90
Figure 3.7. Gating strategy for infiltrating immune cells after myocardial infarct 92
Figure 3.8. Characterization and temporal dynamics of immune cell populations in αMHC.IGF-1Ea hearts after myocardial infarction 93
Figure 3.9. Temporal dynamics of monocytes subpopulations in αMHC.IGF-1Ea hearts after myocardial infarction 94
Figure 3.10. Temporal dynamics of macrophages subpopulations and dendritic cells in αMHC.IGF-1Ea hearts after myocardial infarction 95
Figure 4.1. Representative haematoxylin and eosin staining of TA injured muscle and cardiac injured muscle two days after injury 100
Figure 4.2. IGF-1Ea and IGF-1R mRNA levels in blood monocytes, spleen monocytes, BMdMs, LPS/IFNγ-polarized BMdMs and IL-4-polarized BMdMs 101
Figure 4.3. *In vitro* bone marrow-derived macrophages characterization 102
Figure 4.4. Assessment of BMdMs transfection efficiency through various techniques 24 hours after transfection 104
Figure 4.5. IGF-1Ea expression levels in transfected BMdMs 105
Figure 4.6. Effects of IGF-1Ea overexpression *in vitro* BMdMs 106
Figure 4.7. Experimental design for *in vivo* IGF-1Ea BMdMs immunotherapy 107
Figure 4.8. Representative flow cytometry plots of GFP+ positive BMdMs cells in skeletal muscle 24 hours after i.v. infusion, 48 hours after CTX injury 109
Figure 4.9. Adoptive immunotherapy of CFSE-labelled BMdMs into CTX injured muscle 24h and 6 days after injury 111
Figure 5.1. Rat neonatal cardiomyocytes transfected with pAAV9.IGF-1Ea vector 116
Figure 5.2. AAV9.IGF-1Ea timecourse of expression in the murine heart after intravenous injection 117
Figure 5.3. IGF-1Ea mRNA levels 28 days after ischemia/reperfusion 118
Figure 5.4. Bioluminescence imaging illustrating the distribution of luciferase at several timepoints after intravenous injection of AAV9.IGF-1Ea 119
Figure 5.5. AAV9.IGF-Ea gene transfer experimental design 120
Figure 5.6. IGF-1Ea gene transfer improves cardiac function and left ventricular dilation 28 days after ischemia reperfusion 121
Figure 5.7. IGF-1Ea gene transfer reduces cardiac damage, improves cardiac motion and reduces dilation after ischemia/reperfusion 122
Figure 5.8. IGF-1Ea gene transfer reduces infarct expansion and myocardial remodeling in AAV9.IGF-1Ea treated mice 124

Figure 5.9. Representative masson trichrome staining sections of the scar region in the four groups 28 days after ischemia/reperfusion 125
Figure 5.10. AAV9.IGF-1Ea gene transfer increases the number of BrdU positive cardiomyocytes 28 after ischemia/reperfusion 126
Figure 5.11. Phospho-H3 immunohistochemistry of I/R and AAV9.IGF-1Ea treated groups, 28 days after ischemia/reperfusion 127
Figure 5.12. αSMA immunohistochemistry and vessel quantification in I/R and AAV9.IGF-1Ea treated mice, 28 days after ischemia/reperfusion 128
Figure 5.13. IGF-1Ea gene transfer activates the Akt signaling pathway 129
Figure 6.1. Masson Trichrome representative staining of WT and IGF-1Ea scars after myocardial infarction. 138

List of tables

Table 1.1. Glycan receptors, co-receptors, tissue specificity, AAVs tropism, preclinical and clinical studies of AAVs 42
Table 2.1. Polymerase chain-reaction conditions for αMHC.IGF-1Ea 53
Table 2.2. Reaction components and thermo cycler conditions for RT-PCR reactions 56
Table 2.3. Components and thermocycler conditions for IGF-1Ea PCR 73
Table 2.4. IGF-1Ea plasmid and pAC-cTNT restriction enzyme digestion protocol 74
Table 2.5. Ligation protocol 74
Table 2.6. GC- rich PCR components 78
Table 2.7. ExoSAP sequencing protocol components 79
Table 3.1. Echocardiographic measurements and analysis performed at 1, 3, 5, 7 and 28 days after MI 86
Table 4.1. Percentage of macrophages CD45, CD11b, F4/80 in several organs 24 hours after i.v infusion 108
Table 5.1. Echocardiographic measurements at 3 and 28 days after I/R 123

Chapter 1 – Introduction

1.1 The heart

The main function of the heart is to pump oxygenated blood to the body and deoxygenated blood to the lungs for oxygenation, maintaining body homeostasis. To achieve this goal, two circulatory systems are required. The systemic circulation facilitates the distribution of nutrients, oxygen (O_2) and water and the pulmonary circulation allows the collection of metabolic waste products such as carbon dioxide (CO_2) and the exchange of gases in the lungs. Inside the lungs, the architecture of alveoli and alveolar capillaries facilitates the exchange of oxygen. Deoxygenated (venous) blood flows through the capillaries in close contact with ventilated alveoli and becomes oxygenated (arterial blood). Blood also serves as a vehicle for cells and molecules (Sedmera et al. 2008 and Aird et al. 2011).

Because of its fundamental role, the heart is the first organ formed in the developing embryo. The developing heart receives cellular contributions from three main sources: the cardiogenic mesoderm, the cardiac neural crest and the epicardium-derived cells (EPDC) (Laugwitz et al. 2008). The primitive heart, originated from the cardiogenic mesoderm, is no more than a linear tube composed of myocardial and endocardial layers. In human heart development, contraction of the heart tube begins at around 3 weeks of development, propelling blood in a peristaltic fashion. Soon after initiation of the heartbeat, the myocardium increases in size and the linear heart tube undergoes a series of transitions, which involves a process of looping, the atria and ventricles begin to form. At this stage, a new vascular system is required to support the oxygen demand (Tomanek et al. 2005). Studies performed in chicken eggs, suggests that cardiac neural crest cells, from the dorsal neural tube, migrate to contribute into vascular smooth muscle cells (VSMCs) to the great arteries and, at the same time, proepicardial precursors contact the surface, to form the epicardium (Manner et al. 1993 and Mikawa et al. 1996). The epicardium, in turn, gives rise to EPDCs, multipotent cardiac progenitors (Wessels et al. 2004) with the potential to differentiate into VSMC (Mikawa et al. 1996), endothelial cells (ECs) (Perez-Pomares et al. 2002), cardiomyocytes (Perez-Pomares et al. 2002), cardiac fibroblasts (CF) (Gittenberger et al. 1998). In the chick embryo, EPDCs may also contribute to AV cushion mesenchyme giving rise to the cardiac valves (Gittenberger et al. 1998 and Manner et al. 1999).

Through various processes involving septation, valve formation, cell differentiation, cell proliferation and epicardium formation, the primitive heart evolves into the adult four-chambered heart (Sedmera et al. 2008).

In the four-chambered heart, deoxygenated blood enters the heart from the inferior and superior *vena cava* to the right atrium. Through the tricuspid valve, blood enters into the right ventricle. Immediately after, the valve closes to prevent blood from flowing back into the right atrium. The right ventricle contracts, sending blood through the pulmonary valve to the lungs. Again, immediately after, the pulmonary valve close to prevent backflow. Blood enters the lung capillaries where carbon dioxide is removed and oxygen is picked up (**Figure 1.1**). Oxygenated blood exits the lungs and is sent back to the heart through the pulmonary veins into the left atrium. The mitral valve closes to prevent backflow of the blood into the left atrium. After this, the left atrium contracts and blood enters the left ventricle. The left ventricle is the thickest of the chamber muscles since it has to produce enough pressure to pump oxygenated blood to the entire body. Following left ventricular contraction, blood passes through the aortic valve to the aorta (Aird et al. 2011). The aorta, the largest and main systemic artery of the body, branches off distributing oxygenated blood to all parts of the body (**Figure 1.1**). At the root of the aorta, just after the aortic valve, two coronary arteries branch off to nurture the heart with oxygenated blood. Over time the coronary arteries that supply your heart muscle with oxygen-rich blood may become narrowed or occluded, leading to a heart attack or myocardial infarction (MI) (Section 1.3).

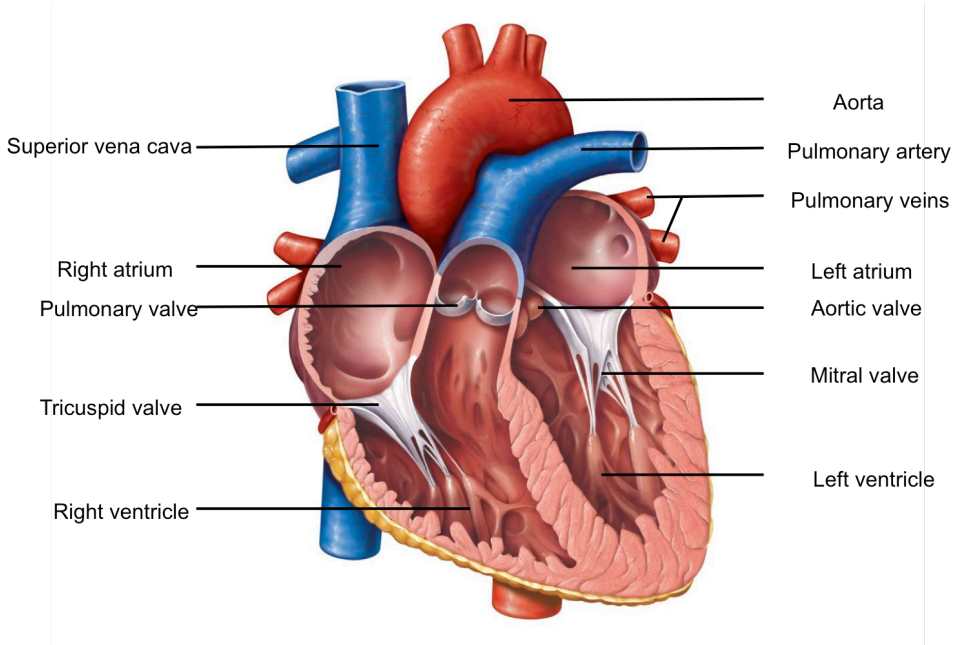


Figure 1.1. Internal view of the 4-chambered healthy heart. The picture depicts right and left atrium, ventricles, the cardiac valves and both systemic (red) and pulmonary circulation (blue). The left ventricle wall thickness allows the heart to gather enough pumping force to propel the blood to the whole organism. Schematics adapted from http://cliparts.co.

1.2 Regeneration of the mammalian heart

Through evolution, higher mammals such as vertebrates have lost the ability to regenerate damaged tissue and appendages, limiting this capacity to organs such as lung or liver. Consequently, scientists have been attempting to answer some fundamental questions for centuries: Why does regeneration occur only in certain organs and not in others? Why was this remarkable ability not preserved or maintained through mammalian natural selection? Is there a regenerative genetic program, hidden deep within the genome? The prevailing view is the heart does not regenerate. Instead, damaged myocardium is replaced by fibrotic scar tissue, leading to a worsening of cardiac function and motion. In the cardiovascular field, three missing hallmarks of regeneration prevent full heart repair: cell replacement, *de novo* vascularisation, and inflammatory resolution.

In other species, however, the heart still preserves this capacity to some degree. Recent research shows that zebrafish are capable of fully regenerating hearts within 2 months after 20% ventricular resection. In this model, regeneration occurs through robust activation and proliferation of cardiomyocytes localised at the leading epicardial edge of the new myocardium (Poss et al. 2002, Poss et al. 2012 and Kikuchi et al. 2010). Interestingly, genetic ablation studies in zebrafish showed reversal of cardiac failure after 60% ablation of total cardiomyocytes. In this model, up-to four-fold increase in cardiomyocyte proliferation was observed compared to resection. Although the mechanism underlying the enhanced regeneration capacity remains unclear, all three missing hallmarks of regeneration to achieve full cardiac repair were achieved: Specific ablation of cardiomyocytes, sparing non-cardiomyocyte tissue, optimally engaged regeneration by promoting cardiomyocyte regeneration, epicardial and endocardial production of retinoic acid, epicardial proliferation, de *novo* vascularisation and macrophage recruitment in absence of a large clot (Wang et al. 2011). Interestingly, the endocardium and epicardium has been proposed to support neovascularisation during zebrafish regeneration. As early as 3-hours after apical heart resection, in zebrafish, robust epicardial and endocardial production of Raldh2 promoted cardiomyocyte proliferation and neovascularisation (Kikuchi et al. 2011)

In summary, injury-induced cardiomyocyte proliferation can overcome scar formation, allowing cardiac muscle to regenerate (Poss et al. 2002, Poss et al. 2012 and Wang et al. 2011). Nonetheless, it is worth mentioning that another teleost animal model, the medaka fish, responded rather differently to cardiac injury. The medaka hearts

displayed an excessive collagen deposition by activated myofibroblasts where existing cardiomyocytes remained steady and no substantial proliferation was observed. Interestingly, Raldh2 gene expression was not found suggesting that the endocardium remained in an inactive state (Ito et al. 2014).

In mammals, the failure of the adult heart to recover from injury has been largely attributed to the ineffective replacement of damaged cardiomyocytes, which withdraw from the cell cycle soon after birth. Cardiac function is maintained through cardiac growth dependent on cellular hypertrophy and proliferation of other cell types acting as a compensatory mechanism. Interestingly, recent studies identified a brief window during the first 7 days of post-natal development, when neonatal mice hearts retains significant regenerative capabilities in response to either resection of the apex or myocardial ischemia by permanent ligation of the left anterior descending artery (Porrello et al. 2011 and Porrello et al. 2012).

Neonatal post-MI mice hearts were characterized by a robust cardiomyocyte proliferation from pre-existing cardiomyocytes and *de novo* formation of large coronary vessels in the infarcted area. Interestingly, not all newly formed cardiomyocytes are derived from pre-existing cardiomyocytes. In fact, neonatal post-MI mouse hearts induced the localized expression of the c-kit and Nkx2.5 expressing cells that contribute to the myogenic and vascular fates (Jesty et al. 2012). Strikingly, fibrotic scar tissue in neonatal mouse hearts is almost completely resolved within 21 days post-MI (Porrello et al. 2011). MI studies on monocyte/macrophage depleted hearts within this brief window during post-natal development indicated that macrophages are essential for *de novo* vascularisation rather than for stimulating fibrosis and scar tissue formation. Interestingly, cardiomyocyte proliferation was not dependent on monocytes/macrophage depletion (Aurora et al. 2014). All these studies indicate that full cardiac repair is achieved when the three missing hallmarks are met, however, the lost of regenerative potential beyond 7 days after birth is yet not fully understood.

1.3 Cardiovascular heart diseases

Cardiovascular heart diseases (CHD), which are mainly disorders of the blood vessels and the heart, are the number one cause of death globally (Go, Alan et al. 2014). In the UK, CHD represent 29% of all deaths and it is estimated that 7 million people are currently suffering from CHD. Among the most common types of cardiovascular diseases, ischemic injury leading to left ventricular dysfunction also known as MI, is the

CHD with the highest death rate (Douglas et al. 2012 and Clyde et al. 2013). From an economic standpoint, the direct and indirect CVD costs are estimated to £19 billion a year to the UK's economy (Cardiovascular disease statistics, BHF, 2014)

1.3.1 Clinical features of myocardial infarction

In pathology, myocardial infarction (MI) is defined as myocardial cell death due to prolonged ischemia (Jaffe et al. 2013). As discussed in Section 1.1, because of the inability of the heart to regenerate, the damaged myocardium becomes necrotic within 2-4 hours after injury. The extent of damage to the myocardium depends both on the collateral circulation of the ischemic zone, which supply the heart with oxygen-rich blood, and the length of time the occlusion is present. The entire process leading to a healed myocardium usually takes at least 5-6 weeks, which by then, if untreated, jeopardises the functionality of the heart (Jaffe et al. 2013 and Clyde et al. 2013). Due to the inability of the heart to regenerated, the healing of the infarcted myocardium, is a process by which the left ventricle undergoes remodeling through a a succession of molecular, cellular, and extracellular changes that culminate in wall thinning, dilation, and fibrosis (Smart et al. 2014). This process is necessary to prevent cardiac rupture, maladaptive remodeling.

In the clinical environment, the symptoms associated with the onset of MI, which results from an imbalance between oxygen supply and demand, are the initial step to recognise and determine if a patient is suffering from a MI event or heart attack. Symptoms typically include chest pain, upper extremity pain, sweating, anxiety and light-headedness. Dyspnoea and fatigue are also observable symptoms of the deficit in oxygen supply as well as the deterioration in heart function (Jaffe et al. 2013). An additional indicator of MI, signalling to clinicians that myocardial injury is present, is the release of cardiac biomarkers into the circulation as a consequence of cardiac injury. The necrosis process discharges specific biomarkers, which are chiefly proteins and peptides from neurohormonal systems, myocardial enzymes and structural proteins. Elevated levels of these biomarkers can be easily detected by performing simple tests to determine their concentration in plasma. Peptides such as BNP (brain natriuretic peptide) and NT-proBNP (pro-brain natriuretic peptide) are associated with ventricular dysfunction. Levels of biomarkers may remain elevated for 2 weeks or more following the onset of myocyte necrosis (Thygesen et al. 2009 and McMurray et al. 2013). These biomarkers have been used in this thesis to evaluate the level of cardiac damage after MI.

1.3.2 Immune system response after myocardial infarction

After MI, the injured myocardium releases inflammatory signals that trigger a battery of cellular processes in order to clean, restore and repair the damaged tissue. The innate immune system is the host's first line of defence against injury and infection. As part of this defence mechanism, myeloid cells such as neutrophils and monocytes are recruited to initiate the inflammatory response, which will lead to a healed myocardium (Nahrendorf et al. 2013). At the site of injury, these two populations release proteolytic enzymes and reactive oxygen species (ROS), which eliminate dead or dying tissue facilitating the repair of the wound (Frangogiannis et al. 2002). Monocytes are primarily produced in the bone marrow from progenitor cells. Upon maturation, monocytes enter the circulation, where they patrol vessels for several days (Auffray et al. 2009 and Skalak et al. 2007). When an injury such as MI occurs, monocytes and neutrophils orchestrate heart's healing process, which in humans, may require up to two weeks (Nahrendorf et al. 2010).

1.3.2.1 Activation of the inflammatory process

Myocardial cell necrosis leads to the release of subcellular components such as mitochondrial membranes, which are capable of triggering the C1, C2, C3 and C4 components of the complement cascade (Pinckard et al. 1975). Complement activation is considered one of the early events triggered by the damaged myocardium with an important and direct role in mediating neutrophil and monocyte recruitment in the injured myocardium, thus initiating the inflammatory process and wound healing (Vakeva et al. 1998). In 1998, Vakeva and collaborators demonstrated that blockade of the complement cascade, by anti-C5 monoclonal antibody, significantly inhibited neutrophil and monocyte infiltration as well as apoptosis and necrosis after MI. Another complement component such as C3b is important for phagocytosis and iC3b is an important ligand for CD11b-mediated neutrophil adherence (Vakeva et al. 1998).

Another key component involved in triggering the inflammatory response are the reactive oxygen species (ROS) generated by neutrophils in the ischaemic myocardium especially after reperfusion, which can directly injure the cell membrane of myocytes and vascular cells (Hori et al. 2009 and Duilio et al. 2001). This process has also been reported to be involved in the activation of inflammatory cascades and cytokine production, which can also trigger the recruitment of neutrophils and monocytes (Dhalla et al. 2000).

1.3.2.2 Neutrophil- and macrophage-mediated inflammatory responses

Akin to an orchestra, inflammation is modulated through control of the timing and pace at which cells are recruited to the injured site. If the rhythm of inflammation is lost due to underlying disease, it may lead to chronic inflammation, considered as unresolved inflammation. Through interactions with chemokine and its receptors expressed by leukocyte subpopulations, the chemokine expression profile in the infarcted myocardium determines the composition of the leukocytic infiltrate. Leukocyte infiltration from blood into the infarcted myocardium requires adhesive interactions with activated vascular endothelial cells involving a family of cell adhesion receptors, the selectins. Neutrophils, first immune cells recruited to the damaged myocardium, represent the primary mechanism for local amplification of the inflammatory process (Jordan et al. 1999 and Frangogiannis et al. 2002). The main function of neutrophils is the clearenace at the injure site through the phagocytosis of dying cells, cellular debris and the reabsorption of the necrotic tissue. These functions are facilitated through at least 3 major mechanisms: (i) ROS release, (ii) release of arachidonic acid metabolites and platelet activating factors, (iii) elastase and protease degranulation (Jordan et al. 1999 and Duilio et al. 2001).

Following the initial burst of neutrophils, other immune cells such as monocytes, macrophages, dendritic cells, lymphocytes and mast cells are also recruited from the bloodstream to the damaged myocardium. In the infarction orchestra, monocytes and macrophages are the major cell types dominating the inflammatory process (Arnold et al. 2007). In this context, macrophages undertake removal of cellular debris and apoptotic neutrophils via phagocytosis; regulate inflammation and protective scar formation. Moreover, macrophages support cell proliferation and re-pattern vascular architecture (Swirski et al. 2013 and Frangogiannis et al. 2014). The participation of macrophages in the body's response to injury is endorsed by their capacity to detect and migrate to sites of tissue damage. To achieve this, macrophages express many chemokine receptors and pattern recognition receptors that enable chemotaxis.

In acute injury, the temporal dynamics of monocytes is controlled by cytokines and chemokines produced during this process (**Figure 1.2**). In mice, from days 1 to 3 after MI, inflammatory Ly-6C^{high} monocytes are recruited *via* the MCP-1/CCR2 chemokine (Uguccioni et al. 1995). From 3 to 5 days, another type of monocyte, Ly-6C^{low} monocytes, are recruited *via* fractalkine/CX3CR1 (Swirski et al. 2013 and Florian et al. 2012). These monocytes may give rise to the inflammatory and reparative macrophage populations,

being temporally regulated by inflammatory macrophages preceding reparative macrophage populations. During the inflammatory phase (**Figure 1.2** and **Figure 1.3**), this first wave of inflammatory monocytes is polarized to inflammatory macrophages and resembles a "demolition crew", removing debris and necrotic cardiomyocytes at the infarct site. Inflammatory macrophages amplify signals such as IL-1β, IL-12 and nitric oxide (NO), phagocytosing cellular debris and releasing chemokines to recruit more inflammatory cells. After the clean-up phase, during the reparative phase (**Figure 1.2**), reparative macrophages support and promote the deposition of new extracellular matrix as a central part of the granulation tissue formed in the wound. In addition, reparative macrophages display an anti-inflammatory profile which promote cell growth and regeneration, as well as serve as mediators on the resolution of the inflammatory process due to high production of IL-10, TGFβ and IGF-1 itself (Danielpour et al. 2006, Frangogiannis et al. 2014 and Bujak et al. 2007). The reparative population further dampens the activity of inflammatory macrophages, assisting progression from the inflammatory to the regenerative phase of repair. Inflammatory macrophages must be tightly regulated since the inflammatory cytokines and ROS species released can directly cause myofibre lysis, exacerbating injury.

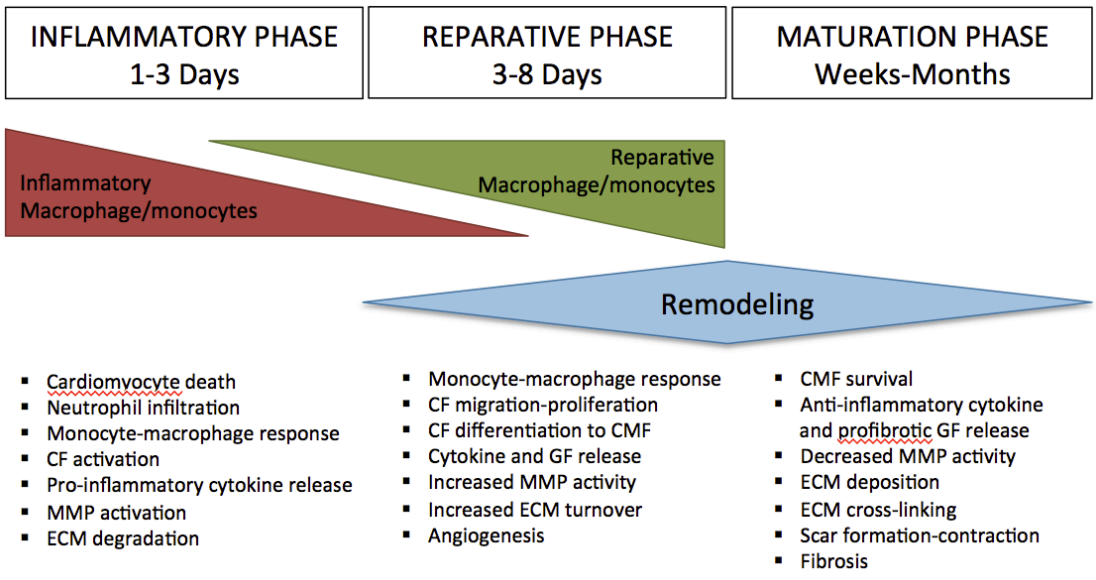


Figure 1.2. Biphasic monocyte/macrophage inflammatory response and remodelling process after myocardial infarction in the mice. CF, cardiac fibroblast; CMF, cardiac myofibroblast; ECM, extracellular matrix; GF, growth factor; MMP, matrix metalloproteinase. Adapted from Nieuwenhoven et al. 2013.

It is important to discuss that the current view on monocyte/macrophage-mediated inflammatory response is still controversial. There is considerable evideance that monocyte subsets and macrophage correspond to each other. However, there is still insufficient knowledge regarding the lineage relationships of monocyte and macrophages after MI (Tacke et al. 2007). Matthias Nahrendorf and colleagues have provided some insights into how this relationship might be (Nahrendorf et al. 2010, Nahrendorf et al. 2013 and Hilgendorf et al. 2014). During myocardial injury, Ly6C^{high} monocytes acquire inflammatory-like macrophage properties. These inflammatory macrophages continue to express Ly-6C, and contribute to inflammation (**Figure 1.3**). Over time, the inflammatory environment changes towards a more reparative environment with a second Ly6C$^{int/low}$ monocytes being recruited. It is still unknown whether macrophages at the reparative phase arise via the differentiation of Ly-6C^{high} monocytes (**Figure 1.3**) and less via differentiation of Ly6C^{low} monocytes or via polarization of inflammatory macrophages to reparative macrophages as suggested by Tonkin et al. 2015.

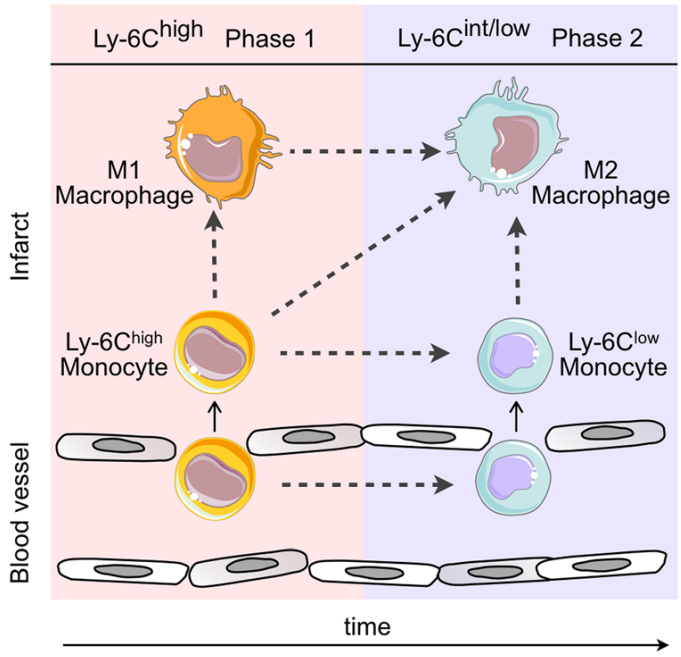


Figure 1.3. Potential lineage relationships of monocytes and macrophages after myocardial infarction. The only lineage relationship which is widely accepted to be happening is the Ly-6C^{high} monocytes contribution to inflammatory Ly6C^{high} macrophages in tissue. The other lineage relationships presented in this figure remain to be experimentally explored in the setting of acute myocardial infarction. Extracted from Nahrendorf et al. 2013.

Furthermore, the resident cardiac tissue macrophages (cTM), which do not rely on the bone marrow for replenishment but rather selfrenewal, from local progenitors or through proliferation cell contribution to wound healing resolution it is still unknown. Pinto and collaborators have provided with new insights on the role of cTM in normal homestatic functions. cTM expression analysis with other adult tissue macrophages exhibit an anti-inflammatory phenotype and the capacity to secrete salutary factors such as IGF-1 (Pinto et al. 2012).

1.3.2.3 Wound healing and heart remodeling

As previously described in Section 1.2, the heart cannot regenerate and therefore other mechanisms are established to preserve, as much as possible, the integrity and stability of the heart. When the inflammatory activity resolves, non-leukocytic cells carry the remodeling process forward in order to replace the missing myocardium with a newly synthesised extracellular collagen matrix (ECCM), the fibrotic scar.

The maturation phase (**Figure 1.2**), following the inflammatory and reparative phase, involves the recruitment and activation of endothelial cells (Zeisberg et al. 2007) and bone marrow cells (Mollmann et al. 2006). Additionally, interstitial and vascular fibroblasts trans-differentiate into cardiac fibroblasts. Recent studies indicated that the conversion from fibroblast to myofibroblast requires the activation of TGF-β (Frangogiannis et al. 2014, Nieuwenhoven et al. 2013 and Bujak et al. 2007) and the removal of pro-inflammatory mediators such as IL-1β**.** These cardiac fibroblasts deposit large amounts of collagen, which preserves the structural and functional integrity of the ventricle, strengthening the emerging scar (Jugdutt et al. 2003).

At histological level, in mice and humans these changes may take months. After MI, the main feature is a thinning in the left ventricular wall accompanied with expansion of the infarct zone. Consequently, the mechanisms previously described induce alterations in the left ventricule (LV) function, filling pressure, wall stress, shape and volume and generates a process called adverse remodeling. These adaptive changes may preserve structural integrity but may also lead over time to infarct expansion, left ventricular dilation, and left ventricular wall thinning and in some cause to infarct rupture and death also know as myocardial infarction-derived heart failure (Van der Laan et al. 2012). Conversely, therapies are designed to provide sufficient healing in order to preserve left ventricular geometry and to prevent heart failure (Nahrendorf et al. 2010).

1.3.3 Current treatments after myocardial infarction-derived heart failure

Over the past decades, treatment for MI has made significant progress; unfortunately, MI remains an unsolved therapeutic target. Current treatments for MI embrace all aspects of the disease process, from changes in lifestyle to surgical intervention. Although heart transplant is still considered today, the number of patients that undergo cardiac replacement is limited mainly due to the low availability of organ donors (McMurray et al. 2013).

When coronary arteries become occluded or narrowed due to coronary heart diseases, invasive interventional strategies are applied in order to improve or restore blood supply. Following the removal of the obstruction, several pharmacological strategies for the treatment of ischemic disease are facilitated to reduce or block cardiac remodeling and prevent heart failure (Minicucci et al. 2011). To boost the reparative capacity of the heart, pharmacological strategies could potentially be combined with cell-based therapies (Ptaszek et al. 2012) and gene transfer therapies (Fang et al. 2013, Kaspar et al. 2005 and Muller et al. 2006).

In order to design successful therapies to ameliorate the adverse effects of heart remodeling, further understanding of the current available treatments is required. A more detailed overview of the main strategies for the treatment of the post-MI condition is presented in the following sections.

1.3.3.1 Interventional cardiology after myocardial infarction

Current interventions for ischemic injury are targeted at physical removal of the obstructions of the heart vessels to restore blood flow to ischemic tissue. These interventions fall into two main categories: coronary artery bypass graft (CABG) surgery and percutaneous coronary intervention (PCI) also called coronary angioplasty (Deb et al. 2013). However, these interventions will only transiently eliminate the symptoms especially if the obstruction is caused by the rupture of an atherosclerotic plaque. The reperfusion that comes after removing the obstruction has the potential to rescue myocardium at-risk, however, for the myocardium that is unable to survive the injury, reperfusion is of little help. In fact, reperfusion of the tissue leads to increased ROS production, which potentially causes adverse effects on the surviving myocardium (Zweier et al. 1988). Research is now focused on promoting the regeneration of the myocardium that is unable to survive through cell- or gene-based approaches which

aims to promote the reparative/regenerative abilities of the heart. These approaches are further discussed in Section 1.4.

1.3.3.2 Pharmacological treatment after myocardial infarction

Several drugs have shown to be the best approach to ameliorate the adverse effects of MI-derived heart failure. The drugs are designed to target the neurohormonal pathways, in particular the pharmacological inhibition of the renin-angiotensin-aldosterone and sympathetic nervous systems. The main drugs are angiotensin-converting-enzyme (ACE) inhibitors and β-blockers which have been demonstrated to prevent left ventricular remodeling and reduce mortality after MI.

ACE inhibitors: ACE inhibitors are considered a first-line therapy for all patients after MI. ACE drugs inhibit the angiotensin-converting enzyme, an important component of the renin-angiotensin aldosterone system. These drugs cause relaxation of blood vessels, as well as decrease blood leading to a decrease in blood pressure and decreased oxygen demand from the heart. ACE inhibitors such as trandolapril (Torp-pedersen et al. 1994), zofenopril (Ambrosioni et al. 1995) and ramipril (Cleland et al. 1993, Pfeffer et al. 1992) have been demonstrated to improve the outcome of patients after MI. The Survival And Ventricular Enlargement (SAVE) trial was the first to report the beneficial effect of the ACE inhibitor captopril on patients after MI (Pfeffer et al. 1992). Results showed that administration of captopril for two years resulted in a 27% reduction in mortality and a 25% reduction in re-infarction rate in patients with left ventricular dysfunction.

β-blockers: β-blockers block the action of endogenous catecholamines (adrenaline) and noradrenaline on the adrenergic beta-receptors, of the sympathetic nervous system. The effect of beta-blockers in the heart is to reduce the heart rate besides a decrease in renin secretion by the kidney, which in turn reduced the heart oxygen demand by lowering extracellular volume and increasing the oxygen-carrying capacity of the blood. The Carvedilol Post-Infarct Survival Control in LV dysfunction (CAPRICORN) trial tested the effects of beta-blocker agents in patients with left ventricular dysfunction after MI and <40% ejection fraction. In this trial, the administration of carvedilol was associated with a 23% decrease in mortality and a 40% reduction in re-infarction rate after 1.3 years (Harris et al. 1992).

Other pharmacological treatments using angiotensin-II receptor blockers (ARB) and aldosterone have shown similar results. Additionally, no differences in mortality or

morbidity were found with these treatments when compared with ACE inhibitors. Thus, both drugs can be used as alternatives to ACE inhibitors.

All the drugs described here improve the course of heart failure after MI, exerting a positive effect on the outcome of the patient as well as mortality and hospitalisation times. Besides the administration of these drugs, diuretics are also given, to relieve the symptoms and signs of congestion (Minicucci et al. 2011).

1.3.3.3 Other post-MI treatments: implantable medical devices

After MI, electrical coupling in the heart becomes compromised at the fibrotic area, which may lead to lethal arrhythmias and potentially sudden death. Implantable medical devices are designed to prevent sudden cardiac death. Implantable medical devices are classified according to their function as (i) rhythm control and (ii) to support the circulation (American Heart association website).

For rhythm control, the implantable cardioverter-defibrillator or ICD device is commonly used and recommended to patients who develop sustained ventricular tachycardia (VT) or ventricular fibrillation (VF) 48h after MI. The device continuously monitors the rhythms of the heart and delivers electrical countershocks to restore normal rhythm (American Heart association website). Another rhythm control device is the well-known pacemaker. Similar to the cardioverter-defibrillator, the pacemaker controls heart rhythm. The pacemaker, however, is recommended when the heart's 'natural pacemaker' is defective, causing the heart to beat either too slow, too fast, or irregularly (American Heart association website). The other most common ICDs are those that support circulation, the so-called left ventricular assist devices or LVAD. In stages of advanced heart failure, this device maintains the pumping ability of the heart when the left ventricle is no longer able to perform such work. LVADs are also known as 'bridge to transplant' devices, mainly because this mechanical pump is implanted in patients waiting for a heart transplant (Frazier et al. 1994 and Birks et al. 2005).

Unfortunately, interventional and pharmacological strategies only boost and reduce the worsening of heart's condition, however, these strategies do not boost the intrinsic capacity of the heart to regenerate and repair itself. Therefore, new therapeutic strategies are being researched to potentially work in synergy with pharmacological strategies to promote heart's own capacity to regenerate and repair itself.

1.4 Therapeutic approaches for myocardial infarction injury

Over the past decade, the use of cellular therapy has emerged as a promising option to treat patients after MI. In order to improve cardiac function in the injured myocardium, two main strategies can be followed: delivering cells from either heterologous or autologous sources to promote repair/regeneration or stimulating the endogenous regenerative capacity of the heart.

1.4.1 Cell-based therapeutic approaches

One of the first cell-based attempts that aimed to achieve improvement of cardiac function through cardiac regeneration involved the use of skeletal myoblasts (Menasche et al. 2008). Although these cells do not have a cardiac origin, the transplantation of these donor cells was reported to improve cardiac functionality after MI. While initial results were promising, further tests carried out shortly after in animal models and in human trials raised concerns and doubts about cell engraftment. The Myoblast Autologous Grafting in Ischemic Cardiomyopathy (MAGIC) trial showed that these cells failed to improve cardiac functionality and ventricular contractile function. Interestingly, skeletal myoblasts did indeed engraft, but instead of differentiating into cardiomyocytes, they became skeletal myocytes. Furthermore, the engrafted skeletal myocytes were not electrically coupled with the healthy myocardium (Menasche et al. 2008).

In 2011, bone marrow-derived cells (BMCs) began to be considered the cell type of choice for cell-based therapies (Chavakis et al. 2010). BMCs have the potential to differentiate into diverse phenotypes. Secondly, BMCs can be easily procured and third, these cells do not require extensive culture techniques (Birks et al. 2005). The work from Piero Anversa and colleagues suggested that stem cells found in the bone marrow could be differentiated into functional cardiomyocytes (Orlic et al. 2001 and Quaini et al. 2002). However, in 2004, the reproducibility of Anversa's experiments was questioned when Charles Murry and collaborators found that, in fact, haemotopoietic stem cells do not transdifferentiate into cardiac myocytes after MI (Sil et al. 2004). Later on, Van Berlo and collaborators found that the endogenous cardiac stem cells (eCSCs) c-kit^{pos} were indeed capable of differentiating into new cardiomyocytes at a rate of approximately 0.03%. These authors concluded that this percentage could not substantially contribute to improve cardiac function to a significant level (Van Berlo et al. 2014).

Many preclinical and clinical trials carried out after these discoveries also produced controversial and conflicting results. Preclinical tests in dogs (Mathieu et al. 2009) and rats (Kim et al. 1999) reported that BMC transplantation improved myocardial function and angiogenesis, and led to a reduction in plasma levels of Nppb (N-terminal probrain natriuretic peptide). In contrast to these finding, studies in sheep (Bel et al. 2003) and pigs (Waksman et al. 2004), reported that BMC therapy produced no improvement in left ventricular function. The reason for these differences are not obvious, but the hypothesis put forward was that perhaps the technique employed to cause the infarction, the specie selected for the study and the site of cell delivery could have been contributing factors for such disappointing results (Bel et al. 2003).

At the clinical level, the use of BMC to treat chronic MI has provided modest benefit in most but not all studies. Unfortunately, the disparity between results has sent researchers back to the bench to gain a clearer understanding on the exact mechanism of action of BMCs. Other aspects that are being considered include the type of donor stem cell, the enhancement of homing capacities, dose and route of administration and improvement of long-term engraftment (Bolli et al. 2001 and Ptaszek et al. 2012). Hypothetically, if the damaged myocardium is replenished, there is no guarantee that electrical coupling will be achieved, thus further studies should tackle that aspect as well.

The clinical trials with the most promising results to date using cell-based therapy for the treatment of MI are the REPAIR-AMI and BALANCE studies. In 2006, the REPAIR-AMI study, the first of this kind, quantified global improvement in left ventricular ejection fraction. Two hundred and four patients were randomized to receive an intracoronary injection of $2.36x10^7$ bone marrow-derived stem cells 3 to 7 days after MI. After 1 year, cell-transplanted patients showed a reduction in death and recurrence of MI (Gersh et al. 2007). The BALANCE study in 2009, following a similar approach as the REPAIR-AMI study, investigated the quantitative improvement in ventricular function and contractility of patients treated with autologous bone marrow cells after MI. From 124 patients, 62 underwent intracoronary bone marrow cell infusion 5 to 9 days after MI. In this case, $6.1\pm3.9 \times 10^7$ bone marrow-derived cells were infused directly into the infarct area *via* an angioplasty balloon catheter. Three months after BMC therapy, patients displayed an improvement in cardiac function and in the stroke volume index. The study also showed a reduction in mortality only in the BMC-treated group (Yousef et al. 2009).

In conclusion, the heart is a remarkable organ, made of various cell types with different functionality. Because of this complexity, a single approach to promote cardiac regeneration has proved to be challenging; therefore, the ideal cardiac regenerative therapy would comprise a combination of key cells working in synergy with paracrine factors to create a permissive environment for the heart to heal or even regenerate. Many other cell types, including mesenchymal stem cells, CD34+/CD133+ cells, adipose-derived cells, iPS cell-derived cardiomyocytes and cardiac-derived cells, are also currently being used in both preclinical and clinical studies with great potential (Ptaszek et al. 2012). Future regenerative therapies will need to combine aspects of stem cell biology, tissue engineering, modulation of the inflammatory response, organ/tissue transplantation, personalised medicine, pharmacological treatments and medical devices.

1.4.1.1 Immunological therapies

The use of macrophages as cell-based therapy to deliver genes to diseased tissues have been studied for many years (Fidler et al. 1994 and Wang et al. 2008). The aim of these studies was to assess the ability of macrophages to "home" to injured sites after local or systemic infusion into humans (Ben-Efrain et al. 1994 and Wiltrout et al. 1983) and mice (Burke et al. 2002). This new interest resides in the fact that only a few current forms of systemic gene delivery, either viral or non-viral, have been shown to penetrate far from the vasculature into damaged tissues, particularly as the vasculature is often disrupted in such tissues. Thus, exploiting the natural tendency of macrophages to migrate into such sites in response to the release of cytokines/chemokines may be key for a new cell-mediated gene delivery system, in other words, monocyte/macrophage adoptive immunotherapy.

It would seem logical to assume that since monocytes, not macrophages, are taken up across the endothelium into normal and pathological tissues, monocytes would prove more effective in "homing" to such tissues (Burke at al.2002). For instance, work in murine models has indicated that mature *ex vivo*-manipulated monocytes are capable of migrating into tissues, where they undergo further maturation and cell division (Kennedy et al. 1998). Although studies in murine models indicated that monocytes are suitable vectors for cell-therapy, the technical difficulties regarding monocyte yield, cell number, isolation procedures, cell culture and monocyte activation, makes macrophages a much better adoptive immunotherapeutic alternative. For these reasons, greater success has been achieved using local administration of macrophages. For example,

Chokri and co-workers reported that greater than 70% of locally-injected LPS/TNFα macrophages homed to the tumour site in mice carrying a subcutaneous melanoma (Chokri et al. 1990). In another study, infusing macrophages, adeno-transfected to express IL-4, to inflamed glomeruli resulted in a remarkable 75% reduction in albuminuria, a sensitive indicator of glomerular damage (Kluth et al. 2000 and Kluth et al. 2001). Other approaches have considered the use of macrophages as delivery vehicles for therapeutic genes.

Macrophages manipulated *ex vivo* have also been shown to be capable of homing to a dystrophic muscle after intravenous (i.v.) administration. The retention of macrophages in these tissues produced a long-term engraftment of up to 2 months (Parrish et al. 1996). As described above, one of the main potential advantages of macrophage adoptive transfer is the ability to circulate the body after i.v injection and target multiple diseased sites, for example, tumour metastases. Unfortunately, these studies have also shown that the majority of the systemically-administered macrophages become trapped in organs such as the lungs, liver and spleen (Burke et al. 2002, Kennedy et al. 1998 and Chokri et al. 1992). Interestingly, better success has been achieved when studying the homing competencies of activated macrophages to atherosclerotic plaques in apolipoprotein E-deficient mice (Patel et al. 1998). Activated macrophages loaded with fluorescent microspheres were used to test new monoclonal antibodies to block macrophage cell adhesion to the atherosclerotic plaque.

Novel approaches are providing new insights suggesting that it might be possible to target macrophages to certain organs or injured sites by specific pre-treatments or even by engineering them to express particular cell surface-expressed proteins. Among these approaches, researchers have engineered *ex vivo*-manipulated macrophages to express certain cytokines or to carry DNA constructs as well as studying trafficking upon injection into a host organism (Fidler et al. 1974 and Andreesen et al. 1998). In another very interesting study, oncolytic viruses were delivered by infiltrating macrophages, which abolished tumor regrowth and extended the survival of tumour-bearing mice (Muthana et. al 2011 and Muthana et. al 2013). This was achieved by cotranducing the oncolytic virus genome with an hypoxia-regulated construct. Following systemic injection, contransduced macrophages reached the area of extreme hypoxia inside the tumour, triggering activation of the hypoxia-regulated element (HRE) and activating the replication of the adenovirus.

To conclude, the data on macrophage adoptive transfer therapy also suggested that may be a relatively risk-free procedure (Fidler et al. 1974 and Andreseen et al. 1998). Therefore, understanding how these cells home is essential for future monocytes/macrophages gene therapies to treat specific inflammatory-driven diseases. In this thesis, Chapter 4 is centred on a series of experiments to determine whether the injury-homing capacity of macrophages can be used to deliver immunomodulatory payloads to the site of injury, with the potential to augment tissue repair and regeneration.

1.4.2 Gene-based therapeutic approaches

Gene therapy is an experimental technique based on the transfer of exogenous nucleic acids to treat or prevent diseases. Such nucleic acids include DNA, mRNA, small interfering RNA (siRNA), microRNA (miRNA) and antisense oligonucleotides (Wolfram et al. 2013). Successful gene therapy does not imply complete gene transfer to all the target cells, rather the transduction of sufficient cells to trigger the desired effect. So far, several gene delivery methods have been developed and tested using non-viral and viral approaches for the treatment of myocardial infarction.

In the cardiac field, Lin and colleagues were one of the first to achieve non-viral gene transfer in adult rat cardiac myocytes. Their approach was to directly inject purified plasmid DNA encoding the β-galactasidose gene into the left ventricular wall. In the study, gene transfer was proven to be successful since cardiac cells started expressing the β-galactasidose gene after 3 days; however, the effect was very much localised to the area of delivery (Lin et al. 1990). A similar study performed in rats, also achieved certain level of gene transfer by directly injecting a luciferase plasmid into the damaged myocardium after ischemia/reperfusion injury (Prentice et al. 1996). Notably, fibrosis and inflammation were observed at the area along the track of the needle (Lin et al. 1990 and Prentice et al. 1996). The conclusion from these studies was that intra-myocardial naked DNA injections were very inefficient with poor delivery and retention, mainly because only a small fraction of target cells expressed the reporter gene after injection. Recent advances in the bioengineering and nanotechnology field have yielded a whole new world of biomaterials, including new polymers (Pack et al. 2005), lipid-based vectors (Semple et al. 2010 and Love et al. 2010) and nanoparticles (Davis et al. 2009), which, in theory, would bring therapeutic nucleic acids to their sites of action.

Viral approaches, on the other hand, have evolved very rapidly, and have been shown to deliver genes much more efficiently into mammalian cells than *via* naked DNA. In fact,

70% of all gene therapy clinical trials are viral-based, using modified viruses such as retroviruses, lentiviruses, adenoviruses (Ads) and adeno-associated viruses (AAVs)(Yin et al. 2014). Over the years, there has been a shifting trend towards Ads and AAV gene therapy, primarily due to the advantages regarding efficiency and efficacy of gene transduction.

1.4.2.1 Viral vectors for cardiac transfer

Retroviruses poorly transduce somatic cells, as they require active cell division for integration. Lentivirus, on the other hand, does not require active cell division to infect cells, however, this type of virus has very low transduction efficiency and moderate success has been achieved predominantly through intramyocardial injection (Nalinda et al. 2012). Ads and AAVs have drawn much more attention over the years since their main advantage is the ability to infect non-diving cells with reasonable efficiency. Although all viral vectors trigger an immune response to some degree, thereby limiting efficiency to a period of a few days to weeks, AAVs are much less immunogenic. This feature together with the fact that AAV gene expression last much longer than equivalent Ad infection, has positioned AAVs as the vector of choice for cardiac gene transfer (Kaspar et al. 2005, Muller et al. 2006 and Walker et al. 2009).

The CUPID trial (Calcium Upregulation by Percutaneous Administration of Gene Therapy in Cardiac Disease) was the first clinical application of AAV vectors for cardiac transfer. In this study, Roger Hajjar and colleagues demonstrated the safety and efficacy of AAV1-SERCA2 delivery in a randomized double blind, placebo controlled, phase 2 study in patients with advanced heart failure (Giacca et al. 2011 and Jessup et al. 2011). Thirty-nine CUPID trial patients were randomized into four groups and treated with 3 doses of AAV1-SERCA2a, low- ($6x10^{11}$), mid- ($3x10^{12}$), high-dose ($1x10^{13}$) and placebo. For these study, seven efficacy parameters were assessed in 5 domains: symptoms, functional status, biomarkers, left ventricular function and remodeling, and clinical outcomes. Six months after gene transfer, both LV end-systolic volume and LV end-diastolic volume were improved when compared with the placebo group, however, improvement in the ejection fraction was not therapeutically relevant (Giacca et al. 2011 and Jessup et al. 2011). Interestingly, in the CUPID study, patients were pre-screened for neutralizing antibodies against the AAV1 in order to find a viable population for the study.

Gene and cell therapy has produced promising results in both preclinical and clinical settings for the treatment of cardiovascular diseases. Nevertheless, safety and possible off-target effects of each of these approaches must be carefully established such that patient welfare and health is prioritized.

1.4.2.2 Adeno-associated virus biology

Adeno-associated virus belongs to the *Parvoviridae* family. This family has evolved in such a manner that in nature, AAV infection is dependent on a helper virus (Berns et al. 1996). The most common helper viruses are the well-known Ad and herpes simplex virus (HSV). Wild-type AAV genomes are very similar to Ad; in fact, AAVs may have evolved from Ad. The genome of AAV has very limited coding capacity, and therefore it relies entirely on the helper virus to replicate and spread. AAV viruses have not yet been associated with any human disease. In humans, in the absence of the helper virus, AAV remains latent inside the host cell. If the helper virus is present, wild-type AAV tends to integrate into a specific locus on chromosome 19 (Kotin et al. 1992). The main difference between Ads and AAVs is related to the genome size and gene types. Ad genomes are linear, double-stranded DNA of approximately 36 Kb. The AAV genome is a single-stranded DNA of approximately 4.7 Kb. The key feature of AAV genomes is the presence of inverted terminal repeats (ITR). The ITRs form T-shaped, base-paired hairpin structures, which promotes replication and facilitates packing (Figure 1.4A and Figure 1.4C).

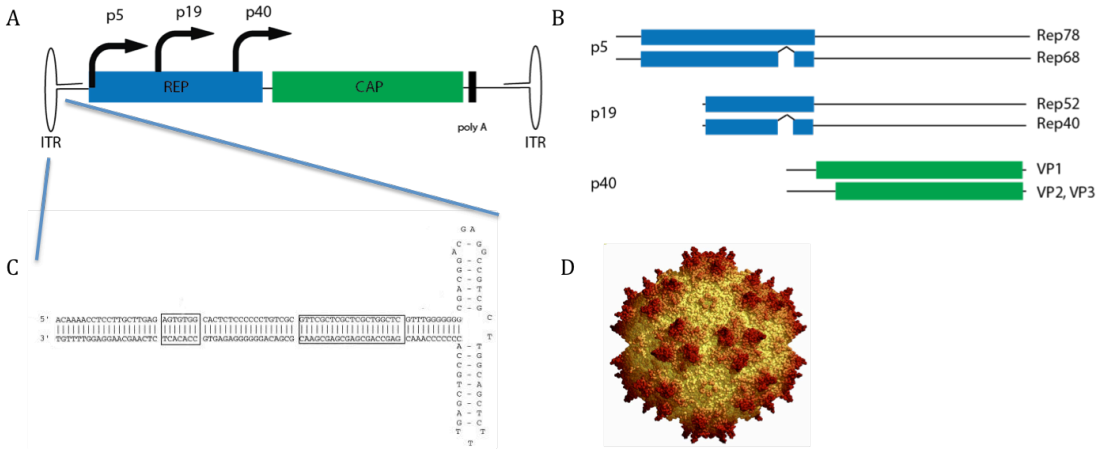


Figure 1.4. Basic structure of a wild-type adeno-associated viral genome. (A) Three viral promoter, p5, p19, p40, controls the transctiption of the two genes REP and CAP. (B) Schematic diagram of the 7 basic protein expression cassette. (C) DNA sequence of the inverted terminal repeats flanking the AAV genome. (D) AAV capsid structure from http://www.rcsb.org/pdb/home/home.do

The AAV genome is comprised of two genes, rep and cap, which encode for four non-structural proteins required for replication (Rep78, Rep68, Rep52 and Rep40) and three structural proteins that constitute the capsid (VP1, VP2, VP3). Three viral promoters, p5, p19 and p40, regulate expression of these two genes (Walker et al. 2009)(**Figure 1.4B**).

Any viral gene-based therapy is founded on the deletion of the rep and cap genes and the incorporation of therapeutic genes. Because the rep and cap genes are removed, integration into the host genome does not occur and the AAV genome remains in an "episomal" manner; however, random integration may occur (Qiu et al. 2008). Wild-type AAV genomes are encapsulated inside an icosahedral particle of roughly 20 nm in diameter made of the three capsid protein VP1, VP2, VP3 in a 1:1:10 ratio. Similar to all viruses, docking of the virion at the surface receptor is necessary for proper infection. VP1, VP2 and VP3 are responsible of such binding (Walker et al. 2009). AAV internalization is a process dependent on binding to a primary receptor and interactions with co-receptors, which will induce AAV internalization *via* clathrin-dependent endocytosis. At the gene level, the capsid genes have hyper-variable regions, which are susceptible to mutations and recombination, thus conditioning AAV tropism to the ability of AAV capsids to bind different cell surface glycans of the target cell (Walker et al. 2009 and Gao et al. 2003)(**Table 1.1**). Diverse tissue tropism determined by the capsid serotype, the lack of pathogenicity and the persistence of viral expression have increased the potential of AAV as a delivery vehicle for gene therapy applications. Indeed, more than 12 human serotypes and 100 nonhuman primate serotypes have been discovered to date. A summary of the main AAV applications can be found in **Table 1.1**. In this thesis, Chapter 5 is focused on a set of experiments to determine whether the use of a particular serotype of adeno-associated virus can efficiently deliver and transfer a therapeutic gene into the heart after MI.

1.4.2.2.1 AAV neutralizing antibodies

In preclinical studies, AAVs have proven to be a very promising tool for delivering therapeutic genes for a myriad of diseases. However, a major concern regarding the use of AAVs for human treatment of diseases is the presence of neutralizing antibodies (Nab) for most of the AAV serotypes. Several studies have revealed that approximately 80% of the population is seropositive for anti-AAV antibodies (Calcedo et al. 2009). Nab can be found against serotypes 1, 2, 3 and 5, in 60% of the population at age 10, which will generally persist into adulthood (Walker et al. 2009). In some cases, a serum dilution of neutralizing antibodies 1/60 can causes 100% transduction inhibition

(Halber et al. 2015). Clinical studies are currently prescreening patients for neutralizing AAV antibodies in order to achieve more efficient AAV approaches.

1.4.2.2.2 Production of recombinant AAVs

For preclinical studies, AAVs are produced by a classic triple transfection of human embryonic kidney cells (HEK293) by three plasmids: AAV cis-plasmid encoding the gene of interest; AAV trans-plasmid containing AAV rep and cap genes; and adenovirus helper plasmid, pDF6. The isolation protocol for the AAV particles differs between laboratories; however, in general, the culture medium containing the vector particles is collected, concentrated using tangential flow filtration, purified by iodixanol gradient ultracentrifugation, followed by further concentration and buffer exchange (Penn Vector Core. University of Pennsylvania website).

Serotype	Receptor	Tissue Organ	Preclinical studies in small animal models	Preclinical studies in large animal models	Clinical studies
AAV 1 (non human primates)[5, 11]	α2-3/ α2-4 N linked SA	Heart Liver Lung Brain Muscle	Mouse[21] , Rat[22] Mouse[25] Mouse[23] Mouse[13] Mouse[24,50]	Pig[44], Sheep[43] Ferret, Pig[45], NHP[46] Cat[41] NHP [42] Rabbit[47], Cat[48], NHP[49], dog[50]	Heart failure (CUPID trial)[55,56] A1ATD[26], LGMD2D[27], LPLD[28]
AAV2 (humans)[5, 11]	HSPG, FGFR1, HGFR, integrins, 37/67 KDa LamR	Brain Eye Heart Joint Liver Lung Muscle	Mouse[13], Rat[1], Mouse[29], Rat[30] Hamster[34], Rat[33],Mouse[2] Mouse[30], Rat[31] Mouse[35,86], Rat[36] Mouse[37] Mouse[38], Rat[39]	Cat[41], NHP[16,77] Dog[69], NHP[78,79] Pig[70] Rabbit[71], horse[72] Dog[73], NHP[80] Rabbit[74], NHP[75] Dog[81], NHP[82]	Alzheimer[51], Batten[52], Canavan[53], Parkinson[54] Inflammatory arthritis[55] CF[55], A1ATD[56], Hemophilia B[57]
AAV3[5]	HSPG, 37/67KDa LamR	Human liver cancer cells			
AAV4 (nonhuman primates)[5]	α2-3 O linked SA	Eye	Rat[40]	Dog[40], NHP[40]	Blindness (Rpe65 mutations)
AAV5 (humans)[5,11]	α2-3 N linked SA, PDGFR	Brain Eye Joint Heart Liver Lung	Mouse[62] , Rat Mouse, Rat[63] Mouse[64] and Rat[65] Mouse[12] Mouse[66] Mouse[67] and Rat[68]	NHP[83] NHP[78,79] NHP[85] NHP[84]	AIP (Phase I completed)
AAV6 (humans)[5, 11]	HSPG, α2-3/ α2-4 N linked SA	Heart Liver Muscle	Rats[7,10] Mouse [12] Mouse[86] Mouse[20]	Dog[87] Dog[86] Dog[84]	
AAV7 (nonhuman primates)[5]	Not determined	Liver	Mouse[89]	NHP[16]	
AAV8 (nonhuman primates)[5, 11]	37/67 KDa LamR	Brain Heart Liver Muscle Pancreas	Mouse[91], Rat[92] Mouse[19], Hamster[19] Mouse[86] Mouse[19], Hamster[19] Mouse[95] , Hamster[96]	 Dog[86], NHP[16] Dog[97], NHP[98]	Hemophilia B[90]
AAV9 (humans)[5]	Galactose, 37/67 KDa LamR	Brain Heart Liver Lung Muscle	Mouse[9,18, 93], Rat[94] Mouse[3,6,8 ,12,15] Rat[10] Mouse[86] Mouse[14] Mouse[99]	Cat[100] Pig[4] Dog[101] Dog[86] Dog[17]	Spinal Muscular Atrophy type 1 (recruiting-Phase 1) Pompe disease (in process but not recruiting – Phase 1)
AAVrh10 (nonhuman primates)		Brain Lung	Mouse[60] and Rat[60] Mouse[61]		Late Infantile Neuronal Ceroid Lipofuscinosis (recruiting – Phase 1)
AAV11[5]					
AAV12 (nonhuman primates)		Muscle Salivary lands	Mouse[59] Mouse[59]		"nasal vaccine"

Table 1.1. Glycan receptors, co-receptors, tissue specificity, AAV tropism, preclinical and clinical studies of AAVs. HSPG, Heparan Sulfate Proteoglycan; α2-4 N linked SA, α2-4 N-linked sialic acid; PDGFR, Platelet-derived growth factor receptor; FGFR1, fibroblast growth factor receptor 1; HGFR, hepatocyte growth factor receptor; 37/67 KDa LamR, 37/67 KDa Laminin receptor. A1ATD a-1 antitrypsin defi ciency, DMD Duchenne muscular dystrophy, LCA Leber

congenital amaurosis, LGMD2D limb-girdle muscular dystrophy type 2D, CF cystic fibrosis, LPLD lipoprotein lipase defi ciency, NHP nonhuman primate; AIP, Acute Intermittent Pophyria. NHP, nonhuman primates. Modified from Walker et al.2009. Information about AAV use on clinical trials can be found at: https://clinicaltrials.gov

1.5 The Insulin-like growth factor family

The insulin growth factor family consists of Insulin-like Growth Factor-1 (IGF-1), Insulin-like Growth Factor-2 (IGF-2), cell surface receptors for both peptides (IGF-1R and IGF-2R) and Insulin Growth Factor-Binding Proteins (IGFBPs).

Insulin-like Growth Factor-1 (IGF-1) is a potent peptide factor involved in a broad range of tissue processes including cell growth and survival, proliferation, differentiation and metabolism, but the molecular basis of these diverse functions is not well understood. Insulin-like Growth Factor-2 (IGF-2), plays a key role in mammalian growth, influencing foetal cell division and differentiation and possibly metabolic regulation in contrast to Insulin-like growth factor 1, which is a major growth factor in adults (Rotwin et al. 1986 and Laron et al. 2001).

1.5.1 Insulin-like growth factor 1 structure and post-translational modifications

The IGF-1 gene spans over 70 Kb of genomic DNA distributed over six exons and five introns (Rotwin et al. 1986) as shown in **Figure 1.5**. IGF-1 is a multi-functional protein due to the fact that alternative splicing generates multiple precursor proteins with N- and C-terminal variability. The diversity of IGF-1 actions mainly derives from the existence of multiple transcription start sites located at exons 1 and 2. Transcripts initiated at exon 1 are spliced to produce an mRNA including exon 1 but not exon 2 (Class I IGF-1), whereas transcription initiated at exon 2 produce transcripts with exon 2, lacking exon 1 (Class II IGF-1) (Rotwin et al. 1986). Interestingly, class II IGF-1 knockout mice have shown that exon 2 deletion is not crucial in normal growth processes, due to compensatory up-regulation of class I transcripts (Temmerman et al. 2010). More complexity is added as the transcription of IGF-1 can also be initiated from alternative promoters, which enable them to initiate the IGF-1 transcription in a mutually exclusive manner (Adamo et al. 1991 and Simmons et al. 1993). In addition, alternative splicing at the 3' end adds a higher level of complexity in the structure and processing of the IGF-1 gene itself, generating carboxy-terminal extension-peptides, or E-peptides. Two main E-peptides can be generated in this process: (i) when exon 4 is spliced to exon 6 (exon 5 skipped), the translation process will add 19 amino acids to

the common 16 amino acids thus generating a 35 amino acid-long E-peptide, also called Ea and, (ii) when exons 1 to 6 are included in the mRNA transcript a second E-peptide is generated called Eb or mechano growth factor (MGF)(Bell et al. 1986 and Jansen et al. 1983)(**Figure 1.5**).

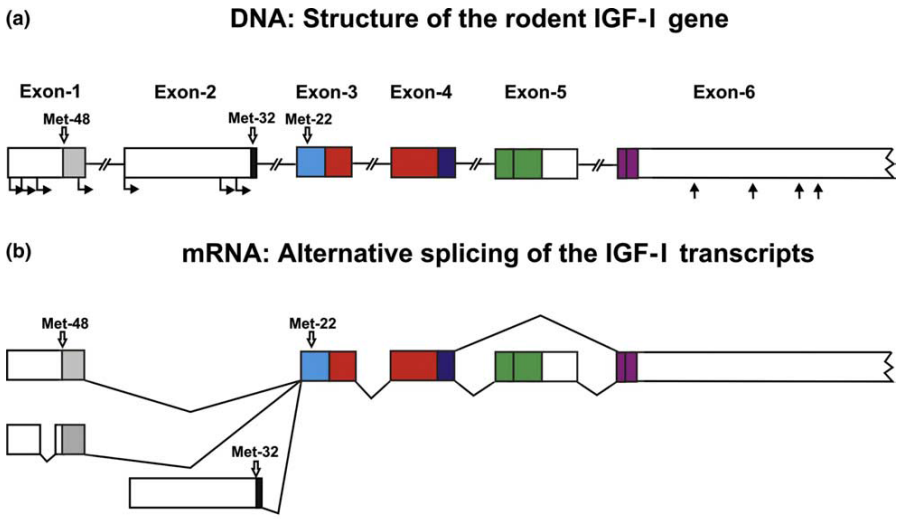


Figure 1.5. Structure of the rodent IGF-1 gene. (A) Multiple transcription sites in exon 1 and 2 (horitzontal arrows). Translation ignition codons (Met) are located in positions, -48 (exon 1), -32 (exon 2) and -22 (exon 3). Poly(A) addition signals are indicated by vertical arrows. (B) differential splicing precursors RNA on the 5'- and 3'- end of the IGF-1 gene. Adapted from Shavlakadze et al. 2005.

The primary structure of IGF-1 is highly conserved in mammals. At the mRNA level, the sequence of mouse and human IGF-1Ea are highly conserved with 94% identity, differing by 4 amino acids only (Bell et al. 1986 and Shavlakadze et al. 2005). In extra-hepatic tissues, where most of the IGF-1 isoforms can be found, the mRNA encoding for the Ea-peptide is the major transcript representing 95% of the total IGF-1 mRNA (Lowe et al. 1988), whereas Eb containing transcripts are more abundant in liver. Because of this, and due to the fact that the majority of the research on IGF-1 has been performed on the IGF-1 mature 7-kDa protein, and also given that sooner or later all the isoforms are processed to form the IGF-1 mature form, very few studies are available in mammals addressing the question of the differential role of all the IGF-1 isoforms (Stewart et al. 1996).

At the protein level, all the mRNA generated by the combination of the different transcriptional regulatory elements give rise to a myriad of IGF-1 proteins, also known

as pre-pro-peptides. The pre-pro-peptides undergo post-translational modifications such as cleavage of the signal peptides, and glycosylation of both the mature and the E-peptides (Shavlakadze et al. 2005) (**Figure 1.6**).

In circulation, IGF-1/2 is a secreted protein with a half-life of less than 10 minutes. Therefore, IGF-1 and IGF-2 bind to IGFBPs with high affinity serving as carrier molecules, modulating their half-life and availability in the circulation and in tissue (Denley et al. 2005 and Forbes et al. 2012).

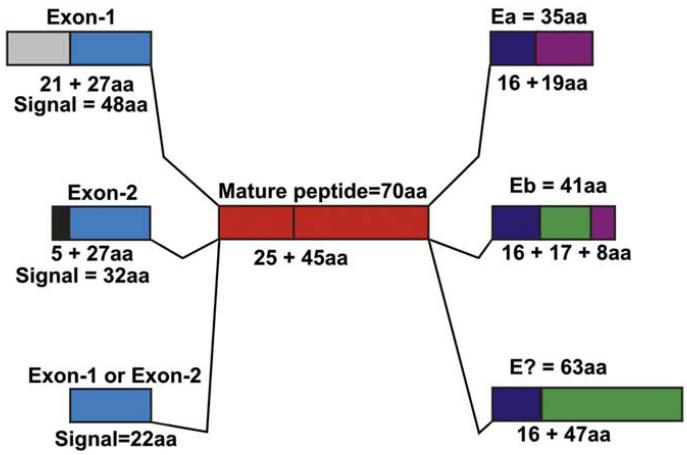


Figure 1.6. Different IGF-1 pre-propeptides cleavage. IGF-1 mature form (red), pro-peptides or signal peptides (N-terminal), and E-peptides (C-terminal). IGF-1Ea (21 Kda), IGF-1Eb (17 Kda) and IGF-1 mature form (7.6 Kda). Adapted from Shavlakadze et al. 2005.

1.5.2 Insulin-like growth factor 1 receptor and signalling pathways

The biological activity of IGF-1 is mediated by the type 1 IGF-receptor (IGF-1R). The IGF-1 receptor and the insulin receptor are α2β2 heterotetrameric transmembrane glycoproteins belonging to the receptor tyrosine kinase family. The α subunits of the receptor are completely extracellular and responsible for ligand binding (Ullrich et al. 1986). The β-subunits of the receptor consist of a short extracellular domain and a large intracellular domain with sites for tyrosine and serine phosphorylation responsible for the signal transduction (Frattali et al. 1993). Differential phosphorylation of IGF-1R leads to the recruitment of other substrates that in turn activates different signal pathways (Butler et al. 1998). Activation of the IGF-1R, can trigger the recruitment of other protein which can be another plausible explanation for why IGF-1 can exert such diverse functions through the same receptor (White et al. 1998) (**Figure 1.7**).

1.5.2.1 MAP-kinase signalling

The MAP kinase pathway is considered to be the main canonical pathway involved in the IGF-1-mediated stimulation of cell proliferation. This pathway involves the phosphorylation of ERK (MAPKK family) by RAS, leading to its nuclear translocation, which in turn induces the expression of molecular markers of cell cycle progression such as c-Jun, c-Fos, Cyclin D1, and cdk4 (Coolican et al. 1997) (**Figure 1.7**).

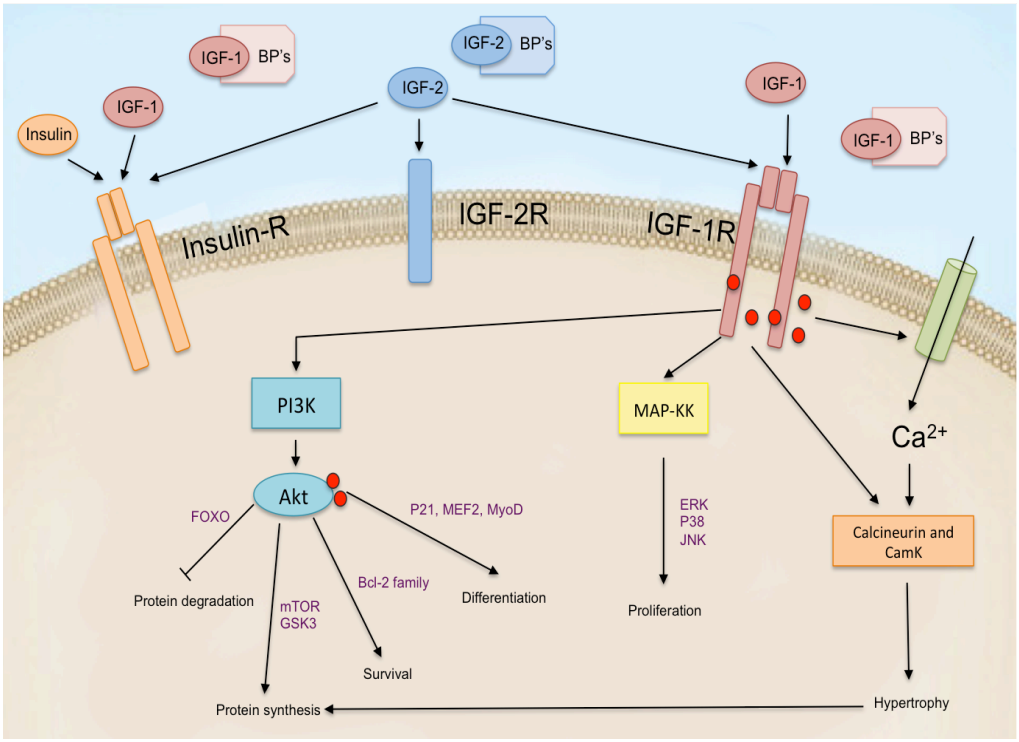


Figure 1.7. IGF-1/IGF-1R signalling pathway. IGF-1R activation by IGF-1 may potentially trigger several pathways such as PI3k, MAP-Kinase, CamK and calcineurin pathways.

1.5.2.2 PI3/AKT-signalling

Upon IGF-1R activation, active PI3-kinase phosphorylates inositol phospholipids. This phosphorylation is required to induce several downstream targets such as Akt. Akt has a diverse set of functions and is the key molecule for protein synthesis. Activation of Akt induces differentiation in several cell types and it is considered the main pro-survival molecule. Downstream of Akt, two main pathways are required; the phosphorylation (and thus inhibition) of glycogen synthase-serine kinase 3α (GSK-3 α), and the phosphorylation and activation of mammalian target of rapamycin (mTOR) (Bodine et al. 2001, Fujio et al. 2000 and Rommel et al. 2001). Other proteins such as the FOXO transcription factor family (Bodine et al. 2001) and members of the Bcl-2 (Brunet et al. 1999 and Datta et al. 1997) family also meditate these pro-survival actions. After

activation of these transcription factors, they exit the nucleus and thus cannot perform their pro-apoptotic transcriptional functions (**Figure 1.7**).

1.5.2.3 Calcineurin signalling

Several studies in skeletal muscle cells have reported a cytoplasmatic serine-threonine phosphatase activation of calcineurin by increased Ca^{2+} levels in myoblasts stimulated with IGF-1 (Kato et al. 2000 and Musaro et al. 1999). Increased intracellular levels of Ca^{2+} lead to the activation of calcineurin, which in turn has an effect on muscle cell differentiation and hypertrophy (**Figure 1.7**). In *in vivo* models, the induction of calcineurin *via* cardiomyocyte-specific overexpression of a calcineurin splicing variant, CnAβ1, promoted infarct vascularization and prevented infarct expansion after MI (Lopez-Olaneta et al. 2014).

1.5.3 IGF-1 isoforms in skeletal muscle regeneration

The main IGF-1 splicing variant expressed in the skeletal muscle in resting muscle is the IGF-1 mRNA for which transcription initiates at exon 1 (Class I IGF-1), encoding the Ea-peptide (Musaro et al. 2001).

After skeletal muscle injury, caused by contusions or exercise-related injury, the splicing variant comprising exons 4 to 6 is up regulated. This splicing variant includes the Eb-peptide in rodents and IGF-1Ec in humans. *In vitro* studies using C2C12 myogenic cells also suggest different roles for IGF-1Ea and IGF-1Eb isoforms. While both isoforms increase myoblast proliferation, IGF-1Eb stimulates proliferation within the first 48 hours (Yang et al. 2002). This role of IGF-1Eb in myoblast and satellite cell proliferation, thus blocking differentiation, is also supported by *in vivo* studies on humans (Hameed et al. 2003) and rats (Hill et al. 2003). Satellite cell proliferate after trauma and after several cell division, satellite cells fuse to damaged myofibers to form new ones.

In mice, muscle-specific overexpression of IGF-1Ea increases the number of myogenic progenitors by promoting the fusion of nascent myocytes enabling increased production of muscle proteins and/or the repair of damaged regions of muscle fibers (Hill et al. 2003 and Lee et al. 2004), fibre size, promotes protein synthesis and healing after injury, increase muscle size-hypertrophy, reduces cachexia, ageing (Musaro et al. 2001). Furthermore, it has been demonstrated that IGF-1 accelerates muscle regeneration by modulating inflammatory cytokines and chemokines (Pelosi et al. 2007). However, little

is know about the role of IGF-1Ea regulating the inflammatory milieu and cell recruitment.

1.5.4 IGF-1 in cardiac repair

There are many studies that have assessed the role of both IGF-1Ea and IGF-1Eb isoforms after cardiac damage. The main pleiotropic effect exerted by IGF-1 is triggered by the activation of its receptor as described in Section 1.5.2. These effects mainly involve anti-apoptotic signals, control of cardiac growth, autophagy inhibition, glucose metabolism facilitation and preventing the ageing of the heart. Although, the signalling pathways that are activated by IGF-1 are well studied, the underlying mechanisms that trigger the activation of either one, two or even all the signalling pathways in order to defeat cardiac death and promote efficient cardiac repair are still not sufficiently understood.

In the rat heart, the expression of IGF-1Ea and IGF-1Eb isoforms is significantly increased after MI. The research corroborates that coronary artery ligation–induced myocardial infarction was followed by an endogenous increase of IGF-1Ea and MGF expression, both at mRNA and protein levels (Stavropoulou et al. 2009 and Carpenter et al. 2008). Anastasia et al. have shown that after MI, the levels of IGF-1Eb were much higher than the IGF-1Ea at both the transcriptional and translational level (Stavropoulou et al. 2009). Other studies performed in sheep have revealed that IGF-1Eb has the ability to reduce the loss of cardiac function and post infarct apoptosis in the peri-infarct zone of sheep myocardium measured by echocardiography (Carpenter et al. 2008). However, the research also implies that the E-peptides (Ea and Eb) play a role in the pathophysiology of rat myocardium, which possesses possibly autonomous biologic actions.

In recent years, our laboratory has demonstrated that the locally-acting IGF1-Ea induces vessel formation after injury and mediates bone marrow mobilization through the expression of specific cytokines (Santini et al. 2011). Furthermore, expressed as a cardiomyocyte-specific transgene or through local cell-mediated delivery, IGF1-Ea accelerates cardiac growth, promotes effective myocardial repair as well as functional restoration after MI (Santini et al. 2007, Santini et al. 2011 and Poggioli et al. (in preparation) (**Figure 1.8**). Santini et al. 2007, also observed decreased apoptosis at the injured site, which is at least in part attributable to IGF-1Ea triggering the up-regulation of UCP-1, metallothionein 2 and the cardioprotective cytokine adiponectin. Despite the

known properties of Akt as a cardioprotective mediator besides the function of IGF-1 as regulator of AKT *via* PI3K, an alternative signalling cascade seems to contribute to IGF-1Ea mediated cardioprotection (Santini et al. 2007, Yasushi et al. 2000 and Takashi et al. 1999).

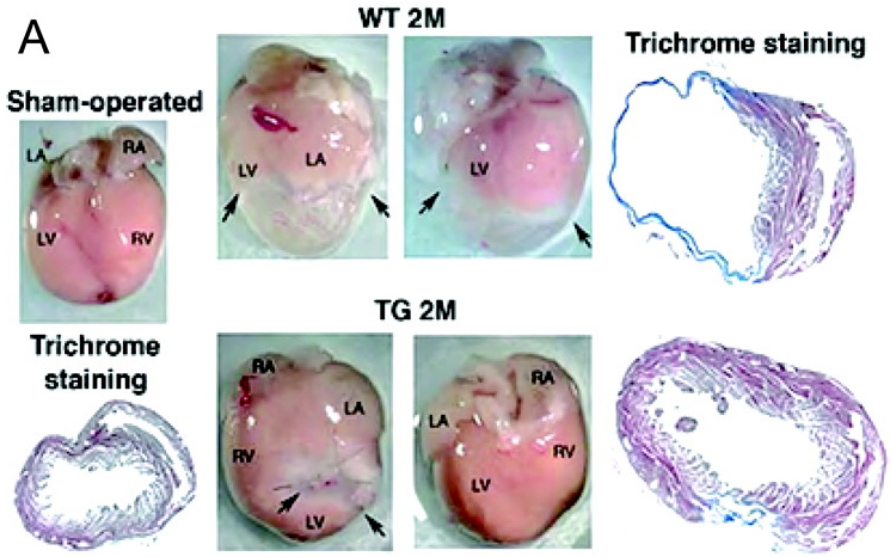


Figure 1.8. Enhanced cardiac repair in αMHC-IGF1Ea transgenic mice after myocardial infarction. Whole mount and histological analysis of sham-operated control (WT) heart (left) and LCA WT and TG hearts (right) 2 months after operation. Arrows indicate fibrotic tissue. LA indicates left atrium; LV, left ventricle; RA, right atrium; RV, right ventricle. Histological analysis by trichrome staining is shown for each treatment. Extracted from Santini et al. 2007.

Interestingly, research on IGF-1Ea in muscle-restricted (Pelosi et al. 2007) and heart-restricted (Santini et al. 2007) prompted a new hypothesis where IGF-1Ea local expression accelerates the regenerative/reparative properties by modulating inflammatory cytokines and chemokines and limiting fibrosis. After skeletal muscle injury, IGF-1Ea supplemental expression significantly down-regulated proinflammatory cytokines, such as tumor necrosis factor (TNF)-alpha and interleukin (IL)-1beta (Pelosi et al. 2007). After heart injury, IGF-1Ea expression resulted in repression of the pro-inflammatory cytokines IL-1β and IL-6, while the anti-inflammatory IL-4 and IL-10 showed higher expression levels when compared to wild-type (WT) animals after cardiotoxin injury (Santini et al. 2007). These results suggests a new role of IGF-1Ea in modulating the environment during muscle repair and the recruitment of myeloid cells however, the molecular and cellular mechanism behind enhanced reparative capacities are still unknown. Chapter 3, of this thesis is designed to unveil the role of IGF-1Ea in the recruitment of monocytes/macrophages.

Furthermore, our group has recently published that the E-peptides bind to the extracellular matrix (ECM) with varying affinities, thereby controlling IGF-1 bioavailability and preventing IGF-1 release into the systemic circulation. Thus, the combinatorial effect of IGF-1 and the E-peptides are a potentially powerful therapy by which IGF-1 can be anchored into the ECM nearby the site of synthesis and/or administration (Hede et al. 2012).

In summary, both *in vivo* and *in vitro* studies have provided a remarkable insight on the actions of IGF-1, although the role of each isoform is still under investigation, IGF-1 has gained a place on the podium as one of the molecules with the highest therapeutic potential to ameliorate the adverse effects of both skeletal muscle and heart injury. Interestingly, all the studies performed using IGF-1 have shown how remarkable and versatile this molecule is in triggering cardiac repair as described in Section 1.5.2. Thus, if tuned properly, it could potentially lead to complete cardiac repair.

1.5.5 IGF-1 therapeutic applications

There are several FDA approved IGF-1-based drugs for the treatment of diseases. IGF-1 treatment is usually in combination with IGF binding protein in order to increase the half-life of IGF-1 in circulation. The most common drugs currently in use to date are Mecasermin (Increlex ®) and Mecasermin rinfabate (IPLEX ®), a binary protein complex of human recombinant IGF-1 and human recombinant IGFBP-3 prescribed for long-term treatment of growth failure in children with severe IGF-1 deficiency.

Interestingly, Raffay S. Khan in 2013 presented a novel delivery vehicle to deliver the IGF-1 protein. The preclinical studies in rat showed that IGF-1 conjugated to a DNA binding agent improved IGF-1 retention at sites of myocardial injury following ischemia reperfusion injury (Khan et al. 2014). Despite the fact that IGF-1 treatment has overall beneficial effects, there are concerns regarding the safety of chronic elevated levels of systemic IGF-1 (Castellano et al. 2009). The main disadvantage of these drugs is the increase in the half-life of IGF-1, thus increasing the levels of IGF-1 in the circulation; this has been associated with severe adverse effects, such as an increased risk of cancer (Gallagher et al. 2010).

However, pharmaceutical companies have not yet achieved a fully functional IGF-1 isoform that could be used as a therapeutic treatment for MI. The problem is in reproducing, *in vitro*, the IGF-1Ea glycosylation pattern in artificial bacterial or yeast

organism, which so far it has not been yet achieved. Although, no function for glycosylation of the Ea-peptide (Eb-peptide has no glycosylations) has so far been reported. The glycosylation patter varies the affinity of these positively charged peptides to the negatively charged ECM (Hede et al. 2012). It has also been speculated that the E-peptides may have a specific receptor independent of IGF-1, which may confer new actions to IGF-1. Consequently, IGF-1Ea gene therapy, rather than the protein itself, is currently the best approach to deliver IGF-1 and the Ea-peptide.

1.5.5.1 Viral delivery of IGF-1

As discussed in the previous section, the challenges that compromise the design of a fully functional IGF-1 isoform have directed IGF-1Ea research towards viral delivery. Research performed in rodents showed that intramuscular injection of an adeno-associated virus serotype 5 encoding IGF-1 rat cDNA under Tet regulation, AAV5.IGF1-tet, improved left ventricular function after MI (Lai et al. 2012). Although the study highlighted the beneficial effects of IGF-1, it also presented several limitations. The serotype 5 works well in rodents, however, is highly immunogenic in humans, thus exhaustive patient pre-screening for Nab should be taken into account to improve efficacy. In addition, AAV vectors were delivered via intramuscular injection rather than intravenous injection limiting the translational scope as well as the efficacy. Interestingly, new AAV serotypes such as AAV9 have shown to have better tropism to the heart than AAV5 (Fang et al. 2013). Furthermore, newly formed serotypes, such as AAV8, AAV9, are capable of crossing the endothelial barrier to provide efficient transgene expression. Regarding cardiac specificity of the transgene, Tet expression was driven by the cytomegalovirus promoter (CMV), which limit heart specificity to intramuscular injections only. Finally, the approach did not engaged de novo vascularisation, nonetheless, reduced apoptosis was achieved (Lai et al. 2012).

Another study focused on IGF-1 angiogenic capabilities, using microSPECT-CT imaging in rats. Intramuscular injection of AAV2-mediated IGF-1 gene transfer significantly improved cardiac function after MI (Dobrucki et al. 2010). The main limitation of this study is again the serotype of choice; the method of delivery (intramuscular) as well as the promoter employed (CMV) which does not confer cardiac specificity (Dobrucki et al. 2010). Successful IGF-1 gene therapies must combine various levels of IGF-1 specificity, first, limiting the expression to the heart with a cardiac specific promoter, and second by using a cardiac-specific serotype in order to achieve successful intravenous delivery after MI.

1.6 Hypothesis and aims

The escalating incidence of acute cardiovascular diseases leading to heart failure underscores the increasingly urgent need for improved therapeutic strategies to limit cardiac tissue damage and improve functional outcomes in a translational setting.

Insulin growth factor splicing variant 4 (IGF-1Ea) is a powerful enhancer of cardiac muscle growth and regeneration, also blocking age-related atrophy and beneficial in multiple skeletal muscle diseases. In the heart, local expression of IGF-1Ea promoted functional restoration associated with reduced infarct expansion, thinning and dilation of the left ventricular wall. The therapeutic potential of IGF-1Ea compared to other isoforms or the mature form mainly relies on its ability to act locally in the area of administration. This thesis examines the efficient gene transfer of IGF-1Ea to the heart and the effects of IGF-1Ea gene delivery on adverse ventricular remodeling after ischemia/reperfusion using cell- or gene-based approaches.

Considering the above observations, the hypothesis behind this thesis is:

> IGF-1Ea gene transfer, delivered either by cell- or viral-based approaches, improves left ventricular function and reduce adverse ventricular remodelling after myocardial infarction.

If successful, the knowledge acquired will be useful to support IGF-1-based cardiac-specific therapies for treatment of MI through the design of new approaches to deliver beneficial factors with the reduced need to perform surgical interventions.

Aims:

1. To understand the underlying mechanisms behind the enhanced repair mediated by IGF-1Ea on inflammation after myocardial infarction by analysing the subtypes of circulating monocytes/macrophages attracted to the infarcted area in our cardiac-specific IGF-1Ea transgenic mice (αMHC.IGF1Ea).
2. To assess whether cultured macrophages can home, carry and deliver IGF-1Ea into the injured heart and investigate their potential beneficial effects on tissue repair.
3. To determine whether intravenous delivery of AAV9-based IGF-1Ea gene transfer can ameliorate the adverse effects of heart remodeling after ischemic injury, as a clinically applicable delivery system.

Chapter 2 - Methodology

2.1 Mouse model

2.1.1 αMHC.IGF-1Ea mice

The αMHC.IGF-1Ea transgenic mice line on under the FVB background was generated in Nadia Rosenthal's laboratory at the EMBL Monterotondo (Santini et al. 2007). The transgenic mouse line was used in Chapter 3. Briefly, the rat IGF-1Ea consensus sequence is under the control of αMHC promoter, limiting expression to the heart muscle. The construct was inserted into the genome by random insertion.

2.1.2 αMHC.IGF-1Ea genotyping

Samples for genotyping were obtained from ear notches. Ear samples were digested at 56°C overnight in digestion buffer (0.5% Igepal CA-630 (Sigma, UK, Cat. 074K0577), 100 mM Tris pH 8, 0.5% Tween 20) with 0.2mg/ml of proteinaise K (Roche Applied, UK, Cat. 03115801001).

Digested samples were vortexed and spinned down. The supernatant containing the DNA was directly used to amplify the IGF-1Ea gene by an standard polymerase chain reaction program (**Table 2.1**). For IGF-1 genotyping the following primers were used:

IGF-1 forward primer: 5'-TTCCTGTCTACAGTGTCTGTG-3'

IGF-1 reverse primer: 5'-GAGCTGACTTTGTAGGCTTCA-3'

Agarose gel electrophoresis (1.5%) were prepared using 1X TAE buffer from a 50x TAE stock, Tris base ($C_4H_{11}NO_3$, MW: 121.14 g/mol), glacial acetic acid (CH_3COOH, MW: 60.05g/mol), 0.5M EDTA stock solution (pH 8.0) (**Figure 2.1**).

Components final concentration	**Volume (µL)**	**Thermocycler conditions**
DNA template	1	35 cycles
DreamTaq Green PCR Master mix (Thermo Scientific. Cat.K1081)	12.5	3 min at 94°C 30 sec at 94°C
Autoclaved, distilled water	10.5	40 sec at 62°C
Primers	1	50 sec at 50°C
		2 min at 72°C
Final volume	25	∞ 4°C

Table 2.1. Polymerase chain-reaction conditions for *αMHC.IGF-1Ea.*

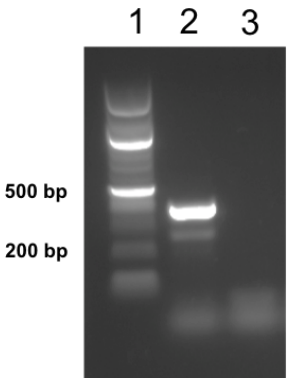


Figure 2.1. IGF-1Ea genotyping PCR product. Lane 1, 100 bp molecular weight laddder. Lane 2, characteristic band at 440 bp for IGF-1Ea αMHC.IGF-1Ea mouse sample. Lane 3, WT mouse sample. 1.5% agarose electroforesis gel.

2.2 RNA extraction and quantification

After sacrificing the mice, hearts were perfused with PBS, and samples from the infarct region, border zone, and remote myocardium were harvested and snap-frozen in liquid nitrogen.

In Chapter 3 and 4, total RNA was extracted according to the TRIzol Reagent protocol (Invitrogen, UK. Cat. 10296028). In Chapter 5, due to the limited amount of tissue, total RNA was isolated using the RNeasy kit from Qiagen, with DNAse on the column (Qiagen, UK. Cat. 74104) which allows that better DNA yields can be extracted.

2.2.1 RNA isolation from cells and from tissue

Total RNA from adherent cells (monolayer) was isolated by removing the culture medium from the culture dish. 1ml TRIzol reagent/35mm dish was directly added to the culture dish surface area. When using either 60mm or 100 mm, 3ml or 8ml of TRIzol were added respectively. Cells were lysed by pipetting up and down several times.

Total RNA from mouse tissue was mechanically disrupted with surgical scissors and placed in a 1.5 mL tube, an appropriate amount of TRIzol was added accordingly, 1 ml TRIzol reagent per 50-100mg. Tissue samples were disrupted with a rotor-stator homogeniser (Polytron PT 2500 E) for 40-50 seconds to disrupt and homogenize the tissue samples.

Samples were incubated at RT for 5 minutes. 0.2 ml of chloroform was added and the samples were centrifuged at 15000g for 15min. The RNA in the aqueous phase was

precipitated with 0.5ml isopropanol and washed with 75% ethanol. The RNA was pelleted, air-dried and re-suspended in DNAse/RNAse free water.

2.2.2 RNA quantification

The RNA yield was quantified using Nanodrop® (Thermo Scientific, Wilmington, USA) device at 260 nm and the purity by the ratio 260/280 nm and 260/230nm. For RNA samples, the ratio between the absorbance measured at 260 nm and 280 nm (A260/A280) should ideally be 2 to indicate good RNA sample purity. Contaminating proteins and some chemicals such as phenol absorb light at a wavelength of 230 nm. A260/A230 ratio between 2.0-2.2 indicates sufficient purity of RNA from these contaminants.

2.2.3 cDNA synthesis

The cDNA was generated according to Quantitect® Reverse Transcription Kit (QIAGEN, UK. Cat. 205313) in a 10µl reaction final volume. In Chapter 3 and 4, 1 µg of total RNA was retrotranscribed. In Chapter 5, due to the limited amount of tissue, 100 ng of total RNA was used instead of 1 µg.

2.2.4 Quantitative Real-Time polymerase chain reaction (qRT-PCR)

Following cDNA synthesis, TaqMan qRT-PCR was performed on an ABI 7900HT Sequence Detection System (Applied Biosystems, Carlsbad, CA, USA) platform using either MicroAmp® Optical 96-Well Reaction Plate or MicroAmp® Optical 384-Well Reaction Plate (Applied Biosystems, Cat. 4306737 and 4309849, respectively). Master mix for all samples and genes of interest (GOIs) was prepared and aliquoted into the reaction plate-well according to **Table 2.2**. For every well, 1 µL of cDNA was loaded on triplicate. Plates were sealed with optical adhesive film (Applied Biosystems, USA. Cat. 4311971) and spinned down for a few seconds. Taqman FAM, VIC predesigned probes were purchased at Applied Biosystems (http://bioinfo.appliedbiosystems.com/genome-database/gene-expression.html).

In this thesis, the TaqMan probes used for the relative quantification of mRNA levels were as follow (Reference code of predesigned probes in brackets):

Chapter 3: IGF-1Ea (Mm00710307_m1), IL-10 (Mm00439614_m1), IL-1β (Mm00434228_m1), CCL2 (Mm00441242_m1), CCL5 (Mm01302427_m1), TGFβ (Mm03024053_m1), Collagen Iα1 (Mm00801666_g1), Collagen Iα3 (Mm01254476_m1), Lox (Mm00495386_m1), MMP2 (Mm00439498_m1), MMP9 (Mm00442991_m1),

TIMP1 (Mm00441818_m1), TIMP2 (Mm004418225_m1), actin, alpha 1, skeletal muscle, ACTA, (Mm00808218_g1), Atrial Natriuretic Peptide, ANP (Mm01255747_g1).

Chapter 4: IGF-1 (Mm00439560_m1), IGF-1Ea (Mm00710307_m1), IGF-1Eb (Mm01228180_m1), IGF-1R (Mm00802831_m1), Il-6 (Mm00446190_m1), Il-10 (Mm00439614_m1), TNF-α (Mm00443258_m1), CCL2-MCP1 (Mm00441242_m1).

Chapter 5: Actin, alpha 1, skeletal muscle, Acta1 (Mm00808218_g1), Nppb/brain natriuretic peptide (BNP) (Mm01255770_g1), Collagen Iα1 (Mm00801666_g1), Collagen Iα3 (Mm01254476_m1), Lox (Mm00495386_m1), Thy1 (Mm00493681_m1), IGF-1Ea (transcript variant 4) (Mm00710307-m1), Luciferase (Mr03987587_mr). GFP expression was quantified using SYBR green primers: FW EGFP: CCA GGA GCG CAC CAT CTT CTT and RV EGFP: GTA GTG GTT GTC GGG CAG CAG.

GAPDH (Applied Biosystems, USA, Cat. 4310893E) was used as housekeeping gene to normalize expression levels.

Components -final concentration For a 96-well plate	**Final Volume (12.5 µL)**	**Thermocycler conditions**
Taqman ® Gene Expression Master Mix	6.25	42 cycles 10 min at 95°C 15 sec at 95°C 1 min at 60°C ∞ 4°C
GOI-FAM (Reference gene GAPDH-VIC)	0.625	
Autoclaved, distilled water	4.625	
Components -final concentration For a 384-well plate	**Final Volume (10 µL)**	
Taqman ® Gene Expression Master Mix	5	
GOI-FAM (Reference gene GAPDH-VIC)	0.5	
Autoclaved, distilled water	3.5	

Table 2.2. Reaction components and thermo cycler conditions for qRT-PCR reactions. Master mix and samples were loaded on triplicates. Taqman ® Gene Expression Master Mix (Applied Biosystems, USA. Cat. 4369016).

2.2.4.1 qPCR data analysis: comparative $\Delta\Delta C_t$ method

Once the PCR cycle is completed; data was exported into Excel and analysed using the LinReg software in order to estimate the efficiency rates and the Ct values (Ruitjer et al. 2009).

At some point of the PCR process, the accumulated fluorescent signal cross the threshold (ie exceeds background level), called the cycle threshold value (C_t). C_t levels are inversely proportional to the amount of target nucleic acid in the sample (ie the lower the C_t value the greater the amount of target nucleic acid in the sample). For relative quantification, the C_t value of the GOI ($C_{t\text{-}GOI}$) is first normalized against the C_t value of a reference gene ($C_{t\text{-}RG}$) (i.e. GAPDH gene in this thesis) to produce the ΔC_t:

$$\Delta C_{t.} = C_{t\text{-}GOI} - C_{t\text{-}RG}$$

Subsequently, the relative expression of the gene of interest for each sample is calculated using the ΔC_t of the sample in the study group ($\Delta C_{t\text{-}ref}$), usually a control or untreated sample and applying the formula:

$$\Delta\Delta C_t \text{ (relative expression of GOI)} = 2^{-\Delta Ct - \Delta Ct\text{-}ref}$$

2.2.4.2 Taqman® probe-based gene expression analysis

TaqMan® probes, also called double-dye oligonucleotides, consist of a fluorophore attached to the 5' end of the probe and a quencher to the 3' end. The reporter fluorescence is suppressed by the proximity to the quencher. For FAM probes, the 5' end emits light at 520 nm upon excitation whereas for VIC® probes, the fluorescence reporter dye VIC®, emits light 580 nm upon excitation. This property makes possible to perform analysis of two genes at the same time in one reaction well. During synthesis, the 5' to 3' nuclease activity of the DNA polymerase, contained in the master mix, cleaves the primer releasing the reporter dye and the quencher dye, resulting in increased fluorescence by a mechanism known as Fluorescence Resonance Energy Transfer (FRET). The machine detects the accumulation of both the fluorophore and quencher released into solution, quantifying the increase in fluorescence of the reported dye (Taqman, applied biosystem website)

2.3 Protein biochemistry

Animals were sacrificed using Schedule One approved methods. The hearts were washed with cold PBS and immediately removed from carcasses, snap frozen in liquid nitrogen and stored at -80C. Tissue samples were disrupted on 500 µl RIPA buffer (Sigma, UK. Cat. R0278) with a rotor-stator homogeniser (Polytron PT 2500 E) for 40-50 seconds to disrupt and homogenize the tissue samples.

2.3.1 Protein extraction and quantification

Proteins were quantified using the *DC* colorimetric protein assay kit following manufacturer's instructions (Bio-Rad Laboratories, UK, Cat. 500-0116) based on standardised protocol from Nadia's group. Briefly, protein samples are exposed to copper tartrate solution in an alkaline medium for a subsequent reduction of protein-copper complexes of the reducing agent (Folin reagent). These two steps result in a colorimetric shift to blue, with a peak absorbance at 750 nm and at 405 nm. The amount of Folin reduced in the reaction is proportional to the amount of amino acids, tyrosine and tryptophan, present in the protein. For protein quantification, a standard curve of known concentration was prepared with Bovine Serum Albumin (BSA) (Sigma, UK. Cat. A9418). Absorbance values were plotted against the amount of proteins and a standard curve was obtained using linear regression (**Figure 2.2**).

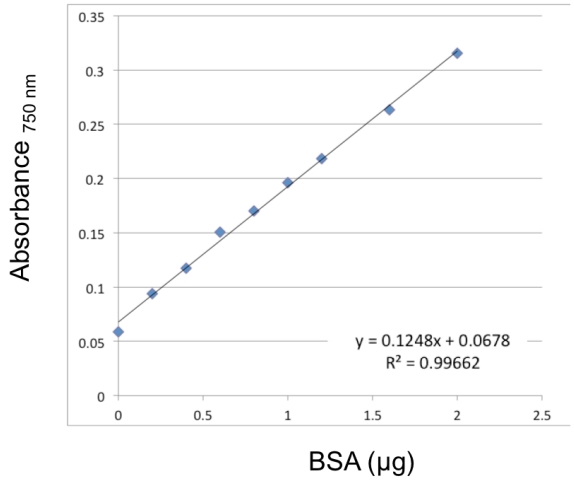


Figure 2.2. Bovine Serum Albumin (BSA) representative standard curve. Concentration curve, from 0.2-2.5 µg/well, of BSA with linear regression analysis. The curve equation and the R^2 are reported. The R-squared value is a measure of goodness-of-fit of linearity. When is >0.99, means that the regression line gives correct predictions. Protein concentration (X) of the unknown samples was calculated by matching their absorbance values (Y) against the standard curve using the graph equation.

2.3.2 Immunoblotting

After quantification, 30-50 µg of protein lysate was denaturalised at 100ºC for 5 min in SDS blue loading buffer (Cell signalling, USA, Cat. 7722) including 1/10 volume 30X DTT (Cell signaling, USA, Cat. 7016). Denatured samples were run in acrylamide 20% tris-HCL/tris-tricine pre-cast gradient gels (Bio-Rad, UK. Cat. 4561091) in running buffer (25mM Tris base, 0.192M Glycine, 0.1% SDS). Following separation, the samples were transferred on a nitrocellulose membrane for 1 hour at 4ºC. Blotted membranes were

blocked in 5% skimmed milk in PBS-T and incubated with the primary antibody O/N at 4ºC. Primary and secondary antibodies were diluted 1:1000 in blocking solution. The following day, blots were washed with PBS-Tween 20 and incubated with the secondary antibody followed by a second wash step. Nitrocellulose blots were incubated with a luminol-based detection reagent (ECL-Amersham/GE healthcare UK. Cat. RPN2232) and proteins bands visualised on an film developer.

In Chapter 4, western blot was performed using the following primary antibodies: anti mouse-IGF-1 (Sigma, UK. Cat. I-8773), and the secondary antibody used was donkey anti-goat IgG-HRP (Santa Cruz, USA. Cat, SC-2020). Alpha-tubulin monoclonal antibody (Sigma, UK. Cat. T6074) was used as a loading control.

In Chapter 5, western blot was performed using the following primary antibodies: anti mouse-IGF-1 (Sigma, UK. Cat. I-8773), anti-phospho-Akt^{Ser473} (Cell signaling, Cat. 9271), anti-Akt (Cell Signaling, Cat. 9272), anti-phosphomTOR$^{Ser\ 2448}$(Cell Signaling, Cat. 2971), anti-mammalian target of rapamycin (mTOR) (Cell Signaling, Cat. 2972) and alpha-tubulin monoclonal antibody (Sigma, UK. Cat. T6074) as described in Blackstock et al. 2014, Panse et al. 2012 and Felkin et al. 2011. The secondary antibody used was donkey anti-rabbit IgG-HRP (GE Healthcare, USA, Cat. NA934). Brightness and contrast were linearly adjusted using power point.

2.4 Immune single cell isolation from heart

To analyse neutrophils, monocytes, macrophages and dendritic cells, a single cell suspension was prepared from hearts before, or at various time points after MI (Day 1, 3, 5, 7, and 28 post-operation). The hearts were mechanically dissociated using surgical scissors and subsequently treated with 4 cycles of 10 min each at 37^{o}C with a 1X Hank's Balanced Salt Solution (HBSS) (Invitrogen, USA. Cat. 14025092) enzymatic dissociation buffer containing 0.1mg/mL Liberase TH Research Grade (Roche Diagnostics, UK. Cat. 05401151001), 50 ug/mL of DNaseI (Roche Diagnostics, UK. Cat. 11284932001), 10mM HEPES (Invitrogen, USA. Cat. 15630-080), and 30mM Taurine (Sigma, UK. Cat. T0625). After each 10 min incubation cycle, the cells were pelleted at 320g for 7min at 4^{o}C and washed with the 1X HBSS media solution containing 20% FBS. Cells were collected and filtered using a 70 μm cell strainer (BD Pharmingen, USA. Cat. 08-771-2). An equal volume of ice cold 1X HBSS containing 10mM HEPES, 30mM Taurine, and 20% Fetal Bovine Serum (FBS) (GE Healthcare, USA. Cat. SH30084.02), was added to the enzyme dissociation buffer. Under these specific cellular isolation conditions, the adult

cardiomyocytes are predominately lysed, as the enzymatic dissociation buffer is potentially toxic to these large, fragile cell types (Oh et al. 2003).

For preparing single cell suspension from other organs such as kidney, liver, lungs, and skeletal muscle tissues, samples were harvested and placed on cold RPMI medium. Thereafter, tissue was finely minced with scalpel and incubated in cell digestion medium containing Collagenase F (Sigma, UK. Cat. C7926) and RPMI, in gentle agitation for 30 minutes at room temperature (RT). After digestion, 4% of FBS and 300U of DNAseI were added to the solution. Cell suspension was then filtered through 70 μm cell strainer and centrifuged 1500rpm for 5min at 4ºC. Resulting pellets were resuspended in PBS and and the number of cells were counted in a Beckman Coulter Vi-Cell XR cell counter (Beckman Coulter).

2.4.1 Flow cytometry and cell sorting

Single cells were incubated in 1X Dulbecco's Modified Eagle Medium (DMEM) solution (Gibco, Life technologies, UK. Cat.12491-015) containing, 2% FBS, 10mM HEPES and incubated for 30 min, on ice, in the dark with the following antibodies:
CD11b-PE (BD Biosciences, USA. Cat. 553311), F4/80-Biotin (eBioscience, USA. Cat. 13-4801-85), CD45-APC-Cy7 (BioLegend, USA. Cat. 103116), CD206-PerCP-Cy5.5 (BioLegend, USA. Cat.141716), Ly6C-APC (eBioscience, USA. Cat. 17-5932-82) and Ly6G-AlexaFluor700 (BioLegend, USA. Cat. 127622).

Samples stained with biotin-labelled primary antibody were incubated with streptavidin-PE-Cy7 secondary antibody (eBioscience, USA. Cat. 25-4317-82) for 30 min, on ice, in the dark, with the 1X DMEM media solution as mentioned above. The samples were washed and re-suspended in fresh 1X DMEM media solution with 1.5 μM Sytox Blue (Invitrogen, USA. Cat. S34857). Cells were re-filtered using 5mL, 35 μm filter cap tubes just prior to sample acquisition. Flow cytometric cell sorting was preformed using a BD FACSAriaI cell sorter (BD Biosciences) equipped with a 355nm UV laser, a 405 nm Violet laser, a 488 nm Blue laser, a 561 nm Yellow-Green laser and a 640 nm Red laser. The antibody cocktail fluorescence minus one (FMO) controls were used as gating controls for analyses to distinguish positive from negative cell staining (**Figure 2.3 and 2.4**).

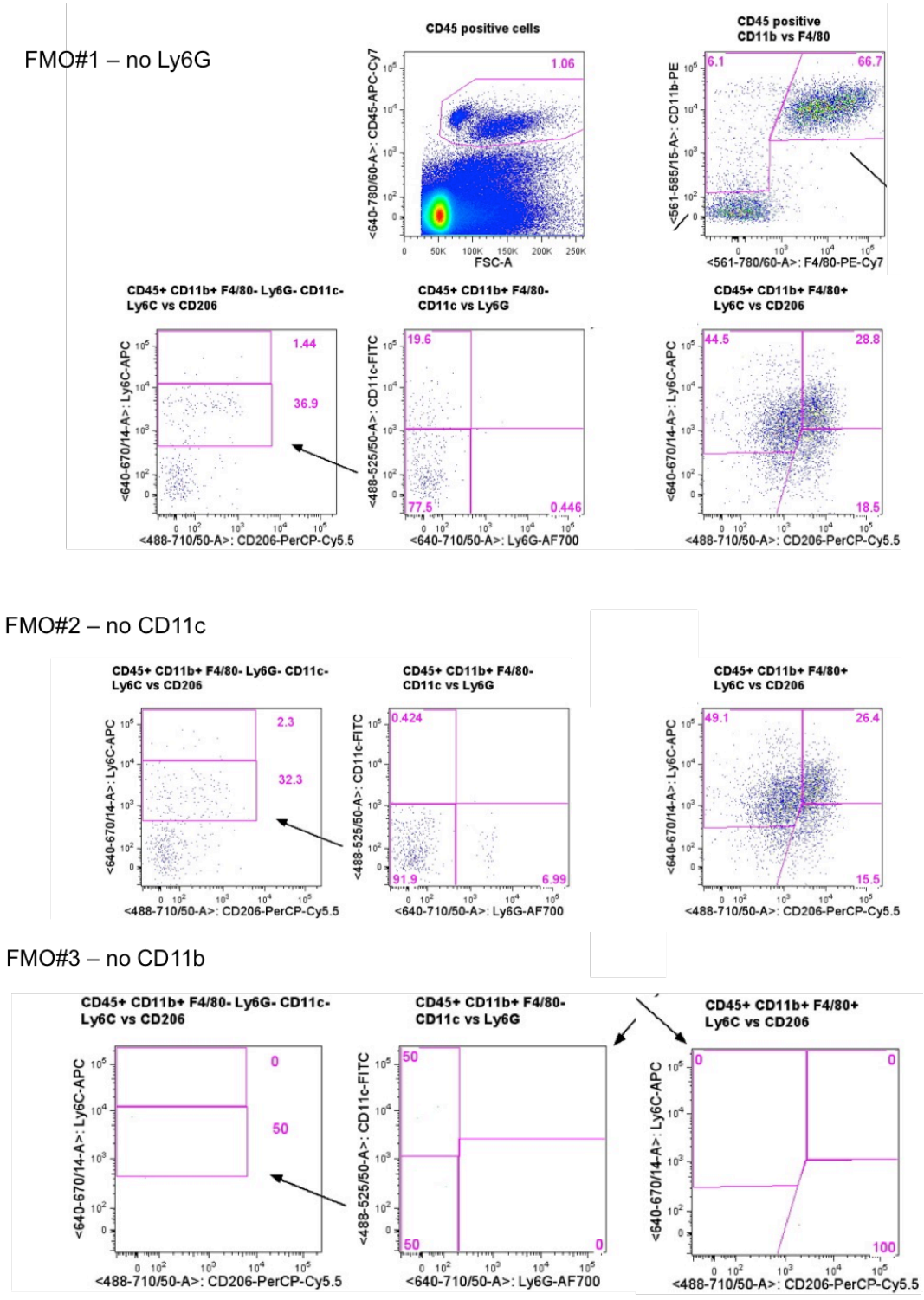


Figure 2.3. Identification of positive stained cells using the Fluorescence Minus One (FMO) strategy for Ly6G, CD11c and CD11b. The FMO strategy was used to appropriately identify positive stained cells and differentiate them from background autofluorescence. Single cell suspensions isolated from hearts of mice uninjured and post-MI were stained with anti-CD11b, -CD45, –Ly-6G, –Ly-6C, -F4/80, -CD206 -CD11c and analyzed by FACS.

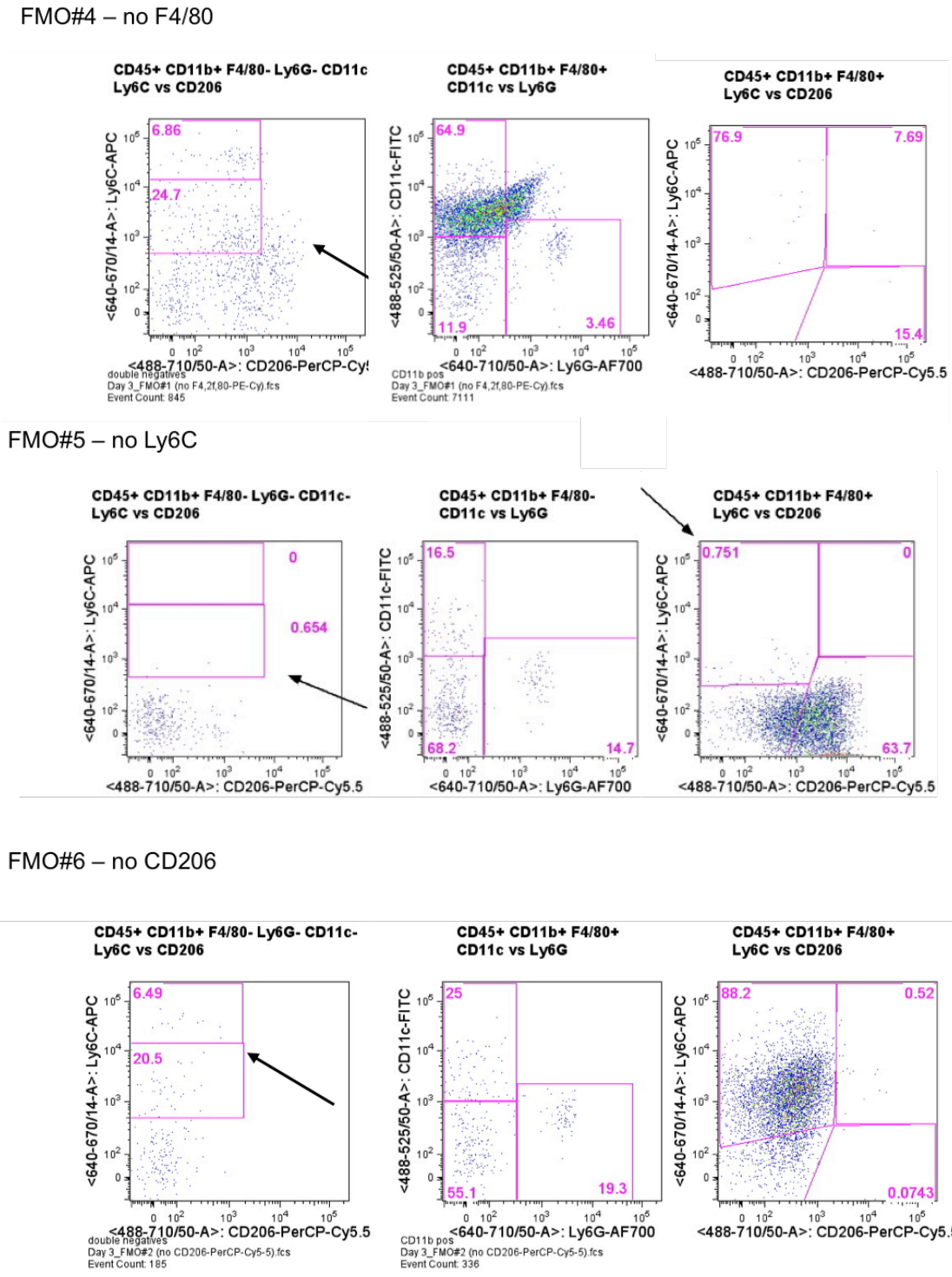


Figure 2.4. Identification of positive stained cells using the Fluorescence Minus One (FMO) strategy for F4/80, Ly6C and CD206. The FMO strategy was used to appropriately identify positive stained cells and differentiate them from background autofluorescence. Single cell suspensions isolated from hearts of mice uninjured and post-MI were stained with anti-CD11b, -CD45, –Ly-6G, –Ly-6C, -F4/80, -CD206 -CD11c and analyzed by FACS.

Immune cells were defined as follows: Total leukocytes (CD45+), neutrophils (CD45+, CD11b+, F4/80-, CD11c-, Ly6G+), monocytes (CD45+, CD11b+, CD11c-, Ly6G-, F4/80-), macrophages (CD45+, CD11b+, CD11c-, Ly6G-, F4/80+) and dendritic cells (CD45+, CD11b+, F4/80-, CD11c+, Ly6G-). Monocytes were further classified as $Ly6C^{high}$ and $Ly6C^{low}$ monocytes on the basis of the Ly6C expression levels. Macrophages were further characterized on the basis of Ly6C and CD206 expression, [i.e. $Ly6C^{high}/CD206^{low}$ (inflammatory macrophages) and $Ly6C^{low}/CD206^{high}$ (reparative macrophages)]. Flow Jo software (version 9. 8.5) (Tree Star, Ashland, OR) was used for analysis.

2.5 Generation and differentiation of bone marrow-derived macrophages

2.5.1 Mouse bone marrow cell isolation

After euthanasia, C57/BL6 mice were sprayed with 70% ethanol and the femurs and tibias from both legs were removed. Fresh muscle was removed using surgical scissors and clean gauze to help with muscle removal. The femurs and tibias were placed in 10 cm plate with cold PBS. Under a tissue culture cabinet, the bones were washed for less than a minute with 70% ethanol. Afterwards, the end of the bones were cut off with scissors and the bone marrow was flushed using a 1 ml syringe filled with RPMI. The fresh bone marrow suspension was homogenized by pipetting up and down then filtered using a 70 μm cell strainer (BD Pharmingen, USA. Cat. 08-771-2) to bring the cells into a single-cell suspension. Finally, cells were counted and cryopreserved (Section 2.5.2) or differentiated into macrophages (Section 2.5.3).

2.5.2 Cryopreservation of mouse bone marrow cells

Isolated bone marrow cells (Section 2.5.1) were centrifuged for 10 minutes at 250g, 5ºC. After centrifugation, cells were resuspended in 1 ml of cell freezing medium at a cell concentration of $6x10^6$ cells/ml (Sigma, UK, Cat. C6164). The freezing aliquots were kept at -80 ºC for a period no longer than 1 month.

2.5.3 Differentiation and culture of bone marrow-derived macrophages (BMdMs)

Freshly or frozen isolated bone marrow cells were plated at a concentration of $6x10^6$ cells per $75cm^2$ flask with 10 ml of differentiation medium containing, RPMI 1640 (Lonza, UK. Cat. BE12-702F/U1) supplemented with 20% FBS (Life technology, Invitrogen, Gibco, UK. Cat. 10270-106), penicillin/streptomycin (P/S) mix (Sigma-Aldrich, Gillingham, UK, Cat. P4333), Sodium pyruvate, 2mM L-glutamine (Sigma, Gillingham, UK. Cat.G8540), 20ng/ml of M-CSF (Preprotech, UK. Cat.AF-315-02), 50μM of β-mercaptoethanol (Sigma, Gillingham, UK. Cat. M6250).

At day 2, another further 10 ml of differentiation medium was added. At day 4, the medium was completely removed and a new fresh 20 ml differentiation medium with half concentration of M-CSF was added. At day 6, the medium was changed to fresh medium with no M-CSF. Finally, at day 7, non-polarized bone marrow-derived macrophages were either stimulated with IL-4 or IFNγ were used for transfection experiments. The schematics of the BMdM differentiation process can be found in Chapter 4, **Figure 4.7A**.

2.5.4 M1/M2 polarization of bone marrow-derived macrophages

At day 7 of differentiation, macrophages were stimulated with 10 ng/ml of IL-4 (Peprotech, UK. Cat. 214-14) to differentiate macrophages towards an M2 phenotype. Alternatively, macrophages were stimulated with 100U/ml of IFN-ϒ (Peprotech, UK. Cat. 200-02) and 1 μg/ml of LPS (Sigma, UK. Cat. L3012) to differentiate macrophage towards an M1 phenotype.

2.5.5 Monocyte isolation from blood and spleen

Monocytes from spleen and blood were isolated from C57/BL6 mice using magnetic CD11b positive selection beads (MACS-Miltenyi biotech, UK. Cat. 130-049-601). To increase the yield prior isolation the cells from spleen and blood were centrifuged on a Bicoll gradient (Biochrome, UK. Cat. L6115), thus the polymorphonuclear (PMN) layer can be obtained. Splenocytes were mashed using the inner rod of a syringe. The suspension was then homogenised by passing the cells through a 70 μm cell strainer (BD Pharmingen, USA. Cat. 08-771-2).

2.5.6 Bone marrow-derived macrophage flow cytometry characterisation.

BMdMs were suspended in 1X Dulbecco's Modified Eagle Medium (DMEM) solution (Gibco, Life technologies, UK. Cat.12491-015) containing, 2% FBS, 10mM HEPES and incubated for 30 min, on ice, in the dark, with the following antibodies:

CD11b-PE (eBioscience, USA. Cat. Cat. 553311), F4/80-APCeF780 (eBioscience, USA. Cat. 47-4801-80), CD45-PECy7 (Biolegend, USA. Cat.1031114), Ly6C-APC (eBioscience, USA. Cat. 17-5932-82) and CD206-488 (eBioscience, USA Cat.53-2069-41). Thereafter, macrophages were centrifuged and washed three times in PBS, 1500rpm for 5 min at 4ºC. All the samples were analysed by flow cytometry on a BD FACS Scan. At least, $1x10^3$ events were collected per sample. Flow Jo software (Version 9. 8.5) (Tree Star, Ashland, OR) was used for analysis.

2.5.7 Bone marrow-derived macrophage CFSE staining

BMdMs were resuspended in a dilution 1:1 of 5 μM CFSE (Life technology, UK, Cat. C34554) in warm serum-free RPMI. Then, incubated for 5 min at 37ºC. Immediately after, BMdMs were put on ice. Precooled RPMI medium was added to dilute the CFSE to reduce cell death. BMdMs were centrifuged, 1500 rpm for 5 minutes at 4ºC, and washed three times in PBS. After centrifugation, BMdMs were used for infusion into mice or for flow cytometry analysis (Chapter 4, **Figure 4.7**).

CellTrace™ CFSE Cell Proliferation Kit, for flow cytometry, (Life technology, UK, Cat. C34554) is widely used for cell tracking and proliferation studies. CFSE readily crosses intact cell membranes. Once inside the cells, intracellular esterases cleave the acetate groups to yield the fluorescent carboxyfluorescein molecule. The succinimidyl ester group reacts with primary amines, crosslinking the dye to intracellular proteins. After the acetate groups are cleaved, it has a peak excitation of 494 nm and peak emission of 521 nm.

2.6 Bone marrow-derived macrophages transfection

BMdMs were transfected using the Amaxa Macrophage Nucleofection Kit (Amaxa Biosystems, USA. Cat. VPA-1009). The day of the experiment 75 cm^2 dishes of BMdMs were washed twice with cold PBS and trypsinased with Trypsin/EDTA solution (Life technologies, UK. Cat. R001100). BMdMs were then incubated for 5 min at 37ºC, then differentiation medium was added to stop the trypsination process. BMdMs were counted and cell density was determined. For transfection, $1x10^6$ BMdMs were resuspended in 100μl of Nucleofector Solution and the appropriate concentration of either pIRES2.eGFP plasmid or pGFP control vector. BMdMs were transferred into a cuvette and placed into the Nucleofector device, Y-001 program. After transfection, the cell suspension was pre-equilibrated with culture medium and gently transferred into a 12-well plate. GFP expression was detected after 2 hours and for up to 72 hours. Optimal BMdMs transfection was determined by comparison with the GFP levels of the control group using the pGFP vector provided by the manufacturer. BMdM-GFP positive cells were also analysed by flow cytometry, on the 488-525/50 laser on a BD FACS Scan. At least, $1x10^3$ events were collected per sample. Flow Jo software (version 9. 8.5) (Tree Star, Ashland, OR) was used for analysis.

2.7 *In vivo* model of cardiac injury

2.7.1 Left descending coronary artery ligation as model myocardial infarction

Myocardial infarction by permanent left coronary artery occlusion was induced in wild-type (WT) and αMHC.IGF-1Ea male mice, 8 to 12 weeks old. Surgeries were performed under mechanical ventilation with 1–2.5% isofluorane. The chest cavity was opened through the left fourth intercostal space. The heart was exposed and the left coronary artery was ligated using 8.0 mm non-absorbable suture (Ethicon-Johnson&Johnson, Germany, Cat. W2808). The coronary artery can be found at 1-2mm below the left atrium, ligation at this point should produce a 20-30% ischemic region. The chest cavity, and skin were sutured using 5.0mm silk sutures (Ethicon-Johnson&Johnson, Germany, Cat. W581). Mortality rate ranged from 20 to 40%, observed between 3 and 5 days in WT mice. Mortality in the αMHC.IGF-1Ea was minimum. Mice received analgesic treatment with buprenorphine (0.3 mg/kg, s.c.) before and after surgery. Mice were housed in individually ventilated cages in temperature-controlled facilities on a 12-hour light/dark cycle on standard diet. All mouse procedures were approved by the Imperial College London Ethical Committee and were in accordance with national and international regulations (UK Home Office Project license 70/7589). A representative picture of an infarcted heart by this method can be found in Chapter 3, **Figure 3.3**.

2.7.2 Ischemia reperfusion injury as a model of myocardial infarction

Myocardial infarction was induced by ischemia-reperfusion (I/R) in C57/BL6 male mice (n=141), 8 to 12 weeks old, obtained from Charles River. Surgeries were performed under general anesthesia with 3–3.5% sevoflurane and mechanical ventilation was provided during the procedure. Mice received analgesic treatment with buprenorphine (0.3 mg/kg, s.c.) after surgery. The infarcts were performed by ligation of the left coronary artery for 45 minutes followed by reperfusion of the artery. The chest cavity was opened through the left fourth intercostal space. The heart was exposed and the left coronary artery was ligated using 8.0mm non-absorbable suture (Ethicon-Johnson&Johnson, Germany, Cat. W2808). The coronary artery can be found at 1-2mm below the left atrium, ligation at this point should produce a 20-30% ischemic region. A plastic canula was employed an knotted along with the left descending coronary artery to facilitate reperfusion. The chest cavity, and skin were sutured using 5.0mm silk sutures (Ethicon-Johnson&Johnson, Germany, Cat. W581). The chest cavity, and skin were sutured with 5.0mm silk sutures (Ethicon-Johnson&Johnson, Germany, Cat.W581). The mortality rate in the first 24 h post-I/R was 38%; no mortality was found afterwards. 1mg/ml of bromodeoxyuridine, BrdU, was administered in the water of all

four groups and renewed every two days. Mice received analgesic treatment with buprenorphine (0.3 mg/kg, s.c.) before and after surgery. Mice were housed in individually ventilated cages in temperature-controlled facilities on a 12-hour light/dark cycle on standard diet. A representative picture of an infarcted heart by this method can be found in Chapter 5, **Figure 5.2**.

2.7.3 Skeletal muscle CTX injury as model for muscle regeneration

Surgical anaesthesia was induced with 3.5-4.5% isofluorane and maintained with 2.5-3% during the procedure. At the beginning of the procedure, mice received analgesic treatment with buprenorphine (0.1 mg/kg, s.c.). Fur was removed and Tibialis Anterior (TA) and quadriceps from 7-8 weeks-old mice were injected with 5µl of cardiotoxin (CTX) at 10µM (Latoxan, France, Cat. L8102). For each TA and quadriceps, 4 and 8 CTX injections of 5µl were perfomed respectively. Muscle samples were harvested at various timepoints after injury. In parallel, TA muscle was embed in paraffin for histological analysis and quadriceps were collected for single cell separation.

2.8 Echocardiography

2.8.1 Transthoracic echocardiography with Vevo 770

Echocardiographic measurements were taken using a high-frequency ultrasound system Vevo 770 (VisualSonics, Canada) with a 30-MHz linear transducer and recorded images were analyzed by using the Vevo 770 workstation software. Mice were anesthetized with 1-2% isofluorane, and the anesthetic flow rate was adjusted to maintain heart rate of approximately 450 ± 50 beats per minute. Furthermore, warmed ultrasound gel and a heating platform were used to maintain body temperature at 37 ± 0.5ºC to minimize variation between mice. The functional analysis was performed at basal level, 1, 3, 5, 7 and 28 days post-MI in anesthetized mice to evaluate left ventricle cardiac function, chamber dimensions, and infarct size. From these analysis, left ventricular end-systolic volume (LVESV), left ventricular end-diastolic volume (LVEDV), left ventricular internal-systolic diameter (LVIDS), left ventricular internal-diastolic diameter (LVIDD), left ventricular posterior wall in diastole (LVPWD), left ventricular posterior wall in systole (LVPWS), left ventricular ejection fraction (LVEF) and fractional area change (FAC) were acquired to perform the analysis

2.8.2 Transthoracic echocardiography with Vevo 2100

Echocardiographic measurements were taken, by a blinded operator, using a high-frequency ultrasound system Vevo 2100 (VisualSonics, Inc) with a 30-MHz linear

transducer and recorded images were analysed by a second blinded operator using the Vevo 2100 workstation software. Transthoracic echocardiography was performed at baseline, 3 and 28 days post-I/R injury in anesthetized mice to evaluate LV cardiac function, chamber dimensions, wall thickness, infarct size and wall motion. Mice were anesthetized with 1-2% isoflurane in oxygen, the anesthetic flow was adjusted to maintain heart rate in approximately 450 ± 50 beats per minute. Furthermore, warmed ultrasound gel and a heating platform were used to preserve body temperature around 37 ± 0.5ºC to minimize variation among mice. Standard 2D and M-mode parasternal long and short axis (at mid-ventricle) views were obtained to assess left ventricular function and chamber dimensions. From these modes, left ventricular end-systolic volume (LVESV), left ventricular end-diastolic volume (LVEDV), left ventricular end-systolic diameter (LVESD), left ventricular end-diastolic diameter (LVEDD) and left ventricular ejection fractional (LVEF) were acquired to perform the analysis.

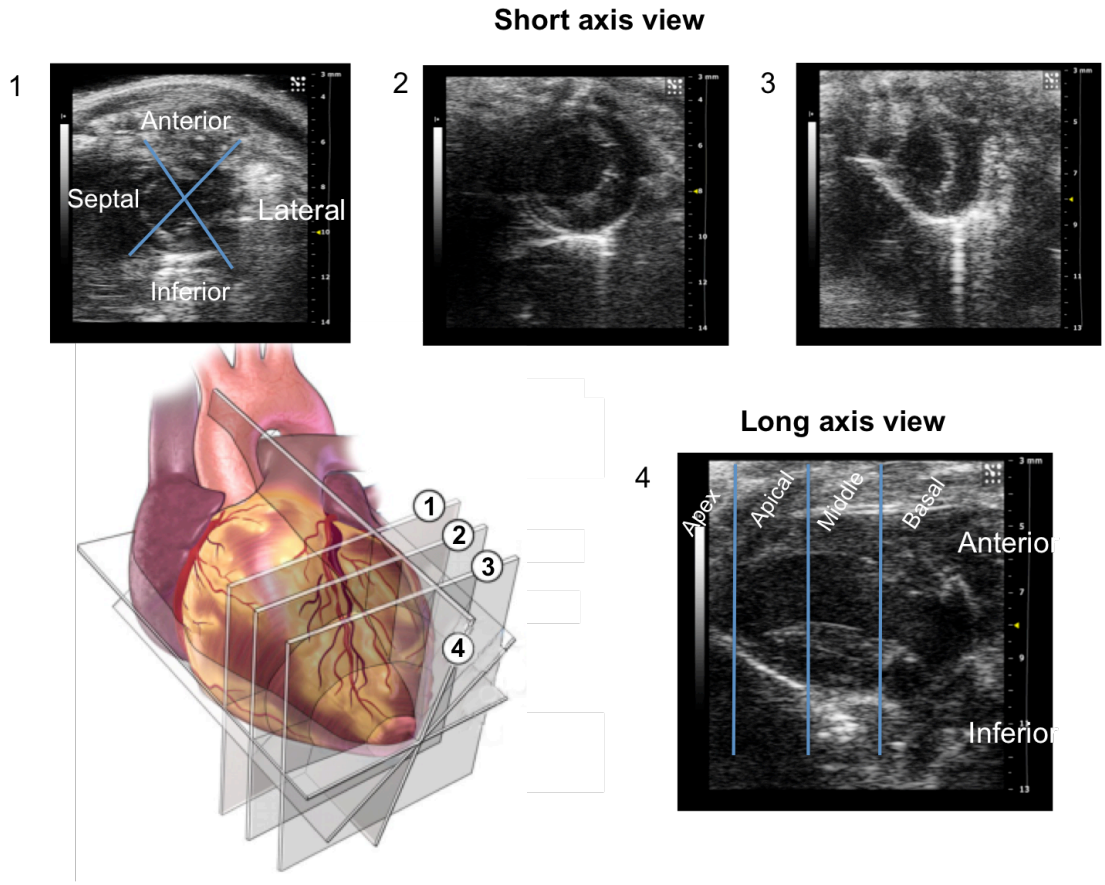


Figure 2.5. Echocardiographic representation of parasternal short and long axis orientation and schematics of LV walls. Global and regional cardiac function was assessed by a 12-based segment model, considering 2D short axis views at 3 levels (base, middle and apex). In each level, the left ventricle was divided in 4 segments (anterior, lateral, inferior and septal) and each segment was score according to the American Society of Echocardiography (Lang et al. 2005). Segment analysis and motion can be found in Chapter 5, **Figure 5.7**.

Left ventricle wall motion score index (WMSI) was calculated in order to assess global and regional cardiac motion by a 12-based segment model, considering 2D short axis views at 3 levels (base, middle and apex). In each level, the left ventricle was divided in 4 segments (anterior, lateral, inferior and septal) and each segment was scored according to the American Society of Echocardiography (1: normal, 2: hypokinetic, 3: akinetic, 4: dyskinetic and 5: aneurysmal) (Lang et al. 2005)(**Figure 2.5** and Chapter 5, **Figure 5.7**).

WMSI is defined as the ratio of the sum of scored individual segment over the total number of segments evaluated. Infarct size was also estimated considering the mean score of individual segments. Only mice that presented two or more cardiac segments with altered motion plus a left ventricular ejection fraction below 45% at 3 days post-surgery were selected for the study. All measurements were carried out in accordance with the recommendations for chamber quantification from the American Society of Echocardiography in conjunction with the European Association of Echocardiography (Lang et al. 2005).

2.9 Histology of paraffin-embedded tissue

After sacrifying the mice, the hearts were perfused with PBS and KCL-arrested-perfused hearts samples were fixed in paraformaldehyde (4% in PBS) for 48h, washed in PBS, dehydrated, and included in paraffin.

2.9.1 Masson's Trichrome Staining

Five-micron thick sections were stained following Masson's trichrome protocol (Masson trichrome Staining reagents, Sigma, UK, Cat. HT15-1KT). Paraffin sections were stained with celestine blue for 5 minutes, washed in tap water, and incubated in haemotoxylin for 5 minutes. Slides were incubated with fucsin acid for 5 minutes, rinsed quickly in distilled water and differentiated in phosphomolybdic acid (1%) for 3-5 minutes. After that, slides were rinsed briefly in water and stained in methyl blue for 2-3 minutes. Finally, slides were washed briefly with distilled water and dehydrated in ascending series of Methanol, cleared in xylene and mounted in DPX (VWR, UK. Cat. 100504-938).

2.9.1.1 Determination of scar length and total fibrosis

Scar length, as method for the quantification of infarct size, was determined in Masson's trichrome-stained sections by using the midline method, which best correlates with functional measurements (Takagawa et al. 2007 and Lopez-Olaneta et al. 2014). In this method, the infarct size is measured as the length of the midline of the infarcted wall, in

which 50% of the wall thickness is composed of scar tissue. Scar length represents the percentage of infarct length with respect to the whole length of the left ventricular circumference. Total fibrosis was quantified in whole heart images obtained at the middle section by ImageJ software (NIH, USA) .

2.9.2 Picrosirius red staining

Five-micron thick sections were stained with Weigart's haematoxylin for 10 minutes followed by a wash in tap water. Sections were incubated with 1% Molybdophosphoric acid for 20 minutes, after a brief wash in distilled water sections were incubated with Sirius red solution for 60 minutes. Slides were washed with distilled water and dehydrated in ascending series of Methanol, cleared in xylene and mounted in DPX.

2.9.3 Heart immunohistochemistry

Prior to immunoperoxidase staining, five-micron thick sections were washed in PBS for 5 minutes. The slides were then immersed in 0.1M citrate buffer (pH 6) and microwaved for 10 minutes before blocking for endogenous peroxidases using 0.3% hydrogen peroxide in PBS for 10 minutes. Sections were washed 3x5 minutes each in PBS and blocked with 3% bovine serum albumin (W/V) (BSA) in PBS for 30 minutes. Sections were incubated separately overnight with the antibodies described below.

The primary antibodies used were, IGF-1 (Sigma, UK. Cat. I-8773) antibody 1:100 dilution, anti-α-smooth muscle actin (Abcam, UK. Cat. Ab5694) 1:400 dilution, and anti-Luciferease (Promega, USA. Cat. -G7451) 1:300 dilution was used. Vessels were quantified by anti-α-smooth muscle actin (αSMA, Sigma, UK, Cat. A5228) 1:200 dilution was used. Mitosis and cell division was quantified by Anti-Phospho-Histone H3 (Ser10) (Cell Signalling, UK, Cat.9701) in a 1:200 dilution.

Primary antibodies were removed by washing the sections 3 times with PBS followed by a second incubation of Biotinylated anti-goat immunoglobulin (Vector laboratories, UK. Cat. I-5000) diluted 1/250 in PBS for 1 hour following 3 times washes in PBS before 1 hour incubation with Avidin-Biotin (Vector laboratories, UK. Cat. PK-4000). Reactivity was detected by using diaminobenzidine tetrahydrochloride (DAB tablets-25mg/ml) (Sigma, UK Cat. D4293) and hydrogen peroxide (0.01% W/V). Sections were then counter stained with haematoxylin and viewed on Ziess Axioskop microscope.

The number of vessels was determined counting the number of αSMA+ vessels divided by the infarct area. Images were digitalised by using a NanoZommer (Hamamatsu, UK) and further quantified by using ImageJ software (NIH, USA).

2.9.4 Heart immunofluorescence

Prior to immunoperoxidase staining, five-micron thick sections were washed in phosphate buffered saline (PBS) for 5 minutes. The slides were immersed in 0.1M citrate buffer (pH 6) and microwave for 10 minutes before blocking for endogenous peroxidases using 0.3% hydrogen peroxide in PBS for 10 minutes. Sections were washed 3x5 minutes each in PBS-Triton 0.3% and blocked with blocking solution (3% bovine serum albumin (W/V) (BSA), 20mM $MgCl_2$, 0.3% Tween, 5% goat serum in PBS) for 1 hour at RT. Samples were also blocked with Avidin/Biotin blocking kit (Vector Labs, USA, SP-2001). After incubation with the primary antibody, sections were washed 3x5 minutes each in PBS-Triton 0.3% and incubated O/N at 4°C.

For BrdU and troponin I immunofluorescence were performed with the following antibodies: Mouse anti-BrdU 1:30 dilution (BD Bioscience, USA, Cat. 347580). Rabbit Anti-cardiac troponin I at 1:100 dilution (Abcam, UK, Cat. ab 47003).

The following day, the slides were incubated with biotinylated anti-rabbit secondary antibody 1:100 (Jackson Immuno Research, USA, Cat.111-066-003) for 1 hour at RT. Finally, slides were incubated with anti-mouse streptavidin-Alexa 488 1:200 (ThermoFisher, USA, Cat. A-11029) and anti-biotin Streptavidin-Cy3 1:200 (Jackson Immuno Research, USA, Cat. 016-160-084). Sections were washed 3x5 minutes each in PBS and DAPI in a 1:1000 dilution. Slides double-stained with anti-BrdU and anti-troponin I were assessed by Zeiss LSM Confocal Microscope System.

2.10. Amplification and purification of IGF-1Ea vector from *E.coli*

The pIRES2.eGFP, in Chapter 4, containing the *Mus musculus* IGF-1Ea consensus cDNA sequence was obtained from Nadia Rosenthal's glycerol stocks. The pIRES2.eGFP vector is a bi-cistronic gene expression cassette, which contains a Kanamycin/Neomycin resistance gene (Kan-Neo). These two genes confers the bacterial host with resistance to each antibiotic allowing artificial selection of those bacterial cells containing the plasmid. In this plasmid, gene expression is driven by the cytomegalovirus promoter (CMV), which regulates the expression of the IGF-1Ea gene and eGFP reporter gene. Transcription ends at a SV40 polyA terminator signal (**Figure 2.6A**).

pIRES2.eGFP glycerol stock of One Shot® TOP10 Chemically Competent *Escherichia coli* (*E. coli*, Invitrogen, USA. Cat. C404010) containing IGF-1Ea plasmid was reactivated by inoculation of 60 µl of glycerol stock into 3 ml of Luria-Bertani, LB, (Sigma, UK. Cat. L3522) and 30 µg/ml of Kanamycin (Sigma, UK. Cat. K1377). After O/N culture at 37 ºC, the bacterial grow was divided and 1 ml was plated into LB Agar plate with Kanamycin, 1 ml was stored as glycerol stock. Finally, the remaining 1 ml was used for isolating the plasmid. The construct was isolated using QIAGEN Plasmid Mini or Midi Kit (QIAGEN, UK. Cat. 12143 and 12123, respectively) according to the manufacture's protocol.

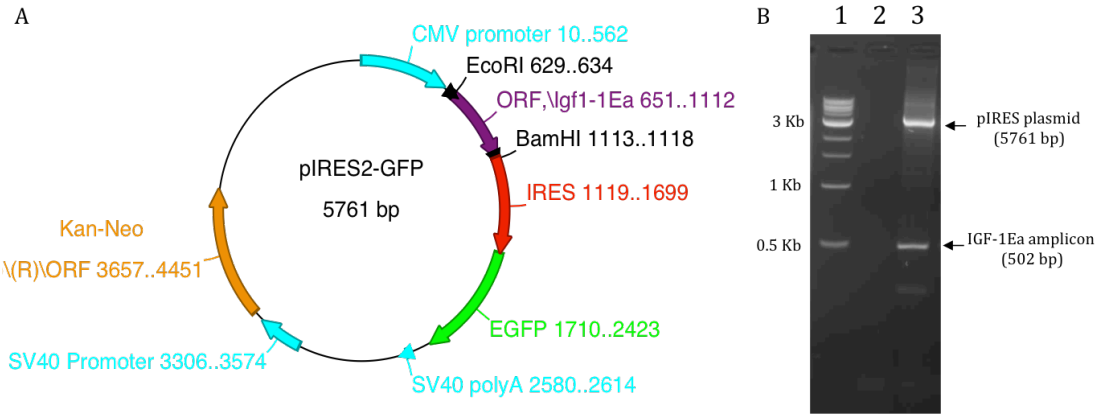


Figure 2.6. Schematic illustration of pIRES2.eGFP backbone and IGF-1Ea PCR product. (A) IGF-1Ea is flanked by the restriction sites EcoRI and BamHI. (B) Amplification of the IGF-1Ea from the pIRES2.eGFP by high efficiency PCR. Lane 1, 1 Kb DNA ladder. Lane 2, negative control. Lane 3, IGF-1Ea amplicon.

2.11 IGF-1Ea cloning strategy: from pIRES2.eGFP to pAAV9.IGF-1Ea

In Chapter 5, the *Mus musculus* IGF-1Ea consensus cDNA sequence was subcloned from the pIRES2.eGFP (Section 2.10) into the destination vector pAC-cTNT (provided by Dr. Juan Bernal, CNIC, Madrid, Spain). The pAC-cTNT plasmid (not shown), later named pAAV9.IGF-1Ea (**Figure 2.7A**), contains all the elements allowing plasmid replication in bacteria as well as serve as viral genomic payload of adeno-associated viral vehicle. The pAC-cTNT plasmid is a bi-cistronic gene expression cassette which expression is driven by the cardiac troponin promoter (cTNT) and an internal ribosomal entry site (IRES) followed by the firefly luciferase reporter gene. The pAC-cTNT also contains SV40 polyA signal and the bi-cistronic cassette is flanked by inverted terminal repeats (ITR), shown as hairpin loops (**Figure 2.7A**). For bacterial amplification, the pAC-cTNT vector also contains a SV40 replication promoter and the Ampicilin resistance gene that confers to the bacterial host resistance to the antibiotic.

The cloning strategy was designed based on the restriction enzyme sites present in the pAC-cTNT limited to EcoRI and NotI restriction sites. Consequently, IGF-1Ea cloning strategy is a two-step cloning strategy as follows, (i) PCR amplification of *Mus musculus* IGF-1Ea consensus sequence in the pIRES2.eGFP by high efficiency PCR with primers containing EcoRI and NotI restriction sites (Section 2.11.1) and (ii) cloning of the IGF-1Ea insert into the plasmid pAC-cTNT destination vector (Section 2.11.2).

2.11.1 Amplification and purification of IGF-1Ea PCR product

The IGF-1Ea sequence, from pIRES2.eGFP, was amplified using the components and PCR cycle described in **Table 2.3.** In order to avoid mutations during IGF-1Ea PCR amplification, Platinum® Pfx High fidelity DNA polymerase. The following primers, showing in bold EcoRI and NotI restriction sites were used:

Forward primer: 5'-GCTTC**GAATTC**TGCAGTCGACGC-3'. In bold, EcoRI sequence.

Reverse primer: 5'-CC**GCGGCCGC**CTACATTCTGTAGG -3'. In bold, NotI sequence.

Component (final concentration)	**Volume (µL) 50 µL reaction**	**Thermocycler conditions 35 cycles**
DNA template (200ng)	1	
$MgSO_4$(1mM)	3	5 min at 94°C
Pfx Amplification Buffer (1X)	5	35X 15 sec at 94°C
dNTPs (0.3mM each)	1.5	30 sec at 55°C
Primer mix (0.3µM Each)	1.5	1 min sec at 68°C
Autoclaved, distilled water	35	10 min at 72°C
***Platinum Pfx DNA polymerase* (1unit/µL)**	0.4	∞ 4°C
PCR Enhancer solution	5	

Table 2.3. Components and thermocycler conditions for IGF-1Ea PCR. Agarose gel electrophoresis (2%) was used to run the PCR product at 100 Volts to verify that a single, discrete band of the correct size was present. Platinum® Pfx High fidelity DNA polymerase was used (Invitrogen ®, UK, Cat No. 11708-013).

The IGF-1Ea PCR product (462 bp) was then subcloned into the pAC-cTNT. After PCR amplification (**Figure 2.6B**) of IGF-1Ea and before cloning into the pAC-cTNT, the PCR product was purified according to the manufacturer's protocol using the QIAquick® Kit (QIAGEN, UK. Cat. 28104). The PCR purification kit is based on a bind-wash-elute procedure where impurities such as primers, nucleotides, enzymes, minerals, oils, salts, which may inhibit the restriction enzyme digestion process, are washed away and pure DNA is eluted with a small volume of water.

2.11.2 IGF-1Ea PCR product digestion and ligation into the pAC-cTNT

Following IGF-1Ea PCR amplification and purification, both the PCR insert and the pAC-cTNT destination vector were digested for 1 hour with EcoRI and NotI restriction enzymes as described in **Table 2.4**.

REAGENT	AMOUNT (µL)
Plasmid DNA	1 µg
EcoRI	1 µL
NotI	1 µL
NEBuffer CutSmart*	5 µL
Total reaction volume	50 µL
Incubation Temperature	37°C
Incubation time	1 hour
Inactivation	65°C – 20min.

Table 2.4. IGF-1Ea plasmid and pAC-cTNT restriction enzyme digestion protocol. *CutSmart: 50mM Potassium Acetate, 20mM Tris-acetate, 10mM Magnesium Acetate and 100µg/ml BSA (pH 7.9 at 25°C). EcoRI (New England BioLabs, USA. Cat. R0101S). NotI (New England BioLabs, USA. Cat. R0189S)

The digestion process generated cohesive 5' and 3' ends in both the pAC-cTNT plasmid and the IGF-1Ea insert. Therefore, in order to facilitate the cloning of the insert in the vector, T4 ligase was used. T4 ligase seals the nicks between adjacent residues of the double-strand break by forming a phosphodiester bond between the 3' hydroxyl and 5' phosphate of adjacent DNA residues. Restriction enzyme digested products, IGF-1Ea insert and pAC-cTNT vector, were ligated as described in **Table 2.5**.

REAGENT	AMOUNT (µL)
Insert:Vector ratio	3:1
Ligase Reaction Buffer	4 µL
Total DNA	<100ng
T4 DNA Ligase	0.1 Units
Distilled water	Up to 20 µL
Incubation temperature	23-26°C
Incubation time	1h – O/N

Table 2.5. Ligation protocol. T4 DNA ligase kit (Life technologies, Thermo Fisher Scientific, UK. Cat. 15224-017).

The final product is the pAAV9.IGF-1Ea plasmid shown in **Figure 2.7**.

2.11.3 One Shot® Stbl3 Transformation

The pAAV9.IGF-1Ea plasmid (**Figure 2.7**) was then used to transform STBL3 competent cells. This step is required to obtain a reasonable amount of pAAV9.IGF-1Ea for downstream protocols.

Transformation was performed according to the manufacturer's protocol using the One Shot®Stbl3™ Chemically competent *E.Coli* (Invitrogen, USA. Cat. C7373-03) using the heat-shock technique (42°C for 45 seconds and then immediately placed on ice). After transformation, the cells were seed on a pre-warmed Ampicilin resistant plate and incubated O/N at 37°C. This particular strain of *E.Coli* is recommended when cloning vectors with inverted terminal repeats (ITR). The strain has been designed to reduce the frequency of homologous recombination preventing intermolecular recombination of the ITR regions, which may compromise vector integrity. As described in the Introduction, Section 1.4.2.2, ITR regions facilitate recombination and DNA packing into the viral vehicle (**Figure 2.8**).

The following day, one half of positive resistant colonies were incubated in 2ml of LB medium, and the other half of the colony was screened for positive insert/plasmid insertion. The screening was performed by PCR for the IGF-1Ea gene and by digesting the vector as described in Sections 2.11.4 and 2.11.5.

2.11.4 Amplification of positive clones, bacterial amplification and plasmid isolation

After O/N culture, the pAAV9.IGF-1Ea plasmid was isolated using QIAGEN plasmid purification Kit according to the manufacturer's instructions (QIAGEN, UK. QIAprep Spin Miniprep Kit Cat. 27106 and Endofree Plasmid Maxi Kit. Cat. 12362). Purified plasmids were eluted with sterile milliQ water and stored at -20°C. The DNA yield was quantified by Nanodrop® (Thermo Scientific, Wilmington, USA) measuring absorbance at 260 nm and 280 nm.

2.11.5 Confirmation of correct IGF-1Ea cloning: PCR and restriction enzyme digestion

In order to verify the correct cloning of the IGF-1Ea insert into the pAC-cTNT destination vector, the DNA was digested using EcoRI and NotI as described in **Table 2.5.** Following endonuclease digestion, 20µL of plasmid was mixed with 6X loading buffer (New England Bio Labs, USA, Cat. B7021S) and loaded on a 1.5% agarose gel as shown **Figure 2.7B**. The digested IGF-1Ea product band observed indicates successful cloning.

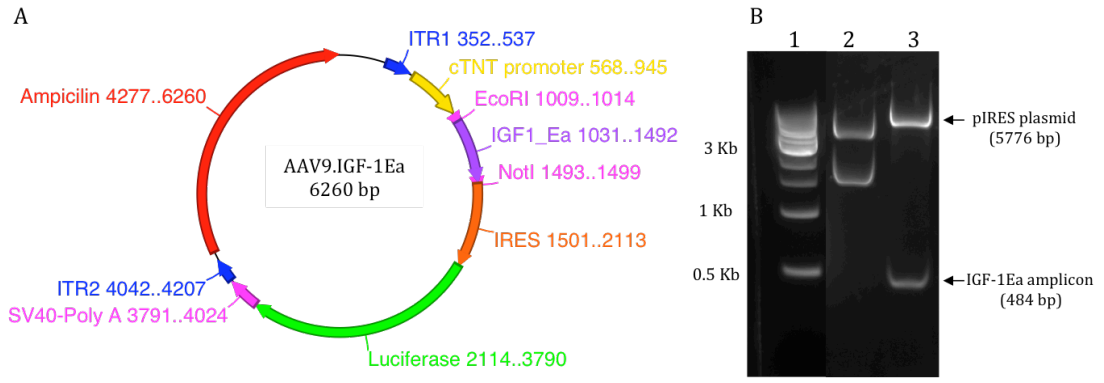


Figure 2.7. Schematic illustration of pAAV9.IGF-1Ea vector backbone and IGF-1Ea restriction enzyme digestion. (A) IGF-1Ea was cloned inside a pAAV9.IGF1Ea under the control of the cardiac troponin promoter. A bi-cistronic gene expression cassette with allows the expression of IGF-1Ea and luciferase via an internal ribosomal entry site (IRES). Transcription ends by a SV40 polyA terminator signal. The IGF-1Ea gene is flanked by the restriction sites EcoRI and NotI. The vector also contains an ampicilin resistance gene that confers to the bacterial host antibiotic resistance. (B) Cloning validation of the recombinant pAAV9.IGF-1Ea plasmid vector by EcoRI and NotI digestion. Lane 1, 1 Kb DNA ladder. Lane 2, original pAAV9 with another GOI. Lane 3, restriction enzyme digestion with the IGF-1Ea gene. 1 Kb plus DNA ladder™ (Invitrogen, USA. Cat. 10787018). EcoRI (New England BioLabs, USA. Cat. R0101S). NotI (New England BioLabs, USA. Cat. R0189S).

2.11.6 pIRES.eGFP and pAAV9.IGF-1Ea sequencing

For sequencing, 150ng per Kb (500-600ng for plasmid over 3Kb), 1 µl of sequencing primer (at ~3.2 pmole) and water was added up to a final volume of 10 ul. Sequences were sent to the MRC sequencing facility. ApE software (http://biologylabs.utah.edu/jorgensen/wayned/ape/) was used for the analysis and comparison of the sequences.

For the pIRES.eGFP, the following primers flanking the IGF-1Ea were designed:

IGF-1 forward primer: 5'-CGTCTTCACACCTCTTCTACC-3'

IGF-1 reverse primer: 5'-GGTAGAAGAGGTGTGAAGACG-3'

For the pAAV9.IGF-1Ea, primers were design to cover the DNA region from ITR1 to ITR2 (**Figure 2.7**), which is the region that will be incorporated inside the adeno-associated viral vehicle, thus, no mutation will pass onto the viral production step.

The primers sequence used for sequencing based on pAAV9.IGF-1Ea backbone, **Figure 2.7A,** were the following:

5' ITR1 forward primer: 5'-GGTGTCGGGGCTGGCTTAACTATGC-3'

5' cTNT forward primer: 5'-CAGTCTGGGCTTTCACAAGACA-3'

5' IGF1.1 forward primer: 5'-GCACATTCCTGCTGGCTCTGCC-3'

3' IGF1.1 reverse primer: 5'-CACTAGTCCAGTGTGGTGGAAT-3'

5' ITR2.1 forward primer: 5'-CCGAAAGGTCTTACCGGAAAAC-3'

5' ITR2.2 forward primer: 5'-GTCGACCGTAGATAAGTAGCATGGCG-3'

Samples for sequencing were submitted to the MRC sequencing facility. Only those samples with no mutations, inverted or deleted regions neither at promoter nor at IGF-1Ea gene level, were carried forward for viral production.

Most importantly, I experienced serious difficulties when sequencing the ITR regions, which delayed the project for months. I seek the assistance of MRC facility people that eventually allowed me to properly sequence the ITR regions and make sure that no mutations were carried forward. The approach is described in the following section.

2.11.7 Sequencing GC-rich regions of the ITRs

As described in the Introduction, section 1.4.2.2, the inverted terminal repeats (ITRs) flanking the pAAV9.IGF-1Ea genome are repeated DNA regions with high GC-rich content forming strong hydrogen bounds and secondary structures, which prevents proper amplification (**Figure 2.8**). These regions are not easily denatured during the sequencing process.

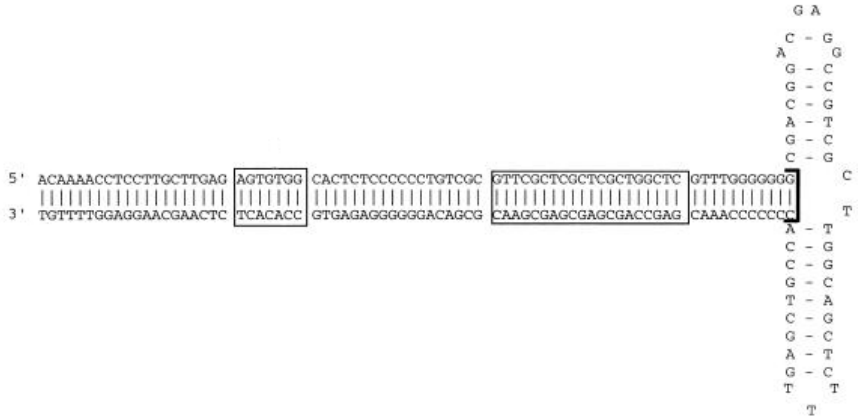


Figure 2.8. Predicted structure of the inverted terminal repeats (ITR) in the pAAV.IGF-1Ea. 3D T-shape structure of the ITR after AAV9.IGF-1Ea delivery into the heart. In the pAAV.IGF-1Ea plasmid, ITR sequences are linear sequences flanking the IGF-1Ea at 5' and 3' (**Figure 2.7**). Inside the virus AAV9, at each end of the genome the ITR form 3D T-shape structures (Chapter 5, **Figure 5.2**).

At MRC facility, we came up with the idea of amplifying the ITR regions by PCR prior to sequencing rather than sending the whole plasmid (Kieleczawa et al. 2006). Therefore, a new protocol was designed to improve amplification efficiencies. A new polymerase, TaKaRA La Taq® (Clontech, France. Cat. RR013A) was used as described to be more efficient when amplifying DNA targets with high GC content. Besides the high efficiency of the TaKaRA La Taq® polymerase, 7-deaza-dGTP was used instead of dGTP. The structure of this GTP analogue stabilizes the hairpin and prevents compressions of the DNA during the amplification phase. The components and the PCR cycle are described in **Table 2.6.**

After ITR PCR amplification, the sample was purified from enzymes and nucleotides. For that, ExoSAP mix, containing 1U each of FastAP and ExoI, was added directly to the PCR tube. The components and reaction protocol is described in **Table 2.7**. For ITR amplification the following primers were used:

ITR1 forward primer: 5'-GGTTCAGGGGGAGGTGTGGGAGG-3'
ITR1 reverse primer: 5' GGAAGCGGAAGAGCGCCCAATAC-3'
ITR2 forward primer: 5'-TGGCTTAACTATGCGGCATCAG-3'
ITR2 reverse primer: 5'-CCAGCCTTTTGTCACCTCCCAG-3'

ITR regions were then sequenced as described in Section 2.11.6 with the same primers as described above.

Component (final concentration)	**Volume 50 µL reaction**	**Thermocycler conditions 35 cycles**
DNA template (100ng)	1 µL	1 min at 94°C
GC Buffer I	25 µL	30X 30 sec at 94°C
dNTP mixture* 400µM each	8 µL	30 sec at 60°C
Primer mix (0.2-1 µM each)	10-50 pmol	1 min at 72°C
Autoclaved, distilled water	10-50 pmol	5 min at 72°C
TaKaRa LA Taq	Up to 50 µL	∞ 4°C
(2.5 units/50µl)	0.5 µL	

Table 2.6. GC- rich PCR components. * 7-deaza-dGTP: 75% 7-deaza-dGTP and 25% dGTP.

ExoSAP Mix Final Concentration	Final volume (30 µL)	Thermocycler conditions
Water	37 µL	
10x SAP Buffer	30 µL	37˚C, 45 min
Exonuclease I (20 U/ µL)	8 µL	80˚C, 15 min
FastAP (1 U/ µL)	25 µL	4˚C hold

Table 2.7. ExoSAP sequencing protocol components. For each PCR, 5µl of ExoSAP mix was added. Exonuclease I (New England BioLabs, Ipswitch, MA, USA. Cat. M0293S) was used to remove overhanging and single stranded DNA fragments. (B) FastAP Thermosensitive Alkaline Phosphatase (Thermo Scientific, Wilmington, USA. Cat. EF06511000) was used to remove the primers, and to dephosphorylate the DNA and dNTPs.

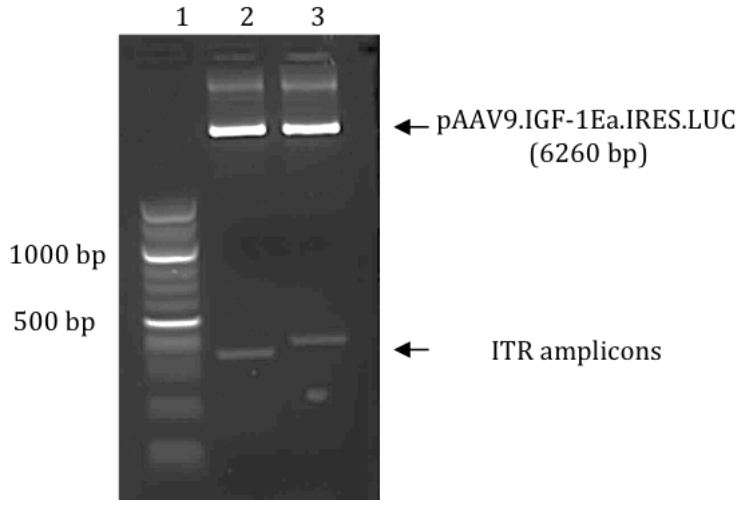


Figure 2.9. ITR PCR product agarose gel. 1.5% Agarose gel showing the ITR PCR product. Lane 1, 100 bp ladder. Lane 2, 5'ITR1 expected size 434 bp. Lane 3, 3' ITR2 expected size 382 bp. Quick-Load® 100 bp DNA Ladder (New England BioLabs, Ipswitch, MA, USA. Cat. N0467S).

2.11.8 pAAV9.IGF-1Ea vector quality control, construction, production, and purification

As described in Section 2.11.2, *Mus musculus* IGF-1Ea consensus sequence was ligated into the pAC-cTNT backbone and construct integrity was confirmed by restriction enzyme digestion and sequencing. AAV9 viruses were produced and purified by Penn Vector Core at the University of Pennsylvania (Gao et al. 2006). Prior packing, the vector was subjected to a series of digestion enzyme quality controls in order to check for vector integrity (**Appendix 1**). The vector was later subjected to genome titrations, sodium dodecyl sulfate–polyacrylamide gel electrophoresis analysis for purity, and transgene expression analysis in HL-1 cells.

2.12 In vivo injections of both GFP- and CFSE-macrophages after CTX injury

CTX injured mice received 1-2 x 10^6 BMdMs/50µl injected intravenously, 24 hours after CTX injury. BMdMs were labelled with either GFP, as described in Section 2.6, or with CFSE.

2.13 AAV9.IGF-1Ea *in vivo* gene transfer

Five hours after ischemic injury, mice were anesthetized with 1.5–2.5% sevoflurane and 50µl of AAV9 virus (in saline) was injected intravenously through the femoral vein using a 29-gauge insulin syringe. AAV9 treatment was performed as follows: one group received 3.5x10^{11} genome copies (GC) of AAV9.GFP as AAV control. For the IGF-1Ea gene transfer, two different viral titers were administered, 3.5x10^{10} GC and 3.5x10^{11} GC of AAV9.IGF-1Ea. After post-viral transfer IGF-1Ea levels were determined by qTR-PCR and western blot.

2.13.1 IVIS - Bioluminescence analysis of in vivo gene transfer

Mice were anesthetized with 1.5-2% isoflurane in oxygen. D-luciferin (Promega, USA. Cat. E1601) at 100 mg/kg in saline was administered to mice via intraperitoneal injection (i.p). 5-10 minutes after D-luciferin administration, all mice were imaged in supine position using a Xenogen IVIS100 imaging system (Caliper Life Sciences, Hopkinton, MA, USA). Organs were immersed in D-luciferin for 1 min and bioluminesce was imaged immediately after using the IVIS 100 imaging system. Images were processed using Living Image software (Caliper Life Sciences). Mean luminescence intensities (photons/s·cm2·sr) were measured from the regions of interest over the mouse hearts.

2.13.2 Detection of serum IGF-1 protein

In Chapter 5, the sera from I/R, AAV9.GFP and AAV9.IGF-1Ea groups were purified for measurements of total IGF-1 using a commercially available ELISA kit specific for rodent IGF-1 (Peprotech 900-K170). IGF-1 serum levels were based on a standard curve generated from recombinant mouse IGF-1, according to the manufacturer's protocol. The assay can accurately detects IGF-1 concentrations ranging from 62–6,000 pg/ml.

2.14 Statistics

In Chapter 3, Two-tailed Student's *t*-test was performed to compare WT vs αMHC.IGF-1Ea at selected time points after MI.

In Chapter 4, One-way ANOVA followed by Dunnett's post-test at different conditions.

In Chapter 5 the following statistical packages were used: One-way ANOVA with Dunnett's Multiple Comparison post-test to compare I/R vs AAV9.GFP, AAV9.IGF-1Ea groups. Two-way ANOVA to compare the 4 groups with Bonferroni post-tests. Two-way ANOVA to compare 3 days vs. 28 days with Bonferroni post-tests. Group differences in qRT-PCR and histological quantifications were analysed by one-way ANOVA followed by Dunnett's post-test to untreated mice. Vessels were analysed by Student's t-test.

Data is presented as mean ± SEM. Data was analyzed with GraphPad-Prism 5.0 (Graphpad Software, Inc., www.graphpad.com), and differences were considered statistically significant at $P < 0.05$.

Chapter 3 – Study of IGF-1Ea-mediated inflammatory response and extracellular matrix remodeling after myocardial infarction in αMHC.IGF-1Ea

3.1 Introduction

After myocardial infarction, the damaged myocardium releases inflammatory signals that trigger a cascade of cellular processes in order to repair damaged tissue, leading to the formation of scar tissue and left ventricular (LV) dysfunction (Introduction, Section 1.3.2). Tissue restructuring after infarction involves the breakdown of the ECM by proteolytic enzymes, mainly the metalloproteinases MMP-2 and MMP-9, balanced by interaction with tissue inhibitors of metalloproteinases (TIMPs)(Vanhoutte et al. 2006). Initially a temporary matrix is formed, primarily composed of collagen type III (Col Iα3), providing a scaffold for the replacement of cells and structural integrity to the heart, thereby reducing the risk of LV dilation and rupture (Caulfield et al. 1979 and Jugdutt et. al. 2003). This is later replaced by collagen type I (Col Iα1) which will constitute the permanent ECM (Jugdutt et al. 2003). Col Iα1 confers tensile strength and resistance to stretch and deformation, while Col Iα3 confers compliance. Their balance determines cardiac tissue stiffness with increased Col Iα3 to Col Iα1 ratio generating a more resilient left ventricle (Jugdutt et al. 2003 and Jugdutt et al. 2003). The newly formed scar tissue acts as scaffold in order to preserve cardiac function due to the loss of contractile myocardium.

Innate immune cells recruited to the injured myocardium from the blood include neutrophils, monocytes, macrophages and dendritic cells (Nahrendorf et al. 2013, Leuschner et al. 2012 and Yan et al. 2013). These cells play a prominent role in remodeling, producing the MMPs that break down the matrix, synthesizing new ECM components and activating fibroblasts to myofibroblasts which will later in the inflammatory process be the main producers of matrix proteins (Jugdutt et al. 2003 and Jugdutt et al. 2003).

The tissue micro-environment at a given time after MI influences the recruitment of immune cells as well as their phenotypic and functional properties. This is especially relevant for the macrophage population, which undergoes a time-dependent shift between inflammatory and reparative functions (Frangogiannis et al. 2014 and Frantz et al. 2014). At early timepoints after injury the majority of macrophages produce inflammatory cytokines and ROS including interleukin IL-1β, IL-12, MMP-9 and nitric oxide. These are termed inflammatory or M1-like macrophages, which express high

levels of Ly6C marker, and function to recruit more inflammatory cells, phagocytose cellular debris and produce growth factors (Vanhoutte et al. 2006). As repair proceeds reparative macrophages predominate, many of which express the CD206 marker. In contrast to the inflammatory macrophages, reparative macrophages are involved in the suppression of inflammation due to high production of IL-10 and TGF-β (Bujak et al. 2007, Frangogiannis et al. 2014 and Cao et al. 2010) and assist in the progression from inflammation to repair. They also perform reparative roles promoting cell growth, angiogenesis and remodeling of the ECM. Additionally, different monocyte populations can be distinguished by the Ly6C marker in the mouse and may preferentially give rise to inflammatory versus reparative macrophages. Understanding the signaling pathways and the lineage relationships of monocytes after MI will support the search for specific therapies, Introduction, **Figure 1.3** (Nahrendorf et al. 2013).

As discussed in the Introduction, Section 1.5.4, IGF-1Ea and its mature circulating form can modulate immune responses and suppress pathological inflammation by modulating regulatory cytokines (Johannesson et al. 2014 and Bilbao et al. 2014). Expressed as a cardiomyocyte-specific transgene (αMHC-IGF.1Ea) or delivered locally to the mouse heart, IGF-1Ea improves functional recovery after cardiac injury, however the cellular and molecular mechanisms behind the enhanced repair in αMHC-IGF.1Ea are not fully understood.

This chapter focuses on investigating whether there is a difference in the immune cell dynamics after myocardial infarction in αMHC-IGF.1Ea hearts and the potential carry-on effect on tissue remodeling.

3.2 IGF-1Ea improves cardiac function after myocardial infarction

In αMHC.IGF-1Ea hearts, the baseline expression of transgenic IGF-1Ea was much higher than the expression of endogenous IGF-1Ea in WT hearts (Average 286-fold) at all experimental time points (**Figure 3.1A** and **3.1B**).

Although far exceeding the expression of endogenous IGF-1Ea, the αMHC.IGF-1Ea transgenic mice provide a suitable model of IGF-1Ea at supraphysiological concentrations of possible therapeutic relevance.

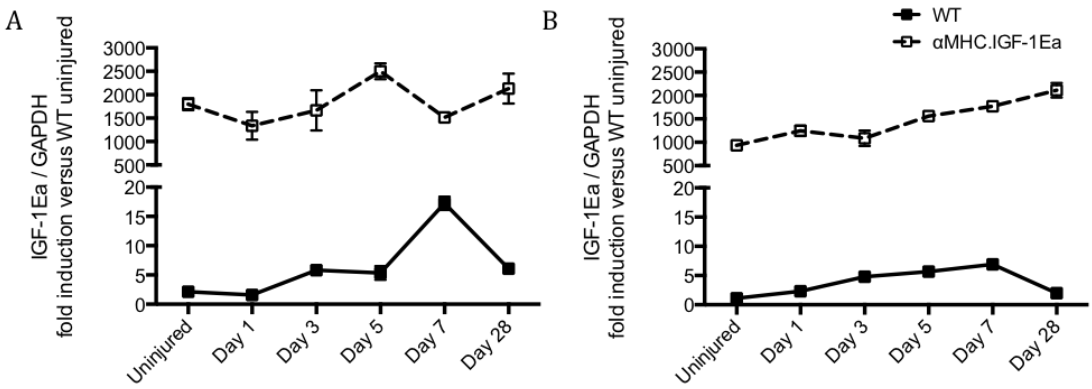


Figure 3.1. IGF-1Ea relative mRNA levels in the heart after myocardial infarct in WT and αMHC.IGF-1Ea mice compared throughout a 28-day timecourse. (A) infarct and (B) remote area (non-ischemic). Infarcted and remote regions were separated using a scalpel and a stereoscopic microscope. Remote regions are septal or inferior non-infarcted areas of the heart as in **Figure 2.5**. Solid lines represent WT mice. Dashed lines represent αMHC.IGF-1Ea mice. n=3 per group. Results are expressed as mean fold induction ± SEM over the values of uninjured hearts.

Endogenous IGF-1Ea expression in WT hearts was measured at 1, 3, 5, 7 and 28 days after MI in both ischemic and remote (Non-ischemic) regions. IGF-1Ea levels increased in both the ischemic and remote regions (**Figure 3.2A**) with a substantially stronger induction in the ischemic area (8-fold over uninjured levels). These results indicate that, similar to other organs, endogenous IGF1-Ea expression is up-regulated after cardiac tissue damage (Philippou et al. 2009, Sanz et al. 2005 and Santini et al. 2007).

To pinpoint the start of functional improvement, echocardiographic analysis was performed before, and 1, 3, 5, 7 and 28 days after MI (**Table 3.1**). One day following MI both groups displayed a reduction in left ventricular ejection fraction (LVEF), however, αMHC.IGF-1Ea hearts showed significant improvement in LVEF by day 7 after MI (**Figure 3.2B** and **Table 3.1**). Left ventricular end systolic/diastolic volumes significantly increased after MI in WT hearts, indicating a sign of left ventricular dilation, while the αMHC.IGF-1Ea hearts did not display any such signs (**Figure 3.2C** and **Table 3.1**).

In support of the functional data, the expression of molecular markers for cardiac damage such as actin-alpha 1 skeletal muscle (ACTA) and atrial natriuretic peptide (ANP) (Cameron at al. 2000 and Sergeeva et al. 2012) were significantly reduced in αMHC.IGF-1Ea compared to WT mice 28 days after MI (**Figure 3.2D** and **3.2E**). The peak

of endogenous IGF-1Ea in the ischemic region of WT mice by day 7, along with the improvement in cardiac function in αMHC.IGF-1Ea as early as day 7, indicates that IGF-1Ea signalling at early time points is key for cardiac repair.

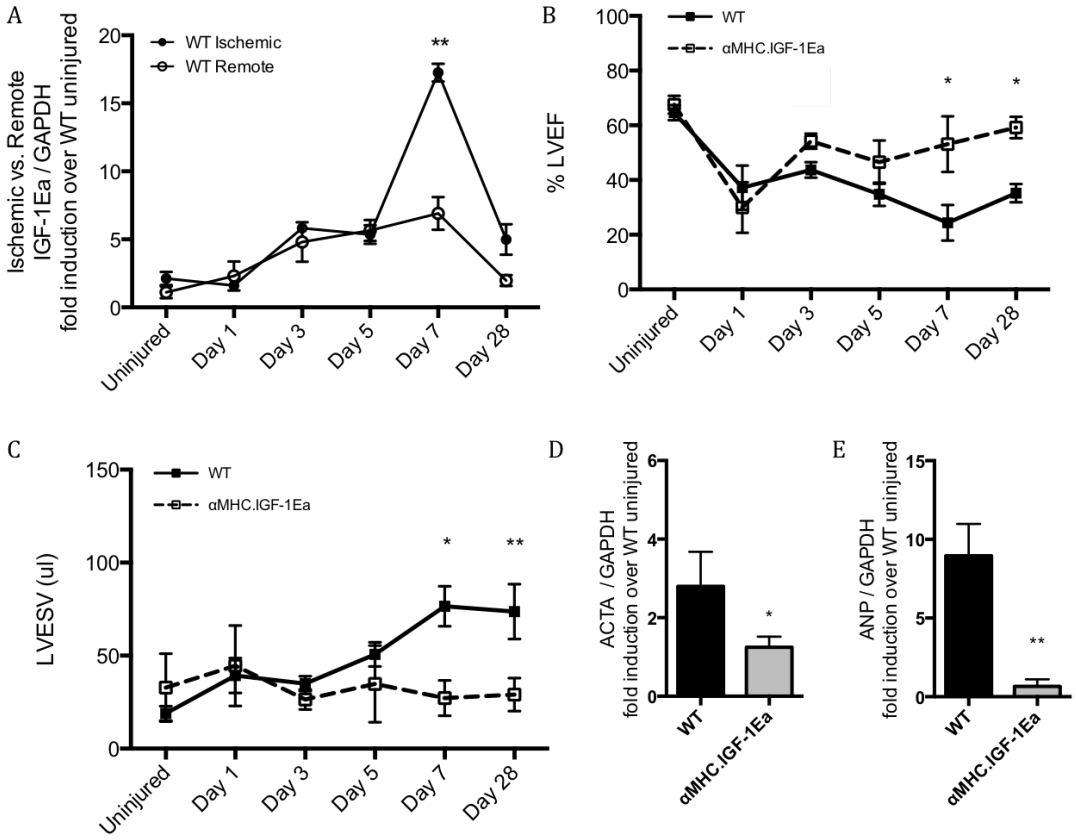


Figure 3.2. Expression of IGF-1Ea improves cardiac function and reduces dilation as early as 7 days after myocardial infarction. (A) mRNA levels of IGF-1Ea in the ischemic and in the remote area of WT hearts at 1, 3, 5, 7 and 28 days following MI. Infarcted and remote regions were separated using a scalpel and a stereoscopic microscope. Remote regions are septal or inferior non-infarcted areas of the heart as in **Figure 2.5**. (B) Left ventricular ejection fraction (LVEF) and (C) left ventricular end systolic volume (LVESV) after myocardial infarction. Solid lines represent WT mice. Dashed lines represent αMHC.IGF-1Ea mice. Levels of (D) actin-alpha 1 skeletal muscle (ACTA 1) and (E) atrial natriuretic peptide (ANP) mRNA expression 28 days after MI. Results are expressed as mean fold induction ± SEM over the values of uninjured hearts. n= 4-6 per group. * $p<0.05$, ** $p<0.005$. Two-tailed Student's *t*-test was performed to compare WT vs αMHC.IGF-1Ea at selected timepoints after MI.

	WT	αMHC-IGF-1Ea	WT	αMHC-IGF-1Ea
	Uninjured		**1 Day**	
LVEDV	52,82±5,246	70,05±10,54	55,09±8,99	67,83±7,35
LVESV	18,91±3,93	32,79±9,10	39,31±9,35	44,57±12,51
LVIDD	3,71±0,26	4,08±0,18	3,44±0,29	3,75±0,30
LVIDS	2,47±0.182	3,01±0,29	3,05±0,52	3,24±0,40
LVPWD	0,83±0,33	1,02±0,07	0,95±0,07	0,85±0,05
LVPWS	1,10±0,071	1,18±0,11	1,07±0,14	0,98±0,19
LVEF	64,652±2,72	67,57±3,21	37,24±8,11&	29,96±9,266&
%FAC	38,80±1,91	37,43±2,36	18,83±4,35&	23,52±7,91
	3 Days		**5 Days**	
LVEDV	57,13±5,271	57,14±4,26	75,610±15,68	59,930±10,355
LVESV	34,97±4,01	26,48±3,14	50,66±6,51	34,82±9,22
LVIDD	3,78±0,07	3,59±0,452	4,06±0,427	3,69±0,24
LVIDS	2,92±0.15	2,75±0,31	3,11±0,33	2,99±0,36
LVPWD	0,86±0,08	0,74±0,04	0,67±0,09	0,88±0,17
LVPWS	1,00±0,09	0,94±0,25	0,70±0,08	1,09±0,18
LVEF	43,72±2,851&	54,17±2,80	34,80±4,24&	46,51±7,95
%FAC	22,51±2,27	28,90±3,11	16,60±2,34&	23,43±4,59&
	7 Days		**1 Month**	
LVEDV	78,95±14,71	56,88±11,5	101,88±20,54&	63,29±6,34
LVESV	76,61±10,81&	27,133±5,793*	73,72±14,80&	29,08±3,37*
LVIDD	4,31±0,32	3,63±0,35	4,38±0,31	3,80±0,16
LVIDS	4,26±0,21&	2,88±0,53*	3,85±0,27&	2,65±0,14*
LVPWD	0,62±0,03	0,70±0,07	0,71±0,05	0,80±0,06
LVPWS	0,60±0,03	0,96±0,96	0,65±0,03	1,05±0,11*
LVEF	24,35±6,52&	53,16±10,24*	35,24±3,38&	59,244±3,949*
%FAC	16,69±4,106&	36,340±3,31*	15,636±2,06&	32,783±2,38*

Table 3.1. Echocardiographic measurements and analysis performed at 1, 3, 5, 7 and 28 days after MI. LVEDV, left ventricular end-diastolic volume; LVESV, left ventricular end-systolic volume; LVIDD, left ventricular internal diameter in diastole; LVIDS, left ventricular internal diameter in systole; LVPWD, left ventricular posterior wall in diastole; LVPWS, left ventricular posterior wall in systole; LVEF, left ventricular ejection fraction; FAC, Fractional area change. Mean values ± SE are shown. n= 4-6 per group.*P<0.05. Two-tailed student t-test was performed to compare WT vs αMHC.IGF-1Ea. &P<0.05. One-way ANOVA for condition time on each group and compared with the uninjured group on that column.

3.3 Altered tissue remodeling in αMHC.IGF-1Ea after injury

Three days after myocardial infarction, WT and αMHC.IGF-1Ea hearts displayed infarcts of equal size, quantified by Masson's trichrome staining (**Figure 3.3A**). However, by 28 days after-MI, αMHC.IGF-1Ea hearts exhibited smaller scar areas compared to WT (**Figure 3.3B, 3.3C** and **3.3D**). This was observed as a reduction in scar length but increased scar thickness, consistent with reduced infarct expansion.

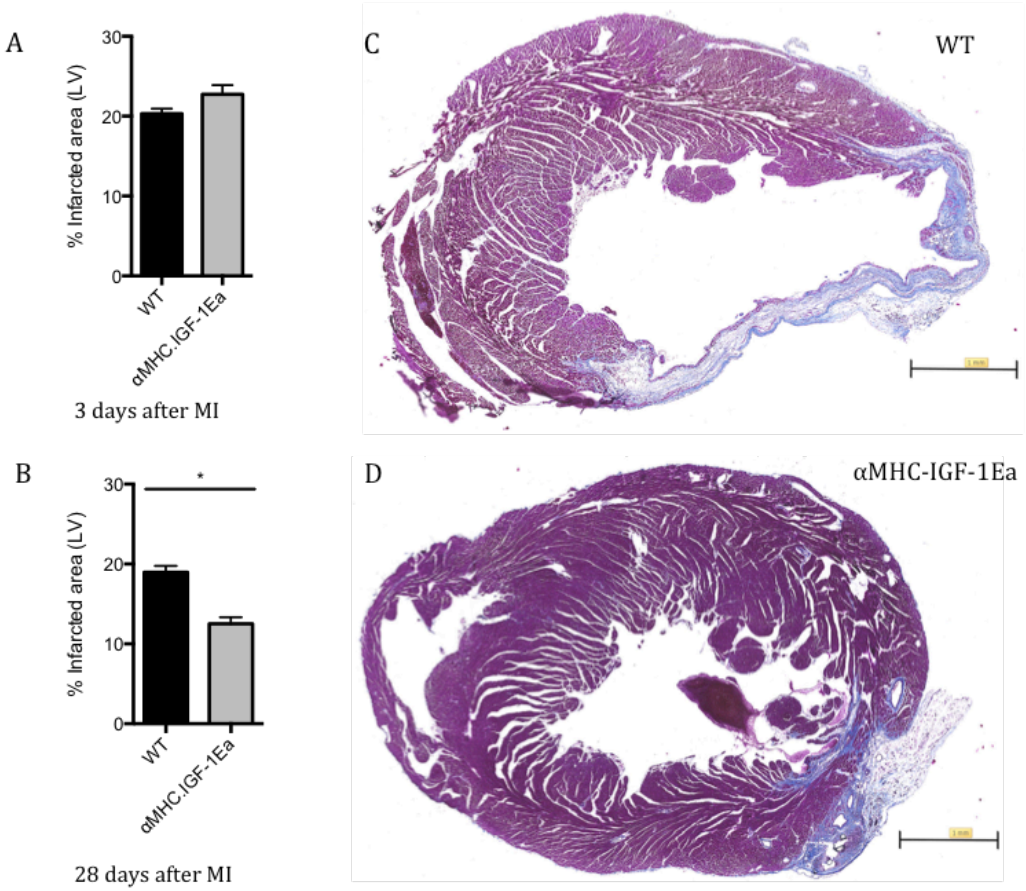


Figure 3.3. IGF-1Ea enhanced repair after myocardial infarction. Quantification of the infarcted area at (A) 3 days and (B) 28 days after MI. n=3. Representative histological sections of (C) WT and (D) αMHC.IGF-1Ea hearts stained with Masson's trichrome 28 days after MI. Scale bar, 1mm. Mean fold induction ± SEM. * $p<0.05$. Two-tailed Student's *t*-test was performed to compare WT vs αMHC.IGF-1Ea at selected timepoints after MI.

As a molecular measurement of fibrosis, TGF-β mRNA levels were significantly lower in αMHC.IGF-1Ea than in WT mice after MI (**Figure 3.4A**). Therefore, expression of genes involved in ECM turnover and synthesis such as MMP-9, MMP-2, TIMP-2, TIMP-1, Col Iα1, Col Iα3 and lysyl oxidase (Lox) at 1, 3, 5, 7 and 28 days after MI were quantified. In WT hearts, MMP9 was up-regulated 3 days after MI, followed by MMP2 at day 7 (**Figure 3.4B** and **3.4C**). Interestingly, neither MMP9 nor MMP2 was significantly up-regulated in αMHC.IGF-1Ea hearts at any time-point. Inhibitors of matrix degradation, TIMP-1 and

TIMP-2, had similar expression in WT and αMHC.IGF-1Ea hearts at all timepoints except for day 7 when TIMP-2 was significantly up-regulated in αMHC.IGF-1Ea hearts compared to WT (**Figure 3.4D** and **3.4E**). Several studies have provided proof that ECM dissolution promotes LV dilation (Jugdutt et al. 2003 and Vanhoutte et al. 2008). Consequently, these results supports the idea of a net overall reduction in matrix breakdown (Figure 3.4A), may contribute to the reduced fibrosis and dilation observed in αMHC.IGF-1Ea hearts (Bujak et al. 2007).

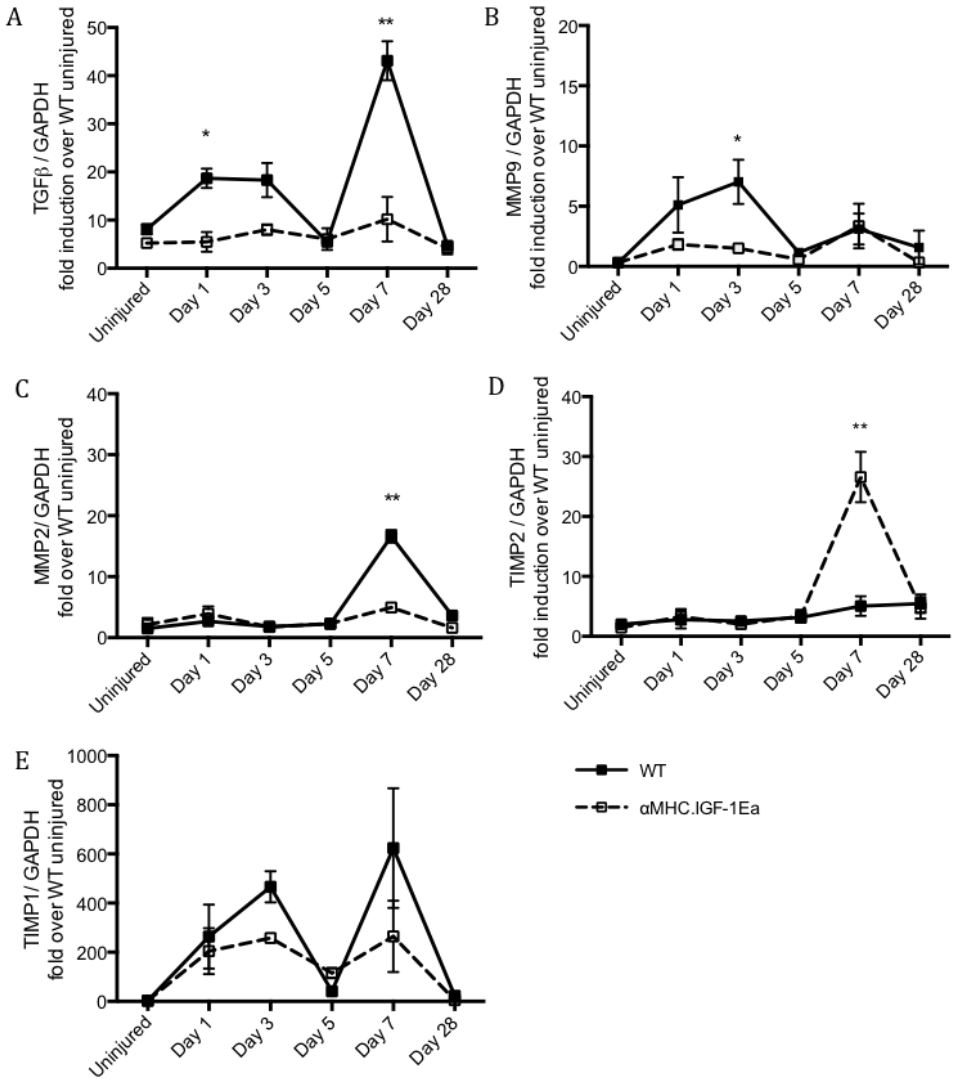


Figure 3.4. Changes in gene expression of extracellular matrix suggesting a distinct remodeling in αMHC.IGF-1Ea mice after myocardial infarction. (A-E) mRNA relative expression was measured at the infarct region. (A) transforming growth factor beta (TGF-β), (B) matrix metalloproteinase 9 (MMP-9), (C) matrix metalloproteinase 2 (MMP-2), (D) tissue inhibitor of metalloproteinase (TIMP) 2 and (E) TIMP1. Mean fold induction ± SEM. Solid lines represent WT mice. Dashed lines represent αMHC.IGF-1Ea mice. n= 4-6 per group. * $p<0.05$, ** $p<0.005$. Two-tailed Student's *t*-test was performed to compare WT vs αMHC.IGF-1Ea at selected timepoints after MI.

Consequently, the composition of the newly synthesised matrix was analysed by measuring mRNA expression of the most abundant cardiac ECM collagens, Col Iα1 and Col Iα3, as well as the collagen cross linker, lox, which increases matrix stiffness. Up-regulation of both collagens was detected by day 3, peaking at day 7 (**Figure 3.5A** and **3.5B**). At this timepoint, WT hearts expressed significantly more of both collagens than did αMHC.IGF-1Ea hearts. Interestingly, a difference in the ratio of the collagens was noted; αMHC.IGF-1Ea hearts expressed more Col Iα3 than Col Iα1 (**Figure 3.5C**). At the peak of collagen up-regulation, lox was also up-regulated in WT hearts, yet this was not observed in αMHC.IGF-1Ea hearts (**Figure 3.5D**). These results indicate that IGF-1Ea overexpression reduces ECM turnover (**Figure 3.4**) after MI and alters the composition of the newly formed matrix (**Figure 3.5**), with preferential expression of Col Iα3 over Col Iα1 and less crosslinking, which likely alters the mechanical properties of the fibrotic area Jugdutt et al. 2003 and Vanhoutte et al. 2008).

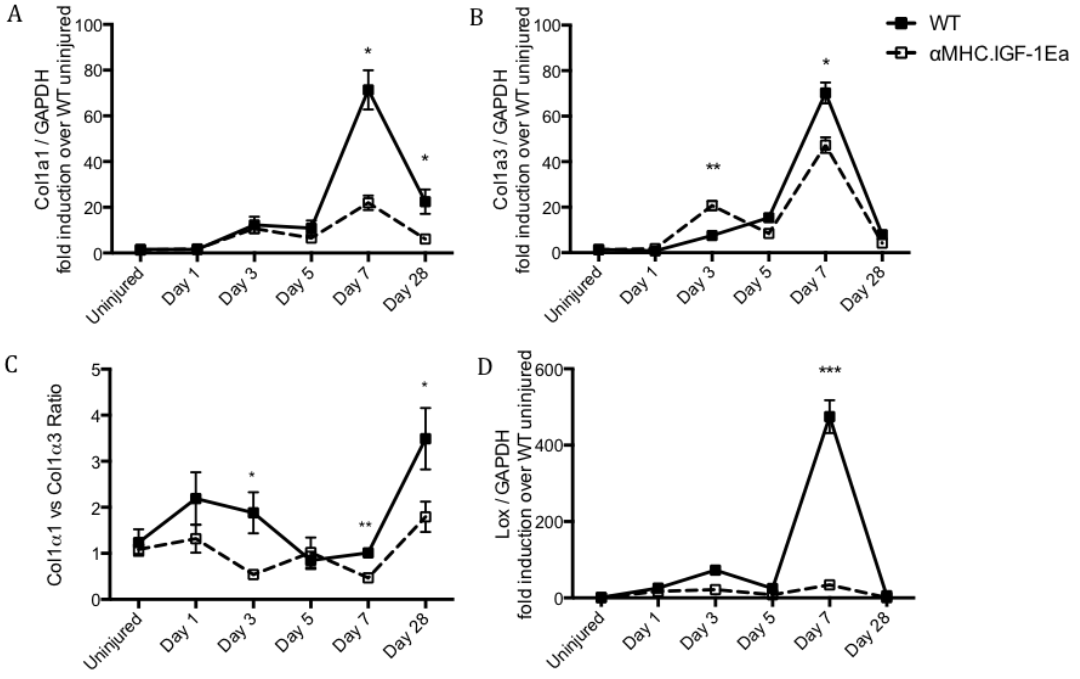


Figure 3.5. Infarct region mRNA levels of matrix genes of the newly synthesised extracellular matrix of αMHC.IGF-1Ea mice. (A-D) mRNA relative expression was measured at the infarct region. (A) Collagen (Col) Iα1, (B) Col Iα3, (C) ColIα1/ColIα3 ratio, (D) lysyl oxidase in the infarct area. Mean fold induction ± SEM. Solid lines represent WT mice. Dashed lines represent αMHC.IGF-1Ea mice. n= 4-6 per group. * $p<0.05$, *** $p<0.001$. Two-tailed Student's *t*-test was performed to compare WT vs αMHC.IGF-1Ea at selected timepoints after MI.

3.4 Distinct chemokine and cytokine production in αMHC-IGF-1Ea hearts after myocardial infarct.

Tissue remodeling after injury is closely tied to the inflammatory process. Therefore, the inflammatory status of the αMHC.IGF-1Ea and WT hearts was compared, monitoring the production of key immune genes IL-1β, IL-10, MCP-1 and CCL5. Expression of the inflammatory cytokine IL-1β was rapidly induced upon injury in WT hearts (66-fold over uninjured) yet was not increased as strongly in αMHC.IGF-1Ea hearts (19-fold over uninjured; **Figure 3.6A**). Similarly the strong up-regulation of MCP-1 in WT hearts was not observed in αMHC.IGF-1Ea hearts (**Figure 3.6B**). By contrast, the immunosuppressive cytokine IL-10 was rapidly up-regulated in α MHC.IGF-1Ea hearts, peaking 1 day after MI, with 3-fold higher up-regulation compared to WT controls.

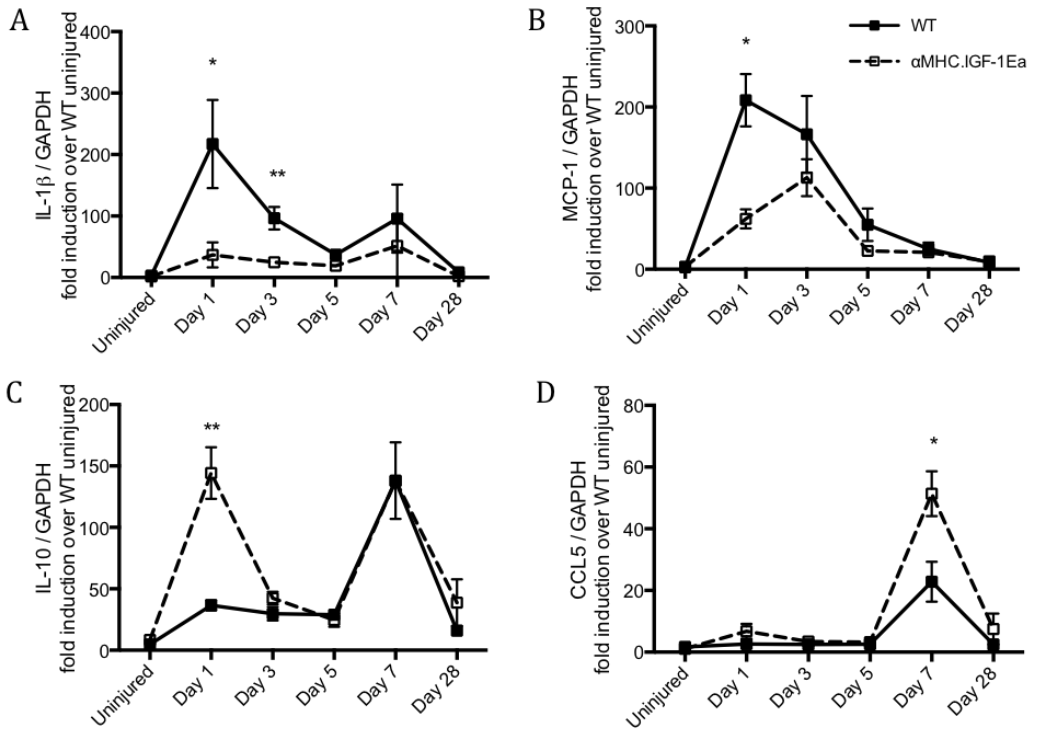


Figure 3.6. Cytokine dynamics in infarcted hearts of αMHC.IGF-1Ea. (A-D) mRNA relative expression was measured at the infarct region. (A) Interleukin (IL)-1β, (B) MCP-1, (C) IL-10 and (D) CCL5 at several time-points after permanent ligation. Solid lines represent WT mice. Dashed lines represent αMHC.IGF-1Ea mice. Mean fold induction ± SEM over the values of uninjured hearts. n= 3 per group. * $p<0.05$, ** $p<0.005$. Two-tailed Student's *t*-test was performed to compare WT vs αMHC.IGF-1Ea at selected timepoints after MI.

Although a second peak of IL-10 mRNA was detected at 7 days after MI, it was comparable in both WT and αMHC.IGF-1Ea hearts (**Figure 3.6C**). CCL5, which is involved in the recruitment of Ly6C^{low} monocytes (Tacke et al. 2007 and Carlin et al.

2013) was up-regulated in αMHC.IGF-1Ea hearts, 7 days after MI (**Figure 3.6D**). These data suggest an early bias towards a less inflammatory environment potentially modulating the recruitment of monocytes in αMHC.IGF-1Ea hearts after myocardial infarction.

3.5 IGF-1Ea modulates myeloid cell recruitment after myocardial infarction.

To document accumulation of the main innate immune cell populations involved in cardiac inflammation after infarct, single cell suspensions (Methodology, Section 2.4) were prepared from whole mouse hearts and analyzed by flow cytometry using the gating strategy shown in **Figure 3.7A-E**. Macrophages were identified as CD45+, CD11b+, CD11c-, Ly6G-, F4/80+ (**Figure 3.7F**), Monocytes, CD45+, CD11b+, CD11c-, Ly6G-, F4/80-, $Ly6C^{high}/Ly6C^{low}$ (**Figure 3.7G**), DC, Dendritic Cells as CD45+, CD11b+, F4/80-, CD11c+, Ly6G- and neutrophils, CD45+, CD11b+, F4/80-, CD11c-, Ly6G+ (**Figure 3.7H**). Inflammatory macrophages as CD45+, CD11b+, CD11c-, Ly6G-,F4/80+$Ly6C^{high}/CD206^{low}$ and reparative macrophages as CD45+, CD11b+, CD11c-, Ly6G-, F4/80+, $Ly6C^{low}/CD206^{high}$ (**Figure 3.7I**).

In WT and αMHC.IGF-1Ea hearts the total number of infiltrating leukocytes (CD45+) gradually increased after MI, both reaching comparable peak numbers at day 5 (**Figure 3.8A**). However at the earlier 3-day timepoint, αMHC.IGF-1Ea hearts contained 49% less leukocytes per milligram of tissue than WT hearts. In examining specific immune cell populations, the difference is partly explained by a 75% reduction in neutrophils (CD45+, CD11b+, F4/80-, CD11c-, Ly6G+; 186 versus 46 cells/mg of tissue, **Figure 3.8B**) and a 67% reduction in monocytes (CD45+, CD11b+, CD11c-, Ly6G-, F4/80-; 191 versus 62 cells/mg of heart, **Figure 3.8C**), however it is mostly due to a reduced presence of macrophages (CD45+, CD11b+, CD11c-, Ly6G-, F4/80+; 58%, 2276 versus 949 cells/mg of heart, **Figure 3.8D**).

These data agree with the reduced MCP-1 expression observed in αMHC.IGF-1Ea hearts (**Figure 3.6B**), as it is the principal chemokine involved in monocyte recruitment (Tacke et al. 2007 and Serbina et al. 2006).

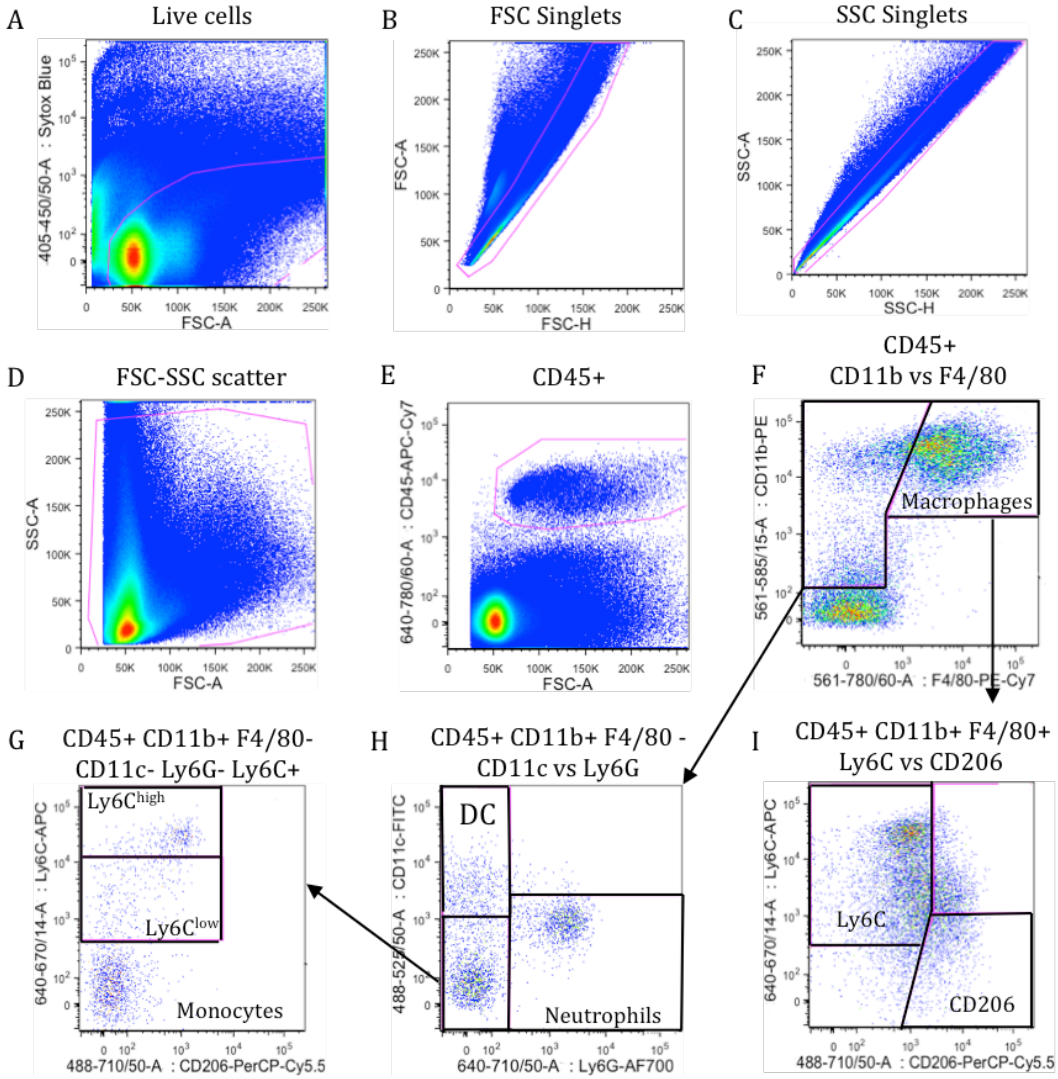


Figure 3.7. Gating strategy for infiltrating immune cells after myocardial infarct. Single cell suspensions isolated from hearts of mice uninjured and after-MI were stained with anti-CD11b, -CD45, –Ly-6G, –Ly-6C, -F4/80, -CD206 -CD11c and analyzed by FACS. (A) live cells, (B and C) Singlets, (D) FSC-SSC scatter, (E) CD45+, (F) Macrophages, CD45+, CD11b+, CD11c-, Ly6G-, F4/80+, (G) Monocytes, CD45+, CD11b+, CD11c-, Ly6G-, F4/80-, $Ly6C^{high}/Ly6C^{low}$, (H) DC, Dendritic Cells, CD45+, CD11b+, F4/80-, CD11c+, Ly6G- and neutrophils, CD45+, CD11b+, F4/80-, CD11c-, Ly6G+, (I) CD45+, CD11b+, CD11c-, Ly6G-,F4/80+$Ly6C^{high}/CD206^{low}$ (Inflammatory macrophages) and CD45+, CD11b+, CD11c-, Ly6G-, F4/80+, $Ly6C^{low}/CD206^{high}$ (Reparative macrophages) based on FMO controls shown in Methodology, Section 2.4.1. Representative plots from WT hearts 3 days after infarction are presented.

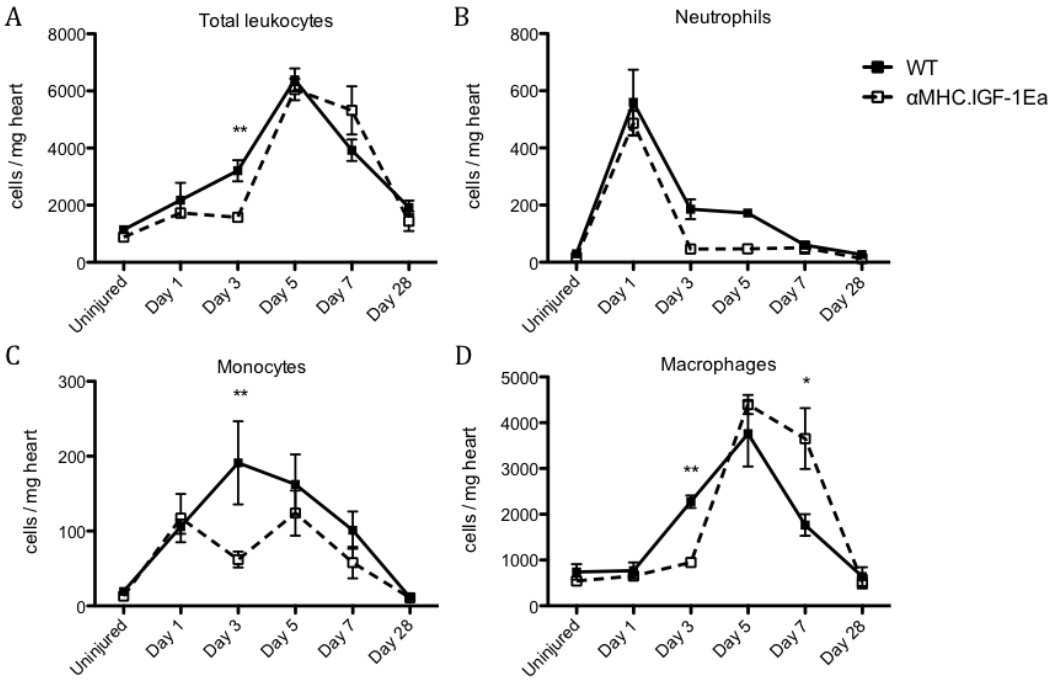


Figure 3.8. Characterization and temporal dynamics of immune cell populations in αMHC.IGF-1Ea hearts after myocardial infarction. Quantification of (A) total leukocytes (CD45+), (B) neutrophils (CD45+, CD11b+, F4/80-, CD11c-, Ly6G+), (C) monocytes (CD45+, CD11b+, CD11c-, Ly6G-, F4/80-), (D) Macrophages (CD45+, CD11b+, CD11c-, Ly6G-, F4/80+). Data is presented as the total number of cells per mg of heart. n= 4-6 per group. Solid lines represent WT mice. Dashed lines represent αMHC.IGF-1Ea mice. Mean values ± SEM are shown.* $p<0.05$, ** $p<0.005$. Two-tailed Student's *t*-test was performed to compare WT vs αMHC.IGF-1Ea at selected timepoints after MI .

The Ly6C surface marker distinguishes two different subsets of monocytes (Frangogiannis et al. 2014 and Frangogiannis et al. 2012). Analysis of the $Ly6C^{high}$ (CD45+, CD11b+, CD11c-, Ly6G-, F4/80- and $Ly6C^{high}$) and $Ly6C^{low}$ (CD45+, CD11b+, CD11c-, Ly6G-, F4/80- and $Ly6C^{low}$) populations revealed that the reduction of total monocyte numbers at day 3 was attributable to a 20% decrease of the $Ly6C^{high}$ population (102 versus 32 cells/mg of heart), whereas the $Ly6C^{low}$ population was not significantly different in WT compared to αMHC.IGF-1Ea (**Figure 3.9A** and **3.9B**).

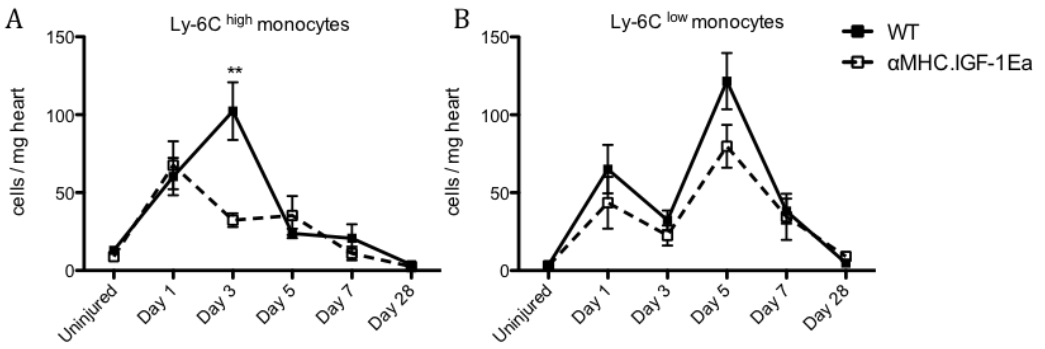


Figure 3.9. Temporal dynamics of monocytes subpopulations in αMHC.IGF-1Ea hearts after myocardial infarction. Monocytes (CD45+, CD11b+, CD11c-, Ly6G-, F4/80-) were further classified as (A) Ly6C^{high} and (B) Ly6C^{low} monocytes. Data is presented as the total number of cells per mg of heart. n= 4-6 per group. Solid lines represent WT mice. Dashed lines represent αMHC.IGF-1Ea mice. Mean values ± SEM are shown. * $p<0.05$, ** $p<0.005$. Two-tailed Student's *t*-test was performed to compare WT vs αMHC.IGF-1Ea at selected timepoints after MI.

To differentiate between inflammatory and reparative macrophage populations, Ly6C and CD206 markers were used. Both Ly6C+ inflammatory (CD45+, CD11b+, CD11c-, Ly6G-, F4/80+ and Ly6C+/CD206-) and CD206+ reparative (CD45+, CD11b+, CD11c-, Ly6G-, F4/80+ and Ly6C-/CD206+) macrophage normalized cell numbers were reduced by 71% and 48% respectively, in αMHC.IGF-1Ea hearts at the 3 day timepoint (522 versus 153 and 596 versus 310 cells/mg of tissue of heart, respectively; **Figure 3.10A** and **3.10B**), however this was significant only for the Ly6C+ population. By day 7 after MI, macrophage dynamics changed and a greater number of total macrophages in αMHC.IGF-1Ea hearts compared to WT was observed, which was mainly due to a 155% preferential increase in the CD206+ population (575 versus 1468 cells/mg heart, **Figure 3.10B**). For this work, only cells that were either Ly6C+/CD206- or Ly6C-/CD206+ were analyzed, although a double positive cell population was found (i.e. CD206+, Ly6C+). However no changes were observed over time between WT and αMHC.IGF-1Ea for the double positive population (**Figure 3.10C**). Dendritic cells (CD45+, CD11b+, F4/80-, CD11c+, Ly6G-) were increased by 48% in αMHC.IGF-1Ea hearts compare to WT 5 days after MI (168 versus 248 cells/mg heart; **Figure 3.10D**).

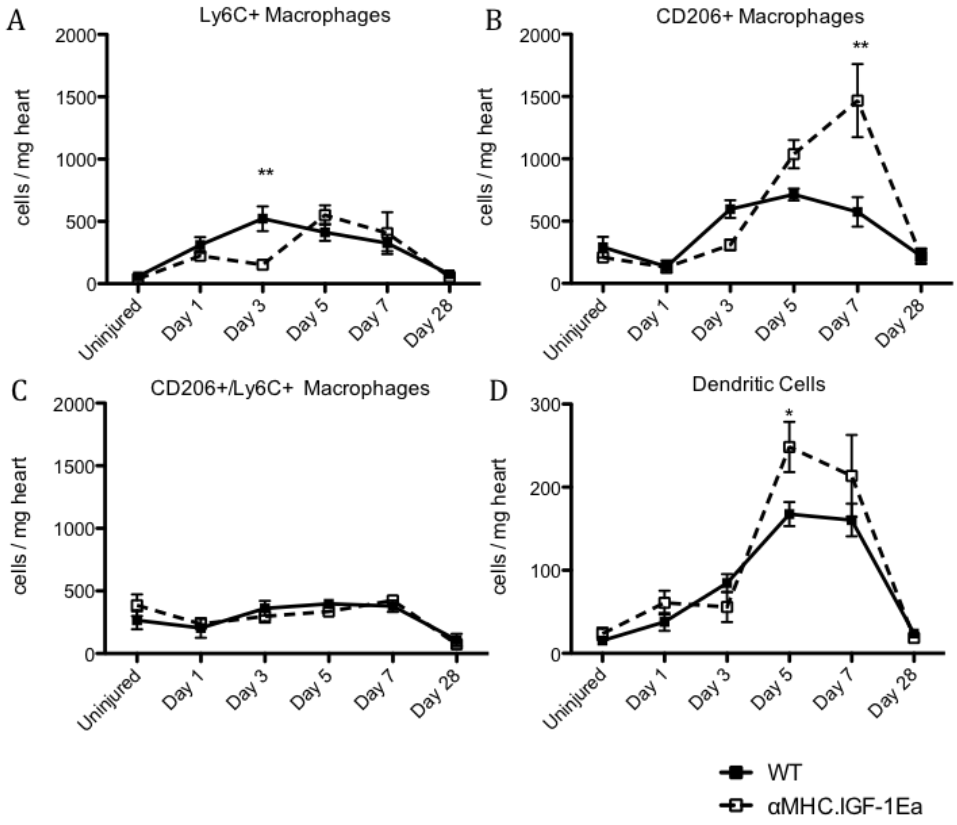


Figure 3.10. Temporal dynamics of macrophages subpopulations and dendritic cells in αMHC.IGF-1Ea hearts after myocardial infarction. Macrophages (CD45+, CD11b+, CD11c-, Ly6G-, F4/80+) were characterized on the basis of Ly6C and CD206 expression as (A) $Ly6C^{high}/CD206^{low}$ (Inflammatory macrophages) and (B) $Ly6C^{low}/CD206^{high}$ (Reparative macrophages). (C) Double CD206+/Ly6C+ population. (D) Dendritic cells were defined as CD45+, CD11b+, F4/80-, CD11c+, Ly6G-. Data is presented as the total number of cells per mg of heart. n= 4-6 per group. Solid lines represent WT mice. Dashed lines represent αMHC.IGF-1Ea mice. Mean values ± SEM are shown. * $p<0.05$, ** $p<0.005$. Two-tailed Student's *t*-test was performed to compare WT vs αMHC.IGF-1Ea at selected timepoints after MI.

In summary, cardiac-restricted expression of an IGF-1Ea transgene limited the early accumulation of innate immune cells at day 3 after MI, with a bias towards the reduction of inflammatory myeloid populations in favour of reparative populations. This reduction paralleled with the lower expression of myeloid chemokines and the less inflammatory milieu observed in the αMHC.IGF-1Ea hearts.

3.6 Discussion

Previous work in our lab showed that local expression of IGF-1Ea promoted functional restoration after MI, and observed reduced infarct expansion, thinning and dilation of

the left ventricular wall (Santini et al. 2007). The work in this chapter indicates that the transcriptional modulation of key ECM remodeling genes, in the IGF-1Ea hearts, is associated with a tempering of the inflammatory myeloid cell response.

Increased MMP expression after injury has been implicated in contributing to scar destabilisation, as transgenic animal model knockouts of either MMP2 or MMP9 have been shown to attenuate LV dilation, rupture and impairment of cardiac function (Hayashidani et al. 2003 and Ducharme et al. 2000). While MMP2 and MMP9 mRNA expression levels were up-regulated in injured WT hearts, this increase was not observed in αMHC.IGF-1Ea hearts. In line with reduced matrix breakdown, mRNA expression of the MMP inhibitor, TIMP2, was significantly increased in αMHC.IGF-1Ea hearts at day 7 after myocardial infarction. Thus IGF-1Ea may prevent adverse cardiac remodeling, in part, by modulating transcription of MMPs/TIMPs.

The production of new matrix components was also altered by the presence of the IGF-1Ea transgene with an overall reduction in collagen synthesis, confirmed in histological stains, and a bias towards expression of Col Iα3 over Col Iα1. In MI patients, turnover of cardiac extracellular matrix can be assessed by using circulating collagen peptides as blood biomarkers and high type I collagen is associated with adverse clinical outcome (Weber et al. 1997 and Iraqi et al. 2009). A prospective multicentre study further showed that especially a low type III/type I collagen ratio at 1 month after MI is predictive of detrimental left ventricular remodeling as well as cardiovascular deaths and hospitalizations for heart failure (Eschalier et al. 2013). Changes in collagen ratios are known to affect the strength and tensile properties of the ECM. It would be interesting to determine whether these properties are modified in the αMHC.IGF-1Ea hearts.

Additionally, IGF-1Ea could promote the changes in collagen deposition by directly acting on fibroblasts as it promotes both their proliferation and activation to myofibroblasts (Simmons et al. 2002 and Hung et al. 2013). Alternatively, IGF-1Ea may influence accumulation and activation of immune cells present at the infarct which in turn regulate myofibroblast activation. Indeed, this fact was observed by a modulation of the inflammatory process in αMHC.IGF-1Ea hearts, with less monocyte ($Ly6C^{high}$) infiltration into the injured myocardium. This effect is associated with reduced expression of the monocyte chemo-attractant MCP-1, although no significant changes were observed in the $Ly6C^{low}$ monocyte population in infarcted hearts, possibly due to

CCL5 up-regulation. It is interesting that while complete depletion of monocytes at any stage of repair leads to poor recovery (Nahrendorf et al. 2007), a more subtle modulation of the monocyte population in the αMHC.IGF-1Ea hearts is associated with improved heart function. Studies abrogating monocyte recruitment using a selective CCR2 inhibitor have resulted in reduced IL-1β, IL-6, MCP-1 and TNFα levels (Chen et al. 2008). IGF-1Ea influences macrophage polarization in skeletal muscle (Tonkin et al. 2015) and we similarly found reduced Ly6C^{high} monocyte and Ly6C+ macrophage normalized cell numbers while CD206+ macrophage numbers were increased by day 7, suggesting that IGF-1Ea promoted a quick progression to the reparative phase of repair by modulating macrophage phenotype. In the αMHC.IGF-1Ea hearts, we observed a decrease in MCP-1, which is the chemokine for CCR2, recently shown to distinguish infiltrating monocytes from the resident macrophage (cTM) population which has a different embryological origin and expresses CD206 (Tacke et al. 2007, Heidt et al. 2014, Epelman et al. 2014 and Pinto et al. 2012). We noted a reduction in the IL-1 β mRNA levels 24 hours after MI. This reduction occurs before the major inflammatory infiltrate. Although, many cells can produce IL-1β, we hypothesised that the activation of cTM towards a more anti-inflammatory environment may lead to the reduction in the inflammatory cytokine IL-1β. It is therefore possible that in our αMHC.IGF-1Ea transgenic mouse model, IGF-1Ea reduces the infiltration of inflammatory Ly6C^{high} monocytes by preventing up-regulation of MCP-1 while still allowing for expansion of the resident macrophage population.

In summary, the αMHC.IGF-1Ea mouse model can modulate several associated aspects of the cellular repair process after MI, including immune cell recruitment, cytokine expression, and matrix turnover. All of these changes occur mainly within the first 7 days after myocardial infarction, at which time a functional improvement can already be measured in αMHC.IGF-1Ea hearts compared to WT controls. These data provide new insights into the mechanism of IGF-1Ea and suggest that early immunodulation is key to successful cardiac repair after injury.

3.6.1 Limitation of the project

The main limitation of this study is the fact that the heart-specific transgene is expressed from the time of embryonic cardiac myogenesis onward, and therefore, does not simulate delivery to humans in a clinically relevant setting. Additionally, the beneficial effects observed in the αMHC.IGF-1Ea hearts, could be explained by either preconditioning effects or by enhancing reparative processes after cardiac injury. In this

thesis, Chapter 5 further addresses these questions as supplemental IGF-1Ea is administered 5 hours after injury, indicating that IGF-1Ea does not have a preconditioning effect.

3.6.2 Outcomes

The study of the immune cell dynamics and the positive remodeling mediated by IGF-1Ea in response to myocardial infarct indicates that IGF-1Ea plays a more active role on modulating the spatial containment of inflammatory cascades leading to effective repair. IGF-1Ea, by reducing infarct expansion, limits the extension of the inflammatory response into the viable myocardium, therefore, limiting fibrosis to the infarcted region. In parallel, IGF-1Ea prevents prolonged or excessive induction of pro-inflammatory signalling reducing the risk of an accentuated injury hence adverse remodeling.

Furthermore, this work suggests that complete cardiac regeneration may not be necessary, but a fine modulation of the inflammatory response may be essential to induce an effective repair and a reduction of the fibrotic tissue. In light of these results, supplemental IGF-1Ea gene therapy, studied in Chapter 4 and 5, is assessed as it contributes to local long-term beneficial remodeling of the heart in response to myocardial infarct.

Chapter 4 – Delivery of therapeutic growth factors to the injured heart by bone marrow-derived macrophages

4.1 Introduction

As described in the Introduction, Section 1.3.2, monocytes and macrophages are principally recognised for their housekeeping roles, modulating inflammation, and comprise the major infiltrating cell population following tissue injury (Nahrendorf et al. 2013, Frantz et al. 2014 and Nahrendorf et al. 2010). The intrinsic injury-homing capacity of macrophages makes them ideal vectors for the delivery of salutary and immunomodulatory payloads to the site of injury, with the potential to augment tissue repair and regeneration (Burke et al. 2002). Moreover, using the body's own homing cells to deliver regenerative gene products to the site of injury might lead to new and powerful cell therapies for heart diseases and other chronic diseases (Tong et al. 2014).

The studies performed in this chapter exploit the homing properties of macrophages to develop tools for the delivery of therapeutic growth factors to an injury site. This chapter assesses whether cultured macrophages can home to the injured muscle and investigates their potential beneficial effects on tissue repair by (1) the generation of homing-competent macrophage cells from the bone marrow, and (2) the characterisation of homed transplanted macrophages following injury. The chapter also explores whether macrophages can deliver an IGF-1Ea therapeutic payload by (1) stimulating endogenous IGF-1Ea, or (2) by 'priming' macrophages with cytokines.

The proposed work supports the development of novel tools to deliver therapeutic factors to injured tissue, which is particularly useful for treatment of injured hearts since no surgical intervention will be necessary, following cardiac injury, to deliver beneficial factors. While proof-of-principle for this approach will be demonstrated in injured skeletal muscle, this approach can be applied to a range of disease contexts where inflammation plays a prominent role. These include rheumatoid arthritis, chronic inflammation and stroke.

4.2 Rationale behind the skeletal muscle injury model

Although extensive experience in myocardial infarction (MI) injury models were acquired, the experiments to characterise the homing competency of cultured macrophages were conducted using the Tibialis Anterior (TA) injury model for the following reasons, (i) the inflammatory and leukocyte infiltration kinetics are almost

identical between the injured TA and MI injury models (Arnold et al. 2007 and Nahrendorf et al. 2007). The TA injury model leads to a local necrotic lesion resulting in a robust inflammatory response, which is a similar response as myocardial infarction (**Figure 4.1**); (ii) using the *in vivo* GFP or CFSE labelling reporter approach, homing to the injured TA and uninjured TA can be assessed simultaneously to determine the homing specificity to injury; (iii) TA injuries do not result in mouse lethality, whereas lethality following cardiac injury can range between 20-40% after surgery (Gao et al. 2010); (iv) TA injuries can be conducted more rapidly than MI, approximately 12 injuries/hour vs 2 injuries/hour, respectively (Arnold et al. 2007 and Tidball et al. 2004).

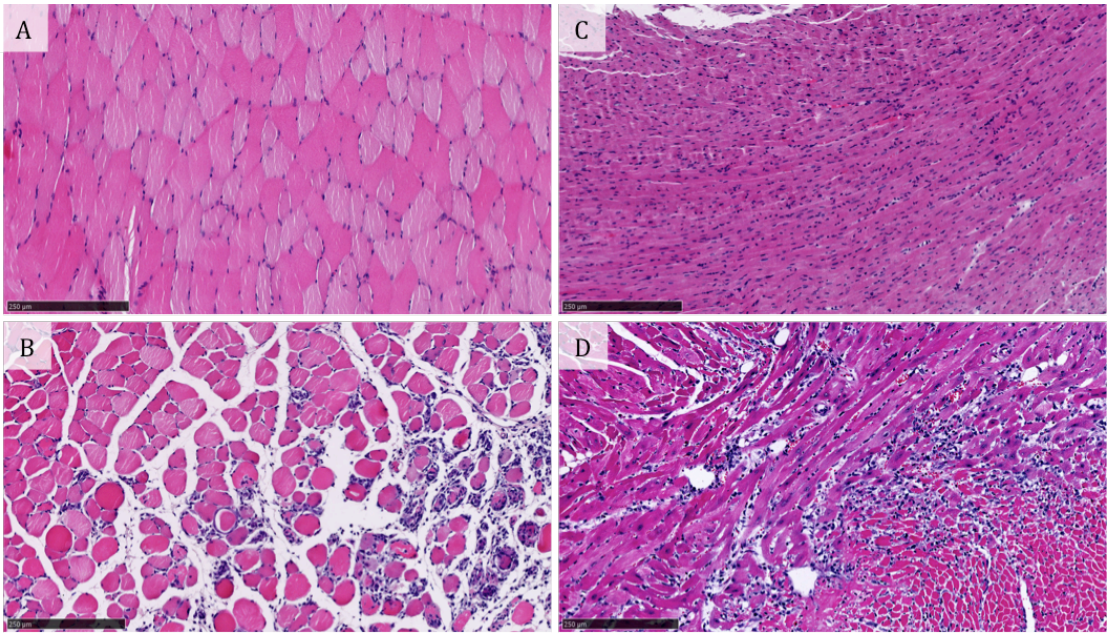


Figure 4.1. Representative haematoxylin and eosin staining of TA injured muscle and cardiac injured muscle two days after injury. (A) Uninjured TA muscle, (B) injured TA muscle, (C) uninjured myocardium and (D) injured myocardium. TA injury is characterise by a large accumulation of inflammatory cells shown here in blue/purple. Scale bar: 250 um.

4.3 IGF-1Ea levels in macrophages and monocytes

To investigate the therapeutic potential of the immune-mediated cell-based therapy, the mRNA levels of IGF-1Ea and IGF-1 receptor (IGF-1R) were assessed in various cell types. BMdMs (Methodology, Section 2.5.3, 2.5.4 and 2.5.5), were the cell type that expressed the highest levels of IGF-1Ea when compared with either blood or spleen monocytes. IFN-γ/LPS-polarization of BMdMs, which induces an M1-like inflammatory phenotype, drastically down-regulated the expression of IGF-1Ea whereas IL-4-polarization of BMdM, which promotes differentiation into M2-like reparative phenotype, induced the

expression of IGF-1Ea by 1.5-fold when compared with control BMdM and 15-fold when compared to blood monocytes (**Figure 4.2A**). Interestingly, the expression of IGF-1R inversely correlated with IGF-1Ea expression after polarization with either stimulus, whereas blood monocytes expressed higher levels of IGF-1R (**Figure 4.2B**).

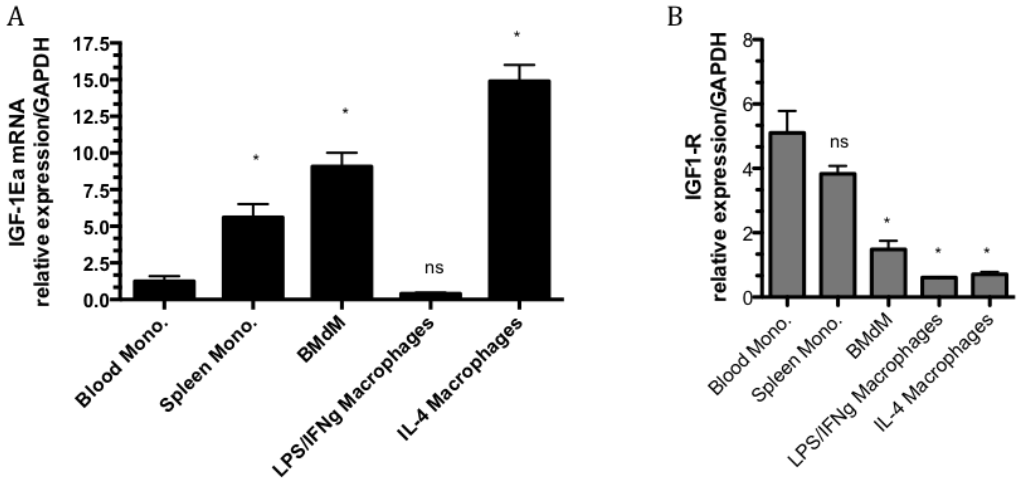


Figure 4.2. IGF-1Ea and IGF-1R mRNA levels in blood monocytes, spleen monocytes, BMdM, LPS/IFNγ-polarized BMdM and IL-4-polarized BMdM. (A) mRNA levels of IGF-1Ea and (B) mRNA levels of IGF-1 receptor in monocytes and macrophages. Mean values ± SEM are shown. * $p<0.001$. One-way ANOVA plus Dunnett's multiple comparison test. n=3 each group.

The results indicated that M2-polarized BMdM were the highest producers of IGF-1Ea (in mRNA levels) in this context, therefore supporting the hypothesis that either BMdM or M2-polarised macrophages may be considered as vectors for the delivery of salutary payloads. Furthermore, IGF-1Ea expression appears to be modulated according to the inflammatory environment that the cells encounter. Further *in vivo* studies in this chapter, Section 4.6, will address the engraftment of these cells after injury as well as the beneficial effect of IGF-1Ea delivery on tissue repair.

4.4 Bone marrow-derived macrophage characterisation for transplantation

Before proceeding with the *in vivo* experiment and due to the heterogeneity of the bone marrow population, the purity of the *in vitro* generated macrophages was evaluated by flow cytometry phenotypic analysis of cell-specific surface markers 6 days after differentiation. Analysis confirmed that, after differentiation, 96.5% of *in vitro* generated macrophages were positive for the macrophages markers CD11b and F4/80 (**Figure 4.3**).

This data indicates that generating BMdMs from the bone marrow results in a basically pure population that can be directly transfected without any further purification step.

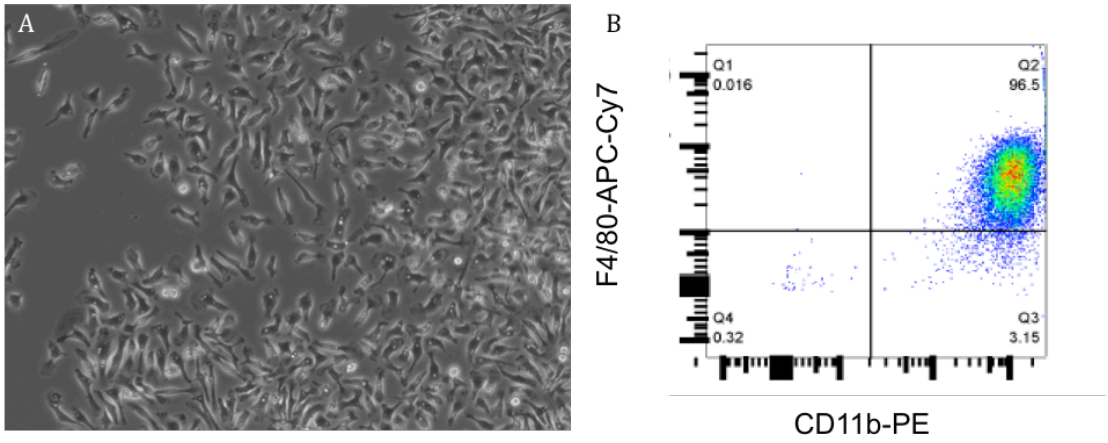


Figure 4.3. *In vitro* bone marrow-derived macrophages characterization. (A) 10x representative Ph2 bright field image of BMdM, (B) flow cytometry plot of BMdM, F4/80-CD11b positive cells after 7 days *in vitro* differentiation. ~100000 events.

4.5 Bone marrow-derived macrophage immunotherapy

To investigate the therapeutic relevant effect of BMdM-mediated IGF-1Ea delivery, endogenous levels of IGF-1Ea were augmented by transfecting BMdMs with the pIRES.eGFP vector (Methodology, Section 2.6). In the pIRES.GFP, the IGF-1Ea expression is driven by the strong CMV promoter. The plasmid also contains an internal ribosome entry site (IRES) followed by the GFP reporter gene.

BMdM were transfected with the pIRES.eGFP plasmid to investigate whether *ex vivo* manipulated macrophages can deliver reparative factors to improve wound healing. Because transfection of non-dividing cells, by which exogenous DNA is incorporated inside of cells, is considered a difficult technique and is associated with significant cell death, the following experiment aimed to optimise the transfection process, thus improving cell viability and increasing IGF-1Ea expression.

BMdMs were transfected at day 6 of differentiation with increasing concentrations of the IGF-1Ea.GFP vector, up to a maximum of 5 µg. Twenty-four hours after transfection, the transfection efficiency was validated by fluorescence microscopy analysis of GFP fluorescence as shown in **Figures 4.4A** and **4.4B**. The analysis demonstrated a variable intensity of GFP fluorescence in the transfected BMdM. This is probably due to the differing number of vector copies that can be transfected into each cell. The transfection

efficiency was also validated by flow cytometry comparing the GFP expression of untransfected BMdM (**Figure 4.4C**) and transfected BMdM with the pIRES.eGFP plasmid (**Figure 4.4D**). Finally, cell viability following transfection was assessed by Sytox staining. Overall, the transfection process itself reduced viability to approximately 60%, which remained the same at all plasmid concentrations (**Figure 4.4E**). From the four DNA concentrations tested, a concentration of 5 μg of plasmid was found to be optimal, balancing viability and IGF-1Ea expression (**Figure 4.4F**). In absolute numbers, only $4.8x10^5$ out of $1x10^6$ BMdM transfected were found to be GFP positive (Total BMdM x cell viability x %GFP = $1x10^6$ x 0.6 x 0.8). Although M1- and M2-like macrophage transfection efficiencies were similar to the BMdM efficiencies (not shown), all cell types showed a transfection efficiency very variable ranging from 45% to 80%.

IGF-1Ea mRNA levels were also quantified by qPCR. Transfection with the highest concentration of the vector (5 μg), induced up to a 100-fold increase in the levels of IGF-1Ea when compared with control non-transfected macrophages and macrophages transfected with the pGFP vector provided by the manufacturer of the transfection kit (**Figure 4.4E**).

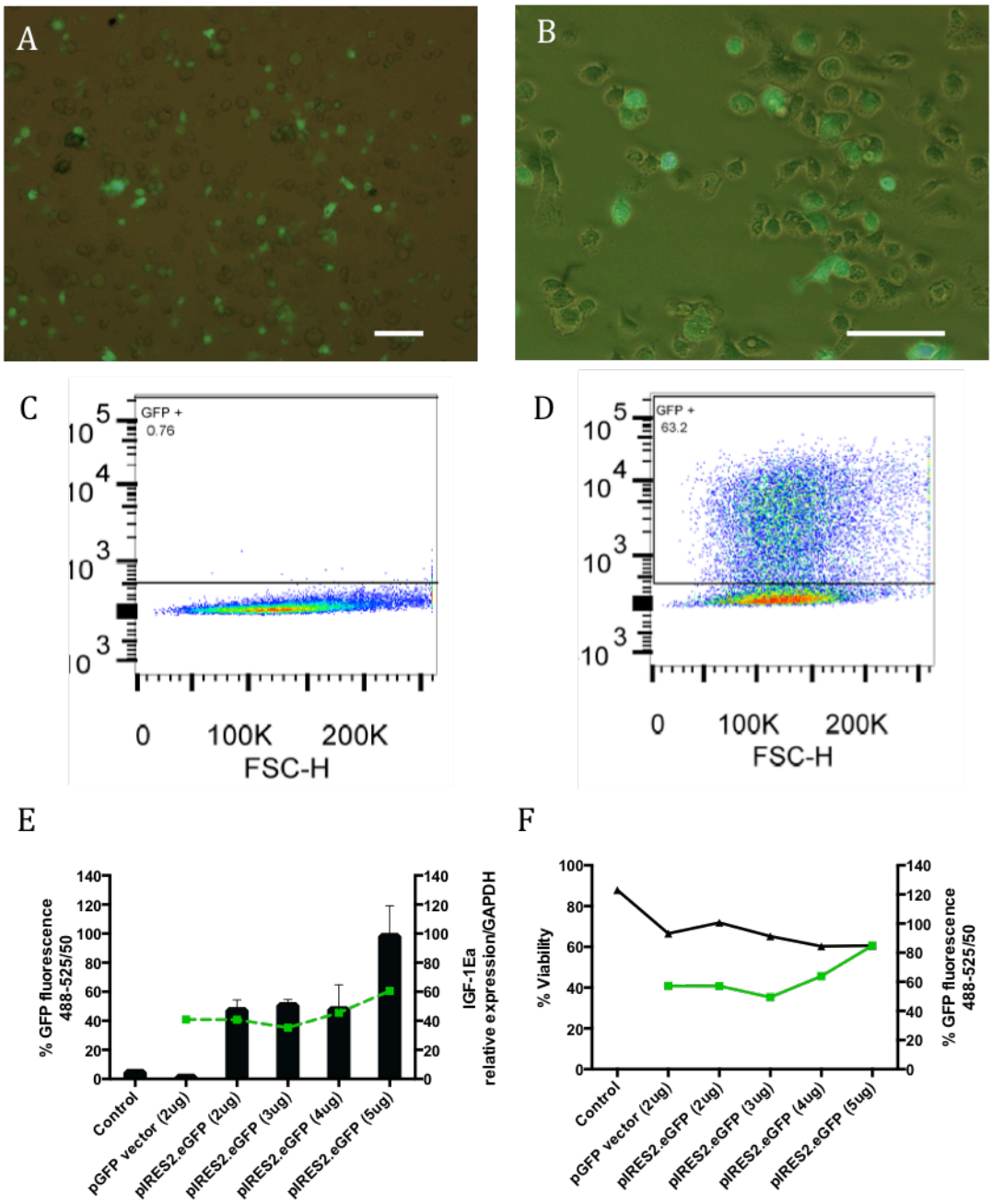


Figure 4.4. Assessment of BMdM transfection efficiency through various techniques 24 hours after transfection. Overlay of bright field and fluorescence field of pIRES2.eGFP transfected macrophages at (A) 100x and (B) 40x magnification. Scale bar, 50 µm. Flow cytometry plot depicting BMdM-GFP positive populations, (C) untransfected (D) with 5 µg of pIRES.eGFP vector. (E) GFP fluorescence (left Y axis) versus IGF-1Ea mRNA levels (left Y axis) in pIRES2.eGFP transfected BMdM, 24h after transfection. (F) Percentage viable cells by Sytox negative staining (left Y axis) and GFP fluorescence (right Y axis). n=12 wells each group. Mean values ± SEM are shown.

To assess IGF-1 protein production, immunoblot analysis was performed as described in Methodology, Section 2.3. BMdMs transfected with 5 µg resulted in a 100-fold increase in IGF-1Ea expression (**Figure 4.5A**). This was mirrored by an increase in detectable IGF-1 protein levels analysed by western blotting (**Figure 4.5B**). Interestingly, the IGF-1Ea propeptide produced by macrophages was initially secreted to the medium, thus, the mature form was not found in transfected BMdMs (**Figure 4.5B**). An IGF-1 immunoblot of conditioned medium from pIRES.eGFP transfected BMdM showed higher levels of IGF-1Ea than the IGF-1 mature form during the first 8-24 hours, however, at 72 hours post-transfection, IGF-1Ea could not be detected by western blot and only IGF-1 mature form was found (**Figure 4.5C**). A possible explanation for this result is that, at this timepoint, the lifespan of transfected BMdMs is limiting IGF-1Ea synthesis. The IGF-1Ea produced was eventually processed and cleaved, consequently, the mature IGF-1 was the only isoform observed 72 hours after transfection.

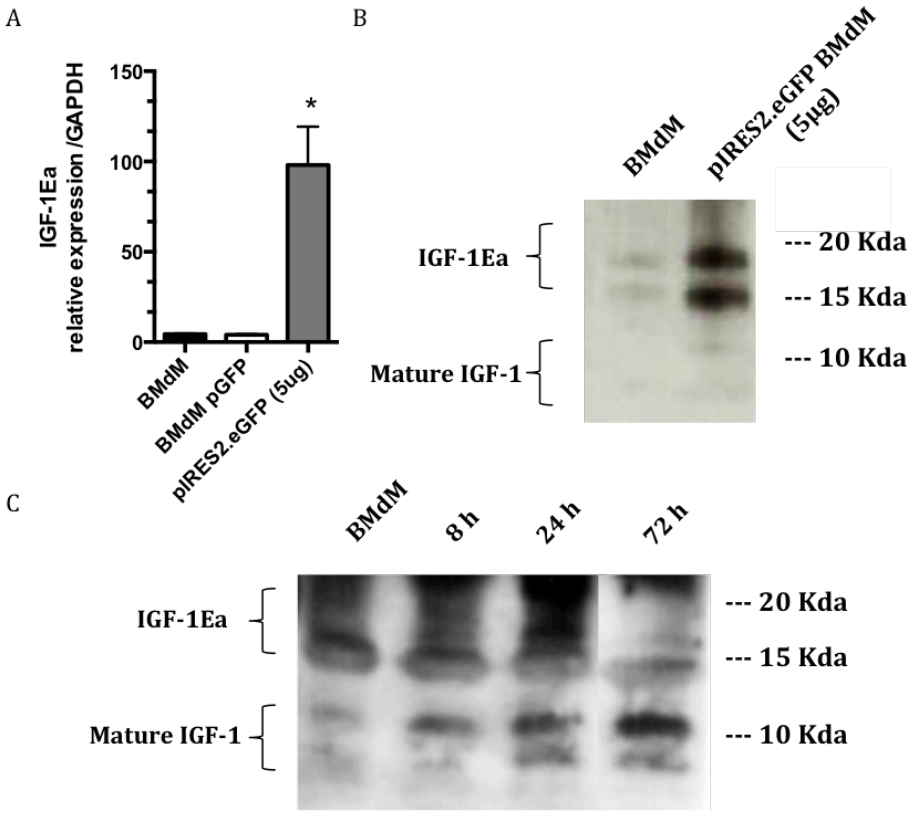


Figure 4.5 IGF-1Ea expression levels in transfected BMdM. (A) IGF-1Ea mRNA levels in BMdM transfected with 5 µg of pIRES2.eGFP. (B) Western blot of IGF-1 and IGF-1Ea protein levels in BMdM transfected with 5 µg of pIRES2.eGFP. Additional bands likely reflect differential glycosylation states, since the rodent Ea-peptide contains two N-linked glycosylation sites. (C) IGF-1 and IGF-1Ea protein levels present in the conditioned medium of transfected macrophages at 8, 24 and 72 hours post-transfection. $1x10^6$ macrophages were transfected. Mean values ± SEM are shown. * $p<0.001$ 1-way ANOVA plus Dunnett's multiple comparison test. n=3 each group.

4.5.1 Effect of IGF-1Ea on transfected BMdM *in vitro*

Previous results from our group have shown that IGF-1Ea overexpression in skeletal muscle and heart dampens pro-inflammatory activity and promotes anti-inflammatory responses (Pelosi et al. 2007 and Santini et al. 2007) Thus, the expression levels of the main cytokines modulated by IGF-1Ea, TNF-α and IL-10, were analysed. After transfection, the inflammatory cytokine TNF-α was up-regulated in both the pGFP and the pIRES2.eGFP group. Interestingly, the levels of TNF-α in BMdMs transfected with IGF-1Ea.GFP were markedly lower (**Figure 4.6A**). Conversely, levels of the IL-10 anti-inflammatory cytokine were increased 150-fold when compared with either non-transfected BMdMs or the pGFP group (**Figure 4.6B**). Although these results allude to an apparent direct autocrine and paracrine effect on BMdMs modulated by IGF-1Ea, further *in vivo* analyses are required to demonstrate specific modulation of the inflammatory process by IGF-1Ea or by the *in vitro* generated BMdMs.

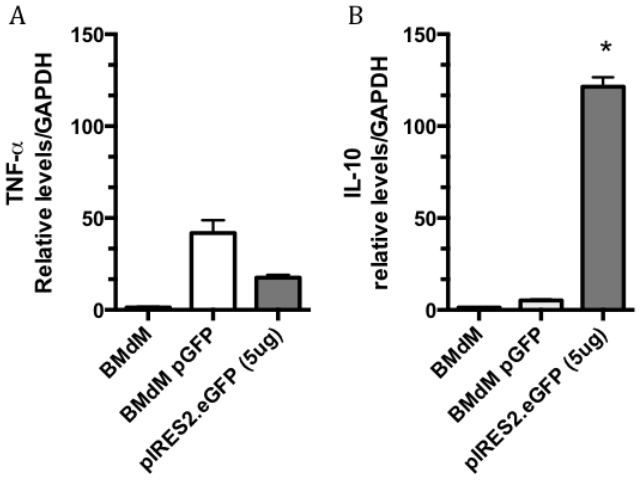


Figure 4.6. Effects of IGF-1Ea overexpression *in vitro* BMdMs. BMdM cultured for 24 hours. mRNA relative levels of (A) TNF-α and (B) IL-10 genes analysed by qPCR. Mean values ± SEM are shown. * $p<0.001$ 1-way ANOVA plus Dunnett's multiple comparison test. n=3 each group.

4.6 Homing of transplanted bone marrow-derived macrophages following TA injury and the effect of 'priming' macrophages with cytokines

In parallel to the work carried out in Section 4.5, the Tibialis Anterior muscle (TA) injury model (Methodology, Section 2.7.3 and 2.12) was performed to evaluate BMdM homing competency. The TA model involves the injection of the snake venom cardiotoxin (CTX) into the right tibialis anterior muscle (Hirata et al. 2003). The homing capacities of BMdMs were determined, before and after priming the cells with LPS/IFN-γ or IL-4 (Methodology, Section 2.5.4). As shown in Section 4.3, M2-like macrophages were the main producers of IGF-1Ea from the selected populations. In order to determine optimal

homing parameters, infusion of both M1- and M2-like BMdMs transfected with pIRES2.eGFP vector as well as BMdM cells at 7 days of differentiation (**Figure 4.7A**), 24 hours post-TA injury (**Figure 4.7B**) were performed. The infusion time was chosen based on leukocyte infiltration kinetics during the acute phases of muscle injury (Nahrendorf et al. 2013 and Tonkin et al. 2015). As described in detail in the Introduction, Section 1.3.2, after MI, inflammatory macrophages (M1-like macrophages) infiltrate into the injury site in great numbers between days 1-3 post-injury, while reparative macrophages (M2-like macrophages) macrophages predominate from days 3-7 post-injury. Therefore, the proposed transplantation window should permit entry of both M1 and M2 polarised macrophages.

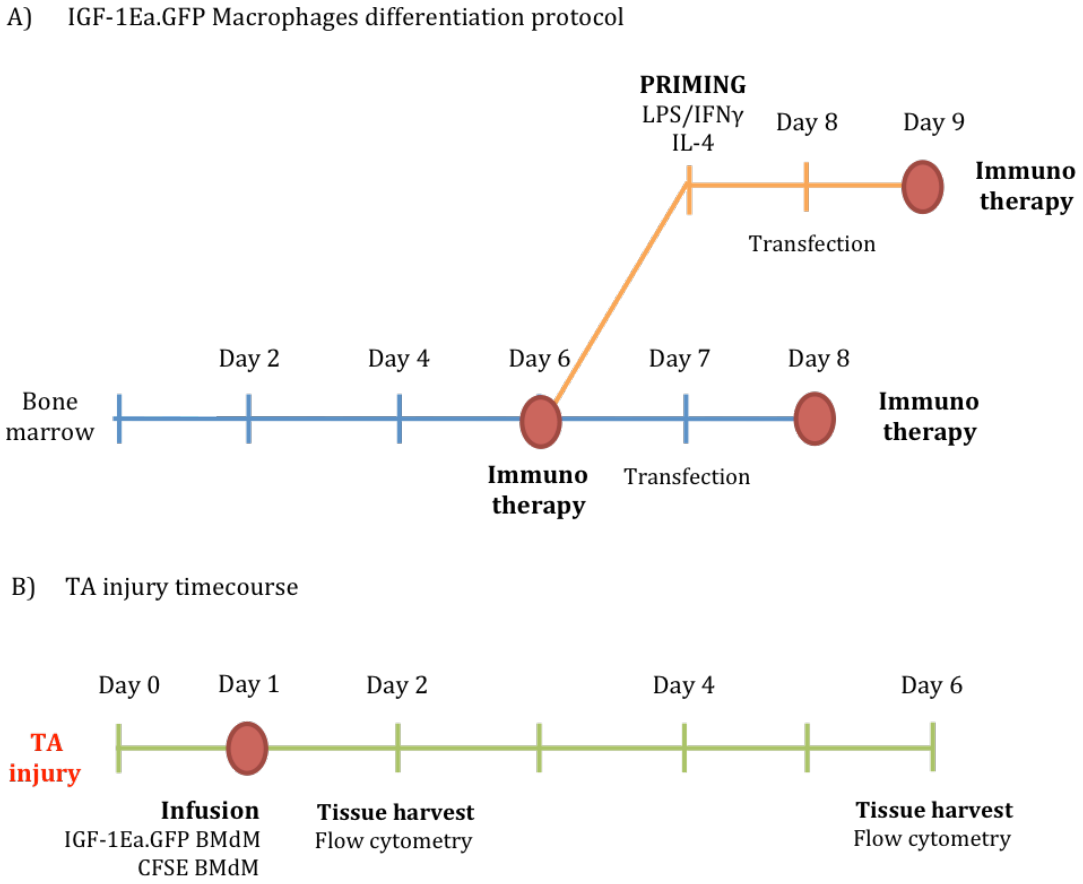


Figure 4.7. Experimental design for *in vivo* IGF-1Ea BMdM immunotherapy. (A) Bone marrow-derived macrophages differentiation process. Red sphere indicates the cells that were selected to assess BMdM homing competency. (B) TA injury timecourse. Selected BMdMs either IGF-1Ea.GFP M1-like BMdMs, IGF-1Ea.GFP M2-like BMdMs and CFSE-labelled BMdMs, were infused intravenously via vein tail 24 hours after TA injury. At either 24 hours or 6 days after infusion, macrophages from the injured TA and uninjured TA were isolated and GFP+ cells were analysed by flow cytometry for the expression of cell surface markers markers, CD45, CD11b, F4/80, Ly6C, CD206.

4.6.1 Homing of IGF-1Ea.GFP M1- and M2-like macrophages

In order to assess BMdMs homing competencies, $2x10^6$ of BMdM cells were infused intravenously (i.v.) (Methodology, Section 2.5 and 2.12), 24 hours after TA injury (**Figure 4.7A** and **4.7B**). Prior infusion, M1-and M2-like BMdMs were transfected as described in Methodology, Section 2.6, transfected BMdMs are named IGF-1Ea.GFP M1- and M2-like macrophage, respectively.

Twenty-four hours after infusion, TA from both legs, injured and uninjured, were obtained and analysed by flow cytometry for GFP fluorescence (Chapter 2, Section 2.12. In order to assess BMdM homing, several organs such heart, kidney and lung were also harvested as controls. Macrophages were analysed according to the expression of the cell surface markers CD45, CD11b and F4/80 (**Figure 4.8A, Figure 4.8B** and **Table 4.1**). GFP fluorescence can be detected in the 488 nm blue laser using a BD FACS ARIAI cell sorter. After infusion, neither IGF-1Ea.GFP M1- nor M2-like BMdM showed any engraftment into the injured muscle (**Figure 4.8C** and **Figure 4.8D**, respectively and **Table 4.1**). Surprisingly, IGF-1Ea.GFP M1-like macrophages preferentially migrated to the kidney (**Figure 4.8E** and **Table 4.1**), but not the lung (**Figure 4.8F** and **Table 4.1**). Conversely, IGF-1Ea.GFP M2-like macrophages preferentially migrated to the lung (**Figure 4.8G** and **Table 4.1**), but not the kidney (**Figure 4.8H** and **Table 4.1**).

	% Total Macrophages	% Total IGF-1Ea.GFP M1-like macrophages	% Total Macrophages	% Total IGF-1Ea.GFP M2-like macrophages
Heart	0.44	0	0.42	0
Kidney	0.54	0.12	0.59	0
Lung	2	0	2.93	0.14
TA injury	50.7	0	49.7	0
TA uninjured	2	0	1.86	0
No cells TA injury	48.3	0		
No cell no injury	1.45	0		

Table 4.1. Percentage of macrophages CD45, CD11b, F4/80 in several organs 24 hours after i.v infusion. Total macrophages were calculated from the total of alive events in the selected tissue (**Figure 4.8A**). IGF-1Ea.GFP M1- or M2-GFP macrophages were calculated from the total macrophage populations (**Figure 4.8B**). Macrophage populations are depicted as CD45+, CD11b+, F4/80+. n=4 mice per group.

Considering the probability of detecting GFP+ cells using this delivery method, the number of GFP-positive cells in lung (for IGF-1Ea.GFP M2-like macrophages) and in the

kidney (for IGF-1Ea.GFP M1-like macrophages) was 2400 and 2800 cells, respectively. The number of events was calculated as follows: IGF-1Ea.GFP M1-like macrophages; $2x10^6$ x 0.0012. IGF-1Ea.GFP M2-like macrophages; $2x10^6$ x 0.0014. Therefore, the homing efficiency to lung and kidney is between 0.12-0.14% for IGF-1Ea.GFP M1/M2-like macrophages (**Table 4.1**).

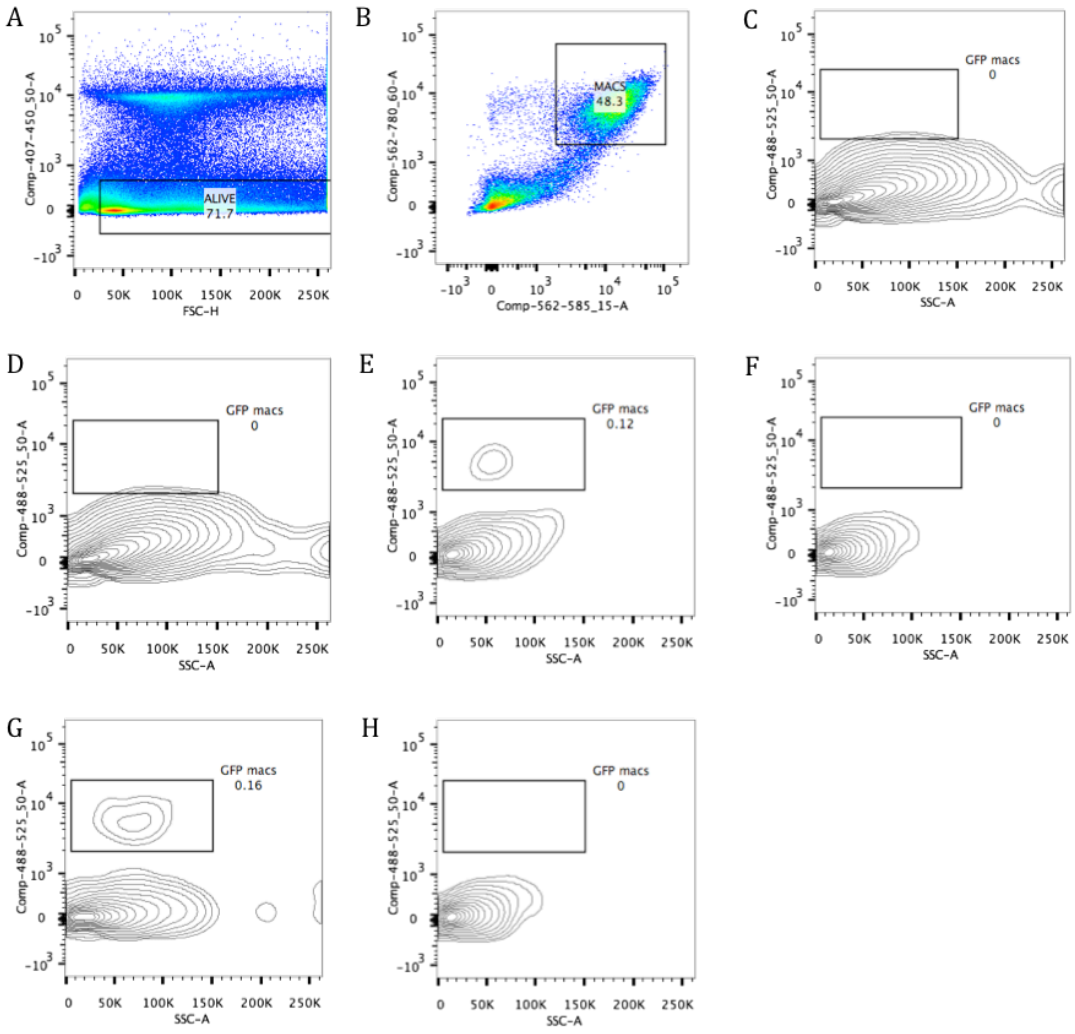


Figure 4.8. Representative flow cytometry plots of GFP+ positive BMdM in skeletal muscle 24 hours after i.v. infusion, 48 hours after CTX injury. (A) Total alive. (B) F4/80-CD11b positive macrophages. (C) IGF-1Ea.GFP M1-like macrophages in CTX injured TA. (D) IGF-1Ea.GFP M2-like macrophages in CTX injured TA. (E) IGF-1Ea.GFP M1-like macrophages in kidney. (F) IGF-1Ea.GFP M1-like macrophages in lung. (G) IGF-1Ea.GFP M2-like in lung. (H) IGF-1Ea.GFP M2-like in kidney. $2x10^6$ total. $1x10^6$ events acquired. n=3 each group. Macrophages populations are depicted as CD45+, CD11b+, F4/80+, GFP+/-.

4.6.2 Homing of CFSE-positive bone marrow-derived macrophages

In parallel with Section 4.6.1, an additional strategy was implemented to test whether non-polarised BMdMs could be a better therapeutic vehicle than the *ex vivo* manipulated IGF-1Ea.GFP M1-/M2-BMdMs. First, the number of macrophages to be infused was increased 5-fold (10×10^6). Secondly, day-7 non-polarised BMdMs were chosen since differentiated macrophages might have reduced plasticity relative to non-polarised BMdMs. Indeed, this is supported by the fact that unfractionated bone marrow cells have improved migration to organs as discussed in the Introduction, Section 1.4.1. Thirdly, CSFE fluorescence-labelled BMdMs represent a much more direct method to label and track BMdMs without the need of transfection, which in turn will increase survival. These modifications should facilitate trafficking and homing of BMdMs, as BMdMs are less affected by *ex vivo* manipulations.

Consequently, approximately 10×10^6 CSFE fluorescence-labelled BMdM were injected i.v. as described in Methodology, Section 2.12. Twenty-four hours after infusion, the TA from both legs, injured and uninjured, were obtained and analysed by flow cytometry for CFSE fluorescence. Spleen and lung were taken as positive controls since these organs have been shown (Section 4.6.1) to strongly retain migrating cells. Flow cytometry analysis indicated that approximately 1500 CFSE-labelled BMdM events (0.004% total macrophages) at the injured site preferentially homed to the injury site as shown in **Figure 4.9A** (as a percentage of total macrophages) and in **Figure 4.9B** (as absolute numbers). Retention was also observed in spleen and lung, with 0.07% of CFSE-labelled BMdM retained in the lungs and 0.03% in the spleen. Thus, in the lung, up to 40–fold more CFSE-labelled BMdM were detected when compared with TA-injured muscle. These data demonstrate that BMdMs can preferentially home to sites of muscle injury; however numbers are very low.

Surprisingly, 6 days after TA injury, the number of engrafted CFSE-labelled BMdMs in the TA injured muscle considerably increased (**Figure 4.9C** and **Figure 4.9D**). Furthermore, CFSE-labelled BMdM retention was not observed in the liver or the lung (not shown). In summary, six days after infusion, approximately 60,000 CFSE-labelled BMdMs were recruited at the injured site (**Figure 4.9C**), representing 0.5 % of the total macrophages at the given time (**Figure 4.9D**).

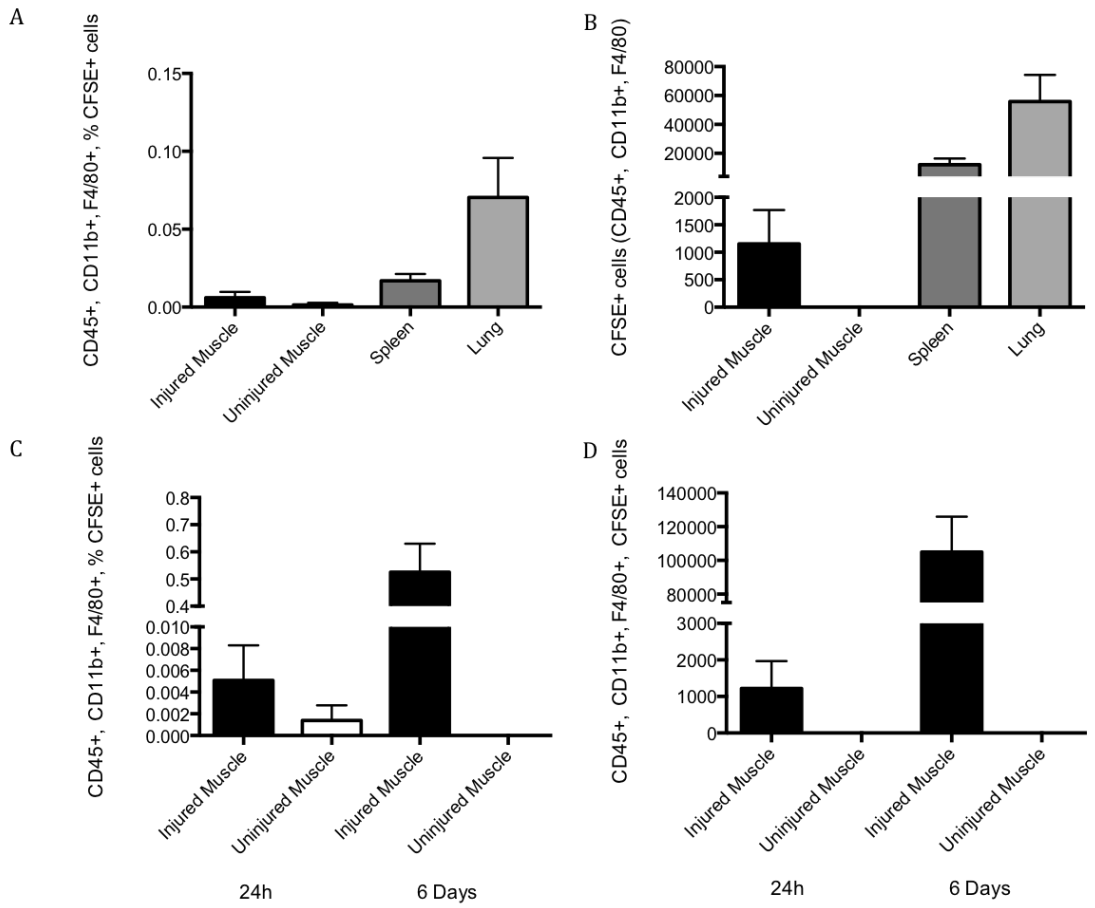


Figure 4.9. Adoptive immunotherapy of CFSE-labeled BMdMs into CTX injured muscle 24h and 6 days after injury. Analysis was performed comparing the capacity of BMdM to migrate into the damaged muscle. (A) Percentage CFSE-labeled BMdM and (B) total numbers of CFSE-labeled BMdMs in the skeletal muscle, spleen and lung, 24 hours after injection (72 hours after TA muscle injury). (C) Percentage CFSE-labeled BMdM (D) total numbers of CFSE-labeled BMdMs in the skeletal muscle, 6 days after injection. Macrophage populations are depicted as CD45+, CD11b+, F4/80+, CFSE+. Mean percentage ± SEM. n > 4 mice per group.

4.7 Discussion

The ultimate aim of this chapter was to develop a strategy to expand a population of macrophages *in vitro* to be used for transplantation into an injured host and evaluate the efficacy of immune-cell mediated delivery of IGF-1Ea to counteract the effects of muscle injury.

Studies performed *in vitro* showed that the environment encountered by macrophages modulated the expression of IGF-1Ea isoform. Interestingly, upon stimulation with IL-4 or reparative environment, macrophages respond by up-regulating the mRNA levels of IGF-1Ea. The opposite trend was observed when macrophages were stimulated with

IFNγ. Regarding the role of the IGF-1R in the IGF-1-mediated immune response, further investigations are required to understand the role of the receptor as a down-regulation of the receptor was observed upon stimulation with TNF-α/LPS but not IL-4.

The *in vitro* studies presented in this chapter indicate that BMdM can be successfully transfected and secrete IGF-1Ea into the culture medium, however, the lifespan of the BMdMs after transfection limits their action after infusion. Furthermore, *in vitro* and *in vivo* studies presented in this chapter show that overexpressing IGF-1Ea in BMdMs is possibly not the best approach for the delivery of salutary factors into the injured muscle. Particularly, the cell-based protocol using IGF-1Ea.GFP M1-/M2-like BMdMs demonstrated that these cells do not home to injured muscles; rather, IGF-1Ea.GFP M1-/M2-like BMdMs differentially homed to either kidney or lung, however, it is most like these cells are retained in such organs. The results shown in Section 4.6 taken together with the fact that the lifespan of IGF-1Ea.GFP M1-/M2-like BMdMs is limited after transfection, restricted the use of IGF-1Ea.GFP M1-/M2-like BMdMs for the treatment of muscle injuries, and specially the heart. Nevertheless, the fact that these cells preferentially home to either lungs or the kidney could open a new line of research for the use of IGF-1Ea.GFP M1-/M2- like BMdMs as desirable cell vehicles for inflammatory-driven diseases affecting these organs. One of the reasons that might explain the reduced homing competency of macrophages can be the cell type chosen. IGF-1Ea.GFP M1-/M2-like BMdMs are fully differentiated cells with limited migratory capacities. Consequently, in Section 4.6.2, non-polarised bone marrow-derived macrophages were used. Experiments using CFSE-labelled BMdMs showed that this population preferentially homed to the injured muscle. However, similar to the results presented in Section 4.6.1, these cells were retained in great measure in organs such as liver and spleen. Interestingly, six days after infusion, no retention was observed in these organs and a relative increase in CFSE-labelled BMdMs number was found at the injured muscle. Consequently, Analysis of IGF-1 overexpression in injured TA after BMdMs infusion was not evaluated because of the low engraftment.

Considering all the data reported in this chapter, it could be concluded that from a therapeutic point of view the use of BMdMs as a vehicle has proven to be very inefficient, with more than 90% of IGF-1Ea.GFP M1-/M2-like BMdMs or CFSE-labelled BMdMs disappearing or undetectable after injection.

The main conclusions of this chapter are that (i) the more differentiated the macrophages become, the less migratory they are. (ii) IGF-1Ea.GFP M1-/M2-like BMdMs transfected with the IGF-1Ea plasmid do not exhibit migration capacity whatsoever but, instead lung and kidney retention is observed. (iii) Using a CFSE-labelled approach, BMdMs displayed some homing capacities although not in adequate numbers to cause a therapeutic effect and, therefore, should not be considered for further translational studies.

One of the hypotheses to explain the disappearance of the majority of the infused cells was that survival might have been compromised due to temperature changes, use trypsin for cell detachment, transition from PBS to blood, or/and the transfection process itself as well as BMdMs are in a more differentiated state than other cells such as monocytes and bone marrow cells. Furthermore, technical difficulties were experienced during the development of this approach including BMdM culture, transfection efficiencies, non-homogenous GFP expression, IGF-1Ea production, and cell survival. Because of these setbacks, proof that engineered macrophages are functional and could potentially enhance healing to injured muscle was ultimately not explored due to technical difficulties described above. Indeed, this work was abandoned at this stage in order to explore other suitable vehicles for IGF-1Ea. Consequently, more cost-effective and time-efficient strategy was pursued, developed and achieved, which is described in Chapter 5.

Nonetheless, if the BMdMs system had succeeded, several techniques would have been used to assess the beneficial effects of this approach. For instance, skeletal muscle regeneration would have been judged as a significant increase in the cross-sectional area of newly formed multinucleated myotubes in skeletal muscle following TA injury (Barton-Davis et al. 1998). Furthermore, flow cytometry analysis studies would have been valuable to characterise macrophage relationships and, to identify the percentage of M1 and M2 macrophages after 1, 3, 5 and 7 days after injury coinciding with M1, M1 to M2 shift, and M2 macrophages, respectively. Finally, real time PCR would have been used to study whether the BMdM therapy modulates the inflammatory response, by studying changes in inflammatory mediators including Il-1β, IL-6, TNF-α, IFN-γ, IL-10, and IL-13.

In addition to this, the extent of skeletal muscle regeneration would have been analysed by quantification of collagen content (fibrosis) using picrosirius red staining, and

quantifying the proportion of multinucleated fibers generated after injury (a marker of extent of regeneration).

4.7.1 Limitation of the approach

The idea behind this approach was indeed very appealing from a therapeutic point of view; however, the main limitations were already encountered at the planning stages, beginning at the time of selecting a suitable cell type as vehicle. Ideally, monocytes should have been the cell of choice. Unfortunately, monocyte isolation procedures are still not well refined, and sufficient numbers cannot be realistically isolated. Furthermore, given that adequate numbers could be isolated, the best available protocol for monocyte transfection has an efficiency of 10-30%, causing high mortality rates (Burke et al. 2002). These two obstacles were one of the main reasons for choosing macrophages instead of monocytes in this chapter.

In summary, both *in vivo* and *in vitro* studies have shown that BMdMs are less suited as vectors for gene therapy than initially thought. *In vitro*, one of the main limitations is the yield of viable BMdMs positively transfected, which is reduced by 50%. Moreover, the heterogeneity in transfection efficiencies generates a less reliable homogenous population, in terms of IGF-1Ea synthesis and delivery. An additional limitation is that macrophage transfection is transient limiting BMdMs lifespan. *In vivo*, the main limitation was the (lack of) BMdMs homing efficiency and the retention in non-target organs such us spleen and lung.

4.7.2 Outcomes

Other macrophage-based approaches are being considered at the moment. In Nadia Rosenthal's group in Australia, luciferase-labelled macrophages (DKO-MΦs) as an alternative to study. They have shown that these macrophages can home to the sites of injury when primed with angiotensin II. Indeed, priming macrophages with angiotensin II significantly improved the homing competency of these cells. Another aspect that is being explored is how to minimise concerns regarding non-autologous allogeneic transplantations, such as rejection.

Additionally, Dr Rosenthal´s group in Australia is also exploring the generation of myeloid cells from iPSCs and testing their homing competencies.

Chapter 5 - Adeno-associated virus type 9 (AAV9) IGF-1Ea gene transfer into the damaged heart after ischemia/reperfusion injury.

5.1 Introduction

Cardiac gene transfer serves as a novel therapeutic approach in the treatment of heart diseases (Introduction, Section 1.4.2). In recent years, the use of AAV has proved to be the most promising gene delivery system for transfer of genes to post-mitotic cells (Gregorevic et al. 2006, Wang et al. 2005 and Walker et al. 2009). In 1998, Prof. Rosenthal successfully delivered AAVs loaded with IGF-1 to aging or dystrophic skeletal muscle (Barton-Davis et al. 1998). In that paper, IGF-1 expression promoted an increase of 15% in muscle mass and 14% in strength in old adult mice.

As described in the Introduction, Section 1.4.2.2, AAV was selected above other serotypes due to high tropism to heart tissue as well as the lack of pathogenicity and persistence of viral expression. There are several studies indicating that the newly produced serotypes AAV, such us AAV5, AAV6, AAV8, AAV9, with so-called cardiac tropism, can achieve greater transduction into the heart muscle than AAV1, AAV2, AAV3, AAV4. In a study in 2012, Hongfei compared intravenous versus intracoronary delivery of several of these AAV serotypes. Of all the serotypes tested, the highest cardiac expression was achieved via intracoronary delivery of AAV9 (Hongfei at al. 2012 and Lai et al. 2012). In another study, Prasad determined that AAV9 was the serotype with the highest transduction efficiency requiring an average of nearly two vector genomes per cell to attain 85% transduction efficiency (Prasad et al. 2011). So far, high efficiency whole heart gene delivery in small animals has only been effectively achieved with AAV serotype 9 (Pacak et al. 2006 and Bostick et al. 2007).

The overall purpose of this chapter was to investigate whether adeno-associated virus (AAV) serotype-9 (AAV9) can (i) successfully deliver IGF-1Ea into the heart after myocardial infarction and (ii) ameliorate the adverse effects of heart remodeling after ischemic injury in a clinically relevant setting.

5.2 pAAV9.IGF-1Ea expression on neonatal cardiomyocytes and AAV9.IGF-1Ea infection of HL-1 cells

Mus musculus IGF-1Ea consensus cDNA sequence was cloned into a pAC-cTNT backbone. Successful cloning was assessed by (i) restriction enzyme analysis and (ii) plasmid sequencing (Methodology, Section 2.11). Following this assessment and prior *in vivo*

work, IGF-1Ea expression levels were evaluated *in vitro* by transfecting rat neonatal cardiomyocytes with the pAAV9.IGF-1Ea vector. Three days after transfection, the IGF-1Ea mRNA levels were 10000-fold increased when compared with the control untransfected cardiomyocytes (**Figure 5.1A**). This increase also correlated with higher levels of IGF-1 protein measured by western blot (**Figure 5.1B**). In a different set of experiments, the luciferase activity of the AAV9.IGF-1Ea virus was assessed by a chemo luminescence assay indicating that the bi-cistronic mRNA was fully functional as Luciferase activity was observed three days after infection (**Figure 5.1C**).

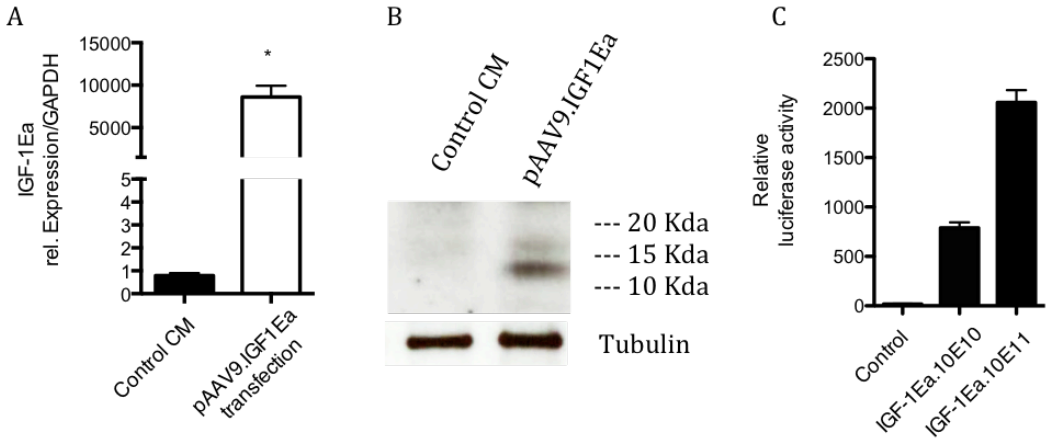


Figure 5.1. Rat neonatal cardiomyocytes transfected with pAAV9.IGF-1Ea vector. IGF-1Ea levels were analysed by (A) qPCR and (B) western blot 3 days after transfection. $1.5x10^4$ neonatal cardiomyocytes were transfected for this experiment, with 500ng of the vector. n=3. (C) Relative luciferase activity of $5x10^5$ HL-1 cells infected with the AAV9.IGF-1Ea virus three days after infection. n=4. Mean values ± SEM are shown. *p<0.05. Two-tailed Student's *t*-test was performed to compare Control CM vs. pAAV9.IGF.1Ea.

5.3 Characteristics of intravenous AAV9.IGF1-Ea gene transfer

To evaluate the therapeutic potential of AAV9-mediated IGF-1Ea gene transfer, we constructed an AAV9 vector encoding the IGF1-Ea mouse cDNA, the expression of which was driven by the cardiac troponin promoter (cTNT). The vector also contained an internal ribosomal entry site (IRES) for the firefly luciferase reporter gene (**Figure 5.2A**), allowing gene delivery to be readily assayed. The *in vivo* transduction levels were first assessed by administering $3.5x10^{11}$ GC of AAV9.IGF1Ea in a single intra-femoral vein injection to C57/BL6 mice.

Quantitative analysis of luciferase and IGF-1Ea expression verified increased levels of mRNA by 3 days post-injection, however, IGF-1Ea levels were not significantly induced

until 7 days post-injection (**Figure 5.2B** and **5.2C**). Immunohistochemistry for luciferase confirmed extensive expression throughout the heart with a mosaic-like pattern (**Figure 5.2D, 5.2E**, **5.2F and 5.2G**) typical of AAV gene transfer (Prasad et al. 2011).

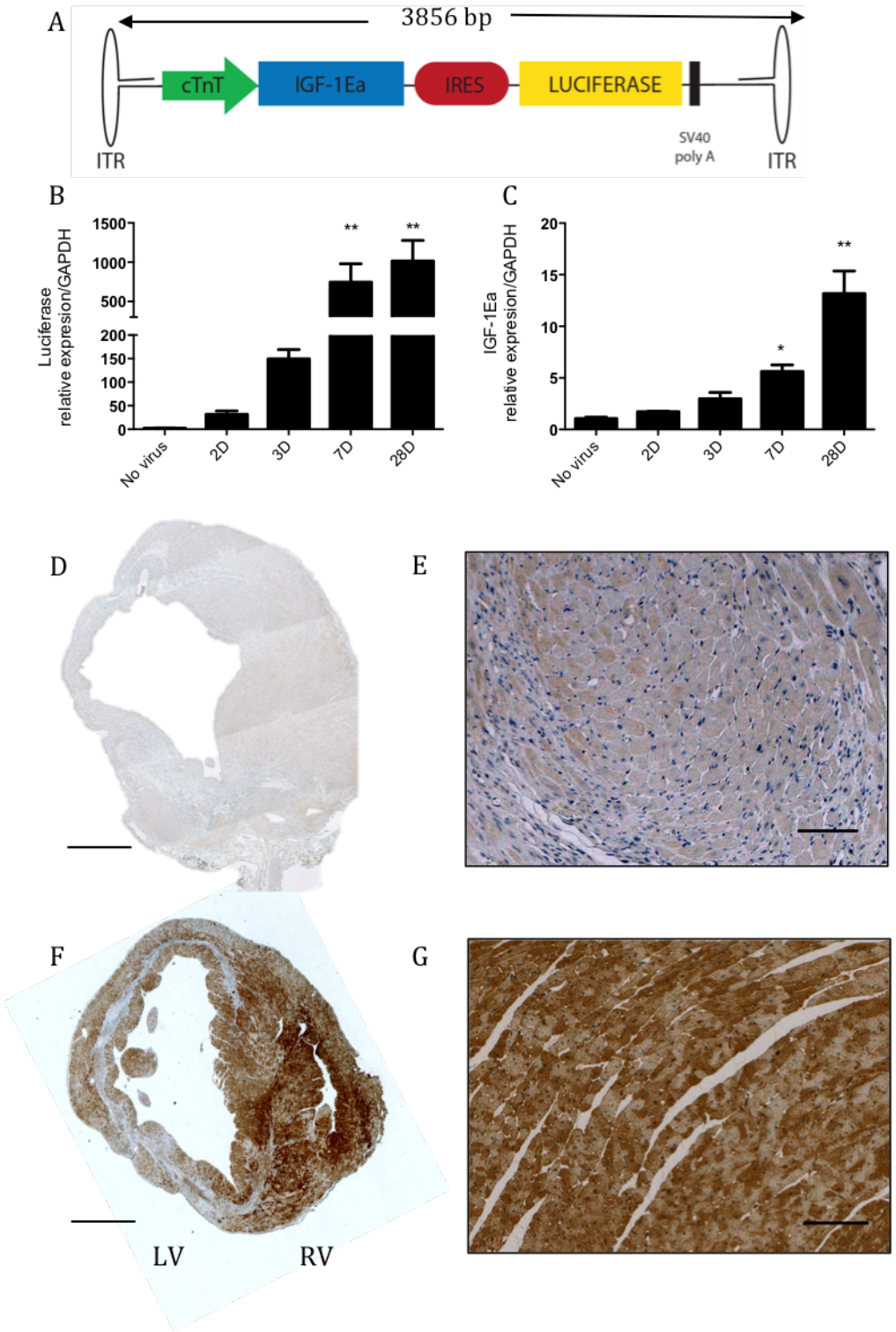


Figure 5.2. AAV9.IGF-1Ea timecourse of expression in the murine heart after intravenous injection. (A) Schematic representation of recombinant AAV vector. The construct contains the IGF-1Ea mouse gene (462 bp) and an internal ribosomal entry site (IRES) followed by the firefly

luciferase reporter gene. The expression of this bi-cistronic DNA is under the control of the cardiac troponin promoter (cTNT), and the SV40 polyA signal, flanked by the AAV inverted terminal repeats (ITR), shown as hairpin loops. The AAV vectors (AAV9.GFP and AAV9.IGF-1Ea) were packaged into AAV9 capsids. Quantitative qPCR analysis of (B) luciferase and (C) IGF-1Ea in the heart at several timpoints after AAV9.IGF-1Ea viral injection. n=3. Mean values ± SEM are shown. *P<0.05, **P<0.001. One-way ANOVA with Dunnett's Multiple Comparison test with I/R group (no virus group). (D-G) Immunohistochemistry of luciferase expression in heart sections 28 days after ischemia/reperfusion (I/R). (D-E) I/R group (no virus group), (F-G) AAV9.IGF-1Ea $3.5x10^{11}$ GC group, 5 hours after I/R. (D and F) whole heart. Scale bar, 1 mm. (F - G) 40x magnification. Scale bar, 250 μm. RV, right ventricle. LV, left ventricle.

By contrast, there was no difference in IGF-1Ea mRNA expression levels between I/R control group and AAV9.IGF-1Ea groups in liver and lung (**Figure 5.3A** and **5.3B**).

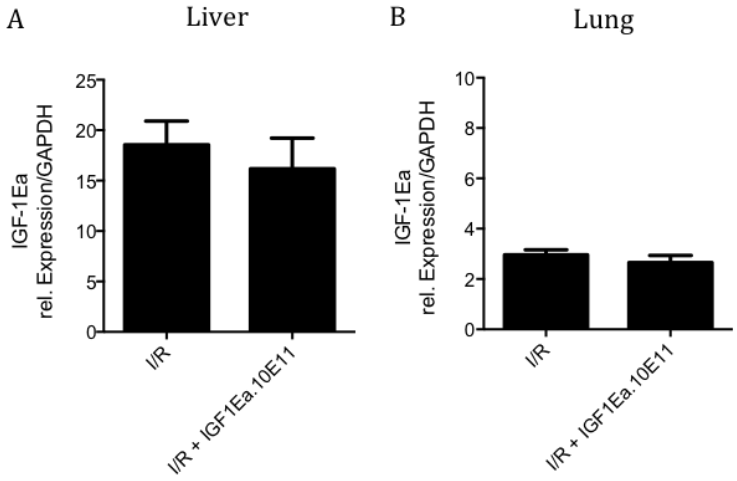


Figure 5.3. IGF-1Ea mRNA levels 28 days after ischemia/reperfusion. (A) liver and (B) lung. n= 5-9 per group. Mean values ± SEM are shown. *p<0.05. Two-tailed Student's *t*-test was performed to compare I/R vs. AAV9.IGF1Ea $3.5x10^{11}$ 28 days after MI.

The *in vivo* expression of luciferase was evaluated at different timepoints. Significant expression of luciferase *in vivo* was seen in the heart at 7 days post-injection. Ectopic expression in the liver was detected at much lower levels than in the heart, as early as 2 days post-injection (**Figure 5.4**), temporarily overriding the specificity of the cTNT promoter. *Ex vivo* imaging detected luciferase expression in the heart as early as 3 days post-injection (**Figure 5.4A, 5.4B** and **5.4C**). Further analysis revealed that the emission of photons at 3 days was blocked by the tissue thickness and composition of the chest (not shown). In conclusion, cardiac expression of IGF-1Ea starting between 3 and 7 days

after i.v injection exhibited robust and sustained gene expression, and bioluminescent imaging of luciferase was an indicator of co-expressed IGF-1Ea.

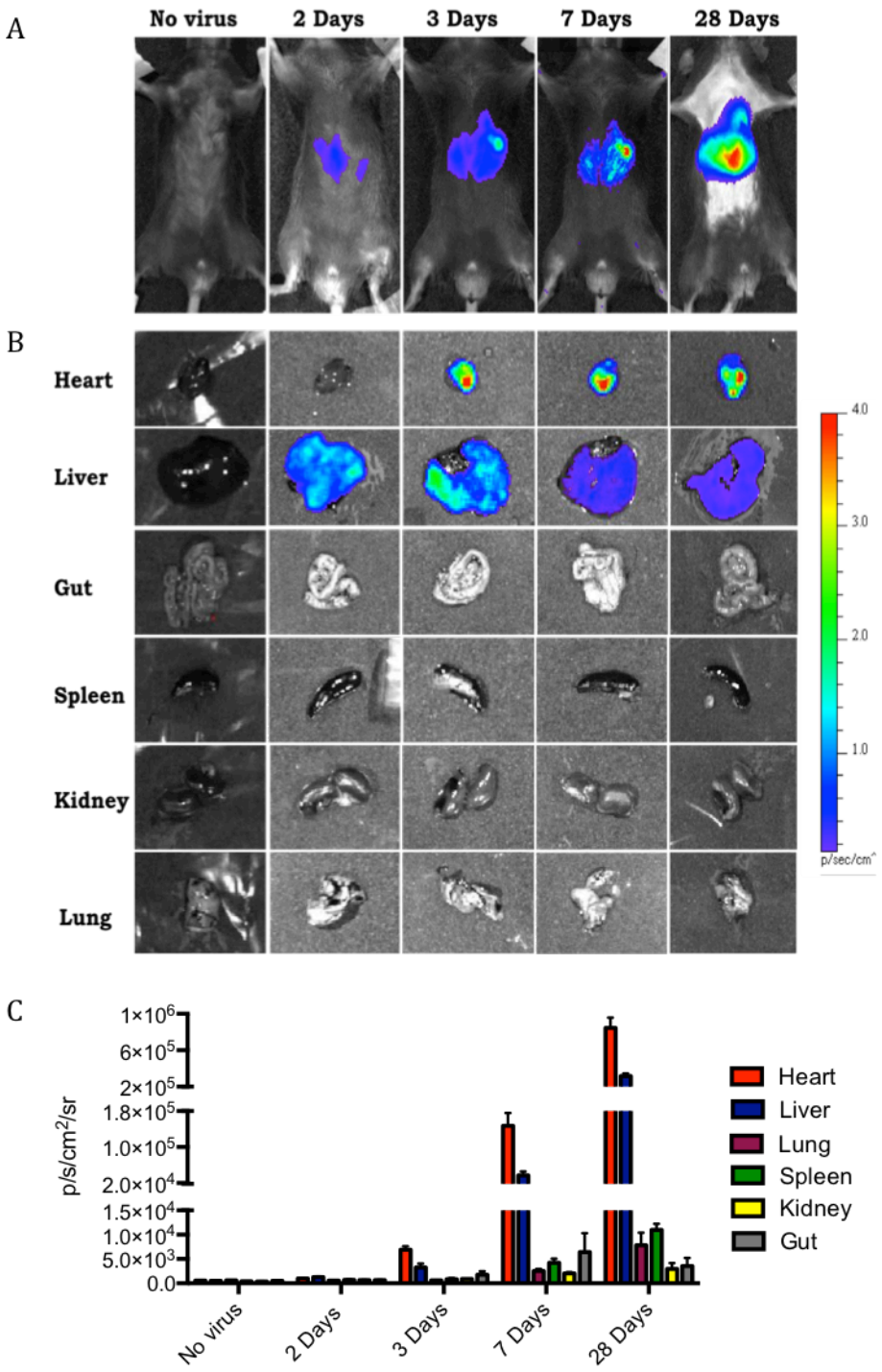


Figure 5.4 Bioluminecesce imaging illustrating the distribution of luciferase at several timepoints after intravenous injection of AAV9.IGF1Ea. *Ex vivo* bioluminescence images of (A) whole body and (B) at indicated organs from mice that received AAV9.IGF1Ea $3.5x10^{11}$ genome copies (GC) at several timepoints. (C) Bioluminescence analysis of AAV9.IGF1Ea.10^{11} specificity after intravenous delivery. Mean values of luciferase shown as average radiance (photons/s/cm2/sr) from the regions of interest and plotted against time in individual organs.

5.4 Echocardiography assessment of AAV9.IGF-1Ea gene delivery after ischemia/reperfusion.

To test the efficacy of virally delivered IGF-1Ea in ameliorating the response to cardiac injury, mice underwent myocardial ischemia for 45 min followed by reperfusion (**Figure 5.5A**). Four groups of animals were compared; I/R group (no virus group) and a group receiving $3.5x10^{11}$ genome copies (GC) of AAV9.GFP (I/R + AAV9.GFP) were used as negative controls; for AAV9.IGF1Ea two different viral titers were tested, $3.5x10^{10}$ GC and $3.5x10^{11}$ GC (I/R + IGF1Ea.10^{10} and I/R + IGF1Ea.10^{11}), respectively based on Jessup et al. 2001. AAV9 administration was performed 5 hours after surgery by intra-femoral vein injection and mice were sacrificed 28 days after injection (**Figure 5.5A**). A significant dose-dependent increase in IGF-1Ea mRNA level was observed in those groups that received the AAV9.IGF1Ea treatment (**Figure 5.5B**). ELISA quantification revealed no differences in IGF-1 serum levels between groups (**Figure 5.5C**), confirming our previous study. IGF-1Ea strongly adheres into the extracellular matrix, retaining the propeptide locally, preventing their release into the circulation, and minimizing the potential hazard of ectopic effects (Hede et al 2012).

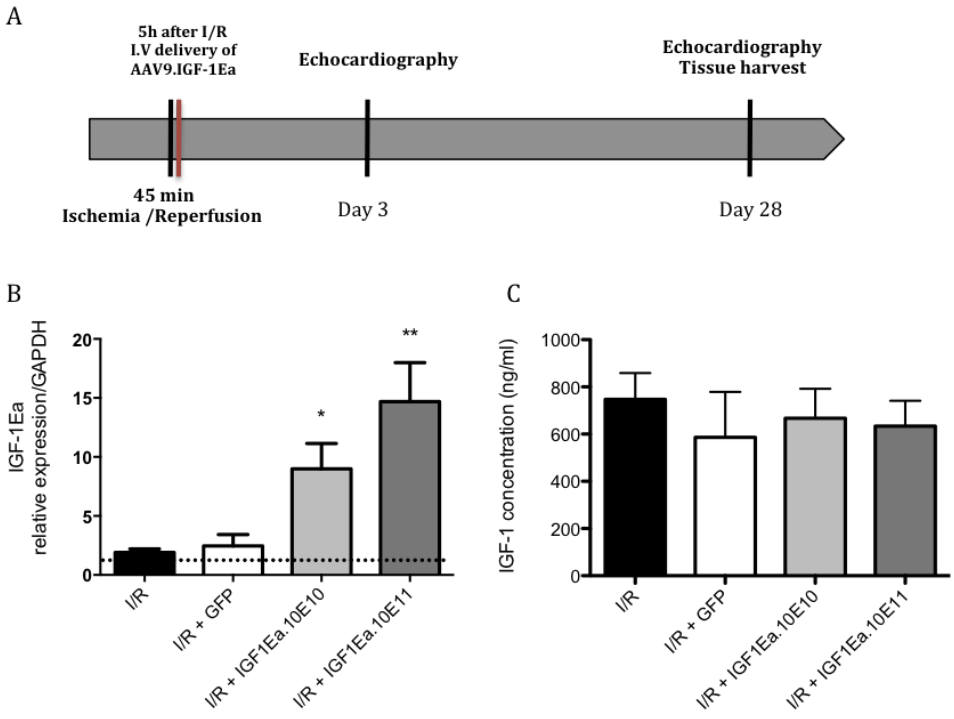


Figure 5.5. AAV9.IGF-1Ea gene transfer experimental design. (A) AAV9.IGF1Ea was administered intravenously, 5 hours after ischemia/reperfusion (I/R) and echocardiographic measurements were taken at 3 days and 28 days. (B) IGF-1Ea mRNA levels in the heart 28 days after I/R and after treatment were quantified by qRT-PCR. n=3-7. (C) Serum concentration of IGF-1, 28 days post-I/R. Mean values ± SEM are shown, n=6-14. *P<0.05, **P<0.001. One-way ANOVA, Dunnett's Multiple Comparison test with I/R group (no virus group).

5.4.1 AAV9.IGF1Ea gene transfer improves global left ventricular function after ischemia/reperfusion.

Echocardiographic analysis at 28 days after I/R revealed improved cardiac function in mice treated with AAV9.IGF1Ea (I/R+IGF1Ea.10^{10} and I/R+IGF1Ea.10^{11}) compared to untreated mice and mice injected with AAV9.GFP (**Figure 5.6A** and **Table 5.1**). LV systolic function in IGF-1Ea overexpressing mice at 28 days was also improved compared to function at 3 days in the same mice. In addition, AAV9.IGF1Ea treated mice showed reduced LV dilation 28 days post-I/R (**Figure 5.6B, Figure 5.6C** and **Table 5.1**) compared to I/R and AAV9.GFP. All four groups showed similar functional worsening in cardiac parameters and chamber dilation 3 days post-I/R regardless of the treatment, suggesting that initial infarct size was analogous among all groups (**Table 5.1**). Notably, functional improvement was more evident in those groups where the highest AAV9.IGF1Ea viral titer was administered.

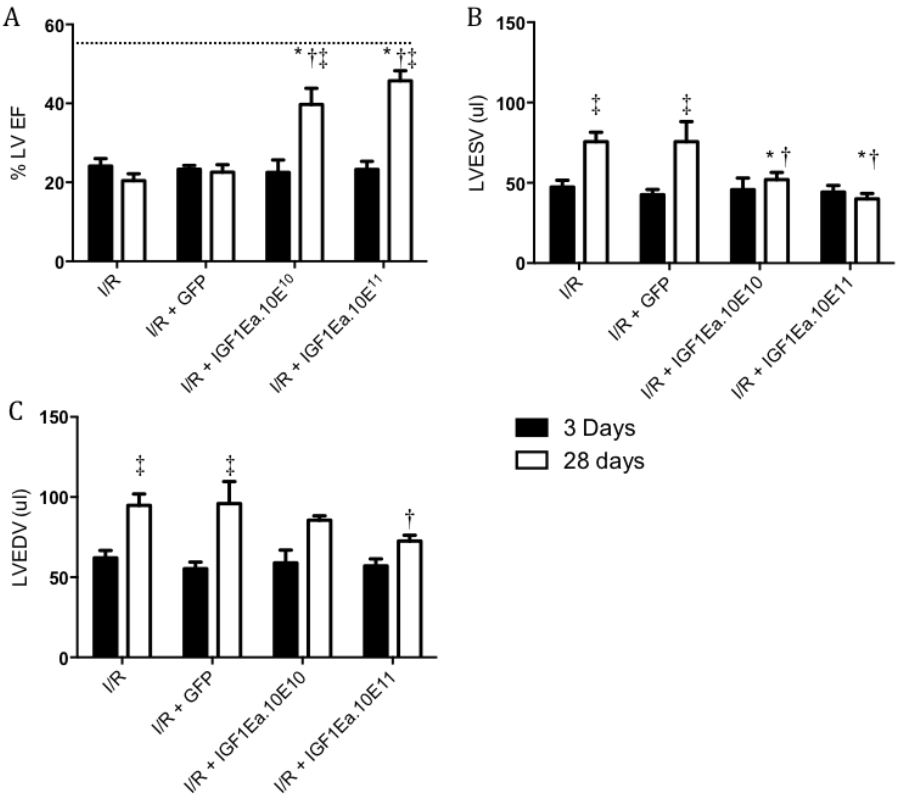


Figure 5.6. IGF-1Ea gene transfer improves cardiac function and left ventricular dilation 28 days after ischemia reperfusion. (A-C) Echocardiographic was performed at 3 and 28 days post-I/R. (A) Left ventricular ejection fraction, LVEF, and (B, C) Left ventricular end systolic and diastolic volumes, LVESV and LVEDV, respectively. Mean values, ± SEM are shown. n= 4-6 per group. *P<0.05 I/R vs. AAV9.GFP, AAV9.IGF1Ea groups. One-way ANOVA with Dunnett's post-test. †P<0.05. Two-way ANOVA to compare the 4 groups with Bonferroni post-tests. ‡ P<0.05. Two-way ANOVA to compare 3 days vs. 28 days with Bonferroni post-tests. The dashed line shows the ejection fraction of basal group.

5.4.2 Left ventricular regional wall motion is enhanced by 28 days after AAV9.IGF1Ea gene transfer.

Quantitative evaluation of LV regional wall motion after infarction and ischemia was performed using echocardiographic analysis. Consistent with the LV systolic functional data, a reduction in the heart failure marker Acta1 was significantly reduced in AAV9.IGF1Ea treated group (**Figure 5.7A**). Improvements in the wall score motion index (WSMI) were also observed in those groups after IGF-1Ea gene transfer (**Figure 5.7B**). Moreover, mice over-expressing IGF-1Ea showed fewer akinetic segments compared to I/R and I/R+GFP control groups (**Figure 5.7C**). In agreement with our evidence that initial infarct size was not changed, no significant difference was observed between the different groups for either WSMI or individual segment assessment at 3 days post-I/R (**Table 5.1**). Both the WSMI and the contraction assessment indicate that AAV9.IGF1Ea treatment improves the overall contractile function of the heart.

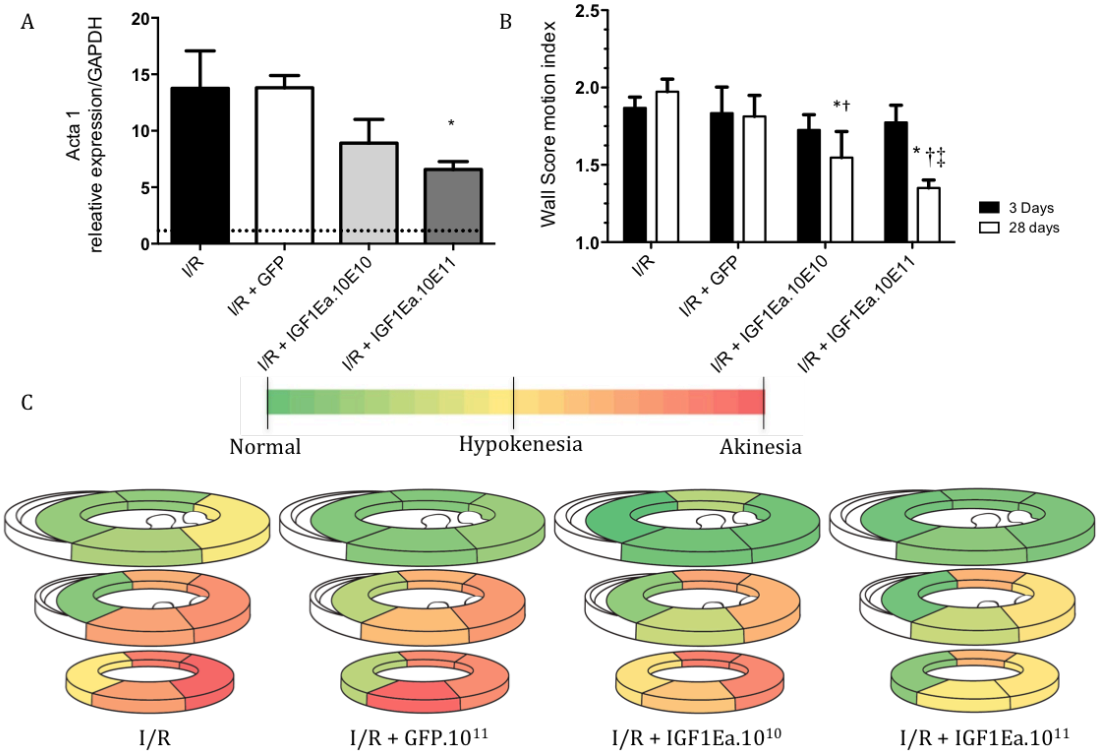


Figure 5.7. IGF-1Ea gene transfer reduces cardiac damage, improves cardiac motion and reduces dilation after ischemia/reperfusion. (A) mRNA levels of α-skeletal actin. (B) Wall score motion index. (C) Segment analysis based on wall motion and systolic thickening. Segment scores are colored coded from green to red representing: normal or hyperkinesis = green, hypokinesis = yellow, akinesis = red. Black bars, 3 days after I/R. White bars, 28 days port I/R. n=7-13. Mean values, ± SEM are shown. *P<0.05 I/R vs. AAV9.GFP, AAV9.IGF1Ea groups. One-way ANOVA with Dunnett's Multiple Comparison post-test. †P<0.05. Two-way ANOVA to compare the 4 groups with Bonferroni post-tests. ‡ P<0.05. Two-way ANOVA to compare 3 days vs. 28 days with Bonferroni post-tests. The dashed line shows the EF of basal group.

	3 Days post I/R			
	I/R	**I/R + AAV9.IGF1Ea 3.5x10^{10} GC**	**I/R + AAV9.IGF1Ea 3.5x10^{10} GC**	**I/R + AAV9.GFP 3.5x10^{11} GC**
LVIDD	3,647±0.1249	3.978±0.1978	3.782±0.1363	3.757±0.1431
LVIDS	2,909±0.129	3.251±0.1334	3.192±0.1345	3.236±0.1563
LVEDV	62,07±4,661	55,3±4,093	58,94±7,967	57,11±4,329
LVESV	47,34±4,199	42,53±3,303	45,73±7,232	44,25±4,031
LVEDA	12.76±0.6272	13.56±0.8405	13.54±1.338	12.43±0.9266
LVESA	9,543±0,5581	9,99±0,6829	10,37±1,017	9,183±0,9007
Number of segments affected	*6.038±0.3645*	*5.4±0.6403*	*5.714±0.5759*	*4.857±0.8071*
Cardiac score	*22,77±3,03*	*21,71±4,11*	*20,71±3,15*	*21,30±4,19*
Wall score motion index	1,90±0,25	1,81±0,34	1.73±0.26	1,78±0,35
	28 Days post I/R			
	I/R	**I/R + AAV9.IGF1Ea 3.5x10^{10}GC**	**I/R + AAV9.IGF1Ea 3.5x10^{10} GC**	**I/R + AAV9.GFP 3.5x10^{11} GC**
LVIDD	4.627±0.1226 ‡	4.705±0.2768 ‡	4.291±0.1993 *	4.016±0.1145 *†
LVIDS	*4.022±0.1352* ‡	3.62±0.2105 ‡	3.183±0.1778	3.216±0.2105 *†
LVEDV	*104.8±8.251* ‡	104.1±15.72 ‡	85.51±2.737	72.6±3.541 †
LVESV	*80.01±5.973* ‡	75.58±12.47 ‡	46.36±3.986 *†	39.89±3.386 *†
LVEDA	*17.04±0.5598* ‡	17.53±1.801 ‡	16.36±1.123	14.07±0.8024
LVESA	*12.24±0.6517* ‡	12.85±1.412 ‡	10.21±0.9048	8.491±0.6365 *†
Number of segments affected	*5.867±0.3326*	6±1.204	4.571±1.077 †	3.7±0.4955 *†‡
Cardiac score	*23,69±3,25*	22,50±7,50	18,57±5,35 *	16,20±1,99 *†‡
Wall score motion index	1,97±0,27	1,88±0,63	1,55±0,45 *†	1,35±0,17 *†‡
HW/BW	7,98±2,14	8,11±1,93	7,99±1,21	7,71±2,87
n	13	7	10	10

Table 5.1. Echocardiographic measurements at 3 and 28 days after ischemia/reperfusion (I/R). LVIDD, left ventricular internal diameter in diastole; LVIDS, left ventricular internal diameter in systole; LVEDV, left ventricular end-diastolic volume; LVESV, left ventricular end-systolic volume; LVEDA, left ventricular end-diastolic area; LVESA, left ventricular end-systolic area. Number of segments affected, number segments with abnormal contractility out of 12 segments in the LV short axis view, as shown in **Figure 5.7C**. Cardiac score, sum of the severity score of each segment with lower values indicating better motion. Wall motion score index, cardiac score divided by the total number of segments. HW/BW, heart weight/body weight. n=7-13. Mean values ± SEM are shown. *P<0.05 I/R vs. AAV9.GFP, AAV9.IGF1Ea groups. One-way ANOVA with Dunnett's Multiple Comparison post-test. †P<0.05. Two-way ANOVA to compare the 4 groups with Bonferroni post-tests. ‡ P<0.05. Two-way ANOVA to compare 3 days vs. 28 days with Bonferroni post-tests.

5.5 IGF-1Ea gene transfer reduces infarct size and cardiac fibrosis

To determine infarct size, infarct expansion and scar thickness after AAV9.IGF1Ea treatment histological analysis was performed. Improved cardiac function in the AAV9.IGF1Ea groups was accompanied by thicker scars when compared with I/R group (no virus group) and I/R + GFP control groups (**Figure 5.8A**). Scar length was also diminished in the IGF-1Ea treated groups (**Figure 5.8B**), suggesting reduced infarct expansion. Total fibrosis was also reduced (**Figure 5.8C**).

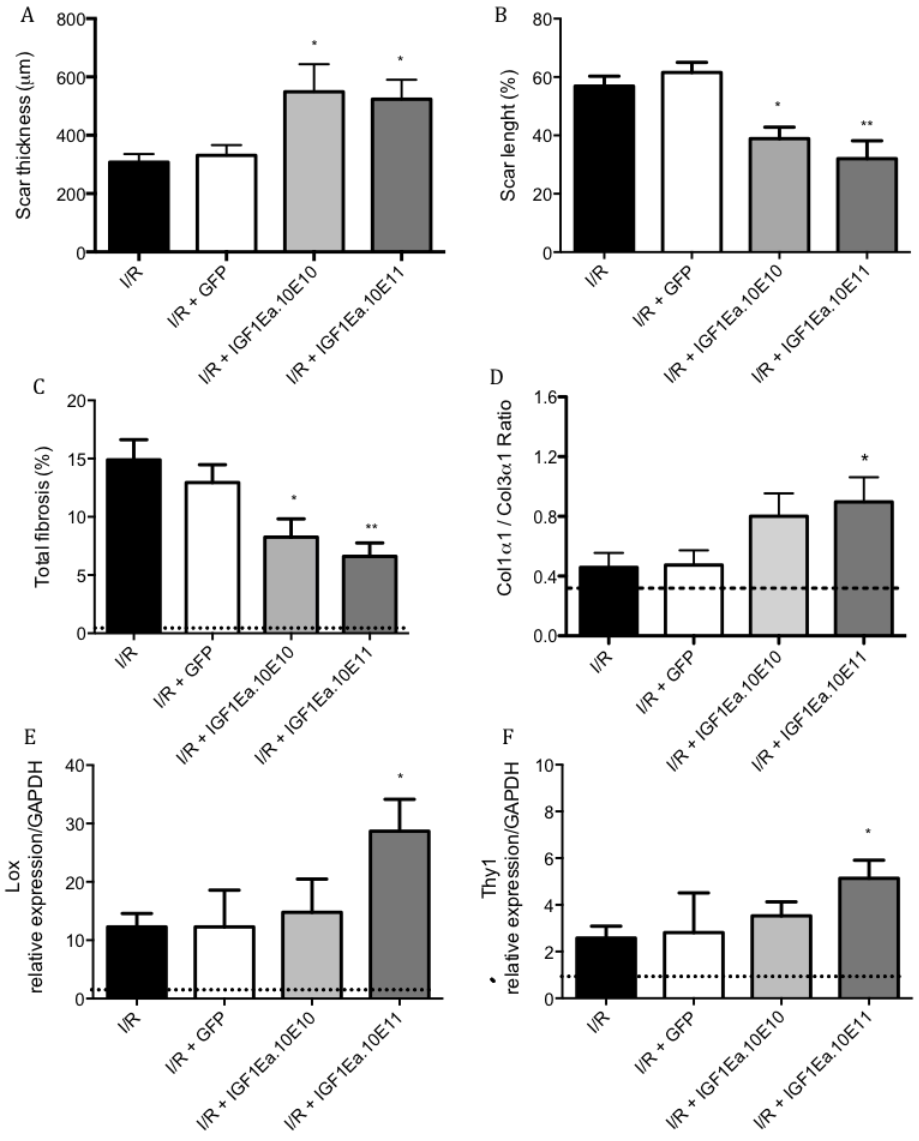


Figure 5.8. IGF1Ea gene transfer reduces infarct expansion and myocardial remodeling in AAV9.IGF1Ea treated mice. (A) Scar thickness, (B) length and (C) total fibrosis were analyzed 28 days post-I/R using histological methods. (D) Col Iα1/Col Iα3 ratio, (E) Lox and (F) Thy1 mRNA relative levels were analyzed by qRT-PCR. n= 5-12 per group. Mean values ± SEM are shown. * $P < 0.05$ I/R vs. all three conditions. One-way ANOVA followed with Dunnett's post-test. From the Masson's trichrome-stained images, infarct scar wall thickness, scar length and total

fibrosis was measured with NIH ImageJ software. Anterior wall thickness was measured at three different points in infarction area of anterior wall perpendicularly and average was taken. Scar length was determined in Masson's trichrome- stained sections using the midline method (Takagawa et al. 2007). The ratio of scar length to left ventricular circumferences of the endocardium and epicardium was determined and expressed as a percentage of infarct size (% of LV) which was calculated as (infarct length/total LV length)×100. Transverse fibrosis and total left ventricular areas were measured and expressed as percent fibrosis. Collagen ratio was calculated as the ratio of Collagen Iα1 and Collagen Iα3 relative expression levels.

Functional and histological findings were confirmed at molecular level by monitoring LV fibrosis markers and the main cell types producing them: collagen 1 (Col Iα1), collagen 3 (Col Iα3), lysyl oxidase (Lox) and Thy1/CD90. Measured 28 days after cardiac gene transfer, the Col Iα1/Col Iα3 mRNA ratio was increased in the AAV9.IGF1Ea groups (**Figure 5.8D**), indicating a difference in extracellular matrix ECM composition. Higher levels of Lox were also detected (**Figure 5.8E**). Lox molecules crosslink collagen and elastin molecules into mature fibers, potentially strengthening the scar. As a measurement of fibroblast proliferation, we quantified Thy1/CD90 levels, which were increased in the AAV9.IGF1Ea group (**Figure 5.8F**).

5.6 BrdU+ nuclei quantification after IGF-1Ea gene transfer

Interestingly, the scars of AAV9.IGF1Ea treated mice were characterised by higher cardiomyocyte content (**Figures 5.9 A-D**).

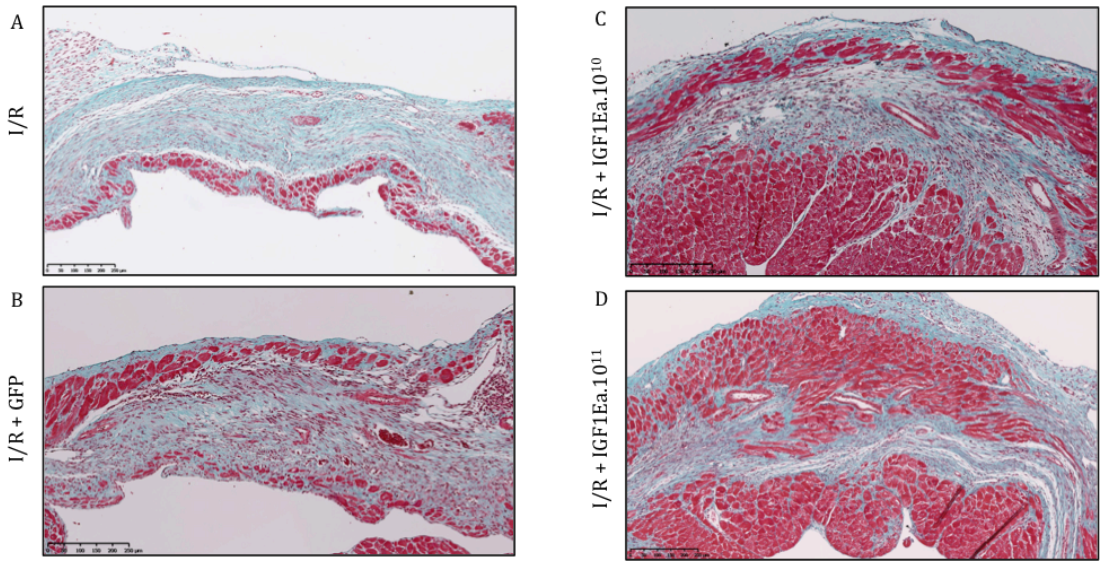


Figure 5.9. Representative masson trichrome staining sections of the scar region in the four groups 28 days after ischemia/reperfusion. Healthy myocardium (red) and fibrosis (blue) are represented. Scale bar, 250 μm.

To assess the generation of new myocardial tissue in the infarcted hearts, mice were given BrdU for 28 days to visualise cumulative DNA synthesis. Consistent with observations in cardiac-specific IGF-1Ea transgenic mice (Santini et al. 2007), the I/R+AAV9.IGF1Ea.10^{11} group moderately increased percentage of BrdU positive cardiomycytes at 28 days post-I/R (**Figure 5.10A, 5.10B** and **5.10C**). The greatest difference was obtained with the I/R+AAV9.IGF1Ea.10^{11} so the higher viral titer was used in preceding experiments. As no significant differences were observed between I/R group (no virus group) and the I/R GFP control groups, only I/R group is presented.

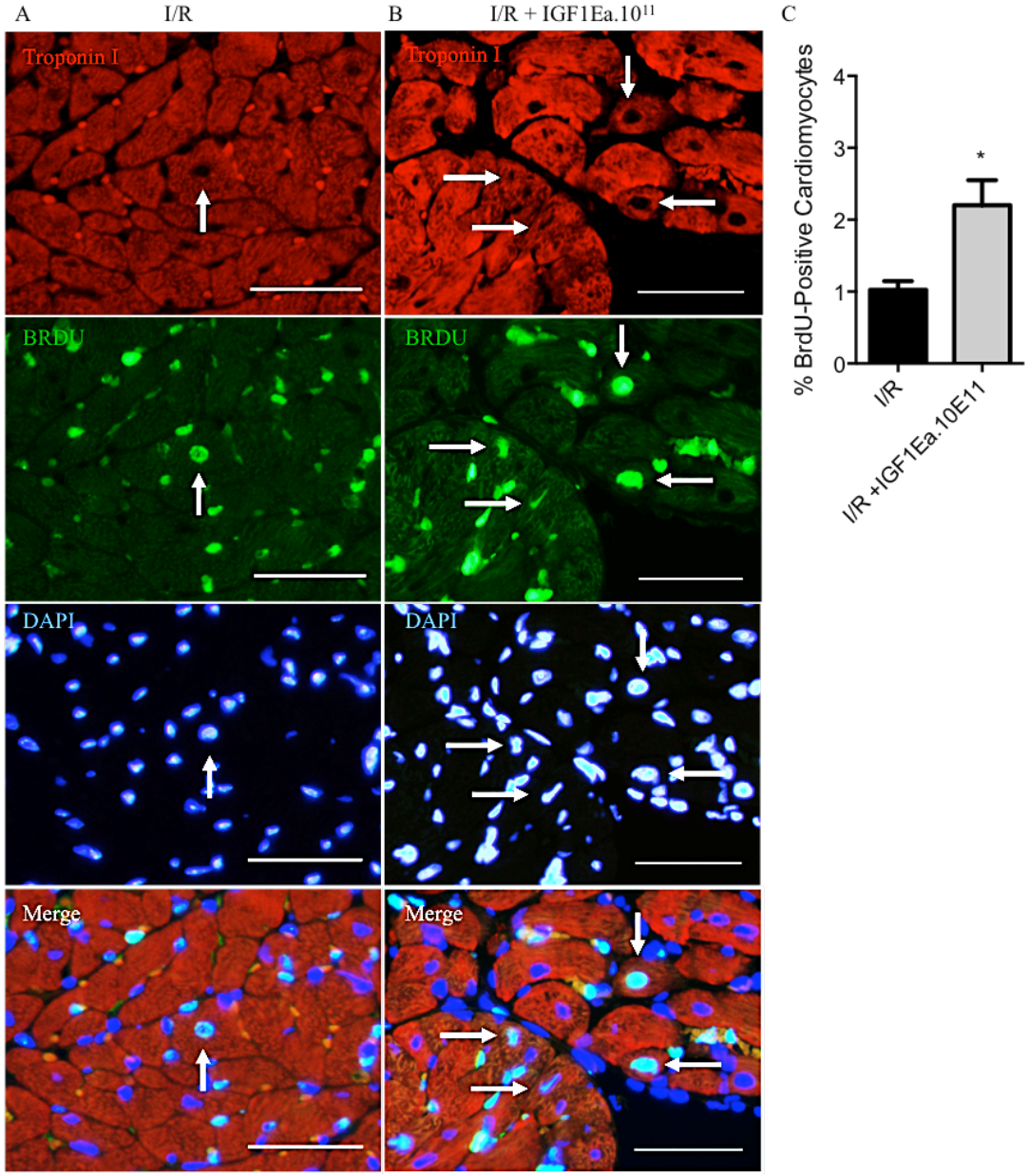


Figure 5.10. AAV9.IGF1Ea gene transfer increases the number of BrdU+ cardiomyocytes 28 after ischemia/reperfusion. (A, B) Representative confocal images of paraffin heart sections 28

days post-I/R of (A) I/R group (no virus) and (B) AAV9.IGF1Ea $3.5x10^{11}$ group. Sections were stained with cardiac troponin I (red, cardiomyocytes), anti-BRDU (green) and DAPI (blue, nuclei). Scale bar, 100 μm. (C) Quantification of BrdU+ cardiomyocytes after *in vivo* labeling. n=3-6. For quantification whole heart sections where analysed for BRDU+ Cardiomycytes. At least three heart sections per heart where analysed. White arrows indicate BrdU positive nuclei. Mean values ± SEM are shown. *p<0.05. Two-tailed Student's *t*-test was performed to compare I/R vs. AAV9.IGF1Ea $3.5x10^{11}$ 28 days after MI.

Phospho-H3 staining, a mitosis marker, did not reveal any significant difference between the groups at 28 days (**Figure 5.11**), suggesting a lack of on-going proliferation at that stage.

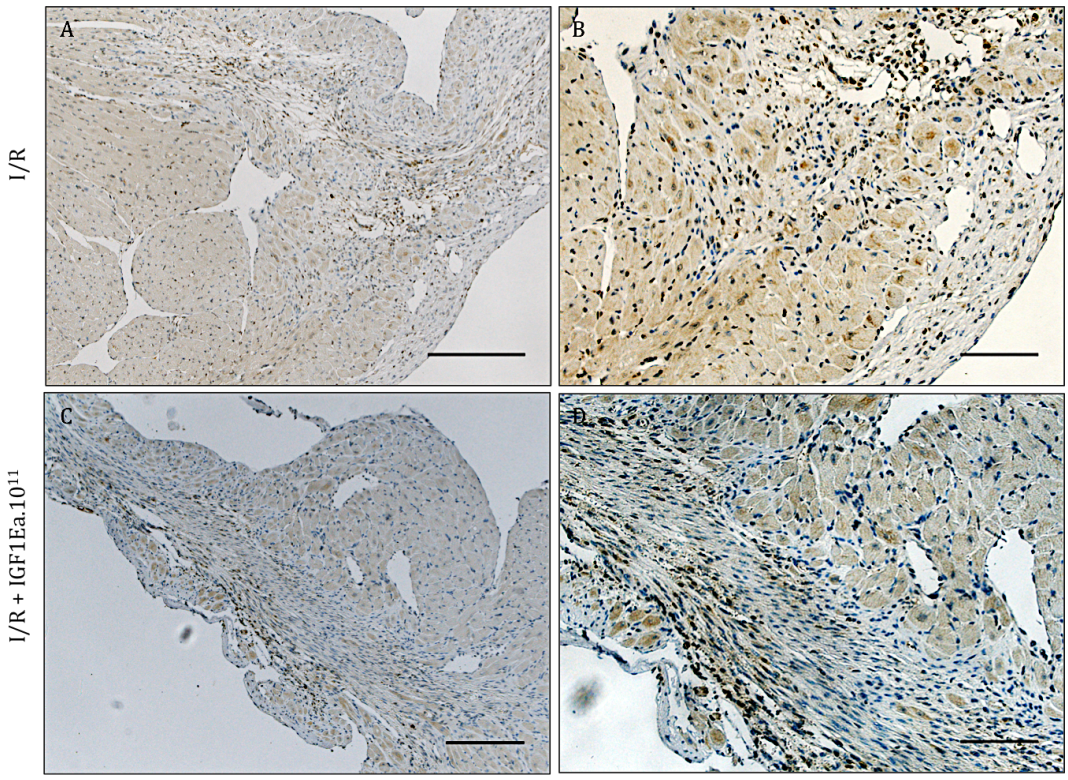


Figure 5.11. Phospho-H3 immunohistochemistry of I/R and AAV9.IGF1Ea treated groups, 28 days after ischemia/reperfusion. (A and B) I/R group (no virus group) and (C and D) IGF-1Ea $3.5x10^{11}$ GC treated, 28 days after ischemia/reperfusion. Scale bar (A and C), 250 um. Scale bar (C and /D), 100 um.

We also assessed whether IGF-1Ea gene transfer promoted enhanced vascularization for proper blood supply to the scars. Indeed, as in IGF-1 transgenic mice (Santini et al. 2011), αSMA immunohistochemistry showed an increase in arterioles in the AAV9.IGF1Ea treated group with the highest AAV9 titer (**Figures 5.12A, 5.12B** and **5.12C**).

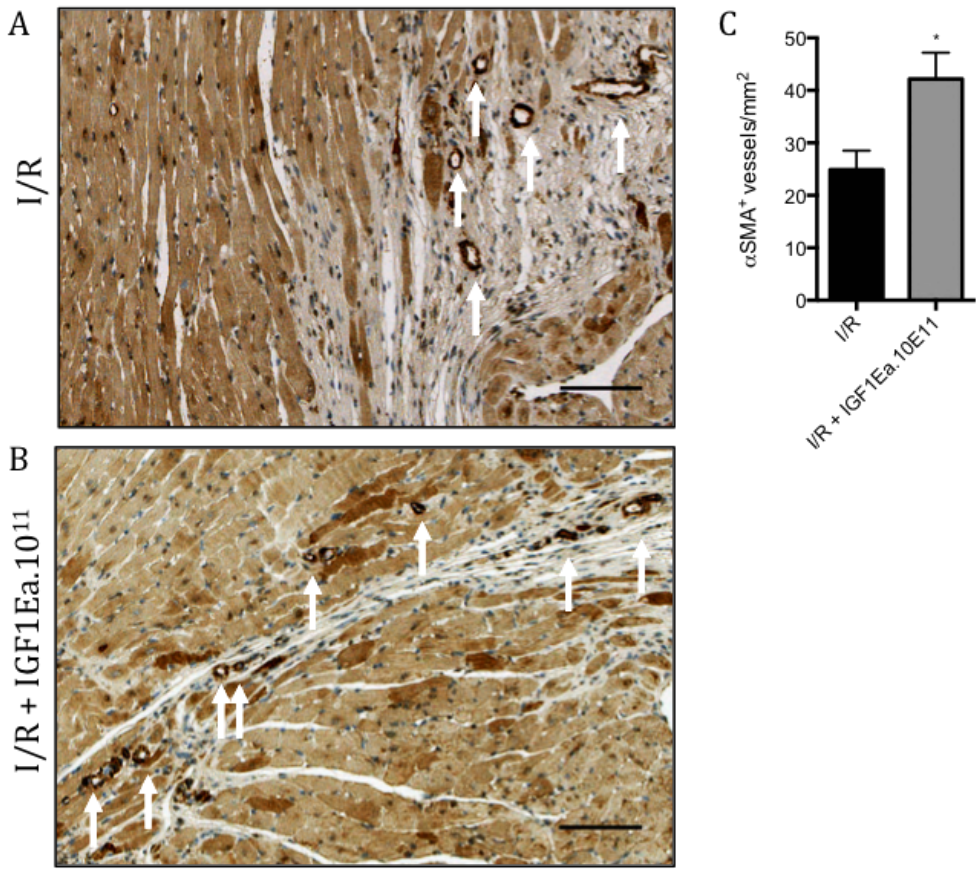


Figure 5.12. αSMA immunohistochemistry and vessel quantification in I/R and AAV9.IGF1Ea treated mice, 28 days after ischemia/reperfusion. αSMA immunohistochemistry of (A) I/R group (no virus group) and (B) AAV9.IGF1Ea $3.5x10^{11}$ treated hearts after ischemia-reperfusion. White arrows indicate αSMA positive vessels. n=4-6. Scale bar, 100 μm. (C) αSMA vessel quantification. For quantification whole heart sections where analysed for αSMA+ cells. At least three heart sections per heart where analysed. Mean values ± SEM are shown. *p<0.05. Two-tailed Student's *t*-test was performed to compare I/R vs. AAV9.IGF1Ea $3.5x10^{11}$ 28 days after MI.

5.7 AAV9.IGF1Ea treatment promotes cardiac Akt-mediated signalling

The main effects of IGF-1 are achieved through the Akt signalling pathway. In the heart, IGF-1 mediates Akt phosphorylation on the serine-473 residue, which indicates Akt activation (Santini et al. 2011). AAV9.IGF1Ea treatment increased IGF-1 protein content in the heart by 1.5 fold when compared with the I/R group. At 28 days post-I/R, mice treated with AAV9.IGF1Ea exhibited a 1.7 fold increase in $^{P\text{-}Ser473}$Akt. Phosphorylation of mTOR, downstream of Akt, was also increased by 1.8 fold after I/R in the AAV9.IGF1Ea treated groups (**Figure 5.13A** and **5.13B**).

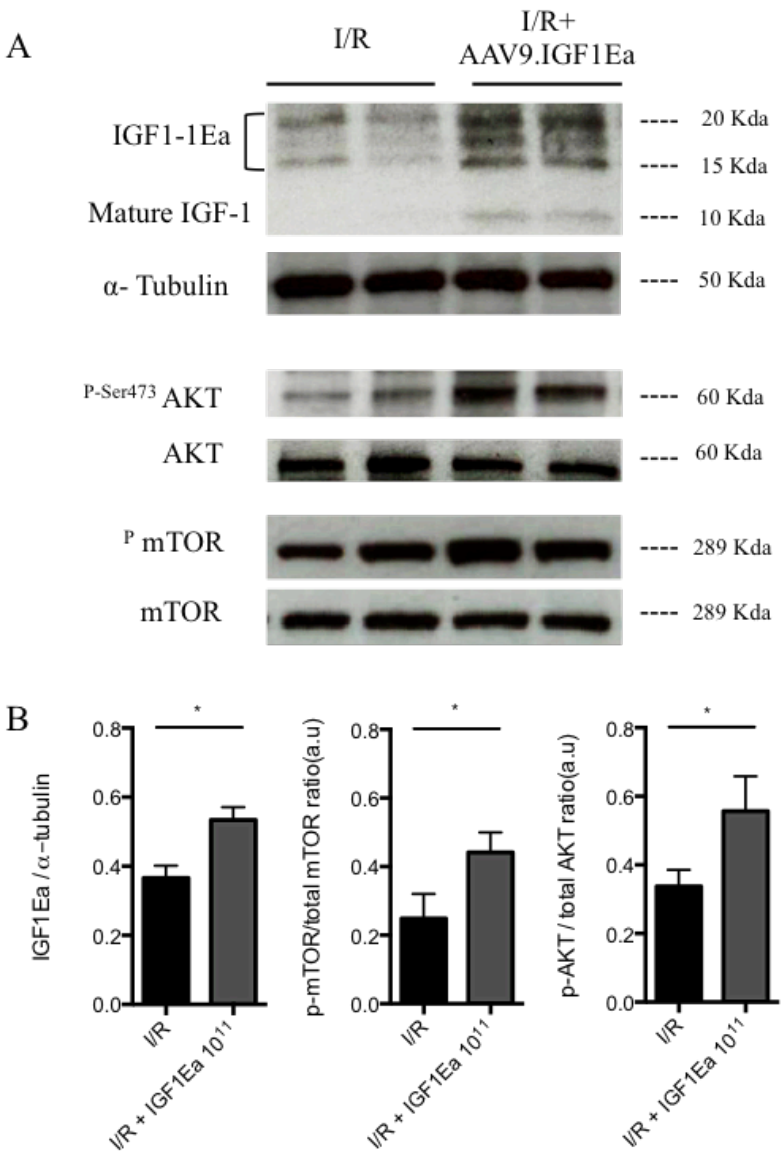


Figure 5.13. IGF-1Ea gene transfer activates the Akt signaling pathway. (A) Representative western blot images of protein extracts from the remote myocardium of I/R and I/R-AAV9.IGF1Ea treated groups 28 days post-I/R. (B) Western blot quantification of IGF-1Ea, p-Akt, and mTOR, 28 days after cardiac transfer by scanning densitometry. n= 6-10 per group. Mean values ± SEM are shown. *p<0.05. Two-tailed Student's *t*-test was performed to compare I/R vs. AAV9.IGF1Ea $3.5x10^{11}$ 28 days after MI.

5.8 Discussion

In this chapter, it is demonstrated for the first time that a single intravenous injection of AAV9.IGF1Ea after ischemic injury induced improvements in LV cardiac function following myocardial infarction. This improvement is through partial recovery of LV contraction and quality motion reducing total fibrosis and infarct expansion limiting adverse remodeling. Interestingly, analysis of the main ECM components, collagen 1 and

collagen 3, showed a skewing in favour of collagen synthesis which may confer different mechanical and physical properties to the infarct. TGF-β is a well know activator of collagen I synthesis by activated fibroblast (Bujak et al. 2007). Consequently, a reduction in total TGF-β levels in the infarcted area, could be explain the reduction in total fibrosis.

As discussed in the Introduction, Section 1.4.2, over the years, the use of AAVs in preclinical (Konkal et al. 2014, Fang et al. 2013 and Kaspar et al. 2005) and clinical studies (Muller at el. 2006 and Giacca et al. 2011) has positioned AAVs as the vector of choice for cardiac gene transfer. This is mainly due to the diverse tissue tropism determined by the capsid serotype, the lack of pathogenicity, low immunogenicity and robust gene expression, achieved with this system (Jessup et al. 2011). This chapter's findings show that single administration of the AAV9 virus provided robust and early onset of IGF-1Ea expression in the heart, with the cTNT promoter providing sufficient expression to achieve therapeutic IGF-1Ea transcription levels after a single systemic injection. AAV9-mediated luciferase gene expression was also detected in the liver at much lower levels, which overrode the cardiac specificity of the cTNT promoter (Prasad et al 2011, Fang et al. 2013 and Kaspar et al. 2005). However, this was not paralleled by an increase in IGF-1Ea mRNA levels in the liver after AAV9.IGF1Ea treatment, indicating that IGF-1Ea overexpression was cardiac-specific. Notably, in this study, we show for the first time that the IGF-1Ea propeptide can be successfully delivered and overexpressed in the heart by this gene therapy approach. The Ea moiety in the IGF-1Ea propeptide, which is efficiently cleaved, anchors IGF-1 to the extracellular matrix in other tissues preventing its clearance and reducing off-target effects (Hede et al. 2012). This feature dampens the risks associated with elevated systemic IGF-1 levels such as hypotension (Cheng et al. 2014) and hypoglycaemia (Kovacs et al. 1999).

As described in the Introduction, Section 1.5, the diverse functions of IGF-1 are mediated through the same receptor (IGF-1R) which upon activation leads to the recruitment of other substrates that in turn activate different signalling pathways (Butler et al. 1998 and Coolican et al. 1997). Upon IGF-1R activation, active PI3-kinase phosphorylates inositol phospholipids (Introduction, Section 1.5.2.2)(Fujio et al. 2000 and Rommel et al. 2001). This phosphorylation is required to induce several downstream targets such as Akt, which promotes protein synthesis and cell survival, among other functions. IGF-1Ea also induces the expression of the calcineurin splicing variant CnAβ (Lara-Pezzi et al. 2007). Interestingly, the effects of AAV9.IGF1Ea are reminiscent of those of CnAβ1 overexpression, which results in Akt activation, improved vascularization of the infarct

region and reduced infarct expansion leading to reduced remodeling and improved cardiac function post-infarction (Prasad et al. 2011 and Felkin et al. 2011). As with previous models of IGF-1 administration, the AAV9 virus was able to induce an increase in the formation of new capillaries (Santini et al. 2011).

Although BrdU+ labelling showed increased percentage of positive cardiomyocites in AAV9.IGF1Ea treated group, no differences were observed with Phospo-H3 staining at 28 days, suggesting that the beneficial effect of IGF-1 is more likely due to improved vascularization of the infarct region, which leads to reduced infarct expansion, in turn reducing dilation and improving LV cardiac function. Regarding the BRDU+ CM. We prompted the question: Does IGF-1Ea induce proliferation of resident CM or homing cardiac stem cells? We have indications suggesting that CM proliferation is originated from c-kit progenitors cells recruited from the bone marrow (Santini et al. 2011). Regarding the improvement in vascular density in the heart could increase the levels of MCP2 and VEGF-A (Santini et al. 2011). We have noted that the scars of the IGF-1Ea treated groups are characterise by an increase number of BRDU+/Phospo-H3 cells. This fact along with the up-regulation of Thy1 suggests that IGF-1Ea supplemental expression activates fibroblast proliferation (Chapter 6).

We have previously shown that cardiac overexpression of IGF-1 in transgenic mice resulted in repression of the pro-inflammatory cytokines IL-1β and IL-6, while the anti-inflammatory IL-4 and IL-10 showed higher expression levels when compared to wild-type (WT) animals after cardiotoxin injury. We found that IGF-1Ea decreased the number of apoptotic cells at the injured site, which is at least in part attributable to the induction of UCP-1, metallothionine 2 and the cardioprotective cytokine adiponectin (Santini et al. 2007) reducing infarct size (Introduction, Section 1.5.4). We hypothesised that IGF-1Ea gene transfer may prevent damaged cardiomycytes to undergo necrosis.

Although the salutary effects of direct intramyocardial injection of IGF-1 expression vectors has been previously documented (Davis et al. 2006, Khan et al. 2014 and Lawrence et al. 2012). This is the first report of sustained effective improvement by virally encoded IGF-1Ea propeptide in a more therapeutically relevant delivery mode.

5.8.1 Limitation of the project

The main disadvantage of the AAV approach is the limited size of the AAV genome (< 5Kb). Additionally, although two levels of cardiac specificity were applied, ectopic

expression was observed in the liver. Thus, the efficiency of IGF-1Ea gene transfer to target the heart was not as specific as expected. On the other hand, as described in the Introduction, Section 1.4.2.2.1, the presence of neutralizing antibodies may play a limiting role if this approach ever reaches human trials. From a wetlab standpoint, sequencing the ITR took longer than expected, delaying the project for several months. However, sequencing of these regions must be performed to make sure that the ITR integrity is preserved. Basically, the supercoiled 3D T-shape structure of the ITRs prevented the amplification of these regions during the sequencing process (Chapter 2, **Figure 2.8**). To overcome this problem, a specific protocol to facilitate sequencing of GC-rich regions was designed as described in Methodology 2.11.7. Another limitation was also found during AAV delivery, we noted that more than 1 cycle of defrosting considerably diminished AAV transduction efficiency. Therefore, each aliquot was used once. From an experimental standpoint, samples should have been harvested at early timepoints, thus, an apoptosis assays should have been performed. At experimental level, IGF-1Ea immunohistochemistry did not provide reliable results do to the sensitivity and specificity of the IGF-1Ea antibody. Consequently, only Luciferase immunohistochemistry was presented.

5.8.2 Outcomes

The escalating incidence of acute cardiovascular diseases leading to heart failure underscores the increasingly urgent need for improved therapeutic strategies to limit cardiac tissue damage and improve functional outcomes in translational settings. This study demonstrates that intravenous delivery of AAV9.IGF1Ea is effective in improving post I/R cardiac function, preventing infarct expansion and dilation. This is attributed to the combined effects of a cardiotropic gene delivery vehicle, AAV9, and the pleiotropic action of IGF-1Ea in the heart.

From a clinical standpoint, intravenous injection is the least invasive mode of delivery for cardiac gene therapy, although higher efficiency could be achieved by delivering the AAV9.IGF1Ea vector via intracoronary infusion during cardiac catheterization in patients. These results provide a rationale to conduct additional studies in larger animals for translation to clinical application.

Chapter 6 – Concluding remarks and future directions

6.1 Concluding remarks

The goal of this thesis was to investigate the potential of new strategies to deliver a beneficial payload to the diseased heart in animal models. Through my PhD, I attempted to combine the knowledge on IGF-1Ea reparative effects with the design of specific clinically relevant therapeutic strategies to deliver IGF-1Ea at the right time after myocardial infarction. Consequently, the main aim of this thesis was (i) to understand the mechanism underlying the IGF-1Ea reparative effects after myocardial infarction, and (ii) to design a suitable cell- or gene-based approach to deliver IGF-1Ea to the infarcted heart promoting cardiac repair and preventing adverse ventricular remodeling in a clinically relevant settings.

In Chapter 3, I have observed improved cardiac function in mice overexpressing cardiac-specific IGF-1Ea as early as 7 days after myocardial infarction. Analysis at gene transcription level revealed that supplemental IGF-1Ea also regulated the expression of key metalloproteinases (MMP-2 and MMP-9), their inhibitors (TIMP-1 and -2) and collagens (Col1α1 and Col1α3) in the first week after injury. Infiltration of inflammatory cells, which direct the remodeling process, was also altered; in particular there was a notable reduction in inflammatory Ly6C+ monocytes at day 3 followed by an increase in anti-inflammatory CD206+ macrophages at day 7. These results indicate that the IGF-1Ea transgene shifts the balance of innate immune cell populations early after infarction, favouring a reduction in inflammatory myeloid cells. This correlates with reduced extracellular matrix degradation and changes in collagen composition that may confer enhanced scar elasticity and improved cardiac function. From this chapter, I uncovered that IGF-1Ea supplemental expression is causing major changes in the resolution of the inflammatory process in the hearts after myocardial infarct. This pinpoints the fact that, in order to enhance repair IGF-1Ea must be present within an early window of 7 days after myocardial infarction.

In Chapter 4 and 5, I have designed two IGF-1Ea therapeutic strategies taking into account that IGF-1Ea must be delivered as early as possible to enhance repair, ideally, within 3-7 days after myocardial infarction. By delivering IGF-1Ea in a clinically relevant setting, I looked to achieve a similar enhancement in repair as found in the αMHC-IGF-1Ea hearts (Introduction, Section 1.5.4).

In the Rosenthal group, numerous projects have attempted to deliver IGF-1Ea into the infarcted myocardium in an efficient way using combinatorial cell/growth factor therapies to improve function following myocardial infarction.

In Chapter 4, I explored the use of BMdMs as a therapeutic vehicle. These cells are found in the infarcted area as early as 2 days after myocardial infarction, thus being a potential vehicle for IGF-1Ea delivery. *In vitro* studies indicated that IGF-1Ea can be overexpressed in BMdMs, however the process is very inefficient. The *in vivo* studies showed that macrophages indeed engrafted into the injured muscle, nonetheless, the process is very inefficient and the numbers of cells retained were just a few, besides, high retention was observed in liver and lung. Taking these two aspects together, IGF-1Ea delivery using BMdMs proved not to be as therapeutically relevant as hoped. At present, we lack a suitable cell-based therapy to deliver IGF-1Ea and confer lasting functional preservation, mainly due to lack of sufficient engraftment of the transplanted cells.

Therefore, I decided to change towards a gene-based therapeutic approach using an adeno-associated virus (AAV) as delivery vehicle. Although it is a completely different approach, studies (Introduction, Section 1.4.2) have shown much better transduction efficiency than cell-based therapies. From a clinical stand point, AAVs are much more tractable than BMdMs as isolation and culture procedures are not required. In particular, I decided to use AAV9 as vehicle, as it has been shown to be the most efficient serotype to achieve high transduction efficiency into the myocardium (Chapter 5).

In Chapter 5, I developed an AAV based, clinically relevant mode of IGF-1Ea delivery to the heart to examine the effects of local IGF-1Ea production on adverse ventricular remodeling after ischemia/reperfusion. A cardiotropic AAV9 vector carrying a cardiomyocyte-specific IGF-1Ea-luciferase bi-cistronic gene expression cassette (AAV9.IGF-1Ea) was administered intravenously to mice 5 hours after ischemia followed by reperfusion (I/R), as a model of myocardial infarction. Virally encoded IGF-1Ea in the heart improved global left ventricular function and LV remodeling, as measured by wall motion and thickness, 28 days after delivery, with higher viral titers yielding better recovery. Thus, the use of AAV9 to deliver IGF-1Ea represents a highly efficient approach for the treatment of myocardial infarction.

6.2 Future directions

The cell- and gene-based therapeutic approaches pursued in this thesis indicated that the most efficient clinically-relevant route to deliver IGF-1Ea is via adeno-associated virus (Chapter 3). Cell-based therapies, particularly, macrophage therapies, point out the main limitations of these approaches, based on the engraftment capacity of these cells (Chapter 4). This suggests that future directions in the IGF-1Ea therapeutic field should be viral-orientated. In contrast to cell-therapy approaches, viral approaches are advancing much faster. In the AAV field, new serotypes are being designed, which have higher and better tropism towards the organ of interest. Although viral approaches using AAV are not perfect, mainly due to the presence of Nab, they appear to be the most promising approach. Regarding AAV9.IGF-1Ea, it is time to bring the study a step forward and to be tested on higher animal models such porcine or eventually to be tested in human trials. Due to the fact that the results on AAV9.IGF-1Ea look very promising for the treatment of myocardial infarction, we have submitted an abstract to a pharmaceutical company, to apply for funding to carry forward this approach to human trial. However, pharmaceutical companies are hesitant to invest in light of existing intellectual property covering many aspects of IGF-1 based therapies, thus limiting the novelty and patentability of AAV9.IGF-1Ea. Although clinical trials are still very far away, more basic research is warranted to refine IGF-1Ea based therapeutic protocols and to explore the mechanism of action whereby growth factor-mediated control of the immune response to damage is a beneficial component of regenerative medicine.

6.3 Future work

For chapter 3

To further investigate the beneficial component of IGF-1Ea in repair I will perform the following experiments:

1) Study of the resident macrophage population (cTM) in the αMHC-IGF-1Ea hearts.

If we compare the number of Ly6C^{low} monocytes and the number of CD206+ macrophages in the injured heart at day 7, the numbers do not add up. There are more CD206+ macrophages than infiltrating monocytes overall. We hypothesised that IGF-1Ea may be stimulating resident macrophage proliferation and polarisation towards an M2 phenotype.

In order to investigate the above hypothesis, we will study the inflammatory response *ex vivo* using a technique developed by Prof. Cesare Terraciano for electrophysiological

purposes. Prof. Cesare Terracciano's group has developed a technique to obtain heart slices, which can be cultured *ex vivo* for a week. I will address the effect(s) that IGF-1Ea exerts on the resident macrophage population in these heart slides after cryoinjury. Consequently, an 'immune' response limited to the resident macrophage populations can be more easily studied in each heart slice. The experiments will be as follow:

Experiment 1: BrdU assays will be performed to compare the proliferative capacities of resident macrophages in WT and αMHC-IGF-1Ea heart slices using the same timepoints as in Chapter 3, 24 hours, 3 days, 5 days and 7 days.

Experiment 2: Flow cytometry analysis will be performed to study the phenotype of the resident macrophages after cryoinjury in WT and αMHC-IGF-1Ea hearts. The phenotype of the resident macrophages will be assessed overtime using the following markers: CD45, CD11b, CD14, Ly6C, CD206. The resident macrophage populations can be characterised by the expression of the CX3CR1 marker as described by Pinto et al. 2012. Additionally, these macrophages populations will be sorted and the expression of inflammatory-mediated markers will be analysed by qPCR.

Experiment 3: qPCR gene expression analysis of whole WT and αMHC-IGF-1Ea heart slices after cryoinjury will be performed. As described in Chapter 3, Figure 3.6, the αMHC-IGF-1Ea hearts are characterise by an early up-regulation of the anti-inflammatory cytokine IL-10 during the first 24 hours after myocardial infarction. Therefore, it will be very interesting to know if whole heart slices and sorted resident macrophages (*Experiment 2*) up-regulate the levels of IL-10 after cryoinjury.

If the resident macrophages display a reparative phenotype after cryoinjury, this will be in accordance with the data in Chapter 3, Figure 3.10. The results will indicate that IGF-1Ea promotes its reparative activity is mediated through the stimulation of the resident macrophage population, this fact could also explain the bias towards the reparative environment found in the αMHC-IGF-1Ea hearts.

2) *Expression of IL-1 β, IL-10, MCP-1, CCL5 and Collagen by macrophages, neutrophils and dendritic cells.*

As discussed in the Introduction, Section 1.5.4 and in Chapter 3, IGF-1Ea modulates several aspects of the inflammatory process, including cytokine expression and matrix turnover genes. It will be interesting to know if the main inflammatory cells studied in Chapter 3 are actually responsible for the cytokines and the matrix turnover expression pattern found in the αMHC-IGF-1Ea hearts.

Although it is not mentioned in this thesis, cell sorting was also performed along with the flow cytometry analysis in Chapter 4. The following cells were sorted at all timepoints: Inflammatory macrophages ($Ly6C^{high}/CD206^{low}$), reparative macrophages ($Ly6C^{low}/CD206^{high}$), neutrophils (CD45+, CD11b+, F4/80-, CD11c-, Ly6G+) and dendritic cells (CD45+, CD11b+, F4/80-, CD11c+, Ly6G-).

It will be interesting to elucidate if IGF-1Ea alters the gene expression profile of these cells, at early timepoints. In particular, a series of qPCR will be performed to further investigate the mechanism underlying the distinct cytokine profile found in the αMHC-IGF-1Ea hearts.

- CCL2, the main ligand for monocyte recruitment, is released by activated neutrophils (Pelletier et al. 2014). Thus, a reduction in the CCL2 mRNA levels in neutrophils in the αMHC-IGF-1Ea hearts, 24 hours after myocardial infarction, could explain the reduced levels of CCL2 found at that particular timepoint in the αMHC-IGF-1Ea hearts.

- The enhanced repair achieved in the αMHC-IGF-1Ea mice, has always been associated with high levels of the anti-inflammatory cytokine IL-10. Reparative macrophages have been identified as one of the main producers of IL-10 after myocardial infarction, facilitating the shift from the inflammatory to the reparative phase (Mosser et al. 2003 and Nahrendorf 2010). Thus, I would like to know if sorted αMHC-IGF-1Ea macrophages at day 1 up-regulate IL-10 mRNA levels, compared to WT macrophages. If so, this can explain the IL-10 up-regulation observed in the αMHC-IGF-1Ea.

- Reparative macrophages are responsible for collagen degradation through the mannose receptor (Madsen et al. 2013). I would like to assess if αMHC-IGF-1Ea

reparative macrophages up-regulate the levels of the mannose receptor upon injury. If so, this fact could explain in part the reduction in the collagen content found in the αMHC-IGF-1Ea hearts.

3) Understanding the distinct composition of the scar tissue in the αMHC-IGF-1Ea hearts after myocardial infarction.

The changes in collagen expression observed in Chapter 3, could be due to proliferation and activation of fibroblast into myofibroblast (Van Nieuwenhoven et al. 2013 and Simmons et al. 2002). This is also supported by the fact that αMHC-IGF-1Ea (Chapter 3, **Figure 3.3** and **Figure 6.1**) and the AAV9.IGF1Ea scars (Chapter 5, **Figure 5.9** and **Figure 6.1**) are characterise by an accumulation of fibroblast-like cells at the scar site, besides the up-regulation of the CD90/Thy1 marker in the scars of the AAV9.IGF1Ea treated group (Chapter 5, **Figure 5.8**). Therefore, I would like to perform immunohistochemistry staining against CD90/Thy1, to confirm that the accumulation of the cells in the scar tissue are fibroblasts.

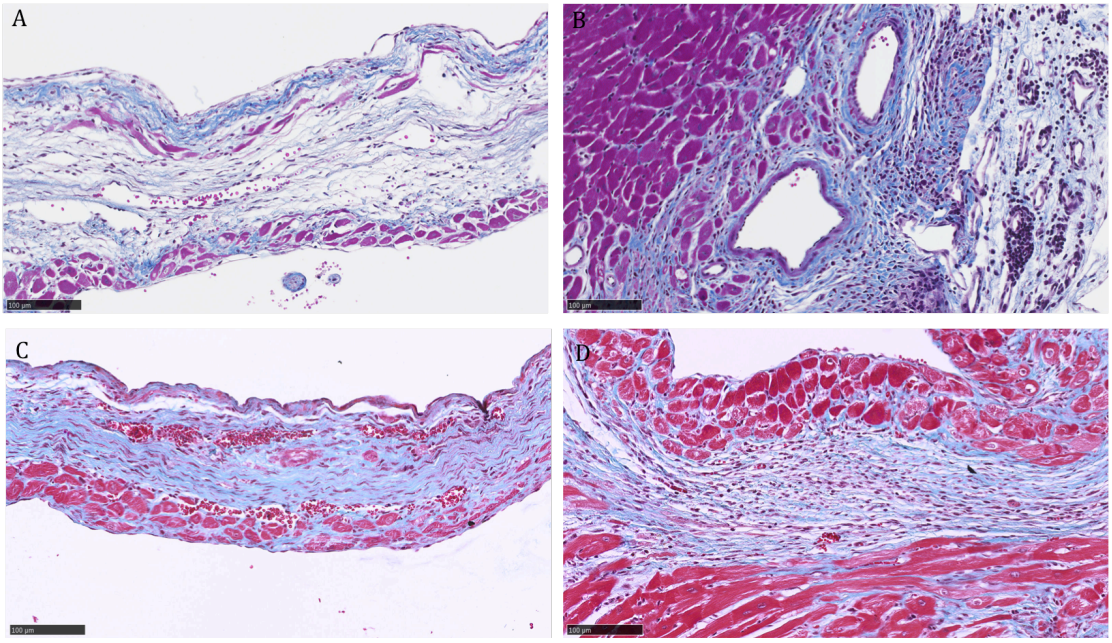


Figure 6.1. Masson Trichrome representative staining of WT and IGF-1Ea scars after myocardial infarction. (A) WT and (B) αMHC-IGF-1Ea scar tissue 28 days after permanent coronary artery occlusion. (C) I/R and (D) AAV9.IGF1Ea treated scar tissue 28 days after ischemia reperfusion. Scale bar, 250μm.

For Chapter 5

There are two main experiments that I would like to perform which will provide us with a better understanding on how to tune IGF-1Ea in future therapeutic approaches.

Experiment 1: One of the most interesting findings of this thesis is the increase in BrdU+ cardiomyocytes that I found after AAV9.IGF1Ea treatment. As discussed in Chapter 5, the increase in BrdU+ cardiomycytes from 1 to 2% does not explain such improvement in cardiac function. However, it will be very interesting to pinpoint when exactly this event occurs, as it would be very helpful to target future IGF-1Ea therapies to that particular timepoint. Thus, I would like to perform a Phospho-H3, Aurora B immunofluorescence timecourse and BrdU studies at 1, 3, 5 and 7 days after ischemia/reperfusion to determine when exactly cardiomyocyte division is occurring.

Experiment 2: The scars of the IGF-1Ea treated mice are characterises by an increase in cardiomyocyte content, which is BrdU negative (**Chapter 5, Figure 5.10**). On the other hand, IGF-1Ea is involved in preventing apoptosis at the injured site (Santini et al. 2007). Therefore, I would like to look for apoptosis by TUNEL assay to determine if IGF-1Ea, indeed promotes survival pathways after AAV9.IGF1Ea administration. TUNEL assay will be performed at the same timecourse as described in *Experiment 1*.

Experiment 3: In order to clarify the composition and structure of the scars analyses of the scars by a polarized microscope will be performed.

Publications and Presentations

Publications

Tonkin, Joanne, Lieve Temmerman, Robert D Sampson, **Gallego-Colon, Enrique**, Laura Barberi, Daniel Bilbao, Michael D Schneider, Antonio Musarò, and Nadia Rosenthal. 2015. "Monocyte/Macrophage-Derived IGF-1 Orchestrates Murine Skeletal Muscle Regeneration and Modulates Autocrine Polarization." *Molecular Therapy* 23 (7): 1189–1200. doi:10.1038/mt.2015.66.

Gallego-Colon, Enrique, Robert D Sampson, Susanne Sattler, Michael D Schneider, Nadia Rosenthal, and Joanne Tonkin. 2015. "Cardiac-Restricted IGF-1Ea Overexpression Reduces the Early Accumulation of Inflammatory Myeloid Cells and Mediates Expression of Extracellular Matrix Remodelling Genes after Myocardial Infarction." *Mediators of Inflammation* 2015: 484357. doi:10.1155/2015/484357.

Gallego-Colon. Enrique, Villalba. M, Cruz. F, Jimenez-Borreguero. J, Sarathchandra. P, Lara-Pezzi. E, Rosenthal. N. Intravenous delivery of adeno-associated virus 9-encoded IGF-1Ea propeptide improves post-infarct cardiac recovery (2015) (Submitted to Circulation Research**, In review**).

Presentations

- Intravenous AAV9 delivery of IGF-1Ea propeptide improves post-infarct cardiac recovery. Imperial College London. National Heart and Lung Institute. PGR Day 2015. W12 Conference.13 July 2015. Hammersmith hospital.

- Intravenous AAV9 delivery of IGF-1Ea propeptide improves post-infarct cardiac recovery. 3rd SRUK/CERU symposium. Oral presentation. 4th July 2015. Hotel Ibis Euston St Pancras. London. UK

- Intravenous delivery of virally-encoded IGF-1Ea improves post-infarct cardiac recovery after ischemia reperfusion. Harefield Heart Science Centre. Magdi Yacoub Institute. 7th June 2015. Harefield. UK

- Intravenous delivery of virally-encoded IGF-1Ea improves post-infarct cardiac recovery after ischemia reperfusion. CardioNet general meeting. Royal Brompton Hospital 7th June 2015. London. UK

- IGF-1Ea modulates the immune system response after myocardial infarct. Seminar meeting. Australian Regenerative Institute (ARMI). Monash University. Clayton. Australia. 15th July 2014. Online seminar.

- Mending a broken heart. II SRUK/CERU Symposium. Oral communication. NH Harrington. 5th July 2014. London, UK.

- IGF-1Ea modulates macrophages response after myocardial infarction. Myocardial Function Seminar. Thursday 3rd July , ICTEM (L-Block) 4th Floor Seminar, Hammersmith campus.

- AAV9 viral-mediated delivery of IGF-1Ea to the diseased heart. CardioNet Late-term review annual meeting. CNIC (Spanish National Centre for Cardiovascular Research). 5-8 May 2014. Madrid. Spain.

- Three-Minutes Thesis Competition. Paul Wood Lecture Theatre, NHLI Education Centre, Royal Brompton Campus. 29th April 2014. Imperial College London.

Abstracts/Posters

- Susanne Sattler, **Enrique Gallego-Colon**, Joanne Tonkin, teresa Kennedy-Lydon, Ekaterina Semenova and Nadia Rosenthal. IGF-1 mediated Treg induction modualtes the immune response after tissue damage. 4th European Congress of Immunology. Vienna, 2015.

- **Enrique Gallego-Colon**, Joanne N. Tonkin, Robert D. Sampson, Marina M. Lopez-Olañeta, Mutsuo Harada, Enrique Lara-Pezzi and Nadia Rosenthal. IGF-1Ea modulates macrophages response after myocardial infarction. SRUK/CERU symposium (2015).

- **Enrique Gallego-Colon**, Joanne N. Tonkin, Robert D. Sampson, Marina M. Lopez-Olañeta, Mutsuo Harada, Enrique Lara-Pezzi and Nadia Rosenthal. IGF-1Ea modulates macrophages response after myocardial infarction. NHLI annual Postgraduate Research Day (2015).

- **Enrique Gallego-Colon**, Joanne N. Tonkin, Robert D. Sampson, Mutsuo Harada, and Nadia Rosenthal. IGF-1Ea modulates macrophages response after

myocardial infarction. Imperial College BHF (British heart foundation) Centre of Research Excellence Symposium (2015)

- **Enrique Gallego-Colon**, Joanne N. Tonkin, Robert D. Sampson, Mutsuo Harada, and Nadia Rosenthal. IGF-1Ea modulates macrophages response after myocardial infarction. Weinstein symposium (2014).

- Susanne Sattler, Bjarki Johanneson, Joanne Tonkin, **Enrique Gallego-Colon**, Daniel Bilbao2 Ekaterina Semenova & Nadia Rosentha. The peptide hormone Insulin-like growth factor-1 affects the immune systemduring physiological and pathological inflammatory responses. 15th International Congress of Immunology (2013).

- **E. Gallego-Colon**, Maria Paola Santini, Joanne Tonkin, Susanne Sattler and N.Rosenthal. Immuno-mending a broken heart. 1st International symposium of the Spanish Society of researchers in the UK (2013).

Awards received during my PhD

- Recipient the British Spanish Society Scholarship/Santander Universities Scholarship. April 2015

- National Prize on Scientific Research. 11th Certamen Universitario Arquimedes 2012. November 2012. Special Award given by Astrazeneca Foundation to the Msc project performed at the CNIC. Research Project: Characterization of human iPS cells as a model for cardiovascular research.

Outreach activities

Television broadcast:

Enrique Gallego's interview to LaSexta noticias, Spanish broadcast TV channel.
http://www.lasexta.com/constantes-vitales/noticias/solo-cientificos-que-emigran-pueden-regresar-espana-antes-dos-anos_2014120800120.html

Press, newspapers:

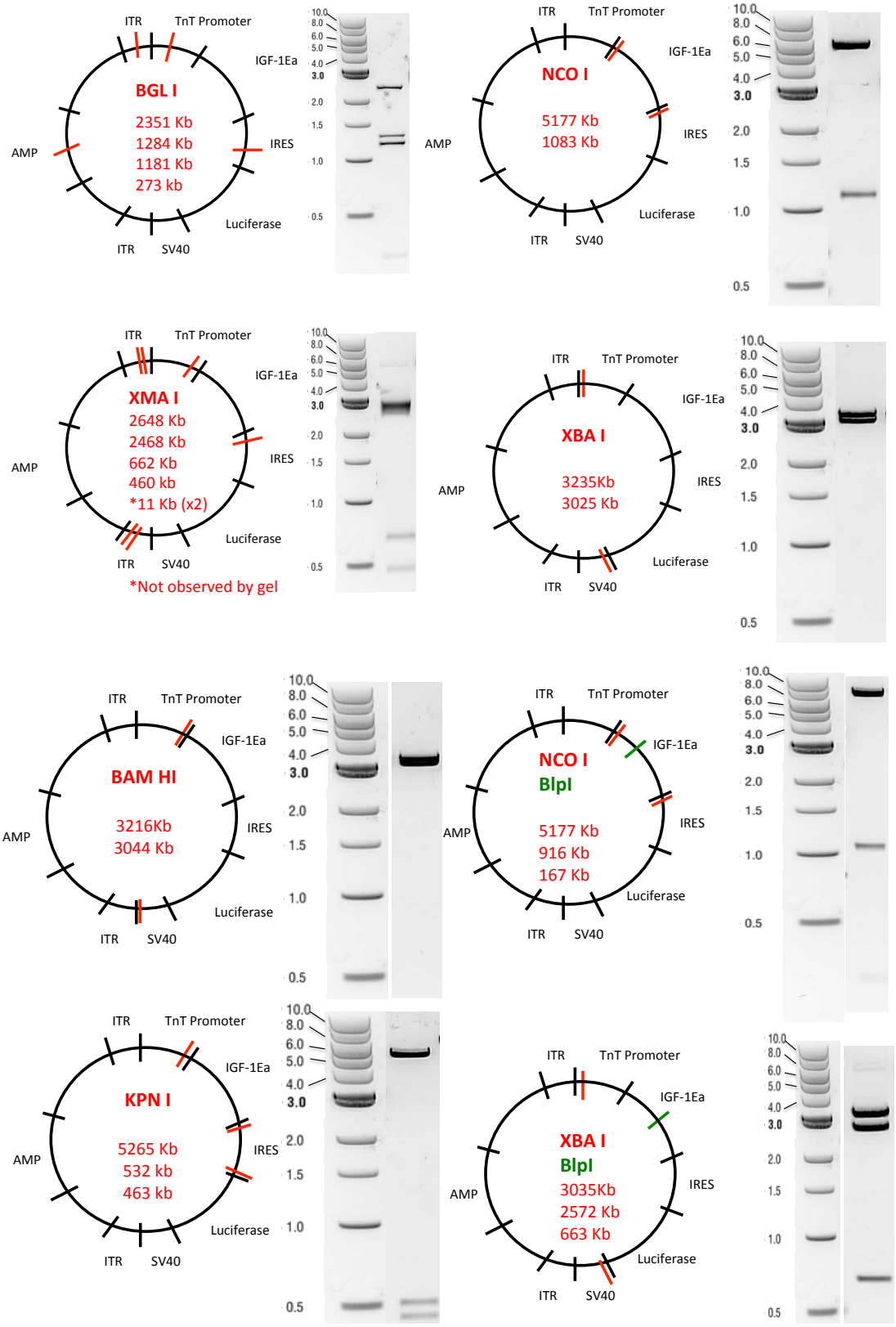
08/04/2015
http://www.laopiniondezamora.es/zamora/2015/04/08/cientifico-corazon/834527.html

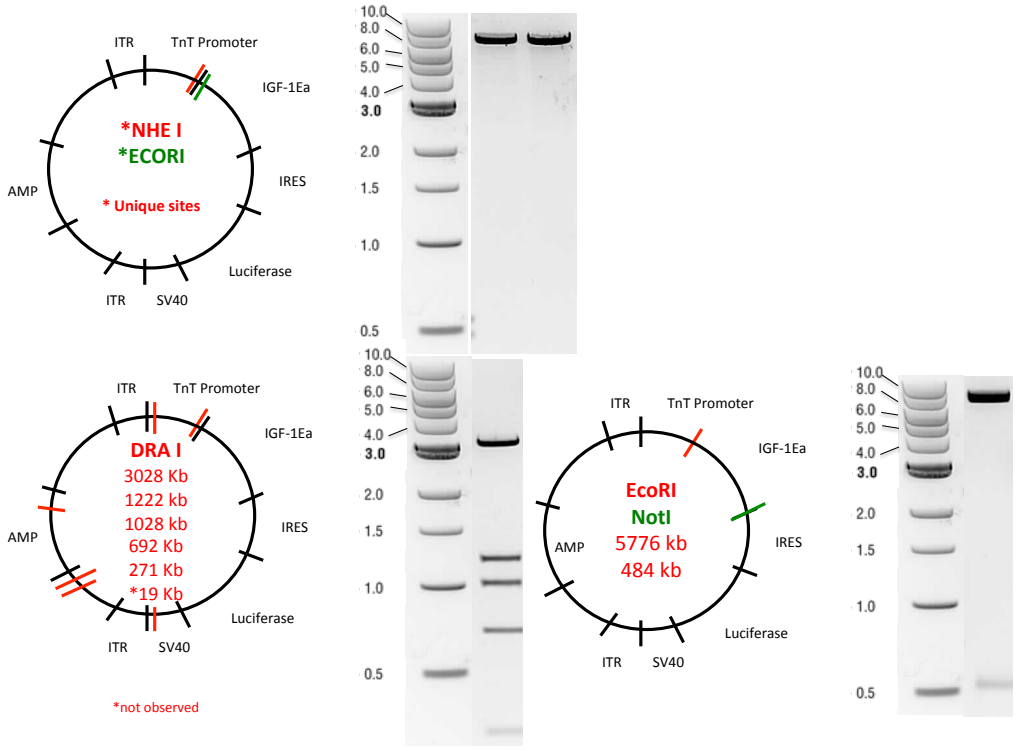
05/10/2014
http://www.laopiniondezamora.es/zamora/2014/10/05/crisis-han-reducido-numero-becas/793277.html

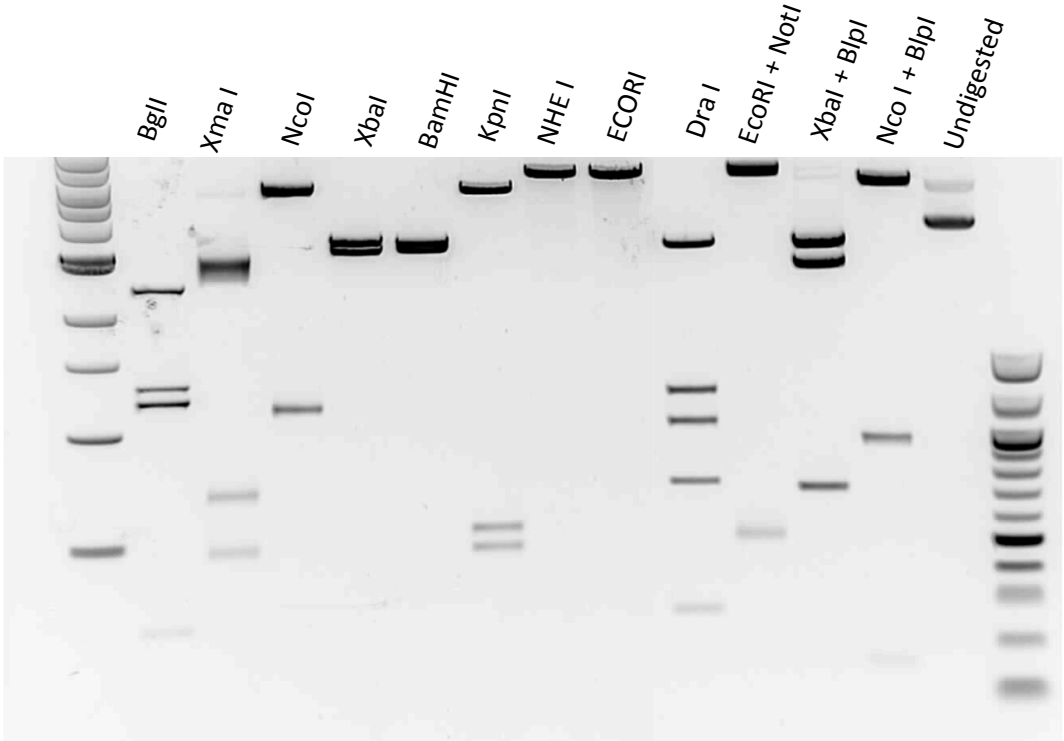
03/12/2012
http://www.astrazeneca.es/prensa/notas-de-prensa-fundacin-astrazeneca/2012/Article/03122012--certamen-arquimides

Appendix 1. pAAV9.IGF-1Ea quality controls

AAV9 viral production required a full characterisation of the plasmid to confirm that all the elements inside the vector were present: 3'ITR/LTR, 5'ITR/LTR, promoter, transgene and polyadenylation signal. The maximum size of an AAV vector from ITR to ITR must be 4.9Kb or below, pAAV9.IGF-1Ea has 2336 bp.




ITR
TnT Promoter
IGF-1Ea
*NHE I
*ECORI
* Unique sites
AMP
IRES
Luciferase
ITR
SV40
10.0
8.0
6.0
5.0
4.0
3.0
2.0
1.5
1.0
0.5
DRA I
3028 Kb
1222 kb
1028 kb
692 Kb
271 Kb
*19 Kb
*not observed
EcoRI
NotI
5776 kb
484 kb


BglI
Xma I
NcoI
XbaI
BamHI
KpnI
NHE I
ECORI
Dra I
EcoRI + NotI
XbaI + BlpI
Nco I + BlpI
Undigested

References

Adamo, M. L., Ben-Hur, H., LeRoith, D., & Roberts, C. T. (1991). Transcription initiation in the two leader exons of the rat IGF-I gene occurs from disperse versus localized sites. Biochemical and Biophysical Research Communications, 176, 887–893.

Adamo, M. et al. Structure, expression and regulation of the IGF-1 gene. Adv. Exp. Med. Med. Biol. 343, 1–11 (1993).

Aird, W. C. (2011). Discovery of the cardiovascular system: From Galen to William Harvey. Journal of Thrombosis and Haemostasis, 9, 118–129.

Ambrosioni, E., Borghi, C., & Magnani, B. (1995). The effect of the angiotensin-converting-enzyme inhibitor zofenopril on mortality and morbidity after anterior myocardial infarction. The Survival of Myocardial Infarction Long-Term Evaluation (SMILE) Study Investigators. The New England Journal of Medicine, 332, 80–85.

Andreesen, R., Hennemann, B., & Krause, S. W. (1998). Adoptive immunotherapy of cancer using monocyte-derived macrophages: rationale, current status, and perspectives. Journal of Leukocyte Biology, 64(4), 419–26.

Arnold, A. Henry, F. Poron, Y. Baba-Amer, N. van Rooijen, A. Plonquet, R. K. Gherardi, and B. Chazaud, "Inflammatory monocytes recruited after skeletal muscle injury switch into antiinflammatory macrophages to support myogenesis.," J. Exp. Med., vol. 204, no. 5, pp. 1057–1069, 2007.

Arnold, L., et al., Inflammatory monocytes recruited after skeletal muscle injury switch into antiinflammatory macrophages to support myogenesis. J Exp Med, 2007. 204(5): p. 1057-69.

Auffray, C., Sieweke, M. H., & Geissmann, F. (2009). Blood monocytes: development, heterogeneity, and relationship with dendritic cells. Annual Review of Immunology, 27, 669–692.

Aurora, E. R. Porrello, W. Tan, A. I. Mahmoud, J. A. Hill, R. Bassel-Duby, H. A. Sadek, and E. N. Olson, "Macrophages are required for neonatal heart regeneration," J. Clin. Invest., vol. 124, no. 3, pp. 1382–1392, Mar. 2014.

Barton-Davis, E. R., Shoturma, D. I., Musaro, a, Rosenthal, N., & Sweeney, H. L. (1998). Viral mediated expression of insulin-like growth factor I blocks the aging-related loss of skeletal muscle function. Proceedings of the National Academy of Sciences of the United States of America, 95(26), 15603–15607.

Bel, A., Messas, E., Agbulut, O., Richard, P., Samuel, J.-L., Bruneval, P., … Menasché, P. (2003). Transplantation of autologous fresh bone marrow into infarcted myocardium: a word of caution. Circulation, 108 Suppl 1, II247–I252.

Bell, G. I., Stempien, M. M., Fong, N. M., & Rall, L. B. (1986). Sequences of liver cDNAs encoding two different mouse insulin-like growth factor I precursors. Nucleic Acids Research, 14(20), 7873–7882.

Ben-Efraim, S., Tak, C., Romijn, J. C., Fieren, M. J., Bonta, I. L. (1994) Therapeutical effect of activated human macrophages on a human tumor line growing in nude mice. Med. Oncol. 11, 7–12.

Berns, K. I., and Giraud, C. (1996) Biology of adeno-associated virus, Curr Top Microbiol Immunol 218 , 1–23.

Bilbao, D., L. Luciani, B. Johannesson, A. Piszczek, and N. Rosenthal. 2014. "Insulin-like Growth Factor-1 Stimulates Regulatory T Cells and Suppresses Autoimmune Disease." EMBO Molecular Medicine 6 (11): 1423–35.

Birks, E.J., Current and future status of the left ventricular device (LVAD)s in the UK. British Journal of Cardiology. , 2005. 12: p. 333-335.

Blackstock, Christopher D, Yusuke Higashi, Sergiy Sukhanov, Shaw-yung Shai, A Michael Tabony, and Patrice Delafontaine. 2014. "Insulin-like Growth Factor-1 Increases Synthesis of Collagen Type I via Induction of the mRNA-Binding Protein LARP6 Expression and Binding to the 5 Stem-Loop of COL1a1 and COL1a2 mRNA".

Bodine, S. C., Stitt, T. N., Gonzalez, M., Kline, W. O., Stover, G. L., Bauerlein, R., Yancopoulos, G. D. (2001). Akt/mTOR pathway is a crucial regulator of skeletal muscle hypertrophy and can prevent muscle atrophy in vivo. Nature Cell Biology, 3(November), 1014–1019.

Bolli, R., Chugh, A. R., D'Amario, D., Loughran, J. H., Stoddard, M. F., Ikram, S., Anversa, P. (2011). Cardiac stem cells in patients with ischaemic cardiomyopathy (SCIPIO): Initial results of a randomised phase 1 trial. The Lancet, 378(9806), 1847–1857.

Bostick, B, a Ghosh, Y Yue, C Long, and D Duan. 2007. "Systemic AAV-9 Transduction in Mice Is Influenced by Animal Age but Not by the Route of Administration." Gene Therapy 14 (22): 1605–9.

Brunet, a, Bonni, a, Zigmond, M. J., Lin, M. Z., Juo, P., Hu, L. S., … Greenberg, M. E. (1999). Akt promotes cell survival by phosphorylating and inhibiting a Forkhead transcription factor. Cell, 96, 857–868.

Bujak, M., & Frangogiannis, N. G. (2007). The role of TGF-beta signaling in myocardial infarction and cardiac remodeling. *Cardiovascular Research*, *74*(2), 184–195.

Burke, B., Sumner, S., Maitland, N., & Lewis, C. E. (2002). Macrophages in gene therapy: cellular delivery vehicles and in vivo targets. Journal of Leukocyte Biology, 72(3), 417–28.

Butler, A A, S Yakar, I H Gewolb, M Karas, Y Okubo, and D LeRoith. 1998. "Insulin-like Growth Factor-I Receptor Signal Transduction: At the Interface between Physiology and Cell Biology." Comparative Biochemistry and Physiology. Part B, Biochemistry & Molecular Biology 121 (1): 19–26.

Butler, A.A., et al., Insulin-like growth factor-I receptor signal transduction: at theinterface between physiology and cell biology. Comp Biochem Physiol B Biochem Mol Biol, 1998. 121(1): p. 19-26.

Calcedo, R., Vandenberghe, L. H., Gao, G., Lin, J., & Wilson, J. M. (2009). Worldwide epidemiology of neutralizing antibodies to adeno-associated viruses. The Journal of Infectious Diseases, 199(3), 381–390.

Cameron, Vicky a. 2000. "Atrial (ANP) and Brain Natriuretic Peptide (BNP) Expression after Myocardial Infarction in Sheep: ANP Is Synthesized by Fibroblasts Infiltrating the Infarct." *Endocrinology* 141 (12): 4690–97.

Cao, Qi, Yiping Wang, Dong Zheng, Yan Sun, Ya Wang, Vincent W S Lee, Guoping Zheng, et al. 2010. "IL-10/TGF-Beta-Modified Macrophages Induce Regulatory T Cells and Protect against Adriamycin Nephrosis." Journal of the American Society of Nephrology : JASN 21 (6): 933–42.

Cardiovascular Disease Statistics 2014. Book. Resource code: G608/1214/CHA. Available on: https://www.bhf.org.uk/publications/statistics/cardiovascular-disease-statistics-2014.

Carlin, Leo M., Efstathios G. Stamatiades, Cedric Auffray, Richard N. Hanna, Leanne Glover, Gema Vizcay-Barrena, Catherine C. Hedrick, H. Terence Cook, Sandra Diebold, and Frederic Geissmann. 2013. "Nr4a1-Dependent Ly6Clow Monocytes Monitor Endothelial Cells and Orchestrate Their Disposal." Cell 153 (2): 362–75.

Carpenter, V., Matthews, K., Devlin, G., Stuart, S., Jensen, J., Conaglen, J., … McMahon, C. (2008). Mechano-Growth Factor Reduces Loss of Cardiac Function in Acute Myocardial Infarction. Heart Lung and Circulation, 17, 33–39.

Castellano, G., Affuso, F., Di Conza, P., & Fazio, S. (2009). The GH/IGF-1 Axis and Heart Failure. *Current Cardiology Reviews*, *5*(3), 203–215.

Caulfield, J B, and T K Borg. 1979. "The Collagen Network of the Heart." Laboratory Investigation; a Journal of Technical Methods and Pathology 40 (3): 364–72.

Chavakis, E., Koyanagi, M., & Dimmeler, S. (2010). Enhancing the outcome of cell therapy for cardiac repair: Progress from bench to bedside and back. Circulation, 121, 325–335

Chen, F. L., Z. H. Yang, Y. Liu, L. X. Li, W. C. Liang, X. C. Wang, W. B. Zhou, Y. H. Yang, and Ren Ming Hu. 2008. "Berberine Inhibits the Expression of TNFα, MCP-1, and IL-6 in AcLDL-Stimulated Macrophages through PPARγ Pathway." Endocrine 33 (3): 331–37.

Chokri, M., Girard, A., Borrelly, M. C., Oleron, C., Romet-Lemonne J. L., Bartholeyns, J. (1992) Adoptive immunotherapy with bispecific antibodies: targeting through macrophages. Res. Immunol. 143, 95–99.

Chokri, M., Lallot, C., Ebert, M., Poindron, P., Batholeyns, J. (1990) Biodistribution of indium-labelled macrophages in mice bearing solid tumors. Int. J. Immunol. 1, 79–84.

Cleland JG., Erhardt L., Murray G., Hall AS., Ball SG. AIRE Study Investigators. Effect of ramipril on mortality and morbidity of survivors of acute myocardial infarction with clinical evidence of heart failure. The Acute Infarction Ramipril Efficacy (AIRE) Study Investigators. Lancet. 1993;342:821–828.

Clyde W., Mariell Jessup, Biykem Bozkurt, Javed Butler, Donald E. Casey, Mark H. Drazner, Gregg C. Fonarow, et al. 2013. "2013 ACCF/AHA Guideline for the Management of Heart Failure: A Report of the American College of Cardiology Foundation/american Heart Association Task Force on Practice Guidelines." Circulation 128: 240–327.

Coolican, S. a, Samuel, D. S., Mcwade, F. J., Ewton, D. Z., & Florini, J. R. (1997). Cell Biology and Metabolism : The Mitogenic and Myogenic Actions of Insulin-like Growth Factors Utilize Distinct Signaling Pathways The Mitogenic and Myogenic Actions of Insulin-like Growth Factors Utilize Distinct Signaling Pathways *. The Journal of Biological Chemistry, 272(10), 6653–6662.

Coolican, Sharon A., Derina S. Samuel, Daina Z. Ewton, Frank J. McWade, and James R. Florini. 1997. "The Mitogenic and Myogenic Actions of Insulin-like Growth Factors Utilize Distinct Signaling Pathways." Journal of Biological Chemistry 272 (10): 6653–62.

Danielpour, D., & Song, K. (2006). Cross-talk between IGF-I and TGF-β signaling pathways. Cytokine and Growth Factor Reviews, 17(1-2), 59–74.

Datta, S. R., Dudek, H., Xu, T., Masters, S., Haian, F., Gotoh, Y., & Greenberg, M. E. (1997). Akt phosphorylation of BAD couples survival signals to the cell- intrinsic death machinery. Cell, 91, 231–241.

Davis, M. E. (2009). The First Targeted Delivery of siRNA in Humans via a Nanoparticle : From Concept to Clinic. Molecular Pharmaceutics, 6(3), 659–668.

Davis, Michael E, Patrick C H Hsieh, Tomosaburo Takahashi, Qing Song, Shuguang Zhang, Roger D Kamm, Alan J Grodzinsky, Piero Anversa, and Richard T Lee. 2006. "Local Myocardial Insulin-like Growth Factor 1 (IGF-1) Delivery with Biotinylated Peptide Nanofibers Improves Cell Therapy for Myocardial Infarction." Proceedings of the National Academy of Sciences of the United States of America 103 (21): 8155–60.

Deb, S., Wijeysundera, H. C., Ko, D. T., Tsubota, H., Hill, S., & Fremes, S. E. (2013). Coronary Artery Bypass Graft Surgery vs Percutaneous Interventions in Coronary Revascularization. Jama, 310(19), 2086.

Denley, A., Cosgrove, L. J., Booker, G. W., Wallace, J. C., & Forbes, B. E. (2005). Molecular interactions of the IGF system. Cytokine and Growth Factor Reviews, 16, 421–439.

Dhalla, N. S., Elmoselhi, A. B., Hatac, T., & Makino, N. (2000). Status of myocardial antioxidants in ischemia – reperfusion injury. Elsevier. Cardiovascular Research, 47, 446–456.

Duilio, C, G Ambrosio, P Kuppusamy, A DiPaula, L C Becker, and J L Zweier. 2001. "Neutrophils Are Primary Source of O2 Radicals during Reperfusion after Prolonged Myocardial Ischemia." *American Journal of Physiology. Heart and Circulatory Physiology* 280 (6): H2649–57.

Dobrucki, L.W. et al., 2010. Analysis of angiogenesis induced by local IGF-1 expression after myocardial infarction using microSPECT-CT imaging. Journal of Molecular and Cellular Cardiology, 48(6), pp.1071–1079.

Douglas S, Philimon Gona, Irene Albano, Martin G Larson, Emelia J Benjamin, Daniel Levy, William B Kannel, and S Vasan. 2012. "A Systematic Assessment of Causes of Death after Heart Failure Onset in the Community: Impact of Age at Death, Time Period, and Left Ventricular Systolic Dysfunction" 4 (1): 36–43.

Ducharme, Anique, Stefan Frantz, Masanori Aikawa, Elena Rabkin, Merry Lindsey, Luis E. Rohde, Frederick J. Schoen, et al. 2000. "Targeted Deletion of Matrix Metalloproteinase-9 Attenuates Left Ventricular Enlargement and Collagen Accumulation after Experimental Myocardial Infarction." Journal of Clinical Investigation 106 (1): 55–62.

Epelman, Slava, Kory J. Lavine, and Gwendalyn J. Randolph. 2014. "Origin and Functions of Tissue Macrophages." Immunity 41 (1). Elsevier Inc.: 21–35.

Eschalier, Romain, Marie Fertin, Renaud Fay, Christophe Bauters, Faiez Zannad, Florence Pinet, and Patrick Rossignol. 2013. “Extracellular Matrix Turnover Biomarkers Predict Long-Term Left Ventricular Remodeling after Myocardial Infarction Insights from the Reve-2 Study.” Circulation: Heart Failure 6 (6): 1199–1205.

Fang, H., Lai, N. C., Gao, M. H., Miyanohara, A., Roth, D. M., Tang, T., & Hammond, H. K. (2013). Comparison of adeno-associated virus serotypes and delivery for cardiac gene transfer. Human Gene Therapy Methods, 23(4), 234–241.

Felkin, Leanne E., Takuya Narita, Renée Germack, Yasunori Shintani, Kunihiko Takahashi, Padmini Sarathchandra, Marina M. López-Olañeta, et al. 2011. “Calcineurin Splicing Variant Calcineurin Aβ1 Improves Cardiac Function after Myocardial Infarction without Inducing Hypertrophy.” Circulation 123 (24): 2838–47.

Fidler, I. J. (1974). Inhibition of Pulmonary Metastasis by Intravenous Injection of Specifically Activated Macrophages Inhibition of Pulmonary Metastasis by Intravenous Injection of Specifically Activated Macrophages1, (May), 1074–1078.

Fidler, I. J. (1994) Therapy of cancer metastasis by systemic activation of macrophages. Adv. Pharmacol. 30, 271–326.

Florian Leuschner, P. J. R., Takuya Ueno, Rostic Gorbatov, Brett Marinelli, Won Woo Lee, Partha Dutta, Ying Wei, Clinton Robbins, Yoshiko Iwamoto, Brena Sena, Aleksey Chudnovskiy, Peter Panizzi, Edmund Keliher, John M. Higgins, Peter Libby, Michael A. Moskowitz, Mikael J. Pittet, Filip K. Swirski, Ralph Weissleder, and Matthias Nahrendorf (2012). "Rapid monocyte kinetics in acute myocardial infarction are sustained by extramedullary monocytopoiesis." The Journal of Experimental Medicine 209(1): 123-137.

Forbes, B. E., McCarthy, P., & Norton, R. S. (2012). Insulin-like growth factor binding proteins: A structural perspective. Frontiers in Endocrinology, 3(March), 1–13.

Frangogiannis, N, C Smith, and M Entman. (2002). “The Inflammatory Response in Myocardial Infarction.” Cardiovascular Research 53 (1): 31–47.

Frangogiannis, N. G. (2014). The inflammatory response in myocardial injury, repair, and remodelling. Nature Reviews. Cardiology, 11(5), 255–65.

Frangogiannis, Nikolaos G. (2012). “Regulation of the Inflammatory Response in Cardiac Repair.” Circulation Research 110 (1): 159–73.

Frantz, Stefan, and Matthias Nahrendorf. 2014. “Cardiac Macrophages and Their Role in Ischemic Heart Disease.” Cardiovascular Research 102 (2): 1–9.

Frattali, A. L., & Pessin, J. E. (1993). Relationship between α subunit ligand occupancy and β subunit autophosphorylation in insulin/insulin-like growth factor-1 hybrid receptors. Journal of Biological Chemistry, 268(10), 7393–7400.

Frazier, O.H., First use of an untethered, vented electric left ventricular assist device for long-term support. Circulation, 1994. 89: p. 2908-2914.

From the American heart association website. http://www.heart.org/HEARTORG/Conditions/HeartAttack/PreventionTreatmentofHeartAttack/Implantable-Medical-Devices_UCM_303940_Article.jsp

Fujio, Y., Nguyen, T., Wencker, D., Kitsis, R. N., & Walsh, K. (2000). Akt promotes survival of cardiomyocytes in vitro and protects against ischemia-reperfusion injury in mouse heart. Circulation, 101, 660–667.

Gallagher, E. J., & LeRoith, D. (2010). The proliferating role of insulin and insulin-like growth factors in cancer. Trends in Endocrinology and Metabolism: TEM, 21(10), 610–618.

Gao, E., Lei, Y. H., Shang, X., Huang, Z. M., Zuo, L., Boucher, M., … Koch, W. J. (2010). A novel and efficient model of coronary artery ligation and myocardial infarction in the mouse. Circulation Research, 107(12), 1445–1453.

Gao, G., Alvira, M. R., Somanathan, S., Lu, Y., Vandenberghe, L. H., Rux, J. J., Calcedo, R., Sanmiguel, J., Abbas, Z., and Wilson, J. M. (2003) Adeno-associated viruses undergo substantial evolution in primates during natural infections, Proc Natl Acad Sci USA 100 , 6081–6086.

Gao, Guangping, You Lu, Roberto Calcedo, Rebecca L Grant, Peter Bell, Lili Wang, Joanita Figueredo, Martin Lock, and James M Wilson. 2006. “Biology of AAV Serotype Vectors in Liver-Directed Gene Transfer to Nonhuman Primates.” Molecular Therapy : The Journal of the American Society of Gene Therapy 13 (1): 77–87.

Gersh, B. J. (2007). Intracoronary Bone Marrow–Derived Progenitor Cells in Acute Myocardial Infarction. Yearbook of Cardiology, 2007, 223–225.

Giacca, M., & Baker, A. H. (2011). Heartening results: the CUPID gene therapy trial for heart failure. Molecular Therapy : The Journal of the American Society of Gene Therapy, 19(7), 1181–1182.

Gittenberger-de Groot, A. C., Vrancken Peeters, M. P., Mentink, M. M., Gourdie, R. G., & Poelmann, R. E. (1998). Epicardium-derived cells contribute a novel population to the myocardial wall and the atrioventricular cushions. *Circulation Research*, *82*(10), 1043–52.

Go, Alan S, Dariush Mozaffarian, Véronique L Roger, Emelia J Benjamin, Jarett D Berry, Michael J Blaha, Shifan Dai, et al. 2014. Heart Disease and Stroke Statistics--2014 Update: A Report from the American Heart Association. Circulation. Vol. 129.

Gregorevic, M. J. Blankinship, J. M. Allen, R. W. Crawford, D. G. Miller, D. W. Russell, and J. S. Chamberlain, "Systemic delivery of genes to striated muscles using adenoassociated viral vectors," vol. 10, no. 8, pp. 828–834, 2006.

Halbert, C. L., Miller, A. D., Mcnamara, S., Emerson, J., Ronald, L., Ramsey, B., & Aitken, M. L. (2015). Prevalence of Neutralizing Antibodies against Adeno-Associated Virus (AAV) Types 2, 5, and 6 in Cystic Fibrosis and Normal Populations: Implications for Gene Therapy using AAV Vectors, 17(4), 440–447.

Hameed, M., Orrell, R. W., Cobbold, M., Goldspink, G., & Harridge, S. D. R. (2003). Expression of IGF-I splice variants in young and old human skeletal muscle after high resistance exercise. The Journal of Physiology, 547, 247–254.

Harris, J. R., Lippman, M. E., Veronesi, U., & Willett, W. (1992). Effect of carvedilol on outcome after myocardial infarction in patients with left-ventricular dysfunction: the CAPRICORN randomised trial. New England Journal of Medicine, 327, 319–328.

Hayashidani, Shunji, Hiroyuki Tsutsui, Masaki Ikeuchi, Tetsuya Shiomi, Hidenori Matsusaka, Toru Kubota, Kyoko Imanaka-Yoshida, Takeshi Itoh, and Akira Takeshita. 2003. "Targeted Deletion of MMP-2 Attenuates Early LV Rupture and Late Remodeling after Experimental Myocardial Infarction." American Journal of Physiology. Heart and Circulatory Physiology 285 (3): H1229–35.

Hede, Marianne Smedegaard, E. S., Agnieszka Piszczek, Emarald Perlas, Nadine Winn, Tommaso Nastasi, Nadia Rosenthal (2012). "E-Peptides Control Bioavailability of IGF-1." Open Access 7(12): e51152.

Heidt, Timo, Gabriel Courties, Partha Dutta, Hendrik B. Sager, Matt Sebas, Yoshiko Iwamoto, Yuan Sun, et al. 2014. "Differential Contribution of Monocytes to Heart Macrophages in Steady-State and after Myocardial Infarction." Circulation Research 115 (2): 284–95.

Hilgendorf, Ingo, Louisa M S Gerhardt, Timothy C Tan, Carla Winter, Tobias A W Holderried, Benjamin G Chousterman, Yoshiko Iwamoto, et al. 2014. "Ly-6Chigh Monocytes Depend on Nr4a1 to Balance Both Inflammatory and Reparative Phases in the Infarcted Myocardium." *Circulation Research* 114 (10): 1611–22.

Hill, M., & Goldspink, G. (2003). Expression and splicing of the insulin-like growth factor gene in rodent muscle is associated with muscle satellite (stem) cell activation following local tissue damage. The Journal of Physiology, 549, 409–418.

Hirata, S. Masuda, T. Tamura, K. Kai, K. Ojima, A. Fukase, K. Motoyoshi, K. Kamakura, Y. Miyagoe-Suzuki, and S. Takeda, "Expression profiling of cytokines and related genes in regenerating skeletal muscle after cardiotoxin injection: a role for osteopontin.," Am. J. Pathol., vol. 163, no. 1, pp. 203–215, 2003.

Hori, M., and K. Nishida. 2008. "Oxidative Stress and Left Ventricular Remodelling after Myocardial Infarction." *Cardiovascular Research* 81 (3): 457–64.

Hung, Chi F, Maryam G Rohani, Sung-Soon Lee, Peter Chen, and Lynn M Schnapp. 2013. "Role of IGF-1 Pathway in Lung Fibroblast Activation." Respiratory Research 14: 102.

Iraqi, Wafae, Patrick Rossignol, Michael Angioi, Renaud Fay, Josette Nuée, Jean Marie Ketelslegers, John Vincent, Bertram Pitt, and Faiez Zannad. 2009. "Extracellular Cardiac Matrix Biomarkers in Patients with Acute Myocardial Infarction Complicated by Left Ventricular Dysfunction and Heart Failure: Insights from the Eplerenone Post-Acute Myocardial Infarction Heart Failure Efficacy and Survival Study (EP." Circulation 119 (18): 2471–79.

Ito, M. Morioka, S. Kimura, M. Tasaki, K. Inohaya, and A. Kudo, "Differential reparative phenotypes between zebrafish and medaka after cardiac injury," Dev. Dyn., pp. 1106–1115, 2014.

Jaffe, A. S. (2013). Third Universal Definition of Myocardial Infarction. Clinical Biochemistry, 46, 1–4.

Jansen, M., van Schaik, F. M., Ricker, a T., Bullock, B., Woods, D. E., Gabbay, K. H., Van den Brande, J. L. (n.d.). Sequence of cDNA encoding human insulin-like growth factor I precursor. Nature.

Jessup, M., Greenberg, B., Mancini, D., Cappola, T., Pauly, D. F., Jaski, B., … Hajjar, R. J. (2011). Calcium upregulation by percutaneous administration of gene therapy in cardiac disease (CUPID): A phase 2 trial of intracoronary gene therapy of sarcoplasmic reticulum Ca2+-ATPase in patients with advanced heart failure. Circulation, 124, 304–313.

Jesty, Sophy a, Michele a Steffey, F. K. Lee, Martin Breitbach, Michael Hesse, Shaun Reining, Jane C Lee, et al. 2012. "C-Kit+ Precursors Support Postinfarction Myogenesis in the Neonatal, but Not Adult, Heart." *Proceedings of the National Academy of Sciences* 109 (33): 13380–85.

Johannesson, B., S. Sattler, E. Semenova, S. Pastore, T. M. Kennedy-Lydon, R. D. Sampson, M. D. Schneider, N. Rosenthal, and D. Bilbao. 2014. "Insulin-like Growth Factor-1 Induces Regulatory T Cell-Mediated Suppression of Allergic Contact Dermatitis in Mice." Disease Models & Mechanisms 7 (8): 977–85.

Jordan, J. E., Zhao, Z. Q., & Vinten-Johansen, J. (1999). The role of neutrophils in myocardial ischemia-reperfusion injury. Cardiovascular Research, 43(4), 860–878.

Jugdutt, Bodh I. 2003. "Remodeling of the Myocardium and Potential Targets in the Collagen Degradation and Synthesis Pathways." Current Drug Targets. Cardiovascular & Haematological Disorders 3 (1): 1–30.

Jugdutt, Bodh I. 2003. "Ventricular Remodeling after Infarction and the Extracellular Collagen Matrix: When Is Enough Enough?" Circulation 108 (11): 1395–1403.

Kaspar, B. K., Roth, D. M., Lai, N. C., Drumm, J. D., Erickson, D. a., McKirnan, M. D., & Hammond, H. K. (2005). Myocardial gene transfer and long-term expression following intracoronary delivery of adeno-associated virus. Journal of Gene Medicine, 7(October 2004), 316–324.

Kato, T., Sano, M., Miyoshi, S., Sato, T., Hakuno, D., Ishida, H., … Ogawa, S. (2000). Calmodulin kinases II and IV and calcineurin are involved in leukemia inhibitory factor-induced cardiac hypertrophy in rats. Circulation Research, 87(August), 937–945.

Kennedy, D. W., Abkowitz, J. L. (1998) Mature monocytic cells enter tissues and engraft. Proc. Natl. Acad. Sci. USA 95, 14944–14949.

Khan, R. S., Martinez, M. D., Sy, J. C., Pendergrass, K. D., Che, P., Brown, M. E., … Davis, M. E. (2014). Targeting extracellular DNA to deliver IGF-1 to the injured heart. Scientific Reports, 4, 4257.

Khan, Raffay S, Mario D Martinez, Jay C Sy, Karl D Pendergrass, Pao-lin Che, Milton E Brown, E Bernadette Cabigas, Madhuri Dasari, Niren Murthy, and Michael E Davis. 2014. "Targeting Extracellular DNA to Deliver IGF-1 to the Injured Heart." Scientific Reports 4: 4257.

Kieleczawa J: Fundamentals of sequencing of difficult templates-an overview. J Biomol Tech 2006;17:207-217.

Kim, E., Sakai, T., & Jia, Z. (1999). Autologous Transplantation of Bone Marrow Cells Improves Damaged Heart Function. Bone, 247–256.

Kluth, D. C., Ainslie, C. V., Pearce, W. P., Finlay, S., Clarke, D., Anegon, I., Rees, A. J. (2001) Macrophages transfected with adenovirus to express IL-4 reduce inflammation in experimental glomerulonephritis. J. Immunol. 166, 4728–4736.

Kluth, D. C., Erwig, L. P., Pearce, W. P., Rees, A. J. (2000) Gene transfer into inflamed glomeruli using macrophages transfected with adenovirus. Gene Ther. 7, 263–270.

Konkal-Matt R. Prasad, PhD, Robert S. Smith, MD, Yaqin Xu, MD, PhD, and Brent A French, PhD. 2014. "A Single Direct Injection into the Left Ventricular Wall of an AAV9 Vector Expressing EcSOD from the Cardiac Troponin-T Promoter Protects Mice Against Myocardial Infarction." J Gene Med 5 (173).

Kotin, R. M., Linden, R. M., and Berns, K. I. (1992) Characterization of a preferred site on human chromosome 19q for integration of adeno-associated virus DNA by non-homologous recombination, EMBO J 11 , 5071–5078.

Kovacs, S. Worgall, P. Schwalbach, T. Steichele, O. Mehls, and L. Rosivall, "Hypoglycemic effects of insulin-like growth factor-1 in experimental uremia: Can concomitant growth hormone administration prevent this effect?" Horm. Res., vol. 51, no. 4, pp. 193–200, 1999.

Lai, N. C., Gao, M. H., Miyanohara, A., & Roth, D. M. (2012). Comparison of Adeno-Associated Virus Serotypes and Delivery Methods for Cardiac Gene Transfer, 241(August), 234–241.

Lai, N.C. et al., 2012. Improved Function of the Failing Rat Heart by Regulated Expression of Insulin-Like Growth Factor I via Intramuscular Gene Transfer. Human Gene Therapy, 23(3), pp.255–261.

Lang, Roberto M, Michelle Bierig, Richard B Devereux, Frank a Flachskampf, Elyse Foster, Patricia a Pellikka, Michael H Picard, et al. 2005. "Recommendations for Chamber Quantification: A Report from the American Society of Echocardiography's Guidelines and Standards Committee and the Chamber Quantification Writing Group, Developed in Conjunction with the European Association of Echocardiograph." Journal of the American Society of Echocardiography : Official Publication of the American Society of Echocardiography 18 (12): 1440–63.

Lara-Pezzi, Enrique, Nadine Winn, Angelika Paul, Karl McCullagh, Esfir Slominsky, Maria Paola Santini, Foteini Mourkioti, et al. 2007. "A Naturally Occurring Calcineurin Variant Inhibits FoxO Activity and Enhances Skeletal Muscle Regeneration." Journal of Cell Biology 179 (6): 1205–18.

Laron, Z. 2001. "Insulin-like Growth Factor 1 (IGF-1): A Growth Hormone." *Molecular Pathology : MP* 54 (5): 311–16. doi:10.1136/mp.54.5.311.

Laugwitz, K.-L., Moretti, A., Caron, L., Nakano, A., & Chien, K. R. (2008). Islet1 cardiovascular progenitors: a single source for heart lineages? *Development (Cambridge, England)*, *135*(2), 193–205.

Lawrence W. Dobruckia, Yoshiaki Tsutsumib, Leszek Kalinowskia, c, Jarrod Deanb, Mary, and E Gavinb, Sabyasachi Senb, Marivi Mendizabald, Albert J. Sinusasa, and

Ryuichi Aikawab. 2012. “Analysis of Angiogenesis Induced by Local IGF-1 Expression after Myocardial Infarction Using MicroSPECT-CT Imaging.” J Mol Cell Cardiol 29 (6): 997–1003.

Lee, S., Barton, E. R., Sweeney, H. L., & Farrar, R. P. (2004). Viral expression of insulin-like growth factor-I enhances muscle hypertrophy in resistance-trained rats. Journal of Applied Physiology (Bethesda, Md. : 1985), 96, 1097–1104.

Leuschner, F., P. J. Rauch, T. Ueno, R. Gorbatov, B. Marinelli, W. W. Lee, P. Dutta, et al. 2012. “Rapid Monocyte Kinetics in Acute Myocardial Infarction Are Sustained by Extramedullary Monocytopoiesis.” Journal of Experimental Medicine 209 (1): 123–37.

Lin, H., Parmacek, M. S., Morle, G., Bolling, S., & Leiden, J. M. (1990). Expression of recombinant genes in myocardium in vivo after direct injection of DNA. Circulation, 82, 2217–2221.

López-Olañeta, M. M., Villalba, M., Gómez-Salinero, J. M., Jiménez-Borreguero, L. J., Breckenridge, R., Ortiz-Sánchez, P., Lara-Pezzi, E. (2014). Induction of the calcineurin variant CnAβ1 after myocardial infarction reduces post-infarction ventricular remodelling by promoting infarct vascularization. Cardiovascular Research, 102(3), 396–406

Love, K. T., Mahon, K. P., Christopher, G., Whitehead, K. A., Querbes, W., Robert, J., … Robert, J. (2010). Correction for Love et al., Lipid-like materials for low-dose, in vivo gene silencing, 107(21), 9915.

Lowe, W.L., Jr., Lasky, S.R., Le roith, D.& Roberts, C.T., Jr. Distribution and regulation of rat insulin-like growth factor I Messenger ribonucleic acids encoding alternative carboxyterminal E-peptides: evidence for differential processing and regulation liver. Mol. Endocrinol 2, 528-535 (1988)

Madsen, D. Leonard, A. Masedunskas, A. Moyer, H. J. Jürgensen, D. E. Peters, P. Amornphimoltham, A. Selvaraj, S. S. Yamada, D. A. Brenner, S. Burgdorf, L. H. Engelholm, N. Behrendt, K. Holmbeck, R. Weigert, and T. H. Bugge, “M2-like macrophages are responsible for collagen degradation through a mannose receptor–mediated pathway,” vol. 202, no. 6, pp. 951–966, 2013.

Mathieu, M., Bartunek, J., El Oumeiri, B., Touihri, K., Hadad, I., Thoma, P., … McEntee, K. (2009). Cell therapy with autologous bone marrow mononuclear stem cells is associated with superior cardiac recovery compared with use of nonmodified mesenchymal stem cells in a canine model of chronic myocardial infarction. The Journal of Thoracic and Cardiovascular Surgery, 138(September), 646–653.

Männer, J. (1993). Experimental study on the formation of the epicardium in chick embryos. *Anatomy and Embryology*, *187*(3), 281–9.

Männer, J. (1999). Does the subepicardial mesenchyme contribute myocardioblasts to the myocardium of the chick embryo heart? A quail-chick chimera study tracing the fate of the epicardial primordium. *The Anatomical Record*, *255*(2), 212–26.

McMurray, J. J. V, Adamopoulos, S., Anker, S. D., Auricchio, A., Böhm, M., Dickstein, K., … Zeiher, A. (2013). ESC Guidelines for the diagnosis and treatment of acute and chronic heart failure 2012: The Task Force for the Diagnosis and Treatment of Acute and Chronic Heart Failure 2012 of the European Society of Cardiology. Developed in collaboration with the Heart. Revista Portuguesa de Cardiologia, 32, e1–641–e61.

Menasché, P., Alfieri, O., Janssens, S., McKenna, W., Reichenspurner, H., Trinquart, L., Hagège, A. a. (2008). The myoblast autologous grafting in ischemic cardiomyopathy (MAGIC) trial: First randomized placebo-controlled study of myoblast transplantation. Circulation, 117, 1189–1200.

Minicucci, M. F., Azevedo, P. S., Polegato, B. F., Paiva, S. a R., & Zornoff, L. a M. (2011). Heart failure after myocardial infarction: Clinical implications and treatment. Clinical Cardiology, 34, 410–414.

Mikawa, T., & Gourdie, R. G. (1996). Pericardial mesoderm generates a population of coronary smooth muscle cells migrating into the heart along with ingrowth of the epicardial organ. *Developmental Biology*, *174*(2), 221–32.

Möllmann, H., Nef, H. M., Kostin, S., Kalle, C. Von, Pilz, I., Weber, M. Elsässer, A. (2006). Bone marrow-derived cells contribute to infarct remodelling, 71, 661–671.

Mosser, "The many faces of macrophage activation.," *J. Leukoc. Biol.*, vol. 73, no. 2, pp. 209–212, 2003.

Müller, O. J., Leuchs, B., Pleger, S. T., Grimm, D., Franz, W. M., Katus, H. a., & Kleinschmidt, J. a. (2006). Improved cardiac gene transfer by transcriptional and transductional targeting of adeno-associated viral vectors. Cardiovascular Research, 70, 70–78.

Musarò, a, McCullagh, K. J., Naya, F. J., Olson, E. N., & Rosenthal, N. (1999). IGF-1 induces skeletal myocyte hypertrophy through calcineurin in association with GATA-2 and NF-ATc1. Nature, 400(1998), 581–585.

Musarò, a, McCullagh, K., Paul, a, Houghton, L., Dobrowolny, G., Molinaro, M., … Rosenthal, N. (2001). Localized Igf-1 transgene expression sustains hypertrophy and regeneration in senescent skeletal muscle. Nature Genetics, 27(february), 195–200.

Muthana, M., Giannoudis, A., Scott, S. D., Fang, H. Y., Coffelt, S. B., Morrow, F. J., … Maitland, N. J. (2011). Use of macrophages to target therapeutic adenovirus to human prostate tumors. Cancer Research, 71, 1805–1815.

Muthana, M., Rodrigues, S., Chen, Y. Y., Welford, A., Hughes, R., Tazzyman, S., … Lewis, C. E. (2013). Macrophage delivery of an oncolytic virus abolishes tumor regrowth and metastasis after chemotherapy or irradiation. Cancer Research, 73(2), 490–495.

Nahrendorf, M., Pittet, M. J., & Swirski, F. K. (2010). Monocytes: Protagonists of infarct inflammation and repair after myocardial infarction. Circulation, 121, 2437–2445.

Nahrendorf, Matthias, and Filip K Swirski. (2013). "Monocyte and Macrophage Heterogeneity in the Heart," 1624–33.

Nahrendorf, Matthias, Filip K Swirski, Elena Aikawa, Lars Stangenberg, Thomas Wurdinger, Jose-Luiz Figueiredo, Peter Libby, Ralph Weissleder, and Mikael J Pittet. (2007). "The Healing Myocardium Sequentially Mobilizes Two Monocyte Subsets with Divergent and Complementary Functions." The Journal of Experimental Medicine 204 (12): 3037–47.

Nalinda B. Wasala, Jin-Hong Shin, and D. D. (2012). The evolution of heart gene delivery vectors. Changes, 29(10), 997–1003.

Oh H, Bradfute SB, Gallardo TD, Nakamura T, Gaussin V, et al. (2003) Cardiac progenitor cells from adult myocardium: homing, differentiation, and fusion after infarction. Proc Natl Acad Sci USA 100: 12313–12318.

Orlic, D., Kajstura, J., Chimenti, S., Jakoniuk, I., Anderson, S. M., Li, B., … Anversa, P. (2001). Bone marrow cells regenerate infarcted myocardium. Nature, 410(6829), 701–705.

Pacak, C. a, Mah, C. S., Thattaliyath, B. D., Conlon, T. J., Lewis, M. a, Cloutier, D. E., Byrne, B. J. (2006). Recombinant adeno-associated virus serotype 9 leads to preferential cardiac transduction in vivo. Circulation Research, 99(4), e3–9. 17) Bostick, B., Ghosh, a,

Pack, D. W., Hoffman, A. S., Pun, S., & Stayton, P. S. (2005). Design and development of polymers for gene delivery. Nature Reviews. Drug Discovery, 4(July), 581–593.

Panse, Kalyani D., Leanne E. Felkin, Marina M. López-Olañeta, Jesús Gómez-Salinero, María Villalba, Lucía Muñoz, Kazuto Nakamura, et al. 2012. "Follistatin-like 3 Mediates Paracrine Fibroblast Activation by Cardiomyocytes." Journal of Cardiovascular Translational Research 5 (6): 814–26.

Parrish, E. P., Cifuentes-Diaz, C., Li, Z. L., Vicart, P., Paulin, D., Dreyfus, P. A., Peschanski, M., Harris, A. J., Garcia, L. (1996) Targeting widespread sites of damage in dystrophic muscle: engrafted macrophages as potential shuttles. Gene Ther. 3, 13–20.

Patel, R. Thiagarajan, J. T. Willerson, and E. T. Yeh, "Inhibition of alpha4 integrin and ICAM-1 markedly attenuate macrophage homing to atherosclerotic plaques in ApoE-deficient mice.," *Circulation*, vol. 97, no. 1, pp. 75–81, 1998

Pelletier, L. Maggi, A. Micheletti, E. Lazzeri, N. Tamassia, L. Cosmi, C. Lunardi, F. Annunziato, S. Romagnani, a Marco, W. Dc, C. Costantini, and M. a Cassatella, "Evidence for a cross-talk between human neutrophils and Th17 cells Evidence for a cross-talk between human neutrophils and Th17 cells," vol. 115, no. 2, pp. 335–343, 2014.

Pelosi, L., Giacinti, C., Nardis, C., Borsellino, G., Rizzuto, E., Nicoletti, C., … Musarò, A. (2007). Local expression of IGF-1 accelerates muscle regeneration by rapidly modulating inflammatory cytokines and chemokines. The FASEB Journal : Official Publication of the Federation of American Societies for Experimental Biology, 21, 1393–1402.

Pérez-Pomares, J.-M., Carmona, R., González-Iriarte, M., Atencia, G., Wessels, A., & Muñoz-Chápuli, R. (2002). Origin of coronary endothelial cells from epicardial mesothelium in avian embryos. *The International Journal of Developmental Biology*, *46*(8), 1005–13.

Pinto, Alexander R., Rosa Paolicelli, Ekaterina Salimova, Janko Gospocic, Esfir Slonimsky, Daniel Bilbao-Cortes, James W. Godwin, and Nadia a. Rosenthal. 2012. "An Abundant Tissue Macrophage Population in the Adult Murine Heart with a Distinct Alternatively-Activated Macrophage Profile." *PLoS ONE* 7 (5).

Pfeffer, M. A., Braunwald, E., Moyé, L. A., Basta, L., Brown, E. J., Cuddy, T. E., … Flaker, G. C. (1992). Effect of captopril on mortality and morbidity in patients with left ventricular dysfunction after myocardial infarction. Results of the survival and ventricular enlargement trial. The SAVE Investigators. The New England journal of medicine (Vol. 327).

Philippou, a., E. Papageorgiou, G. Bogdanis, a. Halapas, a. Sourla, M. Maridaki, N. Pissimissis, and M. Koutsilieris. 2009. "Expression of IGF-1 Isoforms after Exercise-Induced Muscle Damage in Humans: Characterization of the MGF E Peptide Actions in Vitro." In Vivo 23 (4): 567–76.

Pinckard, R. N., Olson, M. S., Giclas, P. C., Terry, R., Boyer, J. T., & O'Rourke, R. a. (1975). Consumption of classical complement components by heart subcellular

membranes in vitro and in patients after acute myocardial infarction. Journal of Clinical Investigation, 56(3), 740–750.

Pinto, A.,R. Paolicelli, E. Salimova, J. Gospocic, E. Slonimsky, D. Bilbao-Cortes, J. W. Godwin, and N. a. Rosenthal, "An abundant tissue macrophage population in the adult murine heart with a distinct alternatively-activated macrophage profile," *PLoS One*, vol. 7, no. 5, 2012.

Pinto, Alexander R., James W. Godwin, and Nadia A. Rosenthal. 2014. "Macrophages in Cardiac Homeostasis, Injury Responses and Progenitor Cell Mobilisation." Stem Cell Research.

Poggioli, T, Daniel Stuckey, Padmini Sarathchandra, Michael D. Schneider, Maria Paola Santini, and Nadia Rosenthal. Cell-mediated Insulin-like growth factor-1Ea propeptide delivery protects from postinjury cardiac dysfunction by modulation of MEK3/6-p38 signalling. (in preparation).

Porrello E., A. I. M., Emma Simpson, Brett A. Johnson, David Grinsfelder, Diana Canseco, Pradeep P. Mammen, Beverly A. Rothermel, Eric N.Olson and Hesham A. Sadek (2012). "Regulation of neonatal and adult mammalian heart regeneration by the miR-15 family." PNAS.

Porrello E., A. I. M., Emma Simpson, Joseph A. Hill, James A. and E. N. O. Richardson, and Hesham A. Sadek (2011). "Transient Regenerative Potential of the Neonatal Mouse Heart." Science 331(6020): 1078-1080.

Poss, K. D. (2002). "Heart Regeneration in Zebrafish." Science 298: 2188.

Poss, K. K. a. K. D. (2012). "Cardiac Regenerative Capacity and Mechanisms." The Annual Review of Cell and Developmental Biology 28: 719-41.

Prasad, K-M R, Y Xu, Z Yang, S T Acton, and B a French. 2011. "Robust Cardiomyocyte-Specific Gene Expression Following Systemic Injection of AAV: In Vivo Gene Delivery Follows a Poisson Distribution." Gene Therapy 18 (1): 43–52.

Prentice, H., Kloner, R. a, Li, Y., Newman, L., & Kedes, L. (1996). Ischemic/reperfused myocardium can express recombinant protein following direct DNA or retroviral injection. Journal of Molecular and Cellular Cardiology, 28(1996), 133–140.

Production and Isolation of AAV vectors: http://www.med.upenn.edu/gtp/vectorcore/production.shtml

Ptaszek, L. M., Mansour, M., Ruskin, J. N., & Chien, K. R. (2012). Towards regenerative therapy for cardiac disease. The Lancet, 379(9819), 933–942.

Qiu, J., and Pintel, D. (2008) Processing of adeno-associated virus RNA, Front Biosci 13 , 3101–3115.

Quaini, F., Urbanek, K., Beltrami, A. P., Finato, N., Beltrami, C. A., Nadal-Ginard, B., Anversa, P. (2002). Chimerism of the transplanted heart. The New England Journal of Medicine, 346(1), 5–15.

Rommel, C., Bodine, S. C., Clarke, B. a, Rossman, R., Nunez, L., Stitt, T. N., … Glass, D. J. (2001). Mediation of IGF-1-induced skeletal myotube hypertrophy by PI(3)K/Akt/mTOR and PI(3)K/Akt/GSK3 pathways. Nature Cell Biology, 3(November), 1009–1013.

Rotwein, P., Pollock, M., Didier, K., Krivis, G., & Sequence, H. I. G. (1986). Organization and Sequence of the Human Insulin-like Growth Factor I. DNA Sequence, (11)

Ruijter, J M, C Ramakers, W M H Hoogaars, Y Karlen, O Bakker, M J B van den Hoff, and a F M Moorman. 2009. “Amplification Efficiency: Linking Baseline and Bias in the Analysis of Quantitative PCR Data.” Nucleic Acids Research 37 (6): e45.

Santini, P. J. L., Giovanna Borsellino, Esfir Slonimski, Elham Zarrinpashenh, Tommaso Poggioli, Nadia Rosenthal. (2011). "IGF-1Ea induces vessel formation after injury and medaites bone marrrow and heart cross-talk through the expression of specific cytokines." Biochemical and Biophysical Research communications. 410: 201-207.

Santini, P. L. T., Laurent Monassier, Catherine Theodoropoulos, Janice Carter, Enrique Lara-Pezzi, Esfir Slonimsky, Ekaterina Salimova, Patrice Delafontaine, Yao-Hua Song, Martin Bergmann, Christian Freund, Ken Suzuki and Nadia Rosenthal (2007). "Enhancing Repair of the Mammalian Heart." Cardiovascular Research 100: 1732-1740.

Sanz, S, J B Pucilowska, S Liu, C M Rodríguez-Ortigosa, P K Lund, D a Brenner, C R Fuller, et al. 2005. “Expression of Insulin-like Growth Factor I by Activated Hepatic Stellate Cells Reduces Fibrogenesis and Enhances Regeneration after Liver Injury.” Gut 54 (1): 134–41.

Sedmera, D., & McQuinn, T. (2008). Embryogenesis of the Heart Muscle. Heart Failure Clinics, 4(3), 235–245.

Semple, S. C., Akinc, A., Chen, J., Sandhu, A. P., Mui, B. L., Cho, C. K., Hope, M. J. (2010). Rational design of cationic lipids for siRNA delivery. Nature Biotechnology, 28(2), 172–176.

Serbina, Natalya V, and Eric G Pamer. 2006. “Monocyte Emigration from Bone Marrow during Bacterial Infection Requires Signals Mediated by Chemokine Receptor CCR2.” Nature Immunology 7 (3): 311–17.

Sergeeva, Irina A, and Vincent M Christoffels. 2013. “Regulation of Expression of Atrial and Brain Natriuretic Peptide, Biomarkers for Heart Development and Disease.”

Biochimica et Biophysica Acta (BBA) - Molecular Basis of Disease 1832 (12). Elsevier B.V.: 2403–13. doi:10.1016/j.bbadis.2013.07.003.

Shavlakadze, T., Winn, N., Rosenthal, N., & Grounds, M. D. (2005). Reconciling data from transgenic mice that overexpress IGF-I specifically in skeletal muscle. Growth Hormone and IGF Research, 15, 4–18.

Sil, A. K., Maeda, S., Sano, Y., Roop, D. R., & Karin, M. (2004). Haematopoietic stem cells do not transdifferentiate into cardiac mycocytes in myocardial infarcts. Nature, 428(April), 660–4.

Stewart, C. & Rotwein, P. Growth, differentation, and survival: multiple physiological functions for insulin-like growth factors. Physiol. Rev. 76, 1005–1026 (1996)

Simmons, J. G., Van Wyk, J. J., Hoyt, E. C., & Lund, P. K. (1993). Multiple transcription start sites in the rat insulin-like growth factor-I gene give rise to IGF-I mRNAs that encode different IGF-I precursors and are processed differently in vitro. Growth Factors (Chur, Switzerland), 9, 205–221.

Simmons, James G, Jolanta B Pucilowska, Temitope O Keku, and P Kay Lund. 2002. "IGF-I and TGF-beta1 Have Distinct Effects on Phenotype and Proliferation of Intestinal Fibroblasts." American Journal of Physiology. Gastrointestinal and Liver Physiology 283 (3): G809–18.

Skalak, R., Raton, B., Dembo, M., Kaverina, I., Small, J. V, Wang, Y. L., … Mondragon, A. (2007). Monitoring of Blood Vessels and Tissues by a Population of Monocytes with Patrolling Behavior, 317(August), 666–670.

Stavropoulou, A., Halapas, A., Sourla, A., Philippou, A., Papageorgiou, E., Papalois, A., & Koutsilieris, M. IGF-1 expression in infarcted myocardium and MGF E peptide actions in rat cardiomyocytes in vitro. Molecular Medicine (Cambridge, Mass.), 15, 127–135.

Swirski, et al. (2013). "Monocyte and Macrophage Heterogeneity in the Heart." Circulation 112: 1624-1633.

Tacke, D. Alvarez, T. J. Kaplan, C. Jakubzick, R. Spanbroek, J. Llodra, A. Garin, J. Liu, M. Mack, N. Van Rooijen, S. a. Lira, A. J. Habenicht, and G. J. Randolph, "Monocyte subsets differentially employ CCR2, CCR5, and CX3CR1 to accumulate within atherosclerotic plaques," J. Clin. Invest., vol. 117, no. 1, pp. 185–194, 2007.

Takagawa, Junya, Yan Zhang, Maelene L Wong, Richard E Sievers, Neel K Kapasi, Yan Wang, Yerem Yeghiazarians, Randall J Lee, William Grossman, and Matthew L Springer. 2007. "Myocardial Infarct Size Measurement in the Mouse Chronic Infarction Model: Comparison of Area- and Length-Based Approaches." Journal of Applied Physiology (Bethesda, Md. : 1985) 102 (6): 2104–11.

Takashi Matsui, L. L., Federica del Monte, Yasuhisa Fukui, Thomas F. Franke, Roger J.Hajjar and Anthony Rosenzweig (1999). "Adenoviral Gene Transfer of Activated Phosphatidylinositol 3'-Kinase and Akt Inhibits Apoptosis of Hypoxic Cardiomyocytes In Vitro." Circulation 100: 2373-2379.

Taqman® probe-based gene expression analysis. http://www3.appliedbiosystems.com/cms/groups/mcb_marketing/documents/generaldocuments/cms_085696.pdf?ICID=mp-taqman-gex-0910

Temmerman, L., E. Slonimsky, and N. Rosenthal. 2010. "Class 2 IGF-1 Isoforms Are Dispensable for Viability, Growth and Maintenance of IGF-1 Serum Levels." Growth Hormone and IGF Research 20 (3). Elsevier Ltd: 255–63.

Thygesen, K., Mair, J., Katus, H., Plebani, M., Venge, P., Collinson, P., … Jaffe, A. S. (2010). Recommendations for the use of cardiac troponin measurement in acute cardiac care. European Heart Journal, 31(2009), 2197–2204.

Tidball, J. G. "Inflammatory processes in muscle injury and repair," AJP Regul. Integr. Comp. Physiol., vol. 288, no. 2, pp. R345–R353, Sep. 2004.

Tomanek, R. J. (2005). Formation of the coronary vasculature during development. *Angiogenesis*, *8*(3), 273–84.

Tong, S. Buch, H. Yao, C. Wu, H. I. Tong, Y. Wang, and Y. Lu, "Monocytes-derived macrophages mediated stable expression of human brain-derived neurotrophic factor, a novel therapeutic strategy for neuroAIDS," PLoS One, vol. 9, no. 2, pp. 1–12, 2014.

Tonkin, J., Temmerman, L., Sampson, R. D., Gallego-Colon, E., Barberi, L., Bilbao, D., Schneider, Michael D, Musarò, Antonio, Rosenthal, N. (2015). Monocyte/macrophage-derived IGF-1 orchestrates murine skeletal muscle regeneration and modulates autocrine polarization. Molecular Therapy.

Torp-pedersen, C. (1994). Effect of ACE inhibitor trandolapril on life expectancy of patients with reduced left-ventricular function after acute myocardial infraction.

Uguccioni, M., D'Apuzzo, M., Loetscher, M., Dewald, B., & Baggiolini, M. (1995). Actions of the chemotactic cytokines MCP-1, MCP-2, MCP-3, RANTES, MIP-1 alpha and MIP-1 beta on human monocytes. European Journal of Immunology, 25, 64–68.

Ullrich, a, Gray, a, Tam, a W., Yang-Feng, T., Tsubokawa, M., Collins, C., … Chen, E. (1986). Insulin-like growth factor I receptor primary structure: comparison with insulin receptor suggests structural determinants that define functional specificity. The EMBO Journal, 5(10), 2503–2512.

Vakeva, a P., Agah, a, Rollins, S. a, Matis, L. a, Li, L., & Stahl, G. L. (1998). Myocardial infarction and apoptosis after myocardial ischemia and reperfusion: role of the

terminal complement components and inhibition by anti-C5 therapy. Circulation, 97(22), 2259–2267.

Van Berlo, J. H., Kanisicak, O., Maillet, M., Vagnozzi, R. J., Karch, J., Lin, S.-C. J., … Molkentin, J. D. (2014). C-Kit+ Cells Minimally Contribute Cardiomyocytes To the Heart. Nature, 509, 337–41.

Van der Laan, a. M., Nahrendorf, M., & Piek, J. J. (2012). Healing and adverse remodelling after acute myocardial infarction: role of the cellular immune response. Heart, 98(Ccl), 1384–1390.

Van Nieuwenhoven, F. a., & Turner, N. a. (2013). The role of cardiac fibroblasts in the transition from inflammation to fibrosis following myocardial infarction. Vascular Pharmacology, 58(3), 182–188.

Vanhoutte, Davy, Mark Schellings, Yigal Pinto, and Stephane Heymans. 2006. "Relevance of Matrix Metalloproteinases and Their Inhibitors after Myocardial Infarction: A Temporal and Spatial Window." Cardiovascular Research 69 (3): 604–13.

Waksman, R., Fournadjiev, J., Baffour, R., Pakala, R., Hellinga, D., Leborgne, L., Rivera, E. (2004). Transepicardial autologous bone marrow-derived mononuclear cell therapy in a porcine model of chronically infarcted myocardium. Cardiovascular Radiation Medicine, 5, 125–131.

Walker, J. M. (2009). Adeno-associated virus biology. Life Sciences (Vol. 531, p. 588).

Wang, J. et al., 2011. The regenerative capacity of zebrafish reverses cardiac failure caused by genetic cardiomyocyte depletion. , 3430, pp.3421–3430.

Wang, Y. Wang, Q. Cao, G. Zheng, V. W. S. Lee, D. Zheng, X. Li, T. K. Tan, and D. C. H. Harris, "By homing to the kidney, activated macrophages potently exacerbate renal injury.," *Am. J. Pathol.*, vol. 172, no. 6, pp. 1491–1499, 2008.

Wang, Z., Zhu, T., Qiao, C., Zhou, L., Wang, B., Zhang, J., Xiao, X. (2005). Adeno-associated virus serotype 8 efficiently delivers genes to muscle and heart. Nature Biotechnology, 23(3), 321–8.

Weber, K T. 1997. Extracellular matrix remodeling in heart failure: a role for de novo angiotensin II generation. Circulation 4065–82.

Wessels, A., & Pérez-Pomares, J. M. (2004). The epicardium and epicardially derived cells (EPDCs) as cardiac stem cells. *The Anatomical Record. Part A, Discoveries in Molecular, Cellular, and Evolutionary Biology*, *276*(1), 43–57.

White, M.F., The IRS-signalling system: a network of docking proteins that mediate insulin action. Mol Cell Biochem, 1998. 182(1-2): p. 3-11.

Wiltrout, R. H., Brunda, M. J., Gorelik, E., Peterson, E. S., Dunn, J. J., Leonhardt, J., Varesio, L., Reynolds, C. W., Holden, H. T. J. (1983) Distribution of peritoneal macrophage

populations after intravenous injection in mice: differential effects of eliciting and activating agents. Reticuloendothel. Soc. 34, 253–269.

Wolfram and J. K. Donahue, "Gene therapy to treat cardiovascular disease.," J. Am. Heart Assoc., vol. 2, p. e000119 (2013).

Yan, Xiaoxiang, Atsushi Anzai, Yoshinori Katsumata, Tomohiro Matsuhashi, Kentaro Ito, Jin Endo, Tsunehisa Yamamoto, et al. 2013. "Temporal Dynamics of Cardiac Immune Cell Accumulation Following Acute Myocardial Infarction." Journal of Molecular and Cellular Cardiology 62. Elsevier Ltd: 24–35.

Yang, S. Y., & Goldspink, G. (2002). Different roles of the IGF-I Ec peptide (MGF) and mature IGF-I in myoblast proliferation and differentiation. FEBS Letters, 522, 156–160.

Yasushi Fujio, T. N., Detlef Wencker, Richard N. Kitsis and Kenneth Walsh (2000). "Akt Promotes Survival of Cardiomyocytes In Vitro and Protects Against Ischemia-Reperfusion Injury in Mouse Heart." Circulation 101: 660-667.

Yin, H., Kanasty, R. L., Eltoukhy, A. a., Vegas, A. J., Dorkin, J. R., & Anderson, D. G. (2014). Non-viral vectors for gene-based therapy. Nature Reviews Genetics, 15(8), 541–555.

Yousef, M., Schannwell, C. M., Köstering, M., Zeus, T., Brehm, M., & Strauer, B. E. (2009). The BALANCE Study: clinical benefit and long-term outcome after intracoronary autologous bone marrow cell transplantation in patients with acute myocardial infarction. Journal of the American College of Cardiology, 53(24), 2262–2269.

Yue, Y., Long, C., & Duan, D. (2007). Systemic AAV-9 transduction in mice is influenced by animal age but not by the route of administration. Gene Therapy, 14(22), 1605–9.

Zeisberg, E. M., Tarnavski, O., Zeisberg, M., Dorfman, A. L., Mcmullen, J. R., Gustafsson, E., Kalluri, R. (2007). Endothelial-to-mesenchymal transition contributes to cardiac fibrosis, 13(8).

Zweier, J.L., Measurement of superoxide-derived free radicals in the reperfused heart. Evidence for a free radical mechanism of reperfusion injury. J Biol Chem, 1988. 263(3): p. 1353-7.

References of Table 1.1 in Chapter 1

1) Ehrengruber, M. U., Hennou, S., Büeler, H., Naim, H. Y., Déglon, N., & Lundstrom, K. (2001). Gene transfer into neurons from hippocampal slices: comparison of recombinant Semliki Forest Virus, adenovirus, adeno-associated virus, lentivirus, and measles virus. *Molecular and Cellular Neurosciences*, *17*(5), 855–871. doi:10.1006/mcne.2001.0982
2) Müller, O. J., Leuchs, B., Pleger, S. T., Grimm, D., Franz, W. M., Katus, H. a., & Kleinschmidt, J. a. (2006). Improved cardiac gene transfer by transcriptional and transductional targeting of adeno-associated viral vectors. *Cardiovascular Research*, *70*, 70–78. doi:10.1016/j.cardiores.2005.12.017
3) Shin, J.-H., Bostick, B., Yue, Y., Hajjar, R., & Duan, D. (2011). SERCA2a gene transfer improves electrocardiographic performance in aged mdx mice. *Journal of Translational Medicine*, *9*(1), 132. doi:10.1186/1479-5876-9-132
4) Fish, K. M., Ladage, D., Kawase, Y., Karakikes, I., Jeong, D., Ly, H., Hajjar, R. J. (2013). AAV9.I-1c delivered via direct coronary infusion in a porcine model of heart failure improves contractility and mitigates adverse remodeling. *Circulation: Heart Failure*, *6*(2), 310–317. doi:10.1161/CIRCHEARTFAILURE.112.971325
5) Zincarelli, C., Soltys, S., Rengo, G., & Rabinowitz, J. E. (2008). Analysis of AAV serotypes 1-9 mediated gene expression and tropism in mice after systemic injection. *Molecular Therapy : The Journal of the American Society of Gene Therapy*, *16*(6), 1073–1080. doi:10.1038/mt.2008.76
6) Pacak, C. a, Mah, C. S., Thattaliyath, B. D., Conlon, T. J., Lewis, M. a, Cloutier, D. E., … Byrne, B. J. (2006). Recombinant adeno-associated virus serotype 9 leads to preferential cardiac transduction in vivo. *Circulation Research*, *99*(4), e3–9. doi:10.1161/01.RES.0000237661.18885.f6
7) Rengo, G., Lymperopoulos, A., Zincarelli, C., Donniacuo, M., Soltys, S., Rabinowitz, J. E., & Koch, W. J. (2009). Myocardial adeno-associated virus serotype 6-betaARKct gene therapy improves cardiac function and normalizes the neurohormonal axis in chronic heart failure. *Circulation*, *119*(1), 89–98. doi:10.1161/CIRCULATIONAHA.108.803999
8) Denegri, M., Bongianino, R., Lodola, F., Boncompagni, S., De Giusti, V. C., E. Avelino-Cruz, J., … Priori, S. G. (2014). Single delivery of an adeno-associated viral construct to transfer the CASQ2 gene to knock-in mice affected by catecholaminergic polymorphic ventricular tachycardia is able to cure the

disease from birth to advanced age. *Circulation*, *129*(25), 2673–2681. doi:10.1161/CIRCULATIONAHA.113.006901

9) Yamashita, T., Chai, H. L., Teramoto, S., Tsuji, S., Shimazaki, K., Muramatsu, S. I., & Kwak, S. (2013). Rescue of amyotrophic lateral sclerosis phenotype in a mouse model by intravenous AAV9-ADAR2 delivery to motor neurons. *EMBO Molecular Medicine*, *5*(11), 1710–1719. doi:10.1002/emmm.201302935
10) Müller, O. J., Schinkel, S., Kleinschmidt, J. a, Katus, H. a, & Bekeredjian, R. (2008). Augmentation of AAV-mediated cardiac gene transfer after systemic administration in adult rats. *Gene Therapy*, *15*(23), 1558–1565. doi:10.1038/gt.2008.111
11) Prasad, K.-M. R., Xu, Y., Yang, Z., Acton, S. T., & French, B. a. (2011). Robust cardiomyocyte-specific gene expression following systemic injection of AAV: in vivo gene delivery follows a Poisson distribution. *Gene Therapy*, *18*(1), 43–52. doi:10.1038/gt.2010.105
12) Lai, N. C., Gao, M. H., Miyanohara, A., & Roth, D. M. (2012). Comparison of Adeno-Associated Virus Serotypes and Delivery Methods for Cardiac Gene Transfer, *241*(August), 234–241. doi:10.1089/hgtb.2012.105
13) Dodge, J. C., Haidet, A. M., Yang, W., Passini, M. a, Hester, M., Clarke, J.,Kaspar, B. K. (2008). Delivery of AAV-IGF-1 to the CNS extends survival in ALS mice through modification of aberrant glial cell activity. *Molecular Therapy : The Journal of the American Society of Gene Therapy*, *16*(6), 1056–1064. doi:10.1038/mt.2008.60
14) Bell, C. L., Vandenberghe, L. H., Bell, P., Limberis, M. P., Gao, G., Vliet, K. Van, … Wilson, J. M. (2011). The AAV9 receptor and its modification to improve in vivo lung gene transfer in mice, *121*(6). doi:10.1172/JCI57367DS1
15) Konishi, M., Kawamoto, K., Izumikawa, M., Kuriyama, H., & Yamashita, T. (2008). Gene transfer into guinea pig cochlea using adeno-associated virus vectors. *The Journal of Gene Medicine*, *10*(6), 610–618. doi:10.1002/jgm
16) Gao, G., Lu, Y., Calcedo, R., Grant, R. L., Bell, P., Wang, L.,Wilson, J. M. (2006). Biology of AAV serotype vectors in liver-directed gene transfer to nonhuman primates. *Molecular Therapy : The Journal of the American Society of Gene Therapy*, *13*(1), 77–87. doi:10.1016/j.ymthe.2005.08.017
17) Yue, Y., Ghosh, A., Long, C., Bostick, B., Smith, B. F., Kornegay, J. N., & Duan, D. (2008). A single intravenous injection of adeno-associated virus serotype-9 leads to whole body skeletal muscle transduction in dogs. *Molecular Therapy : The Journal of the American Society of Gene Therapy*, *16*(12), 1944–1952. doi:10.1038/mt.2008.207

18) Hirai, T., Enomoto, M., Kaburagi, H., Sotome, S., Yoshida-Tanaka, K., Ukegawa, M., … Yokota, T. (2014). Intrathecal AAV serotype 9-mediated delivery of shRNA against TRPV1 attenuates thermal hyperalgesia in a mouse model of peripheral nerve injury. *Molecular Therapy : The Journal of the American Society of Gene Therapy*, *22*(2), 409–19. doi:10.1038/mt.2013.247

19) Wang, Z., Zhu, T., Qiao, C., Zhou, L., Wang, B., Zhang, J., … Xiao, X. (2005). Adeno-associated virus serotype 8 efficiently delivers genes to muscle and heart. *Nature Biotechnology*, *23*(3), 321–8. doi:10.1038/nbt1073

20) Gregorevic, P., Blankinship, M. J., Allen, J. M., Crawford, R. W., Miller, D. G., Russell, D. W., & Chamberlain, J. S. (2006). Systemic delivery of genes to striated muscles using adenoassociated viral vectors, *10*(8), 828–834.

21) Du, L., Kido, M., Lee, D. V., Rabinowitz, J. E., Samulski, R. J., Jamieson, S. W., Weitzman, M. D., and Thistlethwaite, P. A. (2004) Differential myocardial gene delivery by recombinant serotype-specific adeno-associated viral vectors, Mol Ther 10 , 604–608.

22) Palomeque, J., Chemaly, E. R., Colosi, P., Wellman, J. A., Zhou, S., Del Monte, F., and Hajjar, R. J. (2007) Efficiency of eight different AAV serotypes in transducing rat myocardium in vivo, Gene Ther 14 , 989–997.

23) Yan, Z., Lei-Butters, D. C., Liu, X., Zhang, Y., Zhang, L., Luo, M., Zak, R., and Engelhardt, J. F. (2006) Unique biologic properties of recombinant AAV1 transduction in polarized human airway epithelia, J Biol Chem 281, 29684–29692.

24) Lorain, S., Gross, D. A., Goyenvalle, A., Danos, O., Davoust, J., and Garcia, L. (2008) Transient immunomodulation allows repeated injections of AAV1 and correction of muscular dystrophy in multiple muscles, Mol Therapy 16 , 541–547.

25) Paneda, A., Vanrell, L., Mauleon, I., Crettaz, J. S., Berraondo, P., Timmermans, E. J., Beattie, S. G., Twisk, J., van Deventer, S., Prieto, J., Fontanellas, A., Rodriguez-Pena, M. S., and Gonzalez-Aseguinolaza, G. (2009) Effect of adeno-associated virus serotype and genomic structure on liver transduction and biodistribution in mice of both genders, Hum Gene Ther 20 , 908–917.

26) Brantly, M. L., Chulay, J. D., Wang, L., Mueller, C., Humphries, M., Spencer, L. T., Rouhani, F., Conlon, T. J., Calcedo, R., Betts, M. R., Spencer, C., Byrne, B. J., Wilson, J. M., and Flotte, T. R. (2009) Sustained transgene expression despite T lymphocyte responses in a clinical trial of rAAV1-AAT gene therapy, Proc Natl Acad Sci USA 106, 16363–16368.

27) Mendell, J. R., Rodino-Klapac, L. R., Rosales-Quintero, X., Kota, J., Coley, B. D., Galloway, G., Craenen, J. M., Lewis, S., Malik, V., Shilling, C., Byrne, B. J., Conlon, T., Campbell, K. J., Bremer, W. G., Viollet, L., Walker, C. M., Sahenk, Z., and Clark, K. R. (2009) Limbgirdle muscular dystrophy type 2D gene therapy restores alpha-sarcoglycan and associated proteins, Ann Neurol 66 , 290–297.

28) Stroes, E. S., Nierman, M. C., Meulenberg, J. J., Franssen, R., Twisk, J., Henny, C. P., Maas, M. M., Zwinderman, A. H., Ross, C., Aronica, E., High, K. A., Levi, M. M., Hayden, M. R., Kastelein, J. J., and Kuivenhoven, J. A. (2008) Intramuscular administration of AAV1-lipoprotein lipase S447X lowers triglycerides in lipoprotein lipase-deficient patients, Arterioscler Thromb Vasc Biol 28 , 2303–2304

29) Yang, G. S., Schmidt, M., Yan, Z., Lindbloom, J. D., Harding, T. C., Donahue, B. A., Engelhardt, J. F., Kotin, R., and Davidson, B. L. (2002) Virus-mediated transduction of murine retina with adeno-associated virus: effects of viral capsid and genome size, J Virol 76 , 7651–7660. 121.

30) Glushakova, L. G., Timmers, A. M., Pang, J., Teusner, J. T., and Hauswirth, W. W. (2006) Human blue-opsin promoter preferentially targets reporter gene expression to rat s-cone photoreceptors, Invest Ophthalmol Vis Sci 47 , 3505–3513.

31) Takahashi, H., Kato, K., Miyake, K., Hirai, Y., Yoshino, S., and Shimada, T. (2005) Adeno-associated virus vector-mediated anti-angiogenic gene therapy for collagen-induced arthritis in mice, Clin Exp Rheumatol 23 , 455–461.

32) Dai, J., and Rabie, A. B. (2007) Direct AAVmediated gene delivery to the temporomandibular joint, Front Biosci 12 , 2212–2220.

33) Tuuminen, R., Nykanen, A. I., Krebs, R., Soronen, J., Pajusola, K., Keranen, M. A., Koskinen, P. K., Alitalo, K., and Lemstrom, K. B. (2009) PDGF-A, -C, and -D but not PDGF-B increase TGF-beta1 and chronic rejection in rat cardiac allografts, Arterioscler Thromb Vasc Biol 29 , 691–698.

34) Takahashi, H., Kato, K., Miyake, K., Hirai, Y. Yoshino, S., and Shimada, T. (2005) Adeno-associated virus vector-mediated anti-angiogenic gene therapy for collagen-induced arthritis in mice, Clin Exp Rheumatol 23 , 455–461.

35) Snyder, R. O., Miao, C. H., Patijn, G. A., Spratt, S. K., Danos, O., Nagy, D., Gown, A. M., Winther, B., Meuse, L., Cohen, L. K., Thompson, A. R., and Kay, M. A. (1997) Persistent and therapeutic concentrations of human factor IX in mice after hepatic gene transfer of recombinant AAV vectors, Nat Genet 16 , 270–276.

36) Wheeler, M. D., Kono, H., Rusyn, I., Arteel, G. E., McCarty, D., Samulski, R. J., and Thurman, R. G. (2000) Chronic ethanol increases adeno-associated viral transgene expression in rat liver via oxidant and NFkappaB-dependent mechanisms, Hepatology 32 , 1050–1059.

37) Halbert, C. L., and Miller, A. D. (2004) AAV mediated gene transfer to mouse lungs, Methods Mol Biol 246 , 201–212.

38) Yoshimura, M., Sakamoto, M., Ikemoto, M., Mochizuki, Y., Yuasa, K., Miyagoe-Suzuki, Y., and Takeda, S. (2004) AAV vector-mediated microdystrophin expression in a relatively small percentage of mdx myofi bers improved the mdx phenotype, Mol Ther 10 , 821–828.

39) Zaratiegui, M., Castilla-Cortazar, I., Garcia, M., Quiroga, J., Prieto, J., and Novo, F. J. (2002) IGF1 gene transfer into skeletal muscle using recombinant adeno-associated virus in a rat model of liver cirrhosis, J Physiol Biochem 58 , 169–176.

40) Weber, M., Rabinowitz, J., Provost, N., Conrath, H., Folliot, S., Briot, D., Cherel, Y., Chenuaud, P., Samulski, J., Moullier, P., and Rolling, F. (2003) Recombinant adeno-associated virus serotype 4 mediates unique and exclusive long-term transduction of retinal pigmented epithelium in rat, dog, and nonhuman primate after subretinal delivery. Mol Ther 7 , 774–781.

41) 4, C. H., Passini, M. A., Haskins, M. E., and Wolfe, J. H. (2003) Adeno-associated virus vector-mediated transduction in the cat brain, Gene Ther 10 , 1874–1881.

42) Ciron, C., Cressant, A., Roux, F., Raoul, S., Cherel, Y., Hantraye, P., Deglon, N., Schwartz, B., Barkats, M., Heard, J. M., Tardieu, M., Moullier, P., and Colle, M. A. (2009) Human alpha-iduronidase gene transfer mediated by adeno-associated virus types 1, 2, and 5 in the brain of nonhuman primates: vector diffusion and biodistribution, Hum Gene Ther 20 , 350–360.

43) Byrne, M. J., Power, J. M., Preovolos, A., Mariani, J. A., Hajjar, R. J., and Kaye, D. M. (2008) Recirculating cardiac delivery of AAV2/1SERCA2a improves myocardial function in an experimental model of heart failure in large animals, Gene Ther 15 , 1550–1557.

44) Kawase, Y., Ly, H. Q., Prunier, F., Lebeche, D., Shi, Y., Jin, H., Hadri, L., Yoneyama, R., Hoshino, K., Takewa, Y., Sakata, S., Peluso, R., Zsebo, K., Gwathmey, J. K., Tardif, J. C., Tanguay, J. F., and Hajjar, R. J. (2008) Reversal of cardiac dysfunction after longterm expression of SERCA2a by gene transfer in a pre-clinical model of heart failure, J Am Coll Cardiol 51 , 1112–1119.

45) Liu, X., Luo, M., Guo, C., Yan, Z., Wang, Y., and Engelhardt, J. F. (2007) Comparative biology of rAAV transduction in ferret, pig and human airway epithelia, Gene Ther 14 , 1543–1548.

46) Flotte, T. R., Fischer, A. C., Goetzmann, J., Mueller, C., Cebotaru, L., Yan, Z., Wang, L., Wilson, J. M., Guggino, W. B., and Engelhardt, J. F. (2010) Dual reporter comparative indexing of rAAV pseudotyped vectors in chimpanzee airway, Mol Ther 18. 594–600.

47) Flotte, T. R., Conlon, T. J., Poirier, A., Campbell-Thompson, M., and Byrne, B. J. (2007) Preclinical characterization of a recombinant adeno-associated virus type 1-pseudotyped vector demonstrates dose dependent injection site inflammation and dissemination of vector genomes to distant sites, Hum Gene Ther 18 , 245–256.

48) Ross, C. J., Twisk, J., Bakker, A. C., Miao, F., Verbart, D., Rip, J., Godbey, T., Dijkhuizen, P., Hermens, W. T., Kastelein, J. J., Kuivenhoven, J. A., Meulenberg, J. M., and Hayden, M. R. (2006) Correction of feline lipoprotein lipase defi ciency with adeno-associated virus serotype 1-mediated gene transfer of the lipoprotein lipase S447X beneficial mutation, Hum Gene Ther 17 , 487–499.

49) Rivera, V. M., Gao, G. P., Grant, R. L., Schnell, M. A., Zoltick, P. W., Rozamus, L. W., Clackson, T., and Wilson, J. M. (2005) Long-term pharmacologically regulated expression of erythropoietin in primates following AAV-mediated gene transfer, Blood 105 , 1424–1430.

50) Arruda, V. R., Schuettrumpf, J., Herzog, R. W., Nichols, T. C., Robinson, N., Lotfi , Y., Mingozzi, F., Xiao, W., Couto, L. B., and High, K. A. (2004) Safety and efficacy of factor IX gene transfer to skeletal muscle in murine and canine hemophilia B models by adeno-associated viral vector serotype 1, Blood 103 , 85–92.

51) Tuszynski, M. H., Thal, L., Pay, M., Salmon, D. P., U, H. S., Bakay, R., Patel, P., Blesch, A., Vahlsing, H. L., Ho, G., Tong, G., Potkin, S. G., Fallon, J., Hansen, L., Mufson, E. J., Kordower, J. H., Gall, C., and Conner, J. (2005) A phase 1 clinical trial of nerve growth factor gene therapy for Alzheimer disease, Nat Med 11 , 551–555.

52) Worgall, S., Sondhi, D., Hackett, N. R., Kosofsky, B., Kekatpure, M. V., Neyzi, N., Dyke, J. P., Ballon, D., Heier, L., Greenwald, B. M., Christos, P., Mazumdar, M., Souweidane, M. M., Kaplitt, M. G., and Crystal, R. G. (2008) Treatment of late infantile neuronal ceroid lipofuscinosis by CNS administration of a serotype 2 adeno-associated virus expressing CLN2 cDNA, Hum Gene Ther 19 , 463–474.

53) Janson, C., McPhee, S., Bilaniuk, L., Haselgrove, J., Testaiuti, M., Freese, A., Wang, D. J., Shera, D., Hurh, P., Rupin, J., Saslow, E., Goldfarb, O., Goldberg, M., Larijani, G., Sharrar, W., Liouterman, L., Camp, A., Kolodny, E., Samulski, J., and Leone, P. (2002) Clinical protocol. Gene therapy of Canavan disease: AAV-2 vector for neurosurgical delivery of aspartoacylase gene (ASPA) to the human brain, Hum Gene Ther 13 , 1391–1412.

54) Kaplitt, M. G., Feigin, A., Tang, C., Fitzsimons, H. L., Mattis, P., Lawlor, P. A., Bland, R. J., Young, D., Strybing, K., Eidelberg, D., and During, M. J. (2007) Safety and tolerability of gene therapy with an adeno-associated virus (AAV) borne GAD gene for Parkinson's disease: an open label, phase I trial, Lancet 369 , 2097–2105.

55) Mease, P. J., Hobbs, K., Chalmers, A., El-Gabalawy, H., Bookman, A., Keystone, E., Furst, D. E., Anklesaria, P., and Heald, A. E. (2009) Local delivery of a recombinant adeno-associated vector containing a tumour necrosis factor alpha antagonist gene in inflammatory arthritis: a phase 1 dose-escalation safety and tolerability study, Ann Rheum Dis 68 , 1247–1254.

56) Wagner, J. A., Nepomuceno, I. B., Messner, A. H., Moran, M. L., Batson, E. P., Dimiceli, S., Brown, B. W., Desch, J. K., Norbash, A. M., Conrad, C. K., Guggino, W. B., Flotte, T. R., Wine, J. J., Carter, B. J., Reynolds, T. C., Moss, R. B., and Gardner, P. (2002) A phase II, double-blind, randomized, placebo controlled clinical trial of tgAAVCF using maxillary sinus delivery in patients with cystic fibrosis with antrostomies, Hum Gene Ther 13 , 1349–1359.

57) Flotte, T. R., Brantly, M. L., Spencer, L. T., Byrne, B. J., Spencer, C. T., Baker, D. J., and Humphries, M. (2004) Phase I trial of intramuscular injection of a recombinant adeno-associated virus alpha 1-antitrypsin (rAAV2-CB-hAAT) gene vector to AAT-deficient adults, Hum Gene Ther 15 , 93–128.

58) Kay, M. A., Manno, C. S., Ragni, M. V., Larson, P. J., Couto, L. B., McClelland, A., Glader, B., Chew, A. J., Tai, S. J., Herzog, R. W., Arruda, V., Johnson, F., Scallan, C., Skarsgard, E., Flake, A. W., and High, K. A. (2000) Evidence for gene transfer and expression of factor IX in hemophilia B patients treated with an AAV vector, Nat Genet 24 , 257–261.

59) Schmidt, M., Voutetakis, A., Afi one, S., Zheng, C., Mandikian, D., and Chiorini, J. A. (2008) Adeno-associated virus type 12 (AAV12): a novel AAV serotype with sialic acid- and heparin sulfate proteoglycan-independent transduction activity, J Virol 82 , 1399–1406.

60) Klein, R. L., Dayton, R. D., Tatom, J. B., Henderson, K. M., and Henning, P. P. (2008) AAV8, 9, Rh10, Rh43 vector gene transfer in the rat brain: effects of serotype, promoter and purification method, Mol Ther 16 , 89–96.

61) 167. De, B. P., Heguy, A., Hackett, N. R., Ferris, B., Leopold, P. L., Lee, J., Pierre, L., Gao, G., Wilson, J. M., and Crystal, R. G. (2006) High levels of persistent expression of alpha1-antitrypsin mediated by the nonhuman primate serotype rh.10 adeno-associated virus despite preexisting immunity to common human adeno-associated viruses, Mol Ther 13 , 67–76.

62) Alisky, J. M., Hughes, S. M., Sauter, S. L., Jolly, D., Dubensky, T. W., Jr., Staber, P. D., Chiorini, J. A., and Davidson, B. L. (2000) Transduction of murine cerebellar neurons with recombinant FIV and AAV5 vectors, Neuroreport 11 , 2669–2673.

63) Gorbatyuk, M., Justilien, V., Liu, J., Hauswirth, W. W., and Lewin, A. S. (2007) Preservation of photoreceptor morphology and function in P23H rats using an allele independent ribozyme, Experimental eye research 84 , 44–52.

64) Apparailly, F., Khoury, M., Vervoordeldonk, M. J., Adriaansen, J., Gicquel, E., Perez, N., Riviere, C., Louis-Plence, P., Noel, D., Danos, O., Douar, A. M., Tak, P. P., and Jorgensen, C. (2005) Adeno-associated virus pseudotype 5 vector improves gene transfer in arthritic joints, Hum Gene Ther 16 , 426–434.

65) Adriaansen, J., Khoury, M., de Cortie, C. J., Fallaux, F. J., Bigey, P., Scherman, D., Gould, D. J., Chernajovsky, Y., Apparailly, F., Jorgensen, C., Vervoordeldonk, M. J., and Tak, P. P. (2007) Reduction of arthritis following intra-articular administration of an adeno-associated virus serotype 5 expressing a disease-inducible TNF-blocking agent, Ann Rheum Dis 66 , 1143–1150.

66) Kitajima, K., Marchadier, D. H., Burstein, H., and Rader, D. J. (2006) Persistent live expression of murine apoA-l using vectors based on adeno-associated viral vectors serotypes 5 and 1, Atherosclerosis 186 , 65–73.

67) De, B., Heguy, A., Leopold, P. L., Wasif, N., Korst, R. J., Hackett, N. R., and Crystal, R. G. (2004) Intrapleural administration of a serotype 5 adeno-associated virus coding for alpha1-antitrypsin mediates persistent, high lung and serum levels of alpha1-antitrypsin, Mol Ther 10 , 1003–1010.

68) Sandalon, Z., Bruckheimer, E. M., Lustig, K. H., Rogers, L. C., Peluso, R. W., and Burstein, H. (2004) Secretion of a TNFR:Fc fusion protein following pulmonary administration of pseudotyped adeno-associated virus vectors, J Virol 78 , 12355–12365.

69) Acland, G. M., Aguirre, G. D., Ray, J., Zhang, Q., Aleman, T. S., Cideciyan, A. V., Pearce- Kelling, S. E., Anand, V., Zeng, Y., Maguire, A. M., Jacobson, S. G.,

Hauswirth, W. W., and Bennett, J. (2001) Gene therapy restores vision in a canine model of childhood blindness, Nat Genet 28 , 92–95.131.

70) Kaplitt, M. G., Xiao, X., Samulski, R. J., Li, J.,Ojamaa, K., Klein, I. L., Makimura, H., Kaplitt, M. J., Strumpf, R. K., and Diethrich, E. B. (1996) Long-term gene transfer in porcine myocardium after coronary infusion of an adeno-associated virus vector, Ann Thorac Surg 62 , 1669–1676.

71) Ulrich-Vinther, M., Duch, M. R., Soballe, K.,O'Keefe, R. J., Schwarz, E. M., and Pedersen, F. S. (2004) In vivo gene delivery to articular chondrocytes mediated by an adeno-associated virus vector, J Orthop Res 22 , 726–734.\

72) Goodrich, L. R., Choi, V. W., Carbone, B. A., McIlwraith, C. W., and Samulski, R. J. (2009) Ex Vivo Serotype-Specific Transduction of Equine Joint Tissue by Self-Complementary Adeno-Associated Viral Vectors, Hum Gene Ther 20 , 1697–1702.

73) Mount, J. D., Herzog, R. W., Tillson, D. M., Goodman, S. A., Robinson, N., McCleland, M. L., Bellinger, D., Nichols, T. C., Arruda, V. R., Lothrop, C. D., Jr., and High, K. A. (2002) Sustained phenotypic correction of hemophilia B dogs with a factor IX null mutation by liver-directed gene therapy, Blood 99, 2670–2676.

74) Rubenstein, R. C., McVeigh, U., Flotte, T.R., Guggino, W. B., and Zeitlin, P. L. (1997) CFTR gene transduction in neonatal rabbits using an adeno-associated virus (AAV) vector, Gene Ther 4 , 384–392

75) Conrad, C. K., Allen, S. S., Afi one, S. A., Reynolds, T. C., Beck, S. E., Fee-Maki, M., Barrazza-Ortiz, X., Adams, R., Askin, F. B., Carter, B. J., Guggino, W. B., and Flotte, T. R. (1996) Safety of single-dose administration of an adeno-associated virus (AAV)-CFTR vector in the primate lung, Gene Ther 3 , 658–668.

76) Bankiewicz, K. S., Forsayeth, J., Eberling, J. L., Sanchez-Pernaute, R., Pivirotto, P., Bringas, J., Herscovitch, P., Carson, R. E., Eckelman, W., Reutter, B., and Cunningham, J. (2006) Long-term clinical improvement in MPTP-lesioned primates after gene therapy with AAV-hAADC, Mol Ther 20 , 350–360.

77) Ciron, C., Cressant, A., Roux, F., Raoul, S., Cherel, Y., Hantraye, P., Deglon, N., Schwartz, B., Barkats, M., Heard, J. M., Tardieu, M., Moullier, P., and Colle, M. A. (2009) Human alpha-iduronidase gene transfer mediated by adeno-associated virus types 1, 2, and 5 in the brain of nonhuman primates: vector diffusion and biodistribution, Hum Gene Ther 20 , 350–360.

78) Bennett, J., Maguire, A. M., Cideciyan, A. V., Schnell, M., Glover, E., Anand, V., Aleman, T. S., Chirmule, N., Gupta, A. R., Huang, Y., Gao, G. P., Nyberg, W. C., Tazelaar, J., Hughes, J., Wilson, J. M., and Jacobson, S. G. (1999) Stable transgene

expression in rod photoreceptors after recombinant adeno-associated virus-mediated gene transfer to monkey retina, Proc Natl Acad Sci USA 96 ,9920–9925.

79) Lotery, A. J., Yang, G. S., Mullins, R. F., Russell, S. R., Schmidt, M., Stone, E. M., Lindbloom, J. D., Chiorini, J. A., Kotin, R. M., and Davidson, B. L. (2003) Adeno-associated virus type 5: transduction effi ciency and celltype specifi city in the primate retina, Hum Gene Ther 14 , 1663–1671.

80) Gao, G. P., Lu, Y., Sun, X., Johnston, J., Calcedo, R., Grant, R., and Wilson, J. M. (2006) High-level transgene expression in nonhuman primate liver with novel adenoassociated virus serotypes containing selfcomplementary genomes, J Virol 80, 6192–6194.

81) Niemeyer, G. P., Herzog, R. W., Mount, J., Arruda, V. R., Tillson, D. M., Hathcock, J., van Ginkel, F. W., High, K. A., and Lothrop, C. D., Jr. (2009) Long-term correction of inhibitor-prone hemophilia B dogs treated with liver-directed AAV2-mediated factor IX gene therapy, Blood 113 , 797–806.

82) Rivera, V. M., Gao, G. P., Grant, R. L., Schnell, M. A., Zoltick, P. W., Rozamus, L. W., Clackson, T., and Wilson, J. M. (2005) Long-term pharmacologically regulated expression of erythropoietin in primates following AAV-mediated gene transfer, Blood 105 , 1424–1430.

83) Colle, M. A., Piguet, F., Bertrand, L., Raoul, S., Bieche, I., Dubreil, L., Sloothaak, D., Bouquet, C., Moullier, P., Aubourg, P., Cherel, Y., Cartier, N., and Sevin, C. (2010) Effi cient intracerebral delivery of AAV5 vector encoding human ARSA in non-human primate, Hum Mol Genet 19 , 147–158.

84) Flotte, T. R., Fischer, A. C., Goetzmann, J., Mueller, C., Cebotaru, L., Yan, Z., Wang, L., Wilson, J. M., Guggino, W. B., and Engelhardt, J. F. (2010) Dual reporter comparative indexing of rAAV pseudotyped vectors in chimpanzee airway, Mol Ther 18 ,594–600.

85) Nathwani, A. C., Gray, J. T., Ng, C. Y., Zhou, J., Spence, Y., Waddington, S. N., Tuddenham, E. G., Kemball-Cook, G., McIntosh, J., Boon- Spijker, M., Mertens, K., and Davidoff, A. M. (2006) Self-complementary adeno-associated virus vectors containing a novel liver-specifi c human factor IX expression cassette enable highly efficient transduction of murine and nonhuman primate liver, Blood 107 , 2653–2661.

86) Jiang, H., Lillicrap, D., Patarroyo-White, S., Liu, T., Qian, X., Scallan, C. D., Powell, S., Keller, T., McMurray, M., Labelle, A., Nagy, D., Vargas, J. A., Zhou, S., Couto, L. B.,

and Pierce, G. F. (2006) Multiyear therapeutic benefit of AAV serotypes 2, 6, and 8 delivering factor VIII to hemophilia A mice and dogs, Blood 108 , 107–115.

87) Bish, L. T., Sleeper, M. M., Brainard, B., Cole, S., Russell, N., Withnall, E., Arndt, J., Reynolds, C., Davison, E., Sanmiguel, J., Wu, D., Gao, G., Wilson, J. M., and Sweeney, H. L. (2008) Percutaneous transendocardial delivery of self-complementary adeno-associated virus 6 achieves global cardiac gene transfer in canines, Mol Ther 16 , 1953–1959.

88) Wang, Z., Allen, J. M., Riddell, S. R., Gregorevic, P., Storb, R., Tapscott, S. J., Chamberlain, J. S., and Kuhr, C. S. (2007) Immunity to adeno-associated virus-mediated gene transfer in a random-bred canine model of Duchenne muscular dystrophy, Hum Gene Ther 18 , 18–26.

89) Moscioni, D., Morizono, H., McCarter, R. J., Stern, A., Cabrera-Luque, J., Hoang, A., Sanmiguel, J., Wu, D., Bell, P., Gao, G. P., Raper, S. E., Wilson, J. M., and Batshaw, M. L.(2006) Long-term correction of ammonia metabolism and prolonged survival in ornithine transcarbamylase-deficient mice following liver directed treatment with adeno-associated viral vectors, Mol Ther 14 , 25–33.

90) Nienhuis, A. W. (2007) Discussion of human gene transfer protocol 0707–864: an open label dose-escalation study of a self-complementary adeno-associated viral vector (scAAV2/8-LPlhFIXco) for gene therapy of hemophilia B, RAC NIH.

91) Broekman, M. L., Comer, L. A., Hyman, B. T., and Sena-Esteves, M. (2006) Adeno-associated virus vectors serotyped with AAV8 capsid are more efficient than AAV-1 or -2 serotypes for widespread gene delivery to the neonatal mouse brain, Neuroscience 138 , 501–510.

92) Lawlor, P. A., Bland, R. J., Mouravlev, A.,Young, D., and During, M. J. (2009) Effi cient gene delivery and selective transduction of glial cells in the mammalian brain by AAV serotypes isolated from nonhuman primates. Mol Ther 17 , 1692–1702.

93) Foust, K. D., Nurre, E., Montgomery, C. L., Hernandez, A., Chan, C. M., and Kaspar, B. K. (2009) Intravascular AAV9 preferentially targets neonatal neurons and adult astrocytes, Nat Biotechnol 27 , 59–65.

94) Xue, Y. Q., Ma, B. F., Zhao, L. R., Tatom, J. B., Li, B., Jiang, L. X., Klein, R. L., and Duan, W. M. (2010) AAV9-mediated erythropoietin gene delivery into the brain protects nigral dopaminergic neurons in a rat model of Parkinson's disease, Gene Ther 17 , 83–94.

95) Wang, Z., Zhu, T., Rehman, K. K., Bertera, S., Zhang, J., Chen, C., Papworth, G., Watkins, S., Trucco, M., Robbins, P. D., Li, J., and Xiao, X. (2006) Widespread and

stable pancreatic gene transfer by adeno-associated virus vectors via different routes, Diabetes 55 , 875–884.

96) Burger, C., Gorbatyuk, O. S., Velardo, M. J., Peden, C. S., Williams, P., Zolotukhin, S., Reier, P. J., Mandel, R. J., and Muzyczka, N. (2004) Recombinant AAV viral vectors pseudotyped with viral capsids from serotypes 1, 2, and 5 display differential efficiency and cell tropism after delivery to different regions of the central nervous system, Mol Ther 10, 302–317.

97) Ohshima, S., Shin, J. H., Yuasa, K., Nishiyama, A., Kira, J., Okada, T., and Takeda, S. (2009) Transduction efficiency and immune response associated with the administration of AAV8 vector into dog skeletal muscle, Mol Ther 17, 73–80.

98) Rodino-Klapac, L. R., Montgomery, C. L., Bremer, W. G., Shontz, K. M., Malik, V., Davis, N., Sprinkle, S., Campbell, K. J., Sahenk, Z., Clark, K. R., Walker, C. M., Mendell, J. R., and Chicoine, L. G. (2010) Persistent expression of FLAG-tagged micro dystrophin in nonhuman primates following intramuscular and vascular delivery, Mol Ther 18 , 109–117.

99) Pacak, C. A., Sakai, Y., Thattaliyath, B. D., Mah, C. S., and Byrne, B. J. (2008) Tissue specific promoters improve specificity of AAV9 mediated transgene expression following intra-vascular gene delivery in neonatal mice, Genet Vaccines Ther 6, 13.

100) Duque, S., Joussemet, B., Riviere, C., Marais, T., Dubreil, L., Douar, A. M., Fyfe, J., Moullier, P., Colle, M. A., and Barkats, M. (2009) Intravenous administration of selfcomplementary AAV9 enables transgene delivery to adult motor neurons, Mol Ther 17 ,1187–1196.

101) Bish, L. T., Sleeper, M. M., Brainard, B., Cole, S., Russell, N., Withnall, E., Arndt, J., Reynolds, C., Davison, E., Sanmiguel, J., Wu, D., Gao, G., Wilson, J. M., and Sweeney, H. L. (2008) Percutaneous transendocardial delivery of self-complementary adeno-associated virus 6 achieves global cardiac gene transfer in canines, Mol Ther 16 , 1953–1959.